

The role of ERK5 signalling in macrophage behaviour during wound healing

A thesis submitted to the University of Manchester for the degree of Doctor of
Philosophy in the Faculty of Biology, Medicine and Health.

2021

Jason Chu

Division of Pharmacy and Optometry,
School of Health Sciences,
Faculty of Biology, Medicine, and Health.

Contents

List of Figures	5
List of Tables	8
List of Abbreviations	9
Abstract.....	11
Declaration.....	13
Copyright statement.....	13
Acknowledgements.....	14
Chapter 1: Introduction	16
1.1 Background.....	16
1.2 The skin and wound healing	17
1.2.1 Inflammation, tissue formation and remodelling.....	18
1.3 Macrophages in wound healing	22
1.3.1 Functional phenotypes of macrophages - M1/M2 axis.....	26
1.4 Impaired wound healing	30
1.4.1 Current landscape of treatments for impaired wound healing	34
1.5 ERK signalling – a novel therapeutic target for wound healing	36
1.6 Precursor Research.....	43
1.7 Understanding ERK5 signalling in macrophage behaviour and wound healing – hypothesis, aims and objectives.....	45
Chapter 2: Materials and Methods	49
2.1 Cell Lines.....	49
2.2 Treatment Groups	49
2.3 Western Blots.....	50
2.4 MTT and SRB Proliferation Assay.....	52
2.5 <i>In vitro</i> scratch assay.....	53
2.6 Real-Time Quantitative Polymerase Chain Reaction (RT-qPCR).....	53
2.6.1 RNA extraction	53
2.6.2 DNase I Treatment.....	54
2.6.3 Complementary DNA (cDNA) Synthesis.....	54
2.6.4 RT-qPCR Programme.....	54
2.7 Immunofluorescence.....	55
2.8 Animal work	56
2.8.1 Ethics, sources and husbandry	56
2.8.2 Genetic Mouse Models	56
2.8.3 Genotyping.....	58

2.8.4 Genetic modification of ERK5 in keratinocytes	59
2.9 Wounding.....	59
2.10 <i>In vivo</i> OS1 Treatment	59
2.11 Wound Tissue Dissociation	60
2.12 Flow Cytometry	60
2.13 Homogenisation of wounds for RT-qPCR.....	60
2.14 Immunohistochemistry (IHC).....	61
2.15 Positron Emission Tomography (PET) imaging.....	62
2.16 Statistical Analysis.....	62
Chapter 3: Genetic <i>in vivo</i> hyperactivation of ERK5 in keratinocytes drives local inflammation in wound healing	65
3.1 Genetic ERK5 modification had no effect on wound closure.....	66
3.2 H&E analysis show that genetic ERK5 modification in keratinocytes did not influence wound architecture or immune response	69
3.3 FACS analysis show that genetic ERK5 modification did not significantly influence immune response	71
3.4 Assessing changes to immune response in genetic ERK5 modification by histology	74
3.4.1 ERK5 expression is lower throughout the wound region in ERK5KO but similar in CaMEK5 murine models when compared to control	76
3.4.2 Neutrophils are more abundant in both ERK5KO and CaMEK5 murine models	79
3.4.3 F4/80 macrophage profiles are similar in both ERK5KO and CaMEK5 murine models when compared to control	81
3.4.4 iNOS expression levels was lower in ERK5KO and persisted in CaMEK5 murine models.....	83
3.4.5 Arg1 expression profile was similar in both ERK5KO and CaMEK5 murine models.....	86
3.4.6 Collagen deposition was decreased in ERK5KO and CaMEK5 wounds	89
3.5 Discussion.....	92
Chapter 4: Therapeutic inactivation of ERK5 with OS1 in <i>in vitro</i> models of HaCaTs and THP-1s promotes an overall reparative phenotype	102
4.1 <i>In vitro</i> therapeutic degradation of ERK5 in HaCaTs.....	103
4.1.1 OS1 specifically targets and degrades ERK5 protein in HaCaTs	104
4.1.2 OS1 does not affect potential off-target proteins: ERK1/2 and BRD4.....	107
4.1.3. OS1 vs AX inhibition of ERK5 phosphorylation	108
4.1.4 ERK5 inactivation with OS1 had no effect on cell growth.....	110
4.1.5 ERK5 inactivation with OS1 had no effect on cell migration	111
4.1.6 ERK5 inactivation by OS1 promotes the mRNA expression of a range of both inflammatory and repair associated cytokines	113

4.2 <i>In vitro</i> therapeutic degradation of ERK5 with OS1 primes THP-1 macrophages towards a reparative phenotype	118
4.2.1 Morphology and profile of THP-1 macrophages	118
4.2.2 Differentiating M1/M2 –like macrophages by their gene expression of inflammatory and repair associated mediators.....	123
4.2.3 OS1 specifically targets and degrades ERK5 protein in THP-1 cells	125
4.2.4 Identifying changes to cell surface markers by immunofluorescence after ERK5 inactivation with OS1	130
4.2.5 ERK5 expression decreased with OS1 treatment and increased with M1/M2 polarisation.....	132
4.2.6 ERK5 inactivation by OS1 had limited effect on phalloidin expression	136
4.2.7 TSPO expression was largely unchanged by OS1 treatment	138
4.2.8 MR expression was largely unchanged by OS1 treatment.....	141
4.2.9 CD163 expression was largely unchanged by OS1 treatment	143
4.2.10 ERK5 inactivation by OS1 caused transient increase on the mRNA expression of a range of repair mediated cytokines	145
4.3 Discussion	148
Chapter 5: Therapeutic inactivation of ERK5 with OS1 in <i>in vivo</i> models of wound healing promotes a reparative phenotype	158
5.1 Topical OS1 treatment led to decreased ERK5 expression and quicker wound closure .	158
5.2 Therapeutic inactivation of ERK5 with OS1 increased the proportions of macrophage, monocyte and neutrophil populations	162
5.3 Assessing changes to immune response in OS1 treated wounds by histology	166
5.3.1 ERK5 expression decreases throughout the wound region after OS1 treatment	167
5.3.2 ERK5 degradation with OS1 led to reduction in neutrophils	169
5.3.3 ERK5 degradation with OS1 led to modest increase in F4/80 expression at later time points.....	171
5.3.4 ERK5 degradation with OS1 led to no changes in iNOS expression	173
5.3.5 ERK5 degradation with OS1 led to similar but slight increased Arg1 expression at later time points.....	175
5.3.6 ERK5 inactivation with OS1 led to no changes in collagen deposition	177
5.4 OS1 modifies the mRNA expression of various inflammatory associated mediators	180
5.4.1 ERK5 inactivation by OS1 inhibits the mRNA expression of early inflammatory mediators.....	180
5.4.2 ERK5 inactivation by OS1 has limited influence on mRNA expression of chemokine mediators	181
5.4.3 ERK5 inactivation by OS1 has no effect on the mRNA expression of reparative mediators.....	182
5.5 Discussion	185
Chapter 6: Development of macrophage PET imaging modality.....	190

6.1. Inflammatory macrophage infiltration was not successfully identified with TSPO-PET imaging in the wound healing model.....	191
6.2 Reparative macrophage infiltration was not successfully identified with MR-PET imaging in the wound healing model.....	192
6.3 Discussion.....	195
Chapter 7: General Discussion	197
7.1 Aims of PhD:	199
7.2 Genetic <i>in vivo</i> hyperactivation of ERK5 in keratinocytes drive local inflammation in wound healing.....	200
7.3 Therapeutic inactivation of ERK5 with OS1 in <i>in vitro</i> models of HaCaTs and THP-1s promotes an overall reparative phenotype	202
7.4 Therapeutic inactivation of ERK5 with OS1 in <i>in vivo</i> models of wound healing promotes a reparative phenotype	205
7.5 Conclusion	208
7.6 Future Studies	210
7.6.1 Human ex-vivo	210
7.6.2 Diabetic model.....	211
7.6.3 Imaging	212
Chapter 8: References	214

Word Count: 53,652

List of Figures

Figure 1.1. Skin Architecture.....	17
Figure 1.2. Normal wound healing	21
Figure 1.3. Macrophage phenotypes and plasticity.....	29
Figure 1.4. Healthy and Dysfunctional Macrophages.....	31
Figure 1.5. ERK5 structure	37
Figure 1.6. ERK5 signalling and localisation	38
Figure 1.7. ERK5 signalling summary.....	39
Figure 1.8. Genetic ERK5 inactivation improves wound healing in both wild type and diabetic models	44
Figure 2.1. K14CreER-ERK5KO and K14CreER-CaMEK5 Genetically Engineered Models.....	57
Figure 3.1. Genetic ERK5 modification had no effect on wound closure	68
Figure 3.2. Genetic ERK5 modification had no impact on immune infiltration by H&E	70
Figure 3.3. Genetic ERK5 modification did not significantly influence immune profile according to flow cytometry analysis	73
Figure 3.4. Method to assess changes to immune response in genetic ERK5 modification by histology	75
Figure 3.5. ERK5 was lower in ERK5KO wounds but similar in CaMEK5 wounds as determined by immunohistochemistry analysis.....	78
Figure 3.6. Neutrophils were more abundant in both ERK5KO and CaMEK5 wounds as determined by immunohistochemistry analysis.....	80
Figure 3.7. Macrophage presence is unchanged in both ERK5KO and CaMEK5 wounds as determined by immunohistochemistry analysis	82
Figure 3.8. iNOS expression decreased in ERK5KO but persisted in CaMEK5 wounds as determined by immunohistochemistry analysis.....	85
Figure 3.9. Arg1 expression remained unchanged in both ERK5KO and CaMEK5 wounds as determined by immunohistochemistry analysis	88
Figure 3.10. Collagen deposition decreased in ERK5KO and CaMEK5 wounds as determined by immunohistochemistry analysis.....	91
Figure 3.11. Summary wound healing profile of ERK5 modification.....	96
Figure 4.1. OS1 targets and degrades ERK5 in HaCaTs	106
Figure 4.2. OS1 targets and degrades ERK5 in HaCaTs, not affecting potential known off-targets of ERK5 inhibitors: ERK1/2 and BRD4	109
Figure 4.3. OS1 degradation of ERK5 has no effect on HaCaT proliferation and migration.....	112
Figure 4.4. ERK5 inactivation by OS1 promotes gene expression of inflammatory targets	115
Figure 4.5. ERK5 inactivation by OS1 promotes gene expression of reparative targets	117

Figure 4.6. THP-1 macrophage model.....	120
Figure 4.7. Immunofluorescent expression of phalloidin and CD68 in THP-1 macrophages	122
Figure 4.8. Gene expression profile of THP-1 cells.....	125
Figure 4.9. OS1 targets and degrades ERK5 in THP-1s and did not affect proliferation	127
Figure 4.10. OS1 treatment in THP-1s did not affect morphology.....	129
Figure 4.11. OS1 treatment in M0, M1 and M2 THP-1 macrophages degrades ERK5	131
Figure 4.12. Increased expression of ERK5 in M1/M2 THP-1 macrophages which decreased after OS1 treatment	133
Figure 4.13. OS1 decreased expression of ERK5 which was sequestered into the cytoplasm of THP-1 macrophages	135
Figure 4.14. OS1 had limited effect on phalloidin expression in THP-1 macrophages.....	137
Figure 4.15. OS1 had no effect on TSPO expression in THP-1 macrophages within 24h	139
Figure 4.16. OS1 had no effect on TSPO expression in THP-1 macrophages over 72h	140
Figure 4.17. OS1 had no effect on MR expression in THP-1 macrophages.....	142
Figure 4.18. OS1 had no effect on CD163 expression in THP-1 macrophages.....	144
Figure 4.19. ERK5 inactivation with OS1 caused transient increase on the mRNA expression of a range of repair mediated cytokines	147
Figure 4.20. OS1 targets and degrades ERK5 in THP-1s more effectively than CCR2 specific variants	156
Figure 5.1. Topical OS1 mediated ERK5 inactivation increased wound closure rate	161
Figure 5.2. FACS analysis showed that OS1 mediated ERK5 inactivation increased monocyte, macrophage and neutrophil proportions	165
Figure 5.3. Method to assess changes to immune response in OS1 treated wound healing by histology	166
Figure 5.4. ERK5 expression decreased in OS1 treated wounds as determined by immunohistochemistry analysis.....	168
Figure 5.5. Fewer neutrophils were observed in OS1 treated wounds as determined by immunohistochemistry analysis.....	170
Figure 5.6. Macrophage levels increased in OS1 treated wounds as determined by immunohistochemistry analysis.....	172
Figure 5.7. iNOS expression remains unchanged in OS1 treated wounds by immunohistochemistry analysis.....	174
Figure 5.8. Arg1 expression increased in OS1 treated wounds by immunohistochemistry analysis..	176
Figure 5.9. Collagen deposition remain unchanged in OS1 treated wounds by immunohistochemistry analysis.....	179
Figure 5.10. ERK5 inactivation by OS1 has limited effects on gene expression of inflammatory and reparative targets.....	184

Figure 6.1. Development of TSPO and MR PET imaging technology for wound macrophage investigation..... 194

Figure 7.1. ERK5 inactivation drives reparative activity in wound healing 197

List of Tables

Table 2.1. Experimental <i>in vitro</i> Seeding Density	49
Table 2.2. Western Blot Reagents.....	51
Table 2.3. SDS-PAGE Running Gel Composition	52
Table 2.4. RT-qPCR Programme Protocol	55
Table 2.5. Genotyping Primer Sequences and PCR Protocol	58
Table 2.6. List of Antibodies	63
Table 2.7. List of RT-qPCR targets	64

List of Abbreviations

AMP	Antimicrobial peptides
Arg1	Type-I arginase
AX	AX15836
BCA	Bicinchoninic acid
BRD4	Bromodomain protein 4
CaMEK5	Constitutive active (ca) mutant MEK5 K14CreER model
CCL2	C-C Motif Chemokine Ligand 2
COX2	Cyclooxygenase-2
CreER	Mutated estrogen receptor fused with Cre
CT	Computed tomography
DAMPs	Damage associated molecular patterns
Db	Diabetic
DTR	Diphtheria toxin receptor
E-Cad	E-cadherin
ECM	Extracellular matrix
EGR2	Early growth response 2
EMT	Epithelial-to-Mesenchymal
ERK	Extracellular signal regulated kinases
ERK5	Extracellular signal regulated kinase 5
ERK5KO	K14CreER;ERK5 knock-out model
FACS	Fluorescence-activated cell sorting
FGF	Fibroblast growth factor
FPR2	Formyl peptide receptor
G-CSF	Granulocyte colony stimulating factor
GM-CSF	Granulocyte macrophage colony stimulating factor
H&E	Haematoxylin and eosin
IF	Immunofluorescence
IFN- γ	Interferon gamma
IGF-1	Insulin growth factor 1
IHC	Immunohistochemistry
IL	Interleukin
iNOS	Inducible nitrous oxide synthase
JNK	c-Jun N-terminal protein kinases
K14	Keratin 14
LPS	Lipopolysaccharides
MAPK	Mitogen-activated protein kinases
MEF2	Myocyte enhancer-binding factor 2
MEK5	MAPK/ERK5 kinase
MMP	Matrix metalloprotease
MR	Macrophage mannose receptor
MRI	Magnetic resonance imaging
MTT	3-(4,5-dimethylthiazol-2-yl)-2,5-diphenyltetrazolium bromide
N-Cad	N-cadherin
NF- κ B	Nuclear factor- κ B

NLRP	Nod-like receptor protein
NLS	Nuclear localisation signal
NP	Nanoparticles
PAMPs	Pathogen associated molecular patterns
PDGF	Platelet-derived growth factor
PET	Positron emission tomography
pha	Phalloidin
PMA	Phorbol 12-myristate-13-acetate
PR	Proline-rich
PSR	Picosirius red
RIPA	Radioimmunoprecipitation
ROI	Regions of Interest
ROS	Reactive oxygen species
RT-qPCR	Real time quantitative polymerase chain reaction
SDS-PAGE	SDS-polyacrylamide gel electrophoresis
SERS	Surface-enhanced Raman spectroscopy
shERK5	Short hairpin (sh) RNA ERK5 lentiviral transfected HaCaTs
SRB	Sulforhodamine B
SUV	Standard uptake value
TAD	Transactivating domain
TGF- β	Transforming growth factor beta
TIMPs	Tissue inhibitors of metalloproteinases
TLR	Toll-like receptor
TNF- α	Tumour necrosis factor alpha
TSPO	Translocator protein
VCAM-1	Vascular cell adhesion protein 1
VEGF	Vascular endothelial growth factor
WT	Wild type

Abstract

Over 150 million individuals worldwide are affected by impaired wound healing, which can lead to chronic wound pathologies that often require lower limb amputations. Impaired wound healing is particularly prevalent in two growing demographics: aged and diabetic populations. Impaired wound healing continues to persist due to a lack of viable treatment options, exacerbated by an incomplete understanding of the mechanisms of wound healing. Research in this area has highlighted a significant role of dysregulated immune cells in impaired wound healing. We aimed to investigate the role of a key immune cell in wound healing: macrophages and how a known regulator of macrophages in other contexts, ERK5, influences wound healing, using genetic and therapeutic manipulations targeted at ERK5, both *in vitro* and *in vivo*.

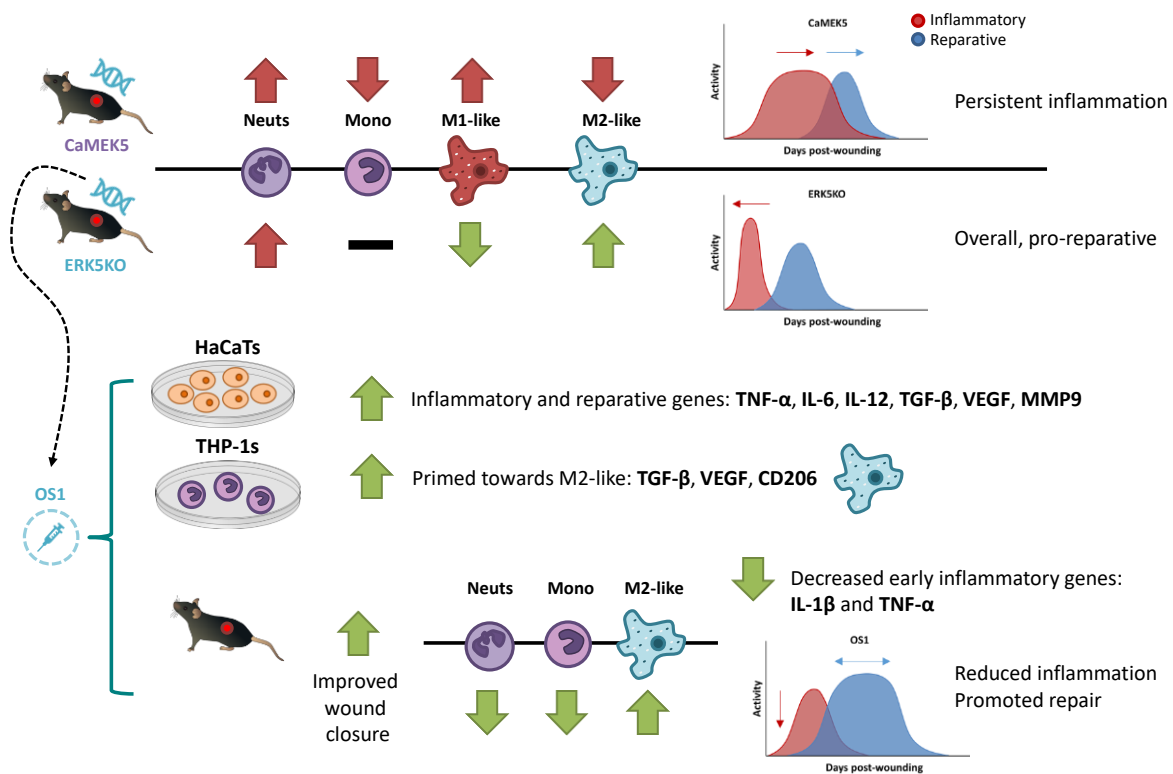
Genetic *in vivo* hyperactivation of ERK5 causes a persistent inflammatory profile in wounds, which aligned with similar observations of aberrant ERK5 signalling contributing to inflammation driven cancer progression. In contrast, genetic inactivation caused a brief increase in inflammation followed by an earlier shift to the resolution phase of wound healing as confirmed by flow cytometry and histology.

This increase in reparative wound signalling in response to targeting ERK5 was also observed in human systems, using an *in vitro* keratinocyte model treated with a novel compound that targets and degrades ERK5, called OS1. Furthermore, using OS1 we were able to prime M0 THP-1 macrophages towards a reparative M2-like phenotype. This OS1-mediated pro-healing wound phenotype was recapitulated *in vivo*, where topical treatment with OS1 (inducing ERK5 loss in the entire wound) increased the rate of wound closure and was associated with an influx of M2-like macrophages and an earlier switch to the resolution phase of wound healing.

This work is the first ever evaluation of the *in vivo* role of ERK5 in wound healing. We discovered that ERK5 signalling drives macrophage polarisation and immune infiltration during wound healing. The findings have the potential to improve diagnosis, stratification and treatment of chronic wounds. This study also provides evidence of the need to deviate from the traditional approach to target ERK5 via kinase inhibitors, since OS1-mediated degradation of ERK5, unlike ERK5 kinase inhibitors, was able to recapitulate the immune phenotypes of ERK5 genetic ablation models.

Overall, this work highlights the potential for OS1 to be used to treat patients with impaired wound healing, such as those associated with diabetes.

Graphical Abstract



Genetic hyperactivation of ERK5 in keratinocytes drives persistent inflammation in wound healing. Conversely, genetic inactivation of ERK5 in keratinocytes induces an initial increase and earlier shift of inflammation, followed by earlier repair activity. This ERK5-reparative phenotype was recapitulated using the novel OS1 therapeutic which targeted and degraded ERK5 *in vitro* and *in vivo* to generate an overall reparative phenotype in cutaneous wound healing.

Declaration

that no portion of the work referred to in the thesis has been submitted in support of an application for another degree or qualification of this or any other university or other institute of learning;

Copyright statement

The author of this thesis (including any appendices and/or schedules to this thesis) owns certain copyright or related rights in it (the “Copyright”) and s/he has given the University of Manchester certain rights to use such Copyright, including for administrative purposes.

Copies of this thesis, either in full or in extracts and whether in hard or electronic copy, may be made only in accordance with the Copyright, Designs and Patents Act 1988 (as amended) and regulations issued under it or, where appropriate, in accordance with licensing agreements which the University has from time to time. This page must form part of any such copies made.

The ownership of certain Copyright, patents, designs, trademarks and other intellectual property (the “Intellectual Property”) and any reproductions of copyright works in the thesis, for example graphs and tables (“Reproductions”), which may be described in this thesis, may not be owned by the author and may be owned by third parties. Such Intellectual Property and Reproductions cannot and must not be made available for use without the prior written permission of the owner(s) of the relevant Intellectual Property and/or Reproductions.

Further information on the conditions under which disclosure, publication and commercialisation of this thesis, the Copyright and any Intellectual Property and/or Reproductions described in it may take place is available in the University IP Policy (see <http://documents.manchester.ac.uk/DocuInfo.aspx?DocID=24420>), in any relevant Thesis restriction declarations deposited in the University Library, the University Library’s regulations (see <http://www.library.manchester.ac.uk/about/regulations/>) and in the University’s policy on Presentation of Theses

Acknowledgements

First, I would like to express my sincerest appreciation to my primary supervisor, Dr Katie Finegan, who gave me the opportunity to conduct a PhD and supported me throughout with advice, encouragement and enthusiasm. I would also like to convey my gratitude to my co-supervisors, Prof Kaye Williams and Dr Kim Mace for their continued experimental assistance and expertise.

I want to thank all the members of the Experimental Oncology Lab, past and present, for their daily support and welcoming a non-cancer researcher into their arms. In particular to my lab family; Lucie Reboud, Olly Smith, Tori Tessyman and Emily Whittleston.

I am grateful for the Histology facility of Peter Walker, Grace Bako and Leah Irlam, for their technical advice and support for the hundreds of paraffin blocks that had to be sectioned. I would also like to thank Peter March, Steve Marsden and Roger Meadows at the Bioimaging facility for their assistance in the thousands of images that came through from histology. Furthermore, thank you to Gareth Howell for his support in flow cytometry and meeting me countless times across the CTF Bridge. In addition, my sincerest thanks to all the BSF and WMIC staff for their support throughout my animal work, in particular Vicky, Hayley, Kleita, Duncan, Lidan and Leonie.

I would also like to express my gratitude to the University of Manchester and the MRC DTP. During my PhD, I had the great privilege of working alongside many inspiring and driven colleagues who ensure PhD programmes are successful. I would like to thank them all for the opportunity to learn so much from them: Melissa Westwood, Jeff Penney, Anna Woolams, Iqra Habib, and Abbie Roberts. And the best of luck to my successors, Jade Talbot and Ioana Emilia Mosneag, and the rest of the MRC DTP student committee.

In addition, the University of Manchester opened up wide opportunities for me to learn about the value of public engagement and teaching. I accidentally found myself consumed by this world, in the best way possible. I am incredibly grateful for the chance I had to work with you all: Jack Barton, Mike Daniels, Kirsty MacIntyre, Donna Littlewood, Laura Hemming, Tarnjit Sidhu, Dee-Ann Johnson, Gavin Humphries, Ruth Ledger and so many others.

PhD life is filled with so many peaks and troughs, and I am thankful for my friends who shared the same experience. I appreciate your time, the calls and the drinks: Kathryn Pennel, Pablo Finkel, Nathan Wong, Valentina Bart, Emily Sey, Sara McDowell, Charlie Rowlands, Alicia

Galdón, Dale Maxwell, Katie Sadler, Sarah Withers, and Lucie Reboud. Yes, Lucie you get an extra shout-out for all your additional support and friendship.

My time in Manchester cannot be described without my involvement in running and Run Wild Manchester. The people of this club showed me how enjoyable running is, and how helpful it can be to balance the trough of the PhD life. I look forward to our next run: Tom Lewis, Molly Glenister-Doyle, Naomi Phillips, Harry McDonald, Alix Tavernier, Laura Sim, Ellie Williams, James Bannister, Aileen Loftus, Ben Dockrell, Millie Pagett and Matt Kotara. In particular, Catraoine McDonnell, my Sunday Runday buddy.

Finally, I would like to thank my parents who have worked countless hard hours to ensure that my sister and I could have a comfortable life and access to education, where they could not. Thank you to my sister Zoe for always keeping me in check and for all your support. You have always been a chaotic and enthusiastic bunch.

Chapter 1: Introduction

1.1 Background

Around 2% of the global population is affected by impaired wound healing, and this places significant strain on the cost of healthcare. The estimated annual cost of addressing chronic wounds in the US was reported at over \$25 billion, and in the UK at around £3 billion. These financial estimations are modest as they do not take into consideration the wider cost on the quality of life for individuals and their families, as well as the socioeconomic cost of an unhealthy workforce (Sen *et al.*, 2009; Järbrink *et al.*, 2016; Martinengo *et al.*, 2019). Moreover, with an ageing population and a rise in diabetes and obesity, particularly in Western civilisations, these co-morbidities further complicate wound healing by altering the skin barrier structure, function and immune response. Consequently, it has been estimated that as many as 25% of diabetics will suffer from diabetic foot ulcers which often lead to lower limb amputations (Bannon *et al.*, 2013; Järbrink *et al.*, 2016).

Wound healing is a multifactorial process, where the underlying mechanism remains incompletely understood. Recent studies have highlighted that macrophages may play an increasingly significant role (Snyder *et al.*, 2016). Effective wound healing requires the coordinated effort of inflammatory macrophages to clear away opportunistic infections followed by timely transition to repair macrophages to facilitate resolution and remodelling. A potentially significant pathway in regulating macrophage behaviour includes extracellular signal regulated kinase 5 (ERK5), which is a member of the mitogen-activated protein kinases (MAPK) family. The role of this kinase pathway has been well studied in cardiac development, tumorigenesis and inflammation (Nithianandarajah-Jones *et al.*, 2012). More recently, its impact in myeloid polarisation has come to light in studies focussing on immune driven

carcinomas and metastasis (Giurisato *et al.*, 2018; Luiz *et al.*, 2020). This opens a potential insight into a parallel investigation in wound repair.

1.2 The skin and wound healing

The skin is the largest organ in vertebrates with a key role as the first line of defence against pathogens. The skin epidermal layer is primarily composed of keratinocytes. Underlying this is the two parts of the dermal layer: the cellular fibroblasts and the extracellular matrix (ECM). At the deepest hypodermic layer, the vascular network is embedded in adipose tissue and interconnected with nerve fibres (Figure 1.1.). Damage to this external barrier triggers the wound healing response (Eming, Martin and Tomic-Canic, 2014).

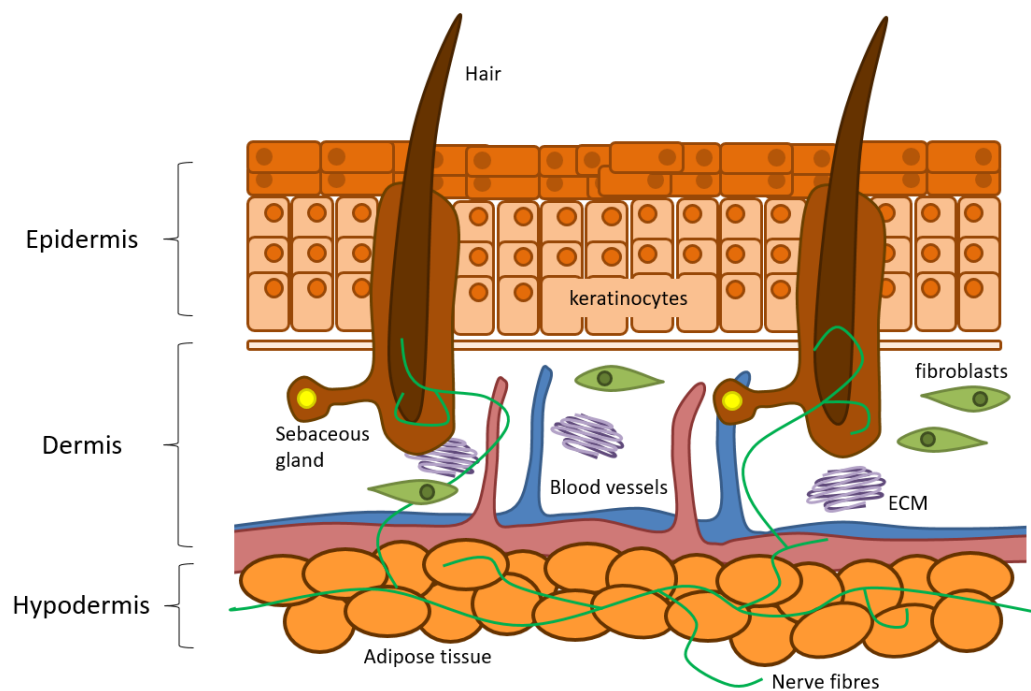


Figure 1.1. Skin Architecture. The skin is composed of three layers: epidermis, dermis and hypodermis, all of which are important in protection against pathogens, maintaining homeostasis and preventing water loss. The outermost layer, epidermis, forms a protective barrier consisting of keratinocytes. Below that is the dermis, composed of connective tissue required for structural strength and elasticity. The hypodermis links the skin to underlying bone, muscle, vasculature and nervous systems. Multiple cell types exist in this region including adipocytes, nerve cells, and fibroblasts.

Wound healing is a highly coordinated series of cellular and molecular mechanisms that are activated to re-establish structural integrity of the skin, at the cost of resultant scar formation. This is orchestrated by a complex combination of local signalling from damaged tissue, pathogenic invasion and the initiation of the inflammatory cascade by activated resident cells. This can be further amplified at a systemic level to recruit distal cells, such as neutrophils and monocytes from circulation. The process of wound healing involves three overlapping phases: inflammation, tissue formation and remodelling. Breakdown at any of these phases can lead to multiple impaired wound healing pathologies (Reinke and Sorg, 2012; Eming, Martin and Tomic-Canic, 2014). These heterogeneous conditions are becoming an increasing burden for human healthcare, with a variety of non-healing chronic ulcers as the leading concern: venous leg ulcer, arterial ulcer, diabetic foot ulcer, and pressure ulcers. These heterogeneous chronic wounds are defined as those that fail to resolve within the expected range of one to three months.

1.2.1 Inflammation, tissue formation and remodelling

The initial stages of wound healing associated inflammation involve haemostasis, a highly regulated process of coagulation, involving the sequential proteolytic activation of zymogens (precursor enzymes). Activation, adhesion, and aggregation of platelets initiate the clotting cascade to produce an insoluble fibrin clot. This provides the provisional wound matrix architecture necessary to recruit immune cells, promote proliferation and act as a reservoir for growth factors (Figure 1.2.A). In parallel, the injured blood vessel undergoes temporary vasoconstriction to reduce blood loss and promote clotting. This is followed by vasodilation and increased vascular permeability to increase blood flow and engorgement of down-stream capillary beds for immune cell recruitment (Adams and Bird, 2009; Reinke and Sorg, 2012).

In response to this rapid vascular change and exposure to damage associated molecular patterns (DAMPs), and pathogen associated molecular patterns (PAMPs), neutrophils are recruited and

transmigrate across the endothelial cell wall of the local capillaries to enter the wound. These are required for the phagocytosis of infectious agents and degradation of necrotic tissue. This involves the release of antimicrobial peptides (AMP), proteases and reactive oxygen species (ROS) (Eming, Krieg and Davidson, 2007; Kovtun *et al.*, 2018). Alongside the influx of neutrophils, circulating monocytes proliferate and are recruited in a C-C Motif Chemokine Ligand 2 (CCL2), vascular cell adhesion protein 1 (VCAM-1) and p-Selectin dependent manner into wounds where they can differentiate into activated macrophages (Koh and DiPietro, 2011; Shi and Pamer, 2011). Macrophages are essential in this inflammatory stage of wound healing to clear cell debris, senescent cells, dead tissues and apoptotic neutrophils. Macrophages are then capable of transitioning towards a reparative phenotype to support the resolution of inflammation.

This functional transition of macrophages highlights a shift towards the tissue formation phase of wound healing (Figure 1.2.B). This is crucial to conceal the exposed wound from the external environment, and is characterised by increased formation of fibrous tissue, epidermal regeneration, wound contraction, and *de novo* angiogenesis (Delavary *et al.*, 2011; Eming, Martin and Tomic-Canic, 2014). Active fibroblasts produce key materials such as collagen, elastin, proteoglycans, and fibronectins, to generate ECM. This provides the architecture to support increased cell growth and proliferation associated with this highly active tissue formation stage (Reinke and Sorg, 2012; Tracy, Minasian and Caterson, 2016). In parallel with this proliferative stage, fibroblasts drive matrix metalloprotease (MMP) activity to breakdown the provisional wound generated during the early haemostatic phase. The coordinated balance of ECM synthesis and MMP activity is required for appropriate angiogenesis, collagen deposition, and the generation of a permanent structural replacement to the initial fibrin clot (Eming, Martin and Tomic-Canic, 2014; Caley, Martins and O'Toole, 2015).

Angiogenesis must occur to re-establish the supply of oxygen and nutrients to wounded tissue. This is initiated by a variety of growth factors, including vascular endothelial growth factor (VEGF), platelet-derived growth factor (PDGF), and fibroblast growth factor (FGF) to trigger a cascade of intracellular signalling events resulting in proliferation and migration of endothelial cells into the wound in cord-like structures. These newly built sprouts elongate to form lumens which interconnect with neighbouring vessels to expand the angiogenic network. As they develop, these early vessel structures change their shape and gene expression to recruit pericytes (contractile cells along capillaries) and smooth muscle cells to stabilise the vessel wall and promote differentiation into arteries and veins (Bauer, Bauer and Velazquez, 2005; Potente, Gerhardt and Carmeliet, 2011; Reinke and Sorg, 2012).

The final phase of wound healing is remodelling, and can be a long process varying from several weeks to one year after injury (Gurtner *et al.*, 2008). This is dependent on injury severity and the health of the wounded individual. Fibroblasts migrate to the wound edge and differentiate to myofibroblasts, a contractile cell that assists with wound closure (Figure 1.2.C). The interaction between fibroblasts and myofibroblasts produces collagen which cross-links with other protein molecules to strengthen the tissue architecture at the expense of scar tissue formation (Darby *et al.*, 2014; Hesketh *et al.*, 2017). Interestingly, scar-free tissue regeneration is only observed in foetal skin. Scarring remains a natural part of adult wound healing and differs from normal tissue in its fibrous composition and elasticity. Pathological scarring only becomes problematic in some surgeries and trauma, such as burns, where the scar tissue extends beyond the margins of the original tissue damage (Eming, Martin and Tomic-Canic, 2014).

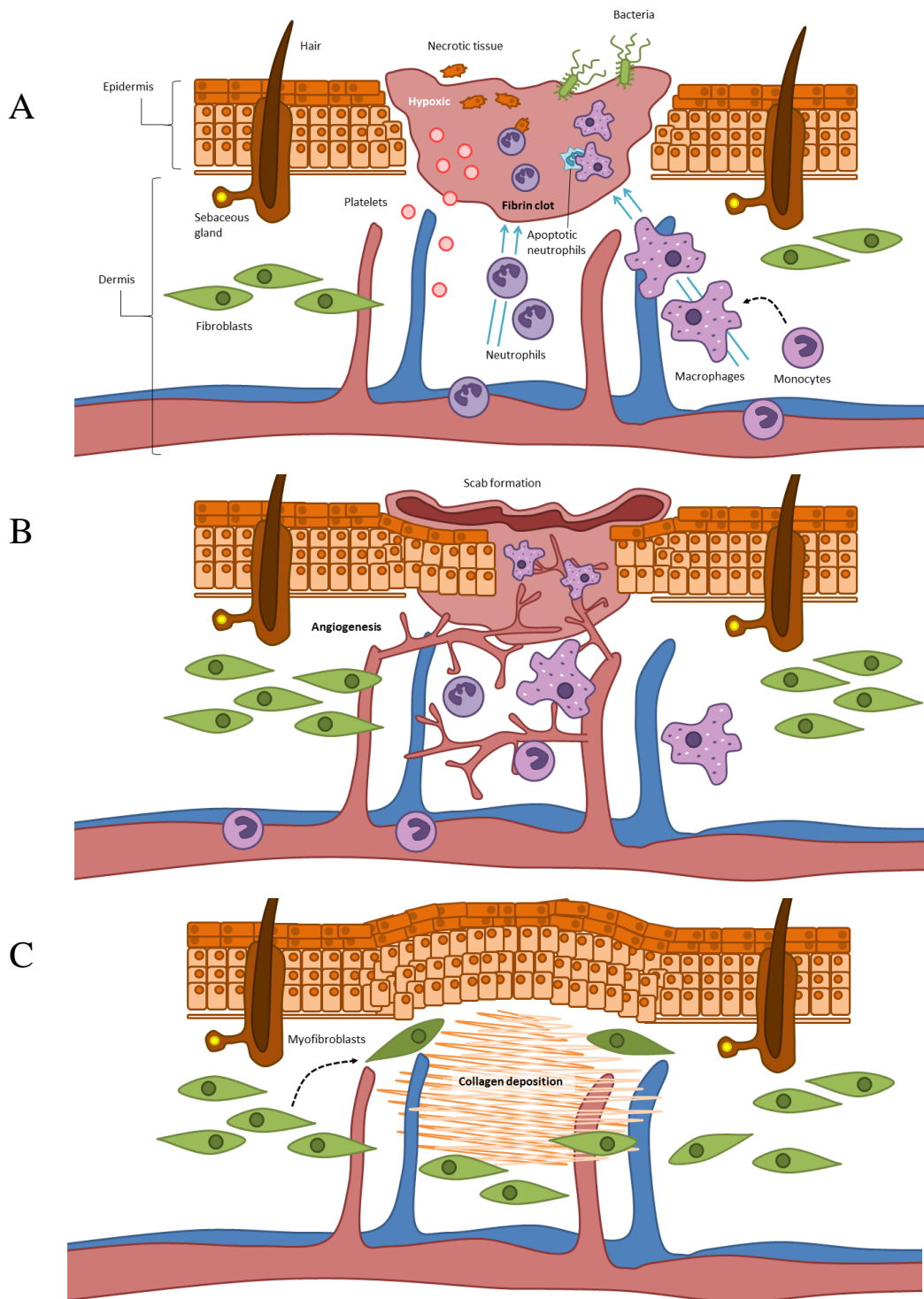


Figure 1.2. Normal wound healing. The process of wound healing involves three overlapping phases of (A) inflammation, (B) tissue formation, and (C) remodelling. (A) Early inflammation involves the clotting cascade to block the initial haemorrhage, followed by an influx of neutrophils and macrophages to clear damage. (B) This highly pro-inflammatory state transitions towards a reparative phase involving angiogenesis and fibroplasia to close the exposed wound. This proliferative tissue formation stage is dominated by fibroblasts and M2- like macrophages. (C) The final phase of wound healing is a prolonged process of remodelling. Over time, fibroblasts at the wound edge can differentiate to myofibroblasts and support collagen deposition, overall wound closure and scar tissue formation.

1.3 Macrophages in wound healing

Macrophages have been highlighted as an important cell in tissue homeostasis and immunity, as well as being implicated as a crucial driver of multiple pathologies including infection, cardiovascular disease, cancer, and obesity (Murray *et al.*, 2014). They are prominent immune cells found in all tissues, either as resident cells or monocyte-derived cells from circulation. Their role in wound healing remains incompletely understood, though studies have found they are crucial in all stages of the process. Their pleiotropic function from host defence, phagocytosis, and support of cell proliferation, resolution and scarring, show that these cells exist in several phenotypic states. Although essential for appropriate wound healing, emerging evidence discussed below show that dysfunctional macrophage behaviour is a significant factor in chronic and diabetic wounds (Delavary *et al.*, 2011; Koh and DiPietro, 2011; Louiselle *et al.*, 2021).

Immediately after injury, resident macrophages are activated by local pro-inflammatory mediators, DAMPs, and PAMPs. Additionally, wounds can often be hypoxic due to disrupted vasculature, and further contribute to activation. Activated resident macrophages subsequently produce a variety of factors to initiate the normal process of inflammation to combat infection and damage. Shortly after, bone-marrow derived monocytes are recruited to the wound bed, where they can differentiate into macrophages. This is facilitated by chemokines such as CCL2, CCL3, and CXCL2, produced by many cells including keratinocytes and macrophages themselves. This can be concurrently driven by platelet derived factors derived from broken down products from the activated complement cascade (Wetzler *et al.*, 2000; Koh and DiPietro, 2011).

Macrophages in the wound environment are required to effectively remove expended neutrophils. They do so by inducing neutrophils to undergo apoptosis, and actively targeting them for phagocytosis (Meszaros, Reichner and Albina, 2000). Failure to remove excess

neutrophil debris contributes to persistence of chemokines (CXCL2 and CCL2), and increased inflammatory mediators (IL-1 β , TNF- α , and cyclooxygenase-2 (COX2)). Additionally these unresolved neutrophils cause inflammatory damage to the wound as they are an abundant source of proteases and ROS, which contribute to breakdown of ECM and endothelial dysfunction. This has been demonstrated from macrophage depletion studies in early murine wounds which exhibit impaired healing associated with accumulation of necrotic cells, high levels of inflammatory mediators and disrupted angiogenesis (Goren *et al.*, 2009; Mirza, DiPietro and Koh, 2009).

Whilst both studies demonstrate an impaired healing profile after macrophage depletion, they were conducted using two different models, which varied in how they targeted macrophages. The macrophages were specifically depleted using a transgenic mouse model that expressed the human diphtheria toxin receptor (DTR) under the control of CD11b in the Mirza *et al* study, while they were under the control of *lysozyme M* (LysM)Cre/DTR in the Goren *et al* study. Interestingly, despite CD11b being expressed on multiple immune cell types including neutrophils, monocytes and macrophages, it has primarily been associated with adhesion and migration of macrophages. Mirza *et al*, successfully show macrophage specific depletion from skin section staining with F4/80, Ly6C and Ly6G antibodies. In their analysis, only F4/80 macrophages were significantly reduced in population after diphtheria toxin induction in the CD11b/DTR mice, whereas monocyte (Ly6C) and neutrophil (Ly6G) populations remained the same as control animals. The Goren *et al* study focussed on LysM which is an antibacterial enzyme lysozyme that is highly expressed in myeloid cells. They found that LysMCre mice induced by diphtheria toxin led to significant depletion of F4/80 macrophages by immunohistochemistry staining sections of the liver and skin. However, interestingly the Goren *et al* study was unable to alter the circulating F4/80 monocyte population from fresh bloods using this model. They argue this may be the result of reduced expression of Cre/DTR on the

cell surface of these higher turnover immature monocyte cells. And so using two similar techniques which target and ablate the myeloid lineage by CD11b or LysM, they highlight the need for macrophages to clear neutrophils, during coordinated wound healing.

Following inflammation, it has become evident that wound macrophages are necessary for the progression of the repair process. Macrophages undergo a transition to exhibit a functional phenotype more characteristic of the M2-like spectrum (further discussed in section 1.3.1). This encompasses a variety of alternatively activated macrophages that are associated with functions such as wound healing, immune regulation and tissue repair. Multiple factors drive this polarisation including tissue iron, chemokines and the successful phagocytosis of neutrophils (Krzyszczuk *et al.*, 2018; Wilkinson *et al.*, 2019). In this state they are a source of several growth factors and cytokines including interleukin (IL)-10, transforming growth factor beta (TGF- β), VEGF, PDGF and insulin growth factor 1 (IGF-1) required to promote cell proliferation, protein synthesis and angiogenesis, as well as suppressing the initial inflammatory phase of wound healing. Macrophages also produce various MMPs, including MMP-2 and MMP-9 and their respective inhibitors, tissue inhibitors of metalloproteinases (TIMPs) that can influence the angiogenic network and subsequent scar tissue by altering the ECM composition (Koh and DiPietro, 2011; Mescher, 2017).

In the latter phases of remodelling, macrophages coordinate with fibroblasts to balance ECM synthesis and MMP-mediated tissue breakdown. This re-establishes an intact epidermis over the exposed wound and promotes scar tissue formation. Accordingly, studies depleting these macrophages at later phases show reduced scar formation, suggesting they are critical driver of pathological fibrosis and scarring (Mirza, DiPietro and Koh, 2009; Brancato and Albina, 2011; Hesketh *et al.*, 2017).

As previously mentioned, the Mirza, *et al* study induced depletion of macrophages under the control of the CD11b promoter. Their studies found that diphtheria toxin induced depletion of macrophages led to reduced granulation tissue and collagen deposition from day 7 post-wounding. Moreover, the macrophage ablation impaired levels of angiogenesis as indicated by reduced CD31 labelling. However, to build on the notion of spatiotemporal influences of macrophages, Lucas *et al*, designed a study to deplete macrophages at differential stages of wound healing, namely as pre-treatment (inflammatory stage), from day 3 onwards (tissue formation stage) and day 8 onwards (remodelling stage). Macrophages were depleted as previously described using the LysMCre/DTR model. They reiterated previous findings that early recruited macrophages were crucial in maintaining healthy granulation, vascularisation and myofibroblast differentiation. Additionally they found that early depletion of macrophages inhibits functional transition of M2-like macrophages, based on the decreased marker expression of Fizz1 and Ym1. Their novel findings of depleting macrophages during the tissue formation stage revealed impaired granulation, haemorrhaging and increased fibrinogen staining. These combination of factors contributed to impairing the epithelium from closing (Lucas *et al.*, 2010). To further support this, they found reduced levels of TGF- β and VEGF, which are known important mediators produced by M2-like macrophages in driving healthy wound closure.

Focussing on scar formation and tissue expansion, other studies have alternatively depleted macrophages with clodronate liposomes. These are actively endocytosed by macrophages to an excess and the accumulation of hydrophilic clodronate initiates apoptosis. Using this system, Zhu *et al*, found that macrophage depletion in a skin graft model led to reduced scar formation and improved collagen remodelling. They found this correlated with reduced myofibroblast differentiation, decreased pro-fibrotic factors including TGF- β and α -SMA. Although these are factors normally required for healthy wound healing, they are found in excess during

hypertrophic scarring, as observed in their control animals (Zhu *et al.*, 2016). Using this clodronate liposome model, depletion of macrophages similarly resulted in reduced vascularisation and reduction of pro-fibrotic factors: TGF- β , VEGF, EGF and FGF (Ding *et al.*, 2019).

These various studies outline that recruited macrophages are significant in controlling ECM composition and thus control the degree of scar formation. In particular, the Lucas *et al* study highlights that selective temporal modulation of macrophages must be taken into consideration for therapeutic strategy (Lucas *et al.*, 2010). In addition, it should be noted that the majority of these macrophage depletion studies occur in murine skin repair, and may in fact differ from the human system. Moreover, these macrophage depletion models indeterminately remove all macrophages including both M1-like and M2-like macrophages. Thus, they were not able to distinguish whether specific functional macrophage phenotypes may have more of an impact on the various stages of wound healing.

1.3.1 Functional phenotypes of macrophages - M1/M2 axis

The pleiotropic functions associated with wound macrophages show they are a heterogeneous population of cells throughout the dynamic timeline of wound healing. Macrophages have classically been described to differentiate into activated M1-like macrophages upon stimulation of pro-inflammatory factors such as interferon gamma (IFN γ) and lipopolysaccharides (LPS). In this phenotypic state they abundantly produce IL-1, IL-6, IL-12, tumour necrosis factor alpha (TNF- α) and inducible nitrous oxide synthase (iNOS), which are all important to scavenge debris and for host defence (Delavary *et al.*, 2011).

Alternatively activated M2-like macrophages are also observed in the wound bed, and are stimulated by IL-4 and IL-13 (Gordon, 2003). M2-like macrophages have been implicated in resolving inflammation and play an important role in supporting wound healing, angiogenesis,

and scar formation through signalling pathways involving IL-10, TGF- β and VEGF (Snyder *et al.*, 2016; Hesketh *et al.*, 2017). Recently, the M2-like cells have been further subdivided as M2a, M2b and M2c, with differing functions associated with type 2 immunity (Th2), immune regulation, and wound healing (Martinez and Gordon, 2014; Roszer, 2015). M2a macrophages are attributed to their similarity to Th2 responses to extracellular parasites and allergic reactions. They are characterised by their production of polyamines, IL-10 and TGF- β . M2b macrophages are associated with Th2 activation, immune regulation and expression of IL-10, TNF, IL-1 and IL-6. Finally M2c are functionally associated with immunosuppression and wound healing. They are recognised by their expression of IL-10, TGF- β and various wound healing mediators such as VEGF and MMPs.

Current simplified models to functionally delineate macrophages into discrete inflammatory M1 and reparative M2 phenotypes are outdated (Figure 1.3.A). Several attempts have been made to specifically identify M1-like macrophages by their expression of CD38, formyl peptide receptor (FPR2), and translocator protein (TSPO), compared to M2-like macrophage expression of early growth response 2 (EGR2), c-Myc, Arg1 and macrophage mannose receptor (MR) (Martinez *et al.*, 2006; Jablonski *et al.*, 2015; Roszer, 2015; Narayan *et al.*, 2017). However, macrophages do not exist in a dichotomous state *in vivo*. Macrophage development and activation is influenced by diverse and complex signals. This is dependent on the timing, the location, and the strength of microenvironmental signals in conjunction with the epigenetic landscape of macrophages.

These epigenetic changes typically include post-translational modification of histones, chromatin proteins and methylation of CpG DNA motifs. These changes to the epigenetic landscape alter the accessibility to encode information on the DNA and thus the binding to key transcription factors including NF- κ B and STATs. Some of the previously mentioned cytokine and growth factor mediators, have been associated with inducing epigenetic changes that can

influence macrophage polarisation. Additionally, the epigenetic landscape of developing monocytes and macrophages may be primed in such a way to limit their pattern of gene expression and functional outcome (Ivashkiv, 2013).

What may be more realistic is that, a spectrum of macrophage phenotypes exists along the M1/M2 axis (Figure 1.3.B). Moreover, macrophages are inherently plastic, and their function can change based on spatiotemporal cues (Mosser and Edwards, 2008; Ginhoux *et al.*, 2016; Smith *et al.*, 2017). One transcriptomic based study stimulated human derived macrophages with 28 different stimuli and generated 9 clusters of macrophage phenotypes (Xue *et al.*, 2014). Moreover, it has been well-established that tissue resident macrophages are functionally and spatially different. A study by Lavin *et al.*, reiterates this by showing macrophages from different tissues exhibit unique transcriptional and epigenetic patterns from over 12,000 macrophage specific enhancers (Lavin *et al.*, 2014).

This suggests that at any single time point, the wound may contain a continuum of macrophage phenotypes including spectral hybrids. For example, populations of wound macrophages have been observed to exhibit M2 associated MR and produce inflammatory cytokines TNF- α and IL-6 (Daley *et al.*, 2010; Koh and DiPietro, 2011). What requires further investigation is the functional difference of macrophage populations during the wound healing phases and the factors that influence its dysregulation in a diseased context.

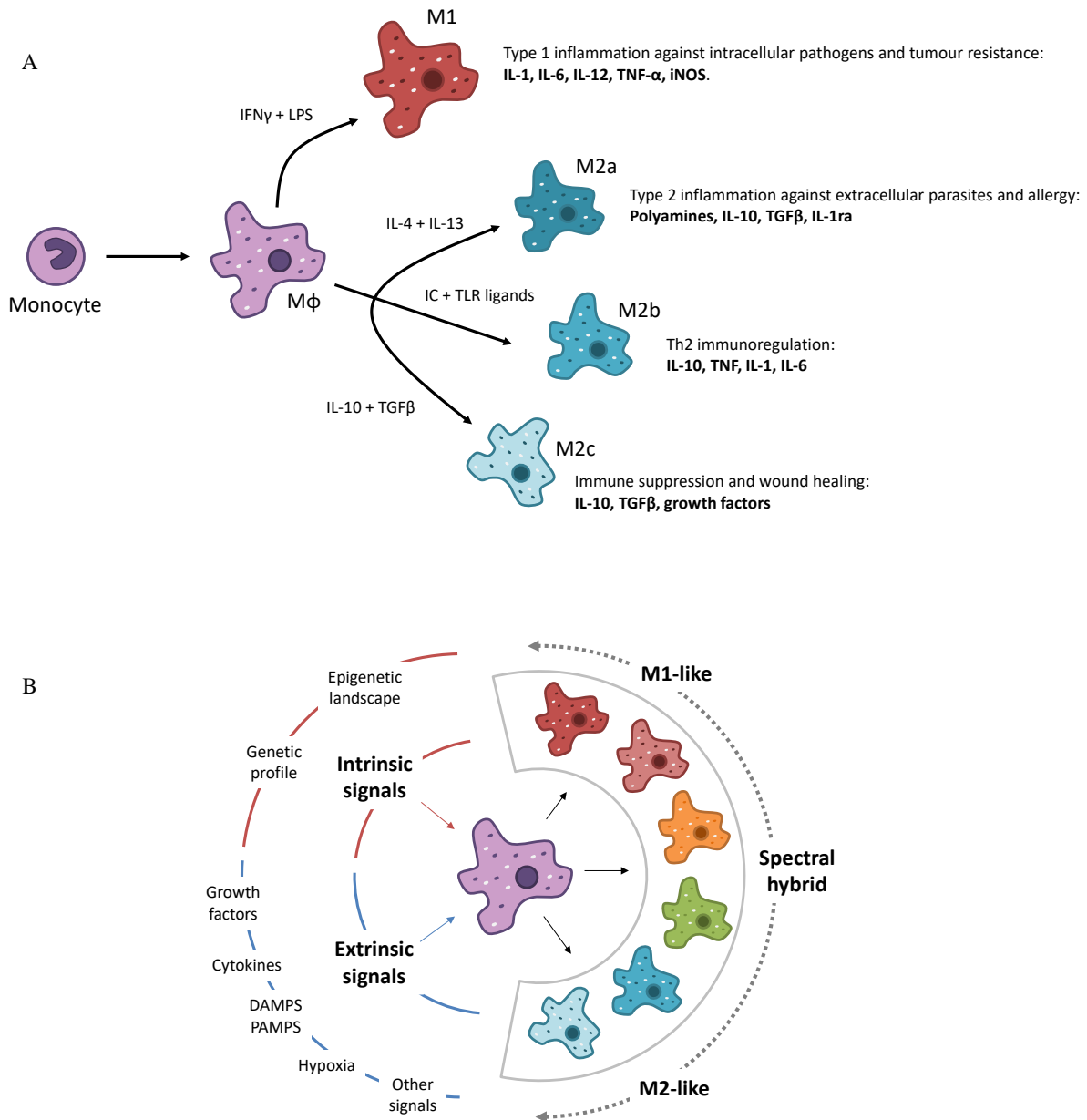


Figure 1.3. Macrophage phenotypes and plasticity. Macrophages play a pivotal role in all phases of the wound healing process, and are dependent on its ability to transition between functionally distinct phenotypes. (A) Historically speaking, macrophages have been categorised by a dichotomy of activation states between M1 and M2. The classical M1 activation reflects the Th1-mediated immunity against intracellular pathogens. The alternative M2 activation has recently been further subdivided to M2a, M2b, and M2c, to distinguish between its different functional activities. These revolve around its role in Th2-mediated immunity against parasitic infections and fungi, immunoregulation, immune suppression and wound healing. (B) However, recent research on macrophages show that this outdated model was in much need of revision. Macrophages are in fact highly plastic and dynamic cells that respond to extrinsic and intrinsic signals in a spatiotemporal-dependent manner to exhibit a spectrum of phenotypes across the M1/M2 axis. Moreover, these differentiated states are not fixed, and can interchange in the context of the microenvironment.

1.4 Impaired wound healing

As previously mentioned, breakdown at any stage of the wound healing process: inflammation, tissue formation or remodelling, leads to chronic wound pathologies. The molecular mechanisms underlying these conditions remain unclear, but several theories have been put forward, including a non-resolving and persistent inflammation. Chronic wounds have been observed with excessive neutrophil infiltration. This coincided with over-production of ROS, neutrophil elastase and MMPs which contribute to ECM damage and degradation of growth factors. Additionally, this can drive transcriptional activation to increase levels of inflammatory cytokines such as IL-1 β , IL-6 and TNF- α (Eming, Krieg and Davidson, 2007; Zhao *et al.*, 2016).

In a systemic review of patient biomarkers in wound healing, various key factors that contribute to inflammation were found. Wound fluid biomarkers in the form of increased levels of MMPs, IL-1, IL-6 and TNF- α was found to be present in non-healing patients (Lindley *et al.*, 2016). Additionally, they found that chronic wounds often were observed with a higher burden of microbial biofilms derived from infections associated with *Staphylococcus* and *Pseudomonas*. Persistent microbial infections can further delay and impair wound healing by inducing a prolonged inflammatory state and sustain recruitment of immune cells.

This overtly inflamed microenvironment results in hypoxia, tissue damage, and blocks the progression of normal wound healing. A combination of existing metabolic disorders such as arterial ulcers and dysregulated vasculature can result in hypoxic conditions in local tissue of wounds and perpetuate an inflammatory cascade. Typically this is driven by DAMP signalling to recruit neutrophils and macrophages, alongside the increased expression of endothelial adhesion molecules in hypoxic tissue (Zhao *et al.*, 2016).

In recent decades it has become increasingly apparent that this failure to progress healing coincides with macrophages unable to effectively make a functional switch and remaining in a pro-inflammatory state (Figure 1.4). Several studies have demonstrated that impaired macrophage populations result in delayed wound healing, re-epithelisation and angiogenesis (Khanna *et al.*, 2010; Delavary *et al.*, 2011; Minutti *et al.*, 2017).

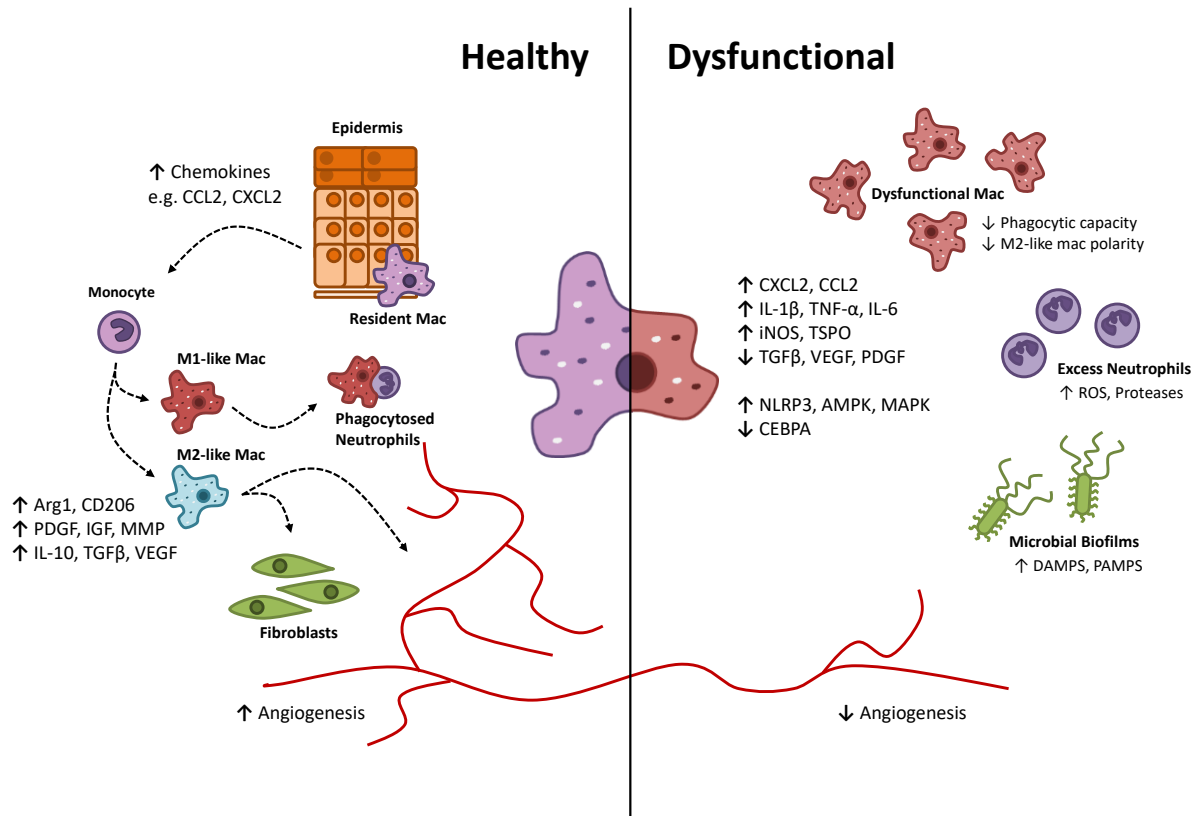


Figure 1.4. Healthy and Dysfunctional Macrophages. In homeostatic conditions, there is cross-talk between the epidermis and residential macrophages to appropriately respond to wounding as the first line of defence and recruit circulating monocytes and neutrophils with chemokines. Upon arrival, these monocytes respond to the local inflammatory environment and polarise towards M1-like macrophages to promote inflammation and phagocytose spent neutrophils. This activity acts as a transition point to facilitate a shift towards repair mechanisms. This regulatory environment promotes the recruitment and polarisation of M2-like macrophages which play a crucial role in signalling immune regulation, repair, and remodelling. However, this coordinated balance can be disrupted in dysfunctional macrophages associated with diabetic and chronic wounds. These macrophages exhibit a persistent inflammatory profile with a reduced phagocytic capacity. This permits neutrophils and microbes to accumulate, accelerating an pathological inflammatory environment. Taken all together, this can create a toxic and damaging microenvironment that prevents transition to repair.

This chronic inflammatory state of macrophages has also been observed in diabetics. This is a condition characterised by chronic hyperglycaemia due to the loss of function of pancreatic beta cells resulting in an inability to produce or use insulin (World Health Organization, 2016). Type 1 diabetes is an autoimmune condition where the immune system inappropriately targets pancreatic beta cells for destruction, rendering them unable to produce effective insulin. This accounts for around 10% of diabetics, and multiple polymorphisms have been identified related to autoreactive islet B-cells or T-cells which have escaped immune tolerance. Type 2 diabetes accounts for the other 90%, and are characterised by insulin resistance associated with aging, obesity and inactive lifestyles. Insulin resistance is when cells are unable to respond adequately to the normal levels of insulin and inappropriately release glucose into the blood. Increased fat build up requires increased activity to breakdown lipids in fat cells, leading to metabolic imbalance and subsequent insulin resistance. Additionally, the presence of excess abdominal fat built up can act as a chronic trigger that drives mitochondrial stress and elevated levels of TNF- α and IL-6 which can hinder beta cell function (Saini, 2010).

Abnormal patterns of macrophage activation have been demonstrated in animal models and diabetes patients. This has been highlighted by persistently high M1-associated markers including NOS2, TNF- α , IL-1 β and MMP9 in late diabetic murine wounds compared to the upregulated M2-associated expression of Arg1 and mannose receptor (MR; and also known as CD206) in non-diabetic wounds (Mirza and Koh, 2011; Bannon *et al.*, 2013). Moreover, studies tracking the sources of these persistently inflamed diabetic macrophages have found them to be primarily bone-marrow derived macrophages (Mace *et al.*, 2009; Wicks, Torbica and Mace, 2014)

Diabetic murine macrophages have also been shown to exhibit increased Toll-like receptor (TLR)4 and nod-like receptor protein (NLRP)-3 inflammasome expression due to altered chromatin patterns, before localising to the wound. In a study by Wicks *et al*, they discovered

reduced acetylation of *Cebpa* in diabetic macrophages. *Cebpa* is a master regulator of myeloid cell differentiation, and its deficiency from the diabetic environment inhibits proper maturation of monocytes and leaves them prone to a pro-inflammatory state (Wicks *et al.*, 2015). These epigenetic changes were triggered by soluble factors present in the diabetic wound environment and may occur early in the bone marrow stem niches to prime them towards an inflammatory phenotype to drive IL-1 β secretion (Wicks, Torbica and Mace, 2014). In the study by Mirza *et al.*, they observed that macrophages isolated from both obese and diabetic human subjects and diabetic murine models exhibited increased levels of NLRP3 inflammasome, caspase-1, IL-1 β and IL-18. Moreover, they found that treating both human and murine bone marrow derived macrophages with diabetic conditioned media led to this similar profile of activated inflammasome and release of IL-1 β and IL-18 (Mirza *et al.*, 2014).

Studies have also revealed that the inflammatory and hyperglycaemic wound environment of diabetics may in fact inhibit M2 polarisation, resulting in an ineffective and mixed macrophage phenotype. This may be in part due to phagocytic defects and altered glucose metabolism associated with diabetic macrophages. This was investigated by Khanna *et al.*, where they found that macrophages isolated from two different *in vivo* models of diabetes had significantly impaired phagocytic capacity and an abundant presence of apoptotic neutrophils in the wound site. Furthermore, the study found increased levels of pro-inflammatory mediators, TNF- α and IL-6, and reduced levels of IL-10. They were able to specifically identify this from the isolated diabetic macrophages, to further support their link between chronic inflammation and metabolic disorder (Khanna *et al.*, 2010). In another study by Ayala *et al.*, they discovered that the hyperglycaemic environment modifies bone marrow-derived macrophage metabolism. Diabetic macrophages had increased levels of phosphorylated AMPK, (AMP-activated protein kinase) a metabolic energy sensor, increased phosphorylated MAPK proteins (SAPK/JNK, stress-activated proteins kinases/Jun amino-terminal kinases; and ERK2) and decreased

expression of TLR4. This altered metabolic and signalling pathway contributed to their inhibited phagocytic capacity (Ayala *et al.*, 2019).

This reduced phagocytosis and capacity to degrade apoptotic cells such as spent neutrophils can also inhibit the production of TGF- β that is typically produced during this macrophage phenotype transition. The loss of this key immune regulatory mediator contributes to the uncontrolled expression of inflammatory mediators in the microenvironment. The combination of aberrant macrophage recruitment and inability for them to transition to reparative phenotypes exacerbates damage in diabetic wounds, in the form of increased necrotic material, uncontrolled inflammatory destruction and inability to transition to the healing phase. It remains unclear, but likely that a combination of these extrinsic factors of the inflammatory diabetic wound and predetermined intrinsic programs in macrophages that lead to an inability to functionally switch from an M1-like to M2-like phenotype (Khanna *et al.*, 2010; Mirza and Koh, 2011).

1.4.1 Current landscape of treatments for impaired wound healing

As previously mentioned, chronic wound pathologies are heterogenous in their causes, development and clinical characteristics. Some of the most common conditions include: venous leg ulcers, arterial ulcers and diabetic foot ulcers. These three are primarily associated with lower leg extremities, persistent inflammation, reduced blood flow and commonly observed in the elderly and diabetics (Eming, Martin and Tomic-Canic, 2014). A thorough patient history assessment is necessary to ensure as full an understanding is possible to the comorbidities and contributing factors that will guide the treatment options.

Current topical wound therapies and dressings have been developed that physically protect the wound site and promote the healing process. Some use hydrocolloids and hydrogels to remove exudate but maintain moisture. Others incorporate collagen products which facilitate a

microenvironment that is favourable at attracting wound healing associated cells and limit protease activity (Cullen *et al.*, 2002). Some developments have focussed on the addition of antimicrobial compounds such as silver which can limit the spread of opportunistic infections (Han and Ceilley, 2017).

More advanced developments have been made which incorporate recombinant growth factors that are typically hampered in chronic wounds. These ensure geographical induction, protection and additional biological complexity to promote healing. Growth factors such as PDGF and FGF have been shown to effectively stimulate the healing process in trials with patients with diabetic foot ulcers and pressure ulcers. However, many of these are partially limited to certain subsets of patients (Mowbray *et al.*, 2008; Han and Ceilley, 2017).

Only a few of these advanced biologics have been approved with Regranex (recombinant PDGF) being a lone drug success. In a wide, randomised, placebo controlled study, they found Regranex to be successful in improving incidence of healing when compared to the standardised regime of ulcer care. Only one out of the four studies showed no significant difference (Wieman, 1998). This may be in part due to the heterogeneous and diverse pool of chronic wound patients. In a study by Chan *et al.*, they used topical application of Regranex on wounds of diabetic mice and this was observed to increase the amount of granulation tissue (Chan *et al.*, 2006). Recently, this drug has primarily been used in conjunction with other wound care therapies for diabetic neuropathic ulcers (Fang and Galiano, 2008).

Topically applied recombinant granulocyte macrophage colony stimulating factor (GM-CSF) and granulocyte colony stimulating factor (G-CSF) have been successfully trialled in those with venous leg ulcers and diabetic foot ulcers (Marques da Costa *et al.*, 1999). Moreover, *in vivo* knockout models reveal that loss of GM-CSF delays wound healing, reduces vascularisation and decreases the expression of IL-6, CXCL2 and CCL2 (Fang *et al.*, 2007).

This remains one of the few immune-targeted therapies in wound healing, but the activity of GM-CSF to promote wound healing may in fact derive from the promotion of repair mechanism such as increased ECM components and associated growth factors, such as TGF- β . Despite persistent inflammation being such a crucial factor in chronic wound healing, it remains elusive as a successful therapeutic target.

The diversity of patients and the wound pathologies also needs to be considered, as their remains a need for a system to stratify patients. This will require a robust methodology to identify a subset or even individual patients by single or multiple biomarker signatures. As previously mentioned in the systematic review by Lindley *et al*, this remains an open field. A range of potential biomarkers have been previously suggested such as β -catenin, microbial biofilms, MMPs and inflammatory cytokines, IL-6 and TNF- α . These can be identified from wound fluids, swabs, and tissue specimens in attempts to delineate between non-healing and healing phenotypes. However, our current diagnostic and prognostic tools in the form of protein identification, cell culture, RT-qPCR and histopathology are currently unable to objectively stratify these patient subsets with confidence. Nonetheless, there are major advances in various “omics” and imaging technology that will help progress this goal of patient-specific treatment plans (Eming, Martin and Tomic-Canic, 2014).

1.5 ERK signalling – a novel therapeutic target for wound healing

A potentially interesting pathway in regulating macrophages in wound healing includes ERK5, which is a member of the MAPK family. Key studies by Giurisato *et al* and Luiz *et al*, have demonstrated that genetic inactivation of ERK5 in the myeloid lineage shifted their phenotypic state towards an anti-tumour and M1-like phenotype. They report that ERK5 mediated signalling can activate STAT3 and c-Myc transcription signalling to modify macrophage polarisation (Gjurisato, Vermi and Tournier, 2016; Luiz *et al.*, 2020).

Other members of this family include extracellular signal regulated kinases (ERK) 1 and 2, c-Jun N-terminal protein kinases (JNK) and the p38 MAPK. ERK5 is the largest of these MAPK with a molecular weight of 115kDa (Figure 1.5). The N-terminal region contains a kinase domain with binding sites to its upstream activator, MAPK/ERK5 kinase (MEK5). ERK5 differs from its family due to its uniquely large C-terminal tail containing two proline-rich (PR) domains, a myocyte enhancer-binding factor 2 (MEF2) domain, a nuclear localisation signal (NLS) and a transactivating domain (TAD) (Nithianandarajah-Jones *et al.*, 2012; Stecca and Rovida, 2019).

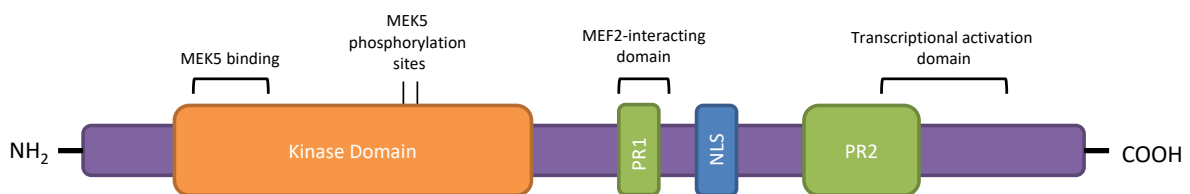


Figure 1.5. ERK5 structure. On the N-terminus of the ERK5, there is a kinase domain with specific binding regions for MEK5, including two amino acid residues for phosphorylation, threonine and tyrosine. The C-terminus is uniquely larger than its MAPK family, and contains two proline rich domains, MEF2-interacting domain, nuclear localisation signal domain and transactivating domain.

Under basal conditions, ERK5 remains in a closed folded conformational state where the N- and C- terminal halves are bound to one another. Due to the reduced NLS activity, ERK5 tends to be localised in the cytoplasm in this conformation. Upon stimulation, MEK5 phosphorylates specific threonine and tyrosine on the kinase domain of the N-terminus of ERK5 and induces a conformational change to an open state (Figure 1.6). This exposes the NLS, to promote localisation into the nucleus to facilitate ERK5 associated transcriptional activity. An additionally unique element of ERK5 is its capacity to autophosphorylate in the C-terminus region, permitting direct regulation of gene transcription (Nithianandarajah-Jones *et al.*, 2012; Pearson *et al.*, 2020).

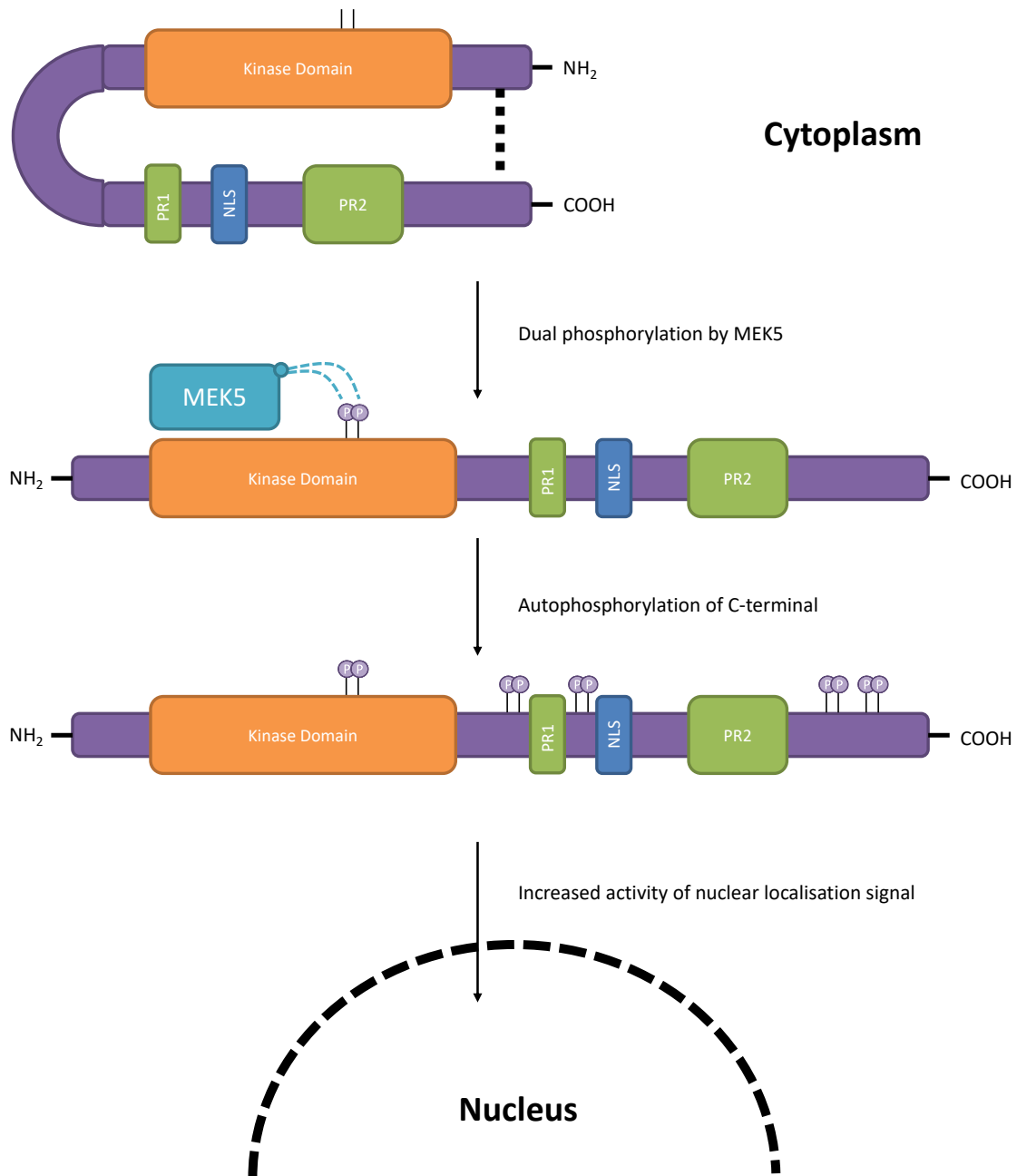


Figure 1.6. ERK5 signalling and localisation. In a quiescent state, unphosphorylated ERK5 is found in a closed conformational state bound together by intermolecular forces between the N- and C-terminal tails. Due to the reduced activity of NLS in this closed state, the protein is predominantly found in the cytoplasm. Phosphorylation activity by MEK5 opens the conformational structure of ERK5 and enables more sites of the C-terminal tail to be phosphorylated. This increased activity of the NLS, promotes its translocation to the nucleus and the subsequent downstream signalling associated with ERK5 and its TAD domain.

This relatively recently identified MAPK, ERK5 responds to mediators including IL-6, VEGF, EGF, PDGF, and physiological conditions such as ischemia, hypoxia, and osmotic and laminar shear-stress (Nithianandarajah-Jones *et al.*, 2012). Its activation regulates a diverse range of processes including cellular proliferation, migration, survival and angiogenesis (Figure 1.7). Early genetic *in vivo* studies revealed that ERK5 deficiency, by genetic ablation of both alleles of the gene, was embryonic lethal due to its crucial role in healthy cardiac development. These studies revealed immature vasculature and defective endothelial organisation and morphology (Kato *et al.*, 1998; Hayashi and Lee, 2004). An additional study was conducted utilising conditional loss of ERK5 under the control of an inducible Mx1-Cre transgene, permitting studies of ERK5 ablation in adult mice. This study by Hayashi *et al.*, further supported that loss of ERK5 caused abnormal vasculature and rounded and apoptotic endothelial cells which led to resultant death by haemorrhaging (Hayashi *et al.*, 2004).

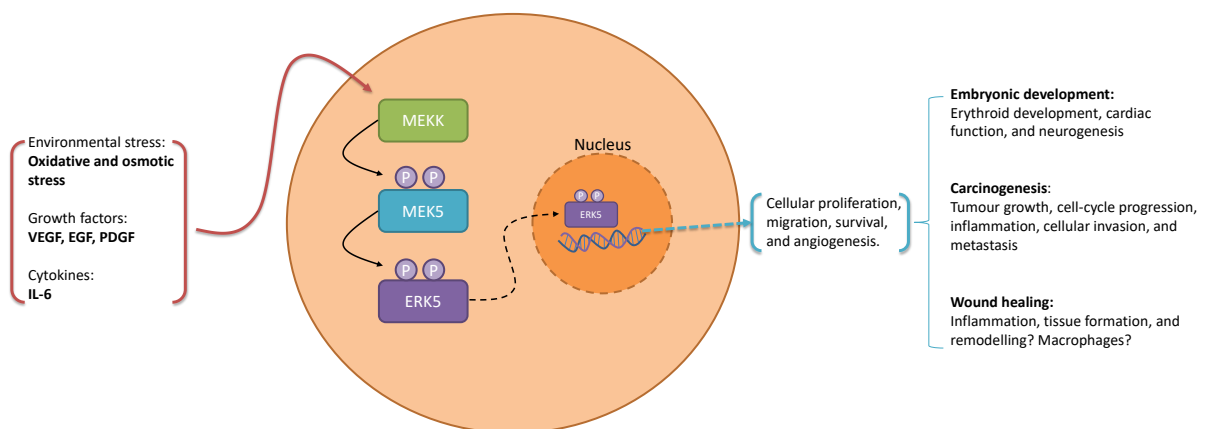


Figure 1.7. ERK5 signalling summary. Extracellular stimuli in the form of environmental stress, growth factors, and cytokines act upon their respective receptors to activate a cascade of kinase events. This is initiated by the phosphorylation of an apical MAPKK (MAPK kinase, also known as MEKK – MAPK/ERK kinase), which sequentially phosphorylates MEK5, and subsequently ERK5. Phosphorylated ERK5 can then translocate to the nucleus to trigger a range of cellular processes from proliferation, migration, and angiogenesis. These physiological responses have been found to influence embryonic development and carcinogenesis. What remains to be determined is the potential role ERK5 signalling may play in wound healing.

Recently, there has been attention drawn to the role ERK5 may have in cancer development, with a focus on its role as a mediator of inflammation and proliferation (Perez-Madrigal *et al.*, 2012; Finegan *et al.*, 2015). They have established ERK5 as an important regulator of the IL-1-COX2 inflammatory signalling pathway which drives skin tumorigenesis. They further demonstrate the potential of anti-ERK5 therapy using XMD8-92, a first generation ERK5 kinase inhibitor, to reduce epidermal proliferation, neutrophil and macrophage infiltration and tumour growth (Finegan *et al.*, 2015). Additionally, increased ERK5 expression has been correlated with invasive and metastatic potential in human colon cancer progression through nuclear factor- κ B (NF- κ B) signalling (Simões *et al.*, 2015). ERK5 inhibition has also been found to decrease inflammatory agonists such as IL-6 and IL-8. Furthermore, ERK5 signalling was needed to promote adhesion of neutrophils in lung endothelial cells. Inhibiting ERK5 was able to limit LPS-induced inflammatory mortality, similar to septic shock (Wilhelmsen *et al.*, 2015). These studies highlight the potential of targeting ERK5 therapeutically to curb the chronic inflammation associated with impaired wound healing.

However, a further study into the specific relationship with myeloid cells revealed that inhibiting ERK5 can polarise tumour associated macrophages towards an anti-tumour and M1-like phenotype and render melanoma cells more vulnerable to cancer therapies (Giurisato *et al.*, 2018). Studies have similarly shown that pharmacological inhibition of MEK5, upstream of ERK5, results in reduced expression of M2-like markers and associated mediators, such as Arg1 and Ym1. Additionally, they found that ERK5 deficient unpolarised macrophages were deficient in these M2-like associated genes, and were primed towards an M1-like phenotype (Luiz *et al.*, 2020).

In the context of atherosclerotic models, they found that inactivation of ERK5 in macrophages led to increase in M1-like and inflammatory associated genes. However, these macrophages were compromised in their phagocytic ability with reduced levels of opsonins and complement

markers. These factors including C1qa, C1qb, and C1qc, are required to facilitate macrophages in successfully targeting cells for phagocytosis. Together, this loss of ERK5 led to inflammatory induced atherosclerotic lesions and increased necrotic cores (Heo *et al.*, 2014). ERK5 has also been found to inhibit vomocytosis, the non-lytic expulsion process to expel live organism engulfed by phagocytes. Here they found that ERK5 inhibition led stimulated vomocytosis, reduced infection, increased inflammatory mediators and reduced M2-like signalling (Gilbert *et al.*, 2017). Together, these studies suggests that ERK5 inactivation could reduce overall inflammation, but still polarise macrophages to remain inflammatory, adding to the complexity of ERK5 signalling in immunity.

As previously mentioned, shear stress can trigger ERK5 activity which can limit functions such as endothelial migration. Thus, studies have found that ERK5 inhibition led to downregulated Krüppel-like factors (KLF)2/4 and increased endothelial migration (Komaravolu *et al.*, 2015). However, in contrast, ERK5 inactivated keratinocytes exhibited altered morphology and disrupted motility, which led to reduced epithelial migration and reduced cell-cell adherence (Arnoux *et al.*, 2008). Moreover, studies have also reported that ERK5 is important in regulating angiogenesis to support tumour expansion and invasion by providing tumours with the necessary network for nutrients and growth factors (Colotta *et al.*, 2009; Rovida *et al.*, 2015). These range of incongruous functional outcomes highlights the breadth of the role of ERK5 and how targeting this protein pathway can be incredibly complex and nuanced in wound repair.

Additionally, it should be noted that recent research using ERK5 kinase inhibitors have found that they often fail to recapitulate the phenotypes observed with genetic inactivation. These studies reiterate that many ERK5 associated functions are independent of kinase activity, and moreover, kinase inhibition itself can trigger other factors to activate ERK5 through its large C-terminal extension (Lochhead *et al.*, 2020). Some of the first generation ERK5 kinase

inhibitors, function through off-target activity on bromodomains, and again show that selective ERK5 kinase inhibition has no biological effect comparable to whole protein ablation (Lin *et al.*, 2016).

In order to replicate the immune-mediated inhibition observed in the ERK5 genetic ablation models, we require a therapeutic system which removes or degrades the whole ERK5 protein from cells, rather than inhibit its catalytic kinase function. This PhD will explore this by assessing a compound developed in-house by our collaborators in the Butterworth Lab, via CRUK Drug Discovery funding. This compound named, OS1, made by Dr Olly Smith, is a heterobifunctional small molecule compound composed of two active regions bound by a linker domain. One arm is specific to ERK5, and the other arm engages with the cell's internal machinery to degrade the target protein. Parallel research within the Finegan Lab (unpublished) has shown its effective pharmacological-knockdown of ERK5 in triple negative breast cancer, inducing an immunological phenotype not observed with ERK5-kinase inhibition alone. These compounds are currently being patented and as a result further detail, such as exact mechanisms of action and structure, cannot be provided in this thesis.

Cancers have often been described as “the wound that never heals”, due to the characteristic dysregulated inflammation, cellular proliferation and migration that promotes tumour development and genetic instability (Hanahan and Weinberg, 2011). With this notion, there is no doubt that similarities exist between the chronic inflammation associated with cancer and impaired wounds such as those associated with diabetes. On that basis, early *in vitro* studies have shown ERK5 activation can inhibit migration of endothelial cells required for angiogenesis and influence the activity of keratinocytes during wound healing (Arnoux *et al.*, 2008; Spiering *et al.*, 2009). However, what remains unanswered is the potential role ERK5 signalling may play in influencing the behaviour of macrophages in the context of impaired wound healing.

1.6 Precursor Research

The Finegan and Mace Labs have previously demonstrated that genetic loss of ERK5 in the keratinocyte resulted in earlier wound healing and reduced inflammation in both healthy and diabetic mice (Db). From the wound closure data, they found that by day 8, ERK5KO wounds were almost at full closure when compared to control mice which were only 50% closed (Figure 1.8.A). A similar pattern of wound closure was also observed in the diseased context of diabetic wounds. Here they compared wound closure between diabetic/ERK5 wild type (WT) mice and diabetic/ERK5KO mice. The wounds of Db/ERK5KO closed at a slightly faster rate compared to their wild type counterparts. The starkest difference was observed on day 12, where the Db/ERK5KO wounds were almost completely closed, while the Db/WT wounds were only 50% closed (Figure 1.8.A).

Furthermore, our initial histological analysis of this study suggested that genetic inactivation of ERK5 in the skin led to delayed and reduced infiltration of macrophages, and increased neutrophil influx at earlier time-points (Figure 1.8.B and C). With this basis, it could be that depleting ERK5 signalling in keratinocytes, manipulates the immune environment to improve wound healing. This similar pattern was observed in the diabetic context, when comparing between Db/WT and Db/ERK5KO, but shifted to a later time. This was as expected due to the chronic inflammatory nature of diabetic wounds.

Given the importance of macrophages role in wound healing, and evidence in cancer studies highlighting the relationship between ERK5 and macrophages, we hypothesise that macrophages can be beneficially manipulated to improve wound healing by targeting the ERK5 signalling pathway.

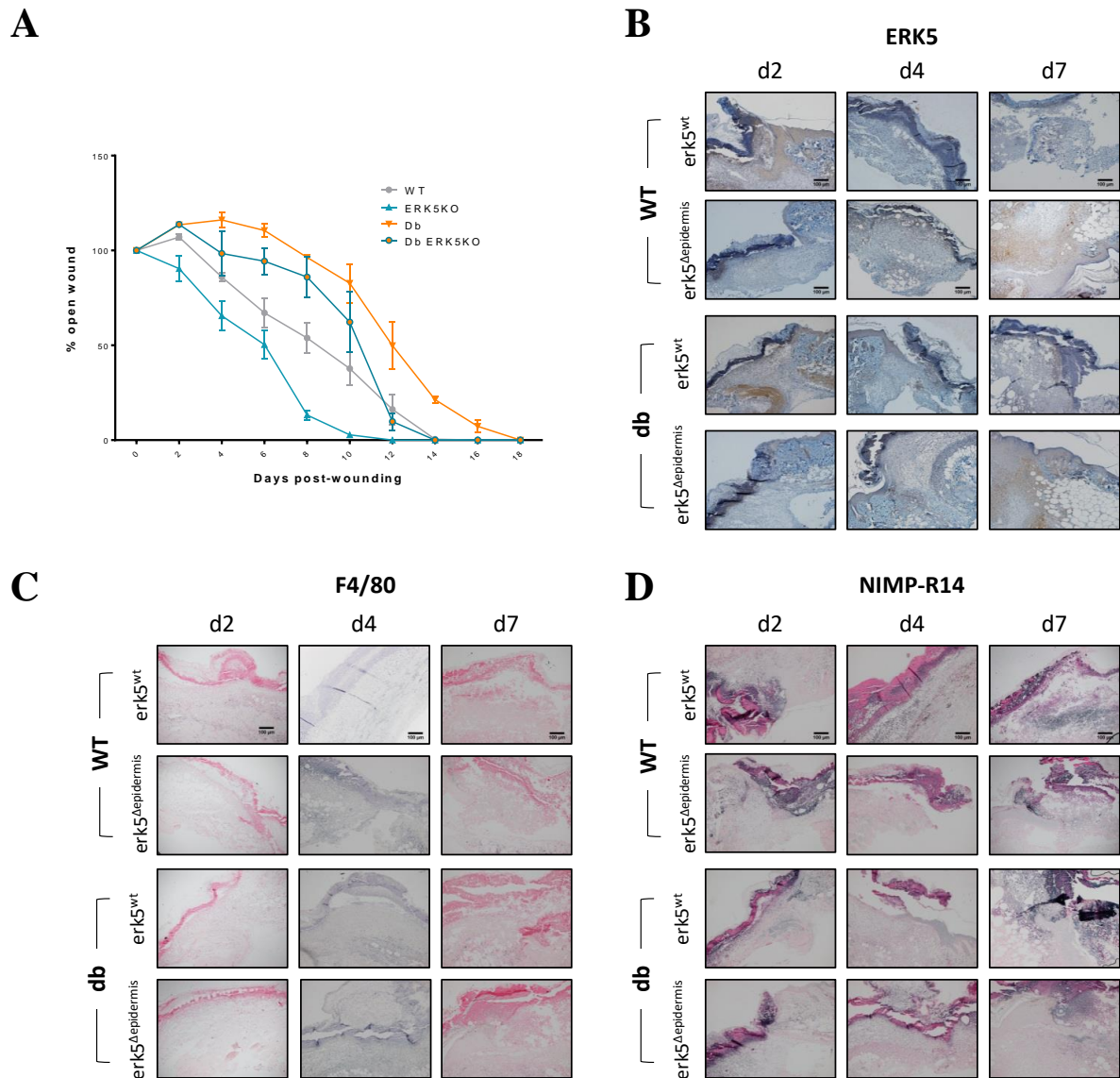


Figure 1.8. Genetic ERK5 inactivation improves wound healing in both wild type and diabetic models. Precursor work by the Finegan and Mace Labs utilised inducible ERK5 epidermis knockout mice, crossed with *Lepr^{db/db}* mice. (A) Wounds were imaged and the area calculated on ImageJ to quantify wound closure. Data points plotted represent the mean of multiple different mice \pm SEM. Representative images of (B) ERK5, (C) F4/80, and (D) NIMP-R14 in wild-type, ERK5KO/WT, WT/db, ERK5KO/db mice over selected time points of day 2, 4 and 7 post-wounding. Black bars = 100 μ m.

1.7 Understanding ERK5 signalling in macrophage behaviour and wound healing – hypothesis, aims and objectives

Impaired wound healing is evidently a complex and multifactorial process, which continues to persist as an issue due to an incomplete understanding of the underlying mechanism and an absence of targeted therapies. Research in recent decades have shown that macrophages are crucial in facilitating healthy wound healing through inflammation, and the transition to repair mechanisms. Additionally, in impaired and diseased context, chronically inflamed and dysfunctional macrophages have been found to be a critical driver of pathology. However, an effective and targeted treatment plan against these inflammatory wound macrophages remains elusive.

ERK5 is a potentially valuable target of interest in elucidating the function of macrophage behaviour in wound healing. Studies in ERK5 signalling have shown it is a key inflammatory driver of IL-1, IL-6 and IL-8 in skin carcinogenesis, and influential in macrophage polarisation. This presents an opportunity to investigate the function of ERK5 signalling in the novel context of wound healing and associated inflammation.

My hypotheses were:

- i) Hyperactivation of ERK5 may contribute to chronic inflammation that disrupts healthy wound healing.
- ii) With the complex and multi-factorial role ERK5 plays, it had the potential to be targeted with the novel compound OS1, to be inactivated and attenuate inflammation and promote repair mechanisms e.g. M2-like macrophage activity.

In order to test these hypotheses, the experimental workflow was broken down into three main aims which utilised genetic models, *in vitro* systems, and *in vivo* translation to fully elucidate

the role of ERK5 and its potential as a therapeutic target to modify inflammation and macrophage behaviour.

- To determine if *in vivo* genetic inactivation and constituent activation of MEK5 affects wound healing and inflammation
- To determine if therapeutic inactivation of ERK5 using novel compound OS1 affects *in vitro* human models of keratinocytes (HaCaTs) and macrophages (THP-1s) in relation to wound healing and inflammation
- To determine if therapeutic inactivation of ERK5 using novel compound OS1 affects *in vivo* model of murine wound healing and inflammation

Answering these aims will enable a wider understanding of ERK5 complexity and its pleiotropic role in influencing inflammation and immunity. Our established genetic models only modify ERK5 in the epidermal layer, permitting specific insight into how ERK5 functions in the keratinocyte layer in the novel context of *in vivo* wound healing. Moreover, we have a unique opportunity to utilise an innovative therapeutic compound and assess the efficacy of degrading ERK5 across multiple cell types in a localised environment. This will provide insight for parallel immune-mediated studies within the Finegan Lab in cancer research models of breast cancer and osteosarcoma. Finally, this research will provide the foundation for future research in *in vivo* chronic wound models such as those associated with diabetes, and assist in developing an ERK5 associated wound biomarker signature to stratify potential patient subsets.

We used an excisional wound model on established genetically modified mice where ERK5 could be selectively inactivated (ERK5KO) and MEK5 constitutively active (CaMEK5). Wounds were left to heal, and collected at d2, d4, and d7 to examine markers of inflammation and wound healing by histology, flow cytometry and wound closure. Expected outcomes were:

- Inhibited inflammation in ERK5KO
- Persistent inflammation in CaMEK5

In order to investigate how ERK5 inactivation influences functions of wound healing and inflammation, we specifically studied *in vitro* models of keratinocytes and macrophages. This permitted an early evaluation of ERK5 signalling in the human context to validate our findings in the murine system, and to isolate the function of ERK5 in the specific cell types. Moreover, we wanted to test how a novel compound, OS1, would compare to existing kinase inhibitors and lentiviral genetic inactivation of ERK5. This was in part to overcome issues in literature where ERK5 kinase inhibition does not reflect whole protein genetic ablation. OS1 differs to existing ERK5-targeted compounds in its ability to degrade the whole protein. Expected outcomes were:

- Degradation of ERK5 in HaCaTs to promote migration and modified gene expression associated with inhibited inflammation and promoted repair markers.
- Degradation of ERK5 in THP-1s to influence unpolarised macrophages towards a repair phenotype.

To address the final aim, we used the excisional wound model on healthy mice and assessed the *in vivo* translatability of topical OS1 application in regulating wound healing and inflammation. Wounds were left to heal, and collected at multiple time points from d4 to d29, after wound closure to examine markers of inflammation and wound healing by histology, flow cytometry, wound closure and novel positron emission tomography (PET) *in vivo* molecular imaging analysis. Expected outcomes were:

- OS1 treatment inhibiting inflammation, and altering macrophage polarisation towards a repair phenotype.

- The dynamics of this macrophage behaviour being observed with PET technology where a single animal can be tracked during the entire wound healing process. This would provide a major advantage over the snapshot pathology approach and provide refinement and reduction in the number of animals needed for this type of research.

The data generated from this study would provide insight into the role ERK5 plays in inflammation and wound healing, and how a novel therapeutic, OS1, influences this pathway after degrading ERK5 in the *in vitro* model of HaCaTs and THP-1s, as well as in *in vivo* murine wounding models. This would open the potential for future research in stratifying chronic wound patients based on their ERK5 or inflammatory macrophage profiles that we describe in this study. Additionally, with our unique access to innovative drug technology, we can assess the efficacy and translatability of topical OS1 treatment in human *in vitro* context and murine *in vivo* system.

Chapter 2: Materials and Methods

2.1 Cell Lines

HaCaTs, and THP-1s were obtained from frozen stocks within the lab and were originally obtained from American Type Culture Collection (ATCC). HaCaT cells were cultured in Dulbecco's modified Eagle's medium (DMEM) – high glucose (Life Technologies), containing 10% Fetal Bovine Serum (FBS) at 37°C in 5% CO₂ humidified incubator. THP-1 cells were cultured in Roswell Park Memorial Intermediate (RPMI) 1640 medium, containing 10% FBS and 1% Penicillin/Streptomycin (Sigma) at 37°C in 5% CO₂ humidified incubator. Cells were seeded at varying densities on different culture dishes dependent on application.

Table 2.1. Experimental *in vitro* Seeding Density

	Seeding Density (cells per well)				
	WB	MTT/SRB	qPCR	IF	Scratch
HaCaT	5x10 ⁴	5x10 ³ – 1x10 ⁴	5x10 ⁴	1x10 ⁴	5x10 ⁴
THP-1	2x10 ⁵	5x10 ³ – 2x10 ⁴	2x10 ⁵	3x10 ⁴	-

2.2 Treatment Groups

Various compounds were used *in vitro* and *in vivo* to modify signalling pathways associated with ERK5 or inflammation. Control samples were treated with DMSO at a concentration matched with the highest drug concentration.

OS1 is a heterobifunctional small molecule made of two active regions bound by a linker domain. One arm binds to the target protein of ERK5 and the other arm engages in our cell's machinery to degrade the target protein. This compound was made in-house by the Butterworth Lab, by Dr Olly Smith.

AX15836 (Tocris), named AX throughout this thesis, is an established, potent and selective ERK5 kinase inhibitor.

Short hairpin (sh) RNA ERK5 lentivirals (*EO3*) were generated by the collaborating Bigger Lab and gifted to us. HaCaTs were stably transfected with ERK5 shRNA-GFP lentiviral particles and polybrene transfection reagent (Sigma-Aldrich) for at least 6h at 37°C in 5% CO₂ humidified incubator. The lentiviral particle medium was removed, and replaced with fresh culture medium. Transfection efficiency was evaluated by observation under a fluorescent microscope. Cells were allowed to be grown to confluence before being GFP-sorted by flow cytometry as performed by the Flow Cytometry Facilities with Dr Gareth Howell. Cells were then referred to as shERK5 HaCaTs.

THP-1 monocyte suspension cells were differentiated into M0 adherent THP-1 macrophages with phorbol-12-myristate-13-acetate (PMA) at 100 ng/ml for 24h. After adherence and differentiation, medium was replaced with fresh medium contain either IFN γ + LPS (20 ng/ml + 1 μ g/ml) or IL-4 + IL-13 (20 ng/ml, both) for 48h to polarise towards M1 or M2 –like THP-1 macrophages.

2.3 Western Blots

Cells were washed in ice-cold PBS and lysed in radioimmunoprecipitation (RIPA) buffer made using the following: 50mM Tris-HCl at pH 7.4, 150mM NaCl, IGEPAL 1%, 1mM EDTA, 1mM PMSF (Fluka), cOmplete™ Mini EDTA-free Protease Inhibitor Cocktail (Roche), 1mM Na₃VO₄ and 1mM NaF. Cells were scraped thoroughly and transferred to an Eppendorf. Cell lysates were sonicated for 10 seconds with a Soniprep 150 sonicator (Sanyo) and then centrifuged at 13,000 x g at 4°C for 10 minutes to clear supernatant.

Protein concentrations was measured by the colorimetric bicinchoninic acid (BCA) protein assay, where the production of Cu²⁺ in this assay is a function of protein concentration and incubation time. 5 μ l of sample lysates were added in duplicate with 200 μ l of working reagent

composed of 4% copper sulphate at a 1:50 ratio in BCA. After incubation at 37°C for 30 minutes, the absorbance was read at 562nm on a μ Quant Microplate Reader (BioTek).

Protein samples were diluted to 20 μ g in dH₂O and 2x SDS sample buffer (Table 2.2) with a working volume of 20 μ l per well. Samples were heated to 95°C for 5 minutes and briefly centrifuged before loading into gel alongside 8 μ l of Precision Plus Protein™ Kaleidoscope™ Prestained Protein Standards (Biorad).

SDS-polyacrylamide gel electrophoresis (SDS-PAGE) running gels were prepared as detailed in Table 2.3. Cell lysates were resolved on 6% or 8% SDS-PAGE in 1x Tris-Glycine Running buffer at 110V until the sample buffer reached the bottom of the gel. The gel was then electrophoretically transferred to an Immuno-Blot® polyvinylidene fluoride (PVDF) Membrane (Biorad) for 100 minutes at 100V in 1x Transfer Buffer (Table 2.2). The membranes were incubated with 5% bovine serum albumin (BSA) for 1 hour and probed overnight at 4°C with primary antibodies to various targets (see Table 2.6) and compared to β -actin or GAPDH, as a control to monitor protein loading. Membranes were further incubated with species specific secondary antibody coupled to horseradish peroxidase (see Table 2.6) for 1h. Immune complexes were detected using the Clarity™ Western ECL Blotting kit (Biorad), and imaged on a ChemiDoc™ XRS+ system with Image Lab™ Software (Biorad).

Table 2.2. Western Blot Reagents

	Make up in dH₂O
RIPA Buffer Stock	50mM Tris-HCl at pH 7.4, 150mM NaCl, IGEPAL 1%, 1mM EDTA
2x SDS Buffer	62.5mM Tris at pH 6.8, 2% SDS, 10% Glycerol, 0.01% Bromophenol Blue, 3% β -mercaptoethanol
10x Tris-Glycine Running Buffer	0.025M Tris, 0.192M Glycine, 0.1% SDS
10x Transfer Buffer	0.025M Tris, 0.192M Glycine
1x Transfer Buffer	10% (10x) Transfer Buffer, 20% Methanol

Table 2.3. SDS-PAGE Running Gel Composition

Running Gels						
	1 Gel		2 Gels		4 Gels	
	6%	8%	6%	8%	6%	8%
dH₂O	5.3 ml	4.6 ml	10.6 ml	9.3 ml	21.2 ml	18.5 ml
30% Acrylamide	2 ml	2.7 ml	4 ml	5.3 ml	8 ml	10.7 ml
1.5M Tris pH 8.8	2.5 ml	2.5 ml	5 ml	5 ml	10 ml	10 ml
20% SDS	100 µl	100 µl	200 µl	200 µl	400 µl	400 µl
10% APS	100 µl	100 µl	200 µl	200 µl	400 µl	400 µl
TEMED	6 µl	6 µl	12 µl	12 µl	24 µl	24 µl

5% Stacking Gel

	1 Gel	2 Gels	4 Gels
dH₂O	3.5 ml	7 ml	14 ml
30% Acrylamide	850 µl	1.6 ml	3.2 ml
1M Tris pH 6.8	650 µl	1.25 ml	2.5 ml
20% SDS	50 µl	100 µl	200 µl
10% APS	50 µl	100 µl	200 µl
TEMED	10 µl	15 µl	40 µl

2.4 MTT and SRB Proliferation Assay

Cells were seeded and treated according to their experimental plans and collected at selected time points of 0, 24, 48, and 72 hours. At this point, 50µl of 3-(4,5-dimethylthiazol-2-yl)-2,5-diphenyltetrazolium bromide (MTT) (Sigma-Aldrich) at 2.5 mg/ml was added to each well and incubated at 37°C for 4 hours. After aspiration of the media, 200µl of DMSO was added to each well. The relative cell number was determined by measuring the absorbance at 562nm using a µQuant Microplate Reader (BioTek).

Cells were similarly assessed by sulforhodamine B (SRB) (Sigma-Aldrich) colorimetric assay as previously described. At the end of each time point, attached cells were fixed with 50µl of cold 50% (wt/vol) trichloroacetic acid (TCA) to each well, and incubated at 4°C for 1 hour. After aspiration of the media, cells were washed with distilled water. Cells were stained with 100µl 0.4% SRB for 10 minutes and rinsed with 1% acetic acid to remove unbound dye. The protein-bound dye was solubilised by addition of 200µl 10nM Tris Base solution to each well, and relative cell number was determined by measuring the absorbance at 510nm using a µQuant Microplate Reader (BioTek).

2.5 *In vitro* scratch assay

For wound scratch assays, HaCaT cells were seeded at 5×10^4 cells per well in 6-well plates. HaCaT cells were cultured for 24 hours to achieve 90% confluence followed by starvation in low serum 2% FBS supplemented media. A 200 μ l sterile pipette tip was used to create a scratch across the cell monolayer. Cells were briefly washed with PBS to remove debris. Cells were then treated according to experimental parameters and incubated in fresh low serum 2% medium at 37°C in 5% CO₂. The scratch gap was imaged at several time points using an Inverted Phase Contrast Microscope (Optika) at 4x objective using the Optika® Vision Pro Software (Optika). The scratch gap area fold change was calculated based on the gap area at 0 hours, which was arbitrarily set as 1 and analysed on ImageJ software.

2.6 Real-Time Quantitative Polymerase Chain Reaction (RT-qPCR)

2.6.1 RNA extraction

RNA was extracted from cells by homogenisation with TRIzol (Ambion). Cells were incubated for 5 minutes in the TRIzol before being mixed thoroughly with 20% volume of Chloroform (Fisher). This mixture was incubated for 3 minutes at room temperature then centrifuged for 15 minutes at 10,000 rpm at 4°C. The upper water phase was carefully transferred into an Eppendorf containing 0.5ml Isopropanol (Fisher), vortexed thoroughly and incubated at -20°C for 20 minutes. The sample was centrifuged for 10 minutes at 10,000 rpm at 4°C and the supernatant removed. The pellet was washed twice with cold 75% ethanol and dissolved in 50 μ l Nuclease-Free Water at 55°C for 10 minutes. The RNA concentration was determined using a NanoDrop Lite (Thermo Scientific) spectrophotometer (OD260/280) and samples were stored at -80°C.

2.6.2 DNase I Treatment

Quantified RNA was diluted to 100 ng/ μ l with Nuclease-Free Water and mixed with 10x Reaction Buffer (RDD) and 10% DNase, in a volume of 20 μ l. This mixture was incubated for 15 minutes at room temperature. The reaction was stopped with addition of 10% volume of 50mM EDTA solution and incubated at 65°C for 10 minutes. Samples were stored at -80°C.

2.6.3 Complementary DNA (cDNA) Synthesis

cDNA was synthesised using of 1 μ g RNA, 1 μ l 10mM dNTP (Bioline) and 1 μ l Hexamer random primers (Roche) and incubated for 10 minutes at 70°C. Samples were briefly centrifuged at 4°C and incubated on ice for 2 minutes. A master mix containing, 4 μ l 5x RT Buffer (Bioline), 0.5 μ l Reverse Transcriptase (Biolabs), 0.5 μ l RNase Inhibitor (Biolabs) and 3 μ l RNase free water, was added to the annealed RNA and incubated for 10 minutes at room temperature, and then 50 minutes at 37°C. The reaction was terminated by incubating at 88°C for 10 minutes. cDNA samples were diluted to a 1:3 ratio in RNase free water and stored at -20°C.

2.6.4 RT-qPCR Programme

For RT-qPCR experiments, 8 μ l of SensiMix: SYBR Green (Bioline) was mixed with 2 μ l of 3.33 μ M primers of target interest (see Table 2.7). This mixture was added with 2 μ l of cDNA and 8 μ l of Nuclease-Free Water for a total reaction volume of 20 μ l. All reactions were run in duplicate in a 96-well plate (Star Lab). The reaction was run on the Stratagene Mx3000P qPCR System (Agilent) on the MxPro QPCR software using the protocol on Table 2.4. The obtained data was analysed using the $\Delta\Delta C_T$ method to quantify relative gene expression.

Table 2.4. RT-qPCR Programme Protocol

Step	Time	Temperature
Step 1 (Pre-heat)	10 minutes	95°C
Step 2	60 seconds	95°C
Step 3	30 seconds	95°C
Step 4	30 seconds	55°C
Step 5	30 seconds	72°C
<i>Repeat steps 3-5 for 40x cycles</i>		
Step 6	∞	10°C

2.7 Immunofluorescence

Cells were seeded as in Table 2.1 onto 8-well Millicell EZ-slides (Millipore) and treated according to their experimental plans until collection. At this point the media was aspirated, cells were washed with PBS and subsequently fixed in 10% formalin for 10 minutes. Fixed cells were washed in PBS and then permeabilised with 0.1% (v/v) Triton-100 in PBS for 10 minutes. Cells were washed with PBS and the non-specific binding sites were blocked by incubating with 1% BSA for 30 minutes. Targets of interest were identified by incubating with 100µl of primary antibody diluted in 1% BSA (see Table 2.6) overnight at 4°C. After washing with PBS, samples were further incubated with species specific secondary antibody coupled to fluorescent tags (see antibody Table 2.6) for 1 hour in the dark at room temperature. Some samples were further incubated with 100µl of 1:200 phalloidin (Invitrogen, A12381) in 1% BSA for 2 hours at room temperature to identify actin filament structures.

The EZ-slides casing was dismantled as described in manufacturer's instruction and slides were washed in distilled H₂O. Samples were incubated with one drop of Mounting Medium with DAPI (abcam) for 5 minutes in the dark at room temperature to visualise the nuclei. A coverslip was added to each slide and allowed to dry at room temperature.

Images were acquired on a 3D-Histech Panoramic-250 microscope slide-scanner using a 20x/0.80 Plan Apochromat objective (Zeiss) and the DAPI, FITC and TRITC filter sets. Snapshots

of the slide-scans were taken using the Case Viewer software (3D-Histech). Images were then processed and analysed using ImageJ.

The Bioimaging Facility microscopes used in this study were purchased with grants from BBSRC, Wellcome and the University of Manchester Strategic Fund. Special thanks goes to Peter March, Roger Meadows, and Steve Marsden, for their help with the microscopy

2.8 Animal work

2.8.1 Ethics, sources and husbandry

Mice were housed at the University of Manchester animal care facility, Biological Service Facility. All procedures were approved by the local ethical review committee and the U.K. Home Office under the Animals (Scientific Procedures) Act, 1986. Mice were used experimentally between the ages of 8 and 16 weeks. Animals were mixed sexes and either C57BL/6J from Charles River, or K14Cre-ERK5 (ERK5KO) and K14Cre-CaMEK5 (CaMEK5) (in-house) from a BALB/C background.

2.8.2 Genetic Mouse Models

We have utilised an established knockout mouse model carrying a transgene encoding an *erk5* gene flanked with LoxP sites and a mutated oestrogen receptor fused with Cre (CreER) under the control of the keratin 14 (K14) promoter. These models were previously validated by the Tournier and Finegan lab by ERK5 histology staining and western blot analysis of processed keratinocytes. Induced deletion of ERK5 in keratinocytes was achieved by intraperitoneal injection of tamoxifen (every day for five days) (Figure 2.1.A). Similarly, we utilised a knock in mouse model carrying a transgene encoding a STOP codon flanked by LoxP sites in front of a constituent active (ca) MEK5 allele. Again, this was under the control of K14-CreER. Induced expression of caMEK5 in the keratinocytes was achieved following intraperitoneal injection of tamoxifen (every day for five days) (Figure 2.1.B). Mice were housed for at least

two weeks before experimental wounding to permit normal skin regeneration in order for ERK5 modification in the basal keratinocytes to replace all the epidermal cells.

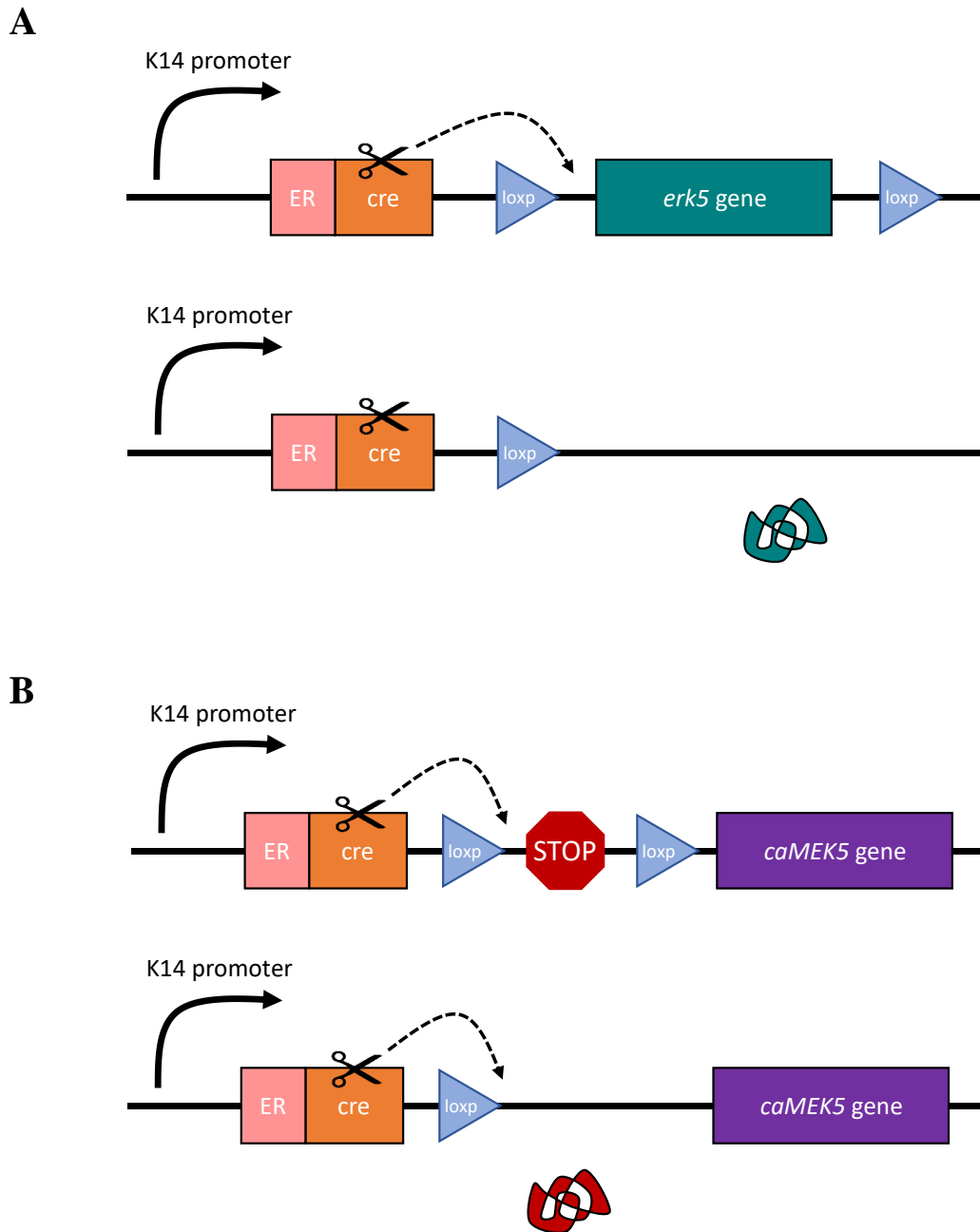


Figure 2.1. K14CreER-ERK5KO and K14CreER-CaMEK5 Genetically Engineered Models. (A) K14CreER-ERK5KO system to inactivate ERK5 and (B) K14CreER-CaMEK5 system to express constitutively active MEK5 and subsequently hyperactive endogenous ERK5.

2.8.3 Genotyping

Mice ear clippings were incubated in a mixture of 100µl DirectPCR Lysis Reagent (Viagen) and 2µl Proteinase K solution (Invitrogen) overnight at 55°C. The reaction was terminated by incubating samples for 1 hour at 85°C and then centrifuged at 13,000 x g for 2 minutes.

Genotype determination was then performed by PCR using primers specific to K14Cre or CaMEK5 on their respective programmes (Table 2.5). From each digested ear clipping, 2µl of sample was processed in a mastermix (Qiagen) containing 2µl Coral Load, 4µl Q-solution, 0.4µl dNTP, 0.2µl of each primer, 0.2µl Taq polymerase and 11µl of dH₂O.

PCR products were run on 1% or 3% Agarose gels at 100V for 45 minutes and imaged under UV. Mice carrying the K14Cre and CaMEK5 transgene were identified by PCR on genomic DNA isolated from ear clipping tissue.

Table 2.5. Genotyping Primer Sequences and PCR Protocol

Primers	Sequence
K14Cre-Forward	CGGTTCGATGCAACGAGTGATGAGG
K14Cre-Reverse	CCAGAGACGGAAATCCATCGCTCG
CaMEK5-Forward	ACCTTTCTGGGAGTTCTCTGC
CaMEK5-Middle	ATGGAAAATACTCCGAGGCGG
CaMEK5-Reverse	TCACTGCATTCTAGTTGTGGTTTG

K14CreERK5	Time	Temperature
Step 1	3 minutes	94°C
Step 2	30 seconds	94°C
Step 3	45 seconds	60°C
Step 4	60 seconds	72°C
<i>Repeat steps 2-4 for 39x cycles</i>		
Step 5	10 minutes	72°C
Step 6	∞	4°C

CaMEK5	Time	Temperature
Step 1	5 minutes	95°C
Step 2	30 seconds	95°C
Step 3	30 seconds	58°C
Step 4	30 seconds	72°C
<i>Repeat steps 2-4 for 32x cycles</i>		
Step 5	10 minutes	72°C
Step 6	∞	4°C

2.8.4 Genetic modification of ERK5 in keratinocytes

Tamoxifen (Sigma; T5648) was dissolved in 100% ethanol at a stock concentration of 20 mg/ml. The stock solution was diluted in Sunflower Oil (Sigma; S5007) to produce a working solution of 2 mg/ml. Tamoxifen in oil could be stored for 1 week at 4°C.

Minimum age of six-week old genetically engineered mice were subjected to intraperitoneal injection of 200µg (100µl of tamoxifen working solution) every day for five days. Two weeks later mice were ready for experimental use.

2.9 Wounding

Animals were anaesthetised with 2.5% isoflurane and 2L/min O₂, the dorsum shaved and sterilised with antiseptic wipes. Anaesthesia was maintained with a nose cone and body temperature regulated using a warming mat at 37°C. Full thickness wounds of 10mm diameter were excised from the lower-back using a template and sterilised surgical scissors. Animals received 1.5 mg buprenorphine at the time of surgery and were housed in separate cages for the duration of the experiment. Animals were given general anaesthesia by isoflurane inhalation prior to OS1 treatment as described in section below and during wound measurements.

Wound circumference was traced on multiple time points, and used to calculate wound closure over the time course on ImageJ software. Tissues were harvested at day 1, 2, 3, 4, 7, 14, 16 and 29 by removing the entire wound area including a 2mm perimeter. Animals were killed by cervical dislocation under general anaesthesia at the time of tissue collection.

2.10 *In vivo* OS1 Treatment

OS1 was prepared fresh at 1µM in 1% methyl-cellulose at a 1:1 ratio overnight at 4°C with mild agitation. OS1 was topically injected into the wound site with a total volume of 50µl per

wound, split into two doses of 25µl in opposing sides of the wound. Animals were dosed every 48 hours for a maximum of 10 doses for the duration of the experiment.

2.11 Wound Tissue Dissociation

Harvested wounds were digested at 37°C with mild agitation for 45 minutes in liberase working solution (Roche) made up of 0.2 mg/ml Liberase DH Research Grade (Roche), 0.25 mg/ml DNase I from bovine pancrease (Sigma) in serum-free media. The liberase reaction was stopped with 10% FBS supplemented media, and the suspension was passed through a 40µm cell strainer (Corning). Single cell suspension was spun at 1300 x g for 3 minutes and re-suspended in 1% FBS supplemented PBS.

2.12 Flow Cytometry

For flow cytometry (referred throughout as FACS; fluorescence activated cell sorting) and analysis, samples were incubated with a panel of immune cell related antibodies (see Table 2.6) for 30 minutes on ice. Samples were spun down at 1300 x g for 3 minutes and washed twice in 1% FBS supplemented PBS. Samples were further fixed in 10% formalin for 15 minutes. Samples were resuspended in 1% FBS supplemented PBS in preparation for flow cytometry processing performed by the Flow Cytometry Facilities with Dr Gareth Howell. Data was analysed using FlowJo (Treestar).

2.13 Homogenisation of wounds for RT-qPCR

A proportion of harvested wounds were flash frozen in dry-ice. Wound tissue was transferred into Precellys Lysing Kit Tubes (2ml) (Bertin) containing 1ml of TRIZol (Ambion) and stored in -80°C. Tissue samples were homogenised using a Precellys Homogeniser (Bertin) at Programme 6 “6500 2x 20s”. Samples were then prepared as described in (RT-qPCR instructions above).

2.14 Immunohistochemistry (IHC)

Mouse skin wound samples were fixed in 10% formalin and embedded in paraffin. Paraffin sections were cut at 5 μ M thickness. Sections were deparaffinised and rehydrated by bathing in xylene and decreasing concentrations of ethanol: 100%, 90% and 70%, before incubation in 2% hydrogen peroxide methanol for 30 minutes. Sections were then further washed in PBS for 3 x 5 minutes.

Antigen retrieval was either performed with 1% trypsin at 37°C for 30 minutes or by heating in 10mM sodium citrate buffer, pH 6.0, at 95°C for 15 minutes in a domestic microwave. After washing in PBS, an ImmEdge™ Hydrophobic Barrier Pen (Vector Labs) was used to draw around each section. Samples were blocked in 10% Normal Goat Serum (Abcam).

Then samples were incubated with primary antibodies specific to ERK5 (Cell Signaling Technology; 3372S), F4/80 (Abcam; ab6640), and NIMP-R14 (Abcam; ab2557) at 4°C overnight. On the following day, samples were washed in PBS and incubated with biotinylated secondary antibody specific to rabbit (Vector Labs; BA-1000) or rat (Vector Labs; BA-9400) at room temperature for 1 hour. Samples were stained with VECTASTAIN® Elite ABC HRP Kit (Vector Lab), according to manufacturer's instructions with DAB (Vector Lab), and counter-stained with Harris Hematoxylin Solution (Sigma-Aldrich). Sections were mounted with aqueous mounting medium.

For collagen staining, samples were deparaffinised as above and incubated with Picro-Sirius Red Solution (Abcam; ab150681) for 30 minutes. Slides were rinsed with two changes of 0.5% Acetic Acid and dehydrated in two changes of 100% ethanol. Sections were mounted with aqueous mounting medium.

Images were acquired on a 3D-Histech Panoramic-250 microscope slide-scanner using a 20x/0.80 Plan Apochromat objective (Zeiss) in brightfield. Snapshots of the slide-scans were taken

using the Case Viewer software (3D-Histech). Images were then processed and analysed using ImageJ. Images were blinded and scored from 0-3 by the degree of brown staining (Figure 3.4).

The Bioimaging Facility microscopes used in this study were purchased with grants from BBSRC, Wellcome and the University of Manchester Strategic Fund. Special thanks goes to Peter March, Roger Meadows, and Steve Marsden for their help with the microscopy

2.15 Positron Emission Tomography (PET) imaging

Animals underwent baseline scans at day 2 or 3 post-wounding, under anaesthesia with 1-2% isoflurane, the tail vein catheterised, placed in the animal bed and transferred to an Inveon pre-clinical PET/CT scanner (Siemens). Mice were injected with [¹⁸F]-DPA-714 or [¹⁸F]-MR-nanobody (synthesised in-house) intravenously via the tail vein before acquisition. Anaesthesia was maintained during image acquisition with a nose cone and temperature monitored throughout. After imaging, animals were recovered in a warmed chamber. Animals were re-scanned at d4, d7, d8, and d14 post-wounding.

Inveon acquired data images were visualised and analysed using Inveon Research Workplace software (Siemens). Regions of Interest (ROI) were drawn manually over wound area and the standard uptake value (SUV) (as an average of voxels) was calculated. Normalisation was performed based on tracer dose and weight of mice to give standardised uptake values. Additional, ROIs were drawn of heart and muscle tissue for alternative quantification and processing.

2.16 Statistical Analysis

Data generated were initially managed through Microsoft Excel. A minimum of three biological replicates were used in each experiment (unless specified), and further biological replicates were added as available. All data shown were analysed using GraphPad Prism 7. Error bars represent standard error of mean (SEM). Comparison between two different groups

were carried out using paired student's t-test. (* denotes P values<0.05, **=<0.01, ***=<0.001, ****=<0.0001. Blank or n.s. denotes not significant.

Table 2.6. List of Antibodies

Target	Species	Reactivity	Conjugate	Application	Dilution	Source	Cat No.
ERK5	Rabbit	Hu, Ms, Rt, Mk	-	IHC, WB	1:200, 1:1000	Cell Signalling Technology	3372S
ERK5	Rabbit	Rat, Human	-	IF	1:100	Abcam	Ab196609
ERK1/2	Rabbit	Hu, Ms, Rt, Mk	-	WB	1:1000	Cell Signalling Technology	9102S
BRD4	Rabbit	Ms, Rt, Hu	-	WB	1:5000	Abcam	Ab128874
β-actin	Mouse	Hu, Ms, Rt	-	WB	1:10000	Sigma Aldrich	A1978
GAPDH	Mouse	Hu, Ms, Rt	-	WB	1:10000	Proteintech	60004-1
NIMP-R14	Rat	Ms	-	IHC	1:200	Abcam	Ab2557
F4/80	Rat	Ms	-	IHC	1:100	Abcam	Ab6640
iNOS	Rabbit	Ms, Rt	-	IHC	1:100	Abcam	Ab15323
Arginase-1	Rabbit	Hu, Ms	-	IHC, IF	1:500, 1:750	Novus	NBP1-54621
TSPO	Rabbit	Ms, Hu	-	IF, IHC	1:1000	Abcam	Ab109497
MR	Rabbit	Ms, Rt, Hu	-	IF	1:750	Abcam	Ab64693
MR*	Rat	Ms, Hu	-	IHC	1:5000	Martinez-Pomares Lab	Notts (5d3)
CD68	Rat	Ms, Hu	-	IF	1:1000	Martinez-Pomares Lab	Notts (FA11)
CD163	Mouse	Hu	-	IF	1:200	Biorad	MCA-1853
CD11b	Rat	Ms	BUV661	FACS	1:100	BD Biosciences	565080
CD25	Rat	Ms	BV421	FACS	1:100	BD Biosciences	564571
CD127	Rat	Ms	PE-CF594	FACS	1:100	BD Biosciences	562419
Ly6C	Rat	Ms	APC-Cy7	FACS	1:100	BioLegend	128026
Ly6G	Rat	Ms	AF-488	FACS	1:100	BioLegend	127625
CD45	Rat	Ms	APC-R700	FACS	1:100	BD Biosciences	565478
F4/80	Human	Ms	PE-Vio615	FACS	1:100	Miltenyi Biotec	130-107-709
iNOS	Rat	Ms	PERCP-eFlour 710	FACS	1:100	Invitrogen	46-5920-82
Arg1	Rat	Ms	PE-Cy7	FACS	1:100	Invitrogen	25-3967-82
Anti-rabbit	Goat	Rb	biotinylated	WB	1:5000	Abcam	Ab97051
Anti-mouse IgG	Goat	Ms	biotinylated	WB	1:2500	Abcam	Ab97040
Anti-rabbit IgG	Goat	Rb	biotinylated	IHC	1:200	Vector Labs	BA-1000
Anti-rat IgG	Goat	Rt	biotinylated	IHC	1:2000	Vector Labs	BA-9400
Anti-Mouse IgG	Goat	Ms	Alexa Flour 488	IF	1:1000	Invitrogen	A11001
Anti-Rat IgG	Goat	Rt	Alexa Fluor 488	IF	1:1000	Invitrogen	A-11006
Anti-Rabbit IgG	Goat	Rb	Alexa Flour 488	IF	1:1000	Invitrogen	A-11008

Table 2.7. List of RT-qPCR targets

Gene	Species	Forward	Reverse
TNF- α	Human	GGAGGACGAACATCCAACCTTCCC	GGTCCCACCCTAAGCCCCA
IL-1 β	Human	TGCACACATGGGATAACGAGGCT	TGAGTCCCGGCGCGTGCAGT
IL-6	Human	TGCAATAACCACCCCTGACC	GTGCCCATGCTACATTTGCC
IL-8	Human	TGGACCACACTGCGCCAACA	CCACAACCCTCTGCACCCAGT
IL-12	Human	TGCCTTCACCACTCCCAAAACC	CAATCTCTCAGAAGTGCAAGGG
TGF β	Human	TACCTGAACCCGTGTTGCTCTC	GTTGCTGAGGTATCGCCAGGAA
MR	Human	CGAGGAAGAGGTTCCGGTTCAC	GCAATCCCGGTTCTCATGGC
VEGF	Human	ATCTTCAAGCCATCTGTGTGC	GCTCACCGCTCGGCTTGT
Vimentin	Human	AGGAACCAATGAGTCCCTGG	ACGAGCCATTTCTCTCTTCA
MMP9	Human	GTACTCGACCTGTACCAGCG	AGAAGCCCCACTTCTTGTCG
SLUG	Human	TGGTTGCTTCAAGGACACAT	GTTGCAGTGAGGGCAAGAA
N-Cadherin	Human	CATCCAGACCGACCCAAACA	GGCACTTGATTTTCTGCAGC
E-Cadherin	Human	CGAGAGCTACACGTTACGG	GGGTGTCGAGGGAAAAATAGG
β -actin	Human	CTACAATGAGCTGCGTGTGG	CAACGTCACACTTCATGATGG
TNF- α	Mouse	agccacgctgtagcaaacaccaa	acaccattccctcacagagcaat
IL-1 β	Mouse	atggcaactgttctgaactcaact	caggacaggtatagattcttcttt
CXCL1	Mouse	cgcacgtgttgacgctccc	tcccgagcgagacgagacca
CXCR2	Mouse	caagtacactgatccagaagagaca	aaaggtttaccttaacaggattcg
CCL2	Mouse	cagctctcttctctccacc	gtgagtgggctgtaactg
TGF β	Mouse	tgacgtcactggagttgtacgg	ggtcatgtcatggatggtgc
VEGF	Mouse	ggagatcctcgaggagcactt	ggcgatttagcagcagatataagaa
β -actin	Mouse	ccaacttgatgatgaaggctttg	attggtctcaagtcaggtacagge

Chapter 3: Genetic *in vivo* hyperactivation of ERK5 in keratinocytes drives local inflammation in wound healing

ERK5 is known to regulate tumour progression and the associated inflammation, thus we wanted to investigate how ERK5 signalling is involved in wound healing. Loss of ERK5 can be embryonic lethal, as it is essential for early murine development (Nithianandarajah-Jones *et al.*, 2012). In order to investigate how inactivation of ERK5 in the skin affects wound healing and the associated local inflammation, we used a mouse model where the ERK5 (*mapk7*) gene was modified with flanking LoxP sites and a mutated oestrogen receptor fused with Cre (CreER) under the control of the keratin 14 (K14) promoter. Compared to the total ERK5 knockout models used by Hayashi *et al.*, this study utilised a genetic model where we could spatially and temporally induce ERK5 inactivation. This was achieved following five days of intraperitoneal injection with tamoxifen which led to ERK5 deletion in basal keratinocytes. Mice were housed for at least a further two weeks before experimental wounding to permit normal skin regeneration in order for ERK5 inactivated basal keratinocytes to replace all the epidermal cells. Additionally, this ensured that no confounding factors from tamoxifen and oestrogen-mediated effects would impact the wound healing process. This mouse model, K14CreER;ERK5 has been shortened to ERK5KO to represent ERK5 keratinocyte specific knockout mice (Finegan *et al.*, 2015).

Conversely, to investigate how hyperactivation of ERK5 in the skin affects wound healing and inflammation, we used another novel mouse model where a STOP codon was flanked by LoxP sites in front of a constitutive active (ca) mutant MEK5 allele, with the inducible form of Cre as above (CreER), under the control of K14 promoter. This induced constitutive activation of MEK5 in the epidermis following intraperitoneal injection with tamoxifen, as previously described, and were housed for at least a further two before experimental wounding. MEK5 is

the upstream kinase of ERK5 in the MAPK pathway, and its constitutively active state in the murine model hyperactivates the endogenous ERK5 in these basal keratinocytes. This mouse model, K14CreER-caMEK5, was shortened to CaMEK5 to represent an epidermal constitutively active MEK5 mouse, which subsequently leads to hyperactivation of ERK5 in the keratinocytes (generated in-house by Dr Blanca Risa).

As summarised previously in chapter 1, one of the first hypotheses was that hyperactivation of ERK5 may contribute to chronic inflammation that disrupts wound healing. Conversely, inactivation of ERK5 would reduce inflammation. Previous work from the Finegan and Mace Labs have conducted wound healing studies until full wound closure using the ERK5KO mice and exhibited improved wound healing, and altered immune profile (Figure 1.8). Therefore our research focused on looking at the earlier phase of wound healing, and how the immune landscape in the first seven days post-wounding may be driving the observed changes in wound closure in these genetically engineered models.

3.1 Genetic ERK5 modification had no effect on wound closure

We verified the ERK5 profile in the epidermis of the mice, by ERK5 specific histology of control, ERK5KO and CaMEK5 mice (Figure 3.1.A). Immunostaining of the gamma and beta regions of the skin sections with an ERK5 antibody confirmed that ERK5 was absent in ERK5KO mice keratinocyte layer. This was compared to the keratinocyte of control mice, and the rest of the non-K14 expressing murine tissue which expressed ERK5 at comparably normal levels, which was explored further in Figure 3.5. ERK5 staining appeared to be slightly upregulated in CaMEK5 keratinocytes when compared to control mice and non-K14 expressing tissue. However, this may in fact be an artefact of the increased nuclear localisation of ERK5 in the keratinocytes of CaMEK5 mice, as a consequence of the hyperactivated state of ERK5. Although, it should be noted that MEK5 mediated phosphorylation of ERK5 often

initiates nuclear localisation of the ERK5 protein, but not exclusively. It is additionally possible that the hyperactive state of ERK5 is more stable and may manifest itself in the appearance of increased levels of ERK5 across the cytoplasm of the cell.

It was also noted that complete ERK5 ablation from the epidermal layer of ERK5KO mice would be impossible. Hair follicles are another structurally important element of the epidermal layer as a key source of cellular regeneration (Sieber-Blum, 2011). However, the follicular bulge expresses cytokeratin 15 (K15) as the prominent marker, as opposed to K14, and so there was residual expression of ERK5 in these hair follicle epidermal regions (Figure 3.1.A, black triangle) which could both influence the ERK5 mediated effects in the wounded skin and provide a source of ERK5 positive keratinocytes to regenerate the epidermal layer.

All wounds exhibited a similar trend in wound closure where they increased by day 2 or 4 and decreased by day 7. This initial increase in wound size is typical of cutaneous excisional model. Control and ERK5KO wounds were largest at day 2, whereas CaMEK5 wounds were largest at day 4. Otherwise, there was no discernible difference in the rate of wound healing between control, ERK5KO and CaMEK5 mice (Figure 3.1.B).

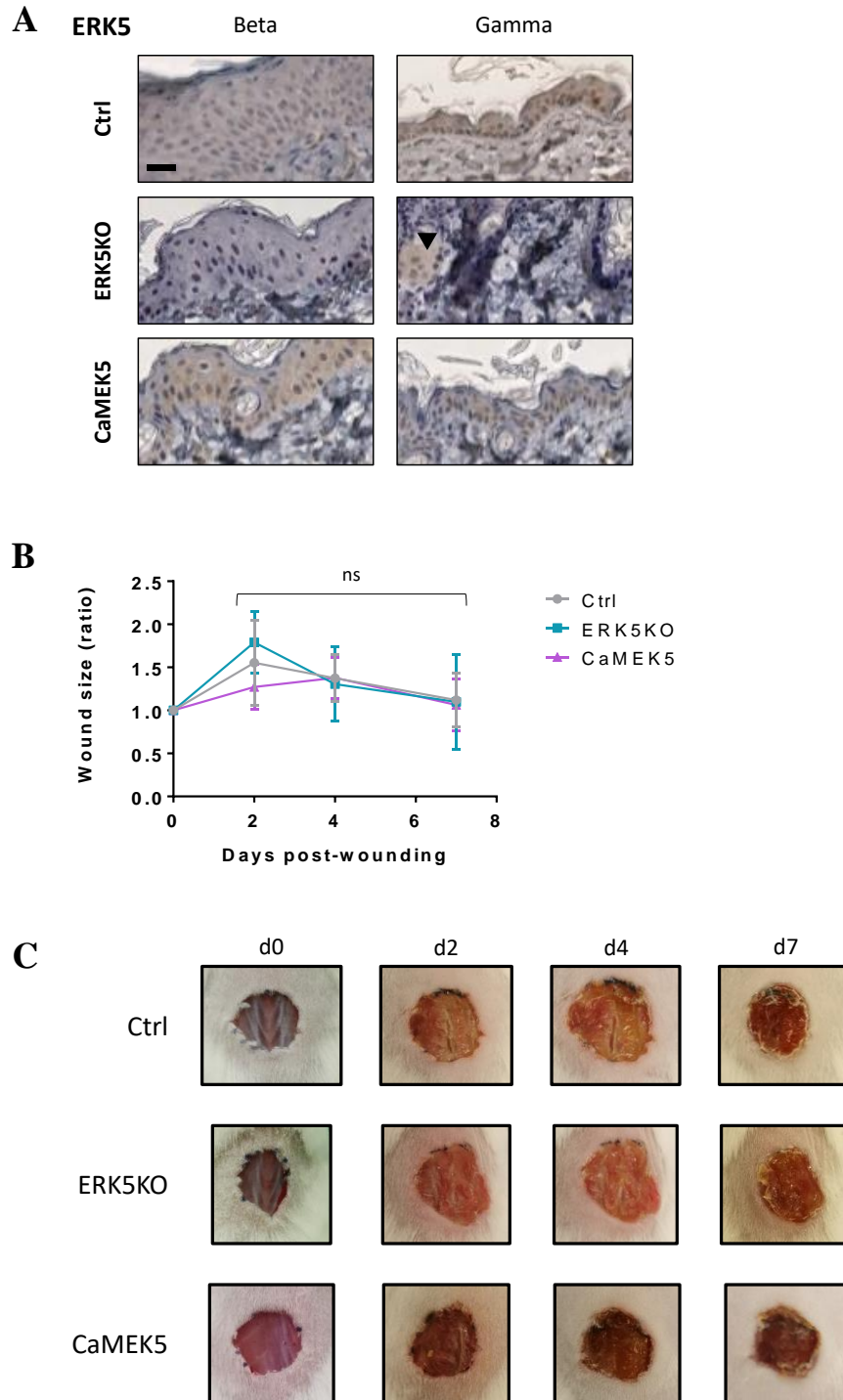


Figure 3.1. Genetic ERK5 modification had no effect on wound closure. Adult ERK5KO or CaMEK5 mice (Cre positive and negative) were induced following intraperitoneal tamoxifen injections to generate ERK5 inactivated or constitutively active MEK5 keratinocytes and compared to control animals. (A) Specific inactivation or hyperactivation in the epidermis of mice was confirmed by immunohistochemistry of wounded skin sections using ERK5 antibodies (brown). Slides were counterstained with Harris Haematoxylin. Black bar = 20 μ M. Black triangle = follicular bulge. (B) Wounds were imaged and the area calculated on ImageJ to quantify the wound closure. Data points plotted represent the mean of multiple different mice \pm SD (d0 = 12, d2 = 12, d4 = 8, d7 = 4). (C) Representative images of wounds in Ctrl, ERK5KO and CaMEK5 mice. (ns = $P > 0.05$, * = $P < 0.05$).

3.2 H&E analysis show that genetic ERK5 modification in keratinocytes did not influence wound architecture or immune response

To delineate the dynamic immune response of the wound healing process, the immune cell population in the wounds over various time points were analysed by flow cytometry and immunohistochemistry. There are various immunological cell types that are crucial and influential in the process, development and persistence of wound healing. Typically, neutrophils are observed as early inflammatory cells, which attract and are then engulfed by incoming monocytes and macrophages. This cascading inflammatory milieu can influence macrophages towards a repair phenotype to stimulate healing and granulation to occur (Ellis, Lin and Tartar, 2018).

Initially we assessed the wound architecture and profile by H&E and observed that inactivation and hyperactivation of ERK5 lead to no obvious physical changes, which was concordant with previous research (Finegan *et al.*, 2015). This reiterates that the genetic model system of K14CreER present no overt physical phenotypes that may impede our investigations into the relationship between ERK5 and wound healing. Initial H&E analysis show there were no difference in immune infiltrates in ERK5KO or CaMEK5 epidermis compared to control (Figure 3.2.A and B). Our analysis was limited to comparison of day 0, 2 and 4 as they are early time points associated with most abundance of inflammatory immune cells.

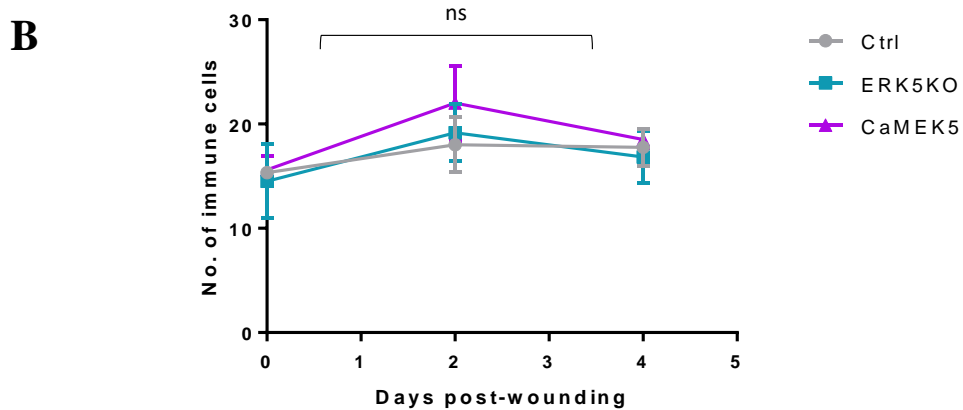
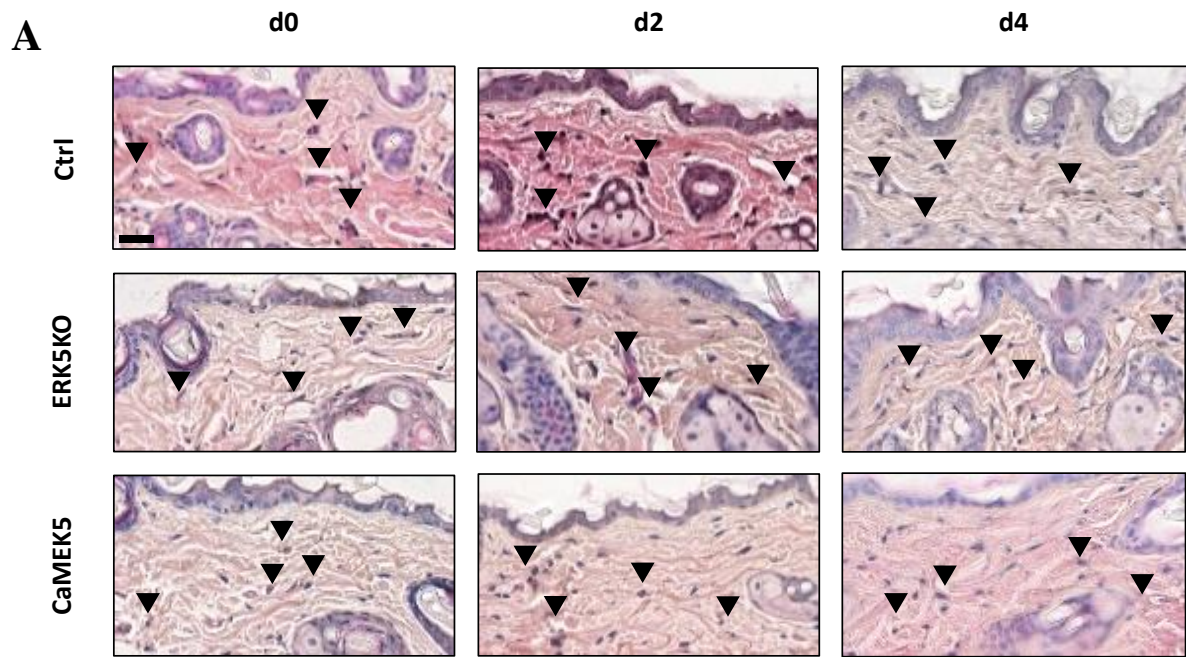


Figure 3.2. Genetic ERK5 modification had no impact on immune infiltration by H&E. (A) Representative H&E images where staining indicates that ERK5 inactivation and hyperactivation had no effect on the architecture of the skin. Further, there was no significant difference in the number of immune infiltrates across ERK5KO, CaMEK5 and control skin at d0 (n=12), d2 (n=4) and d4 (n=4). Black triangles represent site of haematopoietic or immune cells. Black bar = 20µm. (B) Mean number of immune cell infiltrates per mm² in H&E stains. (ns = P>0.05, *=<0.05).

3.3 FACS analysis show that genetic ERK5 modification did not significantly influence immune response

Flow cytometry was used to investigate the immune cell populations in the wounds over various time points: day 0, 2, 4, and 7. Single cell suspensions were collected from the wound tissue and subjected to FACS and gated as shown in (Figure 3.3.A). Immune cell populations were expressed as a percentage of the total cell population collected, and the remaining cells were categorised as “other”.

The number and percentage distribution of immune cells such as granulocytes increased and peaked from day 0 (14.8%) to day 2 (67.4%) in control mice. This was followed by a large decrease on day 4 (28.4%) and more so on day 7 (5.9%) (Figure 3.3.B). This is the typical trend expected as an influx of inflammatory cells were expected by day 2 to deal with potential pathogens and opportunistic dangers arriving in the open wound (Eming, Martin and Tomic-Canic, 2014). By further distinguishing the immune population to neutrophils, macrophages and monocytes, a similar pattern was observed (Figure 3.3.C). And it was notably clear that the dominant population was neutrophils (Ly6G+), particularly on day 2 (52.9%) and day 4 (17.1%).

However there were no significant differences in percentage distribution of various immune cell populations such as macrophages, monocytes, neutrophils and lymphocytes, between the control, ERK5KO, and CaMEK5 mice across the four time points.

Control and ERK5KO mice exhibited a similar trend in profile of increasing neutrophils between day 0 (8.9% vs 10.8%) and day 2 (52.9% vs 57.0%), followed by a decrease, where it was lowest by day 7 (2.9% vs 2.4%). However, CaMEK5 mice at day 2 (14.5%) had low levels of neutrophils, compared to the pattern observed in control and ERK5KO mice (52.9% vs 57.0%) (Figure 3.3.D).

The macrophage population remained largely unchanged between control and ERK5KO mice where they increased from day 0 (2.7% vs 2.0%) to day 2 (3.8% vs 3.9%). Whereas in CaMEK5 mice there was more at day 0 (5.9%) and then reduced by day 2 (1.6%). Following onto day 4, their numbers increased in control (6.3%) and CaMEK5 (2.7%), but fell in ERK5KO (2.0%). And by day 7, all three showed decreased numbers of macrophages but highest in control (2.0%) when compared to ERK5KO (0.8%) and CaMEK5 (1.1%) (Figure 3.3.D).

Likewise, the monocyte population followed a similar pattern in control mice where they increased from day 0 (0.77%) to day 2 (5.98%), before decreasing on day 4 (0.37%) and day 7 (0.1%). ERK5KO and CaMEK5 mice exhibited an almost identical pattern for the monocyte population. The only notable difference, was a reduced population of monocytes at day 2 in the CaMEK5 mice (1.1%).

This study demonstrated the typical pattern of immune cell influx during wound healing of increased neutrophils at early stages, followed by the arrival of macrophages. However, there was minimal difference between the experimental groups. Therefore, modifying ERK5 in the keratinocytes to be hyperactivated or ablated did little to influence the immune cell population in the cutaneous wound site by FACS analysis.

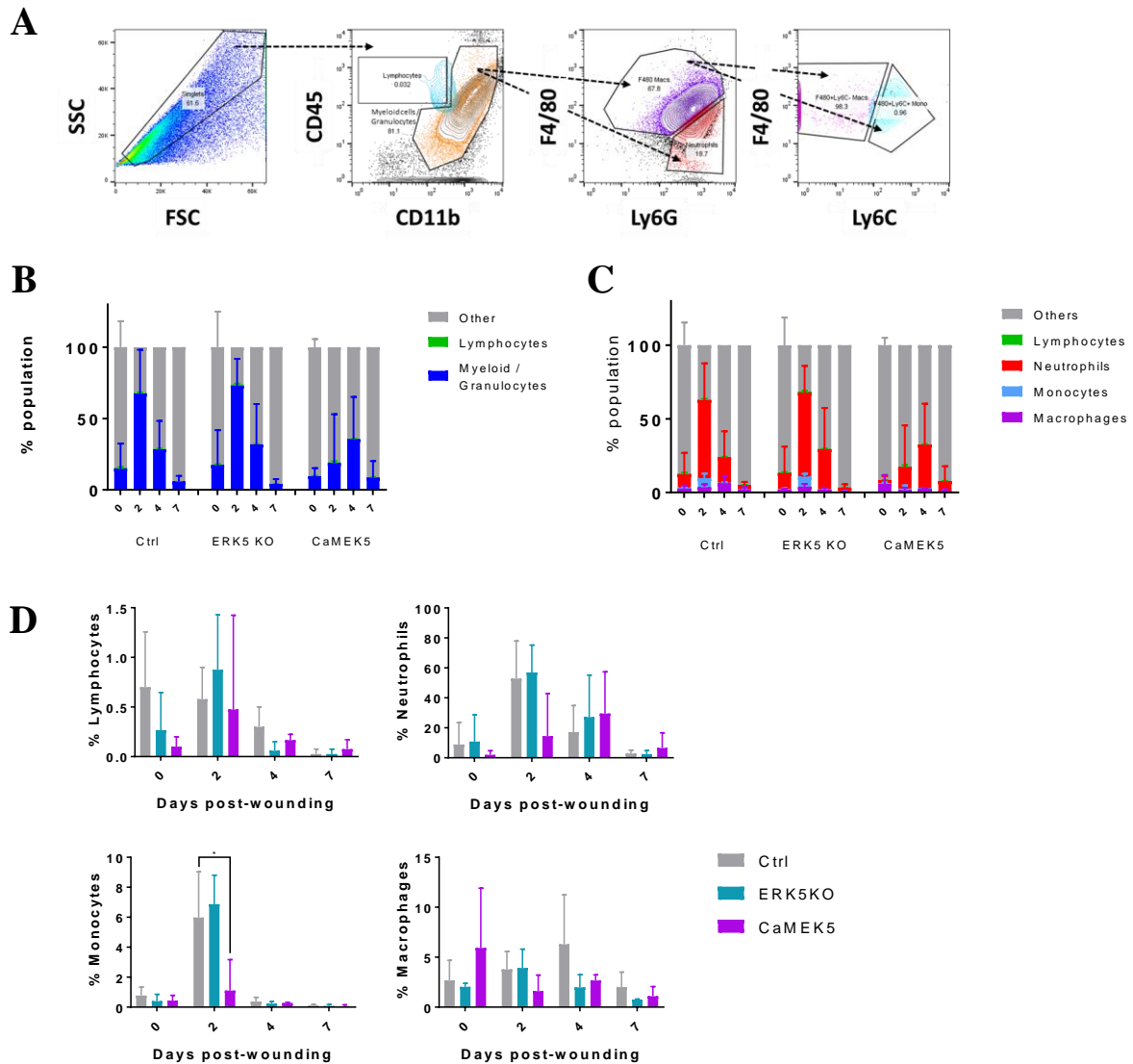


Figure 3.3. Genetic ERK5 modification did not significantly influence immune profile according to flow cytometry analysis. Various populations of immune cells were quantitatively evaluated in wound tissue collected at day 0, 2, 4, and 7 by flow cytometry. (A) Representative flow cytometry plots of the gating strategy. Live cells were gated according to size and granularity. Lymphocytes and myeloid/granulocytes were distinguished according to CD45 and CD11b expression. Macrophages and neutrophils were identified from the myeloid/granulocyte population based on their expression of F4/80 and Ly6G. Monocytes were further distinguished from the macrophage population according to their expression of F4/80 and Ly6C. (B) Quantified population distribution of lymphocytes, granulocytes and other cells in control, ERK5KO and CaMEK5 wounds on day 0, 2, 4 and 7, as a percentage of total cells. (C) Quantified population distribution of macrophages, monocytes, neutrophils and lymphocytes in control (n=12), ERK5KO (n=12) and CaMEK5 (n=12) wounds on day 0, 2, 4, and 7, as a percentage of total cells. (D) Separated graphs indicating the percentage population distribution of lymphocytes, neutrophils, monocytes and macrophages. (ns= $P > 0.05$, *= $P < 0.05$).

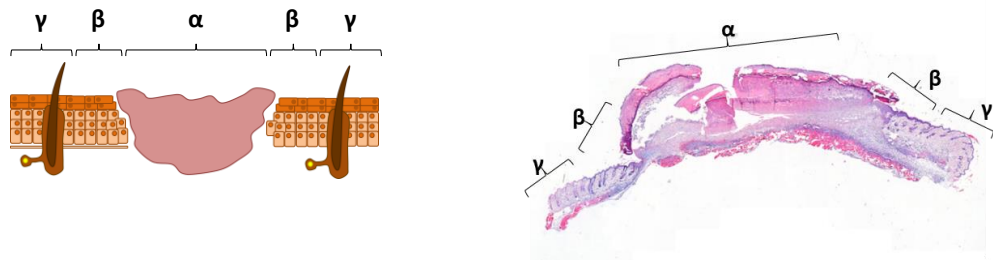
3.4 Assessing changes to immune response in genetic ERK5 modification by histology

Wounded tissue excised from mice was assessed by histology for macrophages (F4/80), neutrophils (NIMP-R14), M1-like polarity (iNOS), M2-like polarity (Arg1), collagen (Picrosirius red) and ERK5 expression. F4/80 is a well-established and robust marker for mature murine macrophages. These include a range of tissue-resident macrophages: Langerhans cells, Kupffer cells, peritoneal macrophages and microglia (Gordon, Plüddemann and Martinez Estrada, 2014; Bio-Rad Laboratories Inc., 2015). NIMP-R14, collectively represents murine Ly6G and Ly6C and is utilised as a consistent marker for granulocyte differentiation and neutrophils. Additionally, its therapeutic use induces neutropenia *in vivo* to inhibit inflammation (Stackowicz, Jönsson and Reber, 2020).

As previously mentioned in chapter 1, delineating M1-like and M2-like macrophages can be a difficult process. Here we focused on using the established differentiation of nitric oxide activity in murine macrophages by categorising M1-like macrophages with iNOS, and M2-like macrophages with Arg1. Inflammatory macrophages often use nitric oxide to kill bacterium, whereas reparative macrophages utilises arginase-1 in fibrosis and immune suppression (Gordon, Plüddemann and Martinez Estrada, 2014; Orecchioni *et al.*, 2019). The caveat remains that this is a simplified notion to identify macrophages into two discrete populations. Additionally, these are all established markers only for murine immune cells, and are not completely translatable to the human system.

IHC on the three regions of the wound; alpha (centre of wound), beta (wound-edge) and gamma (healthy skin) (Figure 3.4.A), was semi-quantitatively assessed and scored out of three (zero = negative, one = low, two = positive, three = high positive), as in (Figure 3.4.B).

A



B

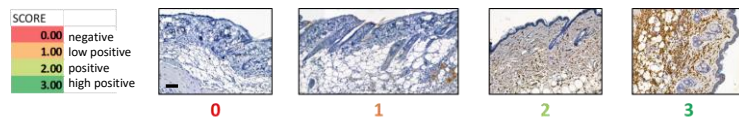


Figure 3.4. Method to assess changes to immune response in genetic ERK5 modification by histology. (A) Wound schematic depicting the three regions of the wound: alpha (α), beta (β), and gamma (γ). (B) Representative images of the scoring system of immunohistochemistry staining intensity: (0) = negative, (1) = low positive, (2) = positive, and (3) = high positive. Black bar = 50 μ m.

3.4.1 ERK5 expression is lower throughout the wound region in ERK5KO but similar in CaMEK5 murine models when compared to control

We have demonstrated that our genetic murine model can successfully inactivate or hyperactivate ERK5 in the keratinocyte layer of wounds after tamoxifen induction (Figure 3.1.A). However, it remained important to assess the levels of ERK5 expression across the whole wound region to understand how ERK5 modulation in the epidermis can influence the expression of this protein in the local microenvironment. It has been shown that genetic inactivation within the keratinocytes, can have proximal changes in ERK5 in immune cells in the skin that drives tumorigenesis (Finegan *et al.*, 2015). These are driven by paracrine signalling from neighbouring cells whereby the loss of ERK5 in the keratinocytes results in a modified transcriptional landscape and downstream mediator production of inflammatory and growth factors, IL-1 β , IL-6, IL-8, VEGF, and FGF (Stecca and Rovida, 2019). Assessing the full wound and immune environment for ERK5 expression provides an insight into whether the ERK5 signal has diffused across a gradient due to genetic epidermal modification. Moreover, various studies along this theme again show the significance of ERK5 in the myeloid lineage and in generating inflammatory macrophages that are anti-tumour (Giurisato *et al.*, 2018; Luiz *et al.*, 2020).

In control mice, ERK5 expression increased slightly after wounding, and was moderately observed from day 2 to day 7 across all three wound regions (Figure 3.5.A). ERK5KO mice exhibited slightly lower ERK5 expression across the whole wound environment in day 2 (Ctrl - α 1.25, β 1.56, γ 0.92 vs ERK5KO - α 0.33, β 0.56, γ 0.56) and day 4 (Ctrl - α 1.50, β 1.17, γ 1.00 vs ERK5KO - α 1.00, β 0.80, γ 0.73) compared to control mice (Figure 3.5.C). It should be considered, this is a stark contrast to the overt loss of ERK5 expression observed in Figure 3.1.A, where analysis was focussed on the keratinocyte layer. Data from the whole wound ERK5 staining here, indicates that ERK5 inactivation in this specific epidermal layer had a

limited effect on the ERK5 expression on the rest of the compartments in the cutaneous wound environment.

CaMEK5 mice exhibited similar profiles of ERK5 expression compared to control, but was slightly lower in day 4 (Ctrl - α 1.50, β 1.17, γ 1.00 vs α CaMEK5 - 0.89, β 0.44, γ 1.00) (Figure 3.5.C). The similarity in the profile despite the genetic modification of ERK5 activity in the keratinocyte suggests that hyperactivation of ERK5 in the keratinocyte does not have a substantial proximal effect on ERK5 expression of the other regions of the skin and cutaneous wound site within the days investigated (day 0, 2, 4, and 7 post-wounding).

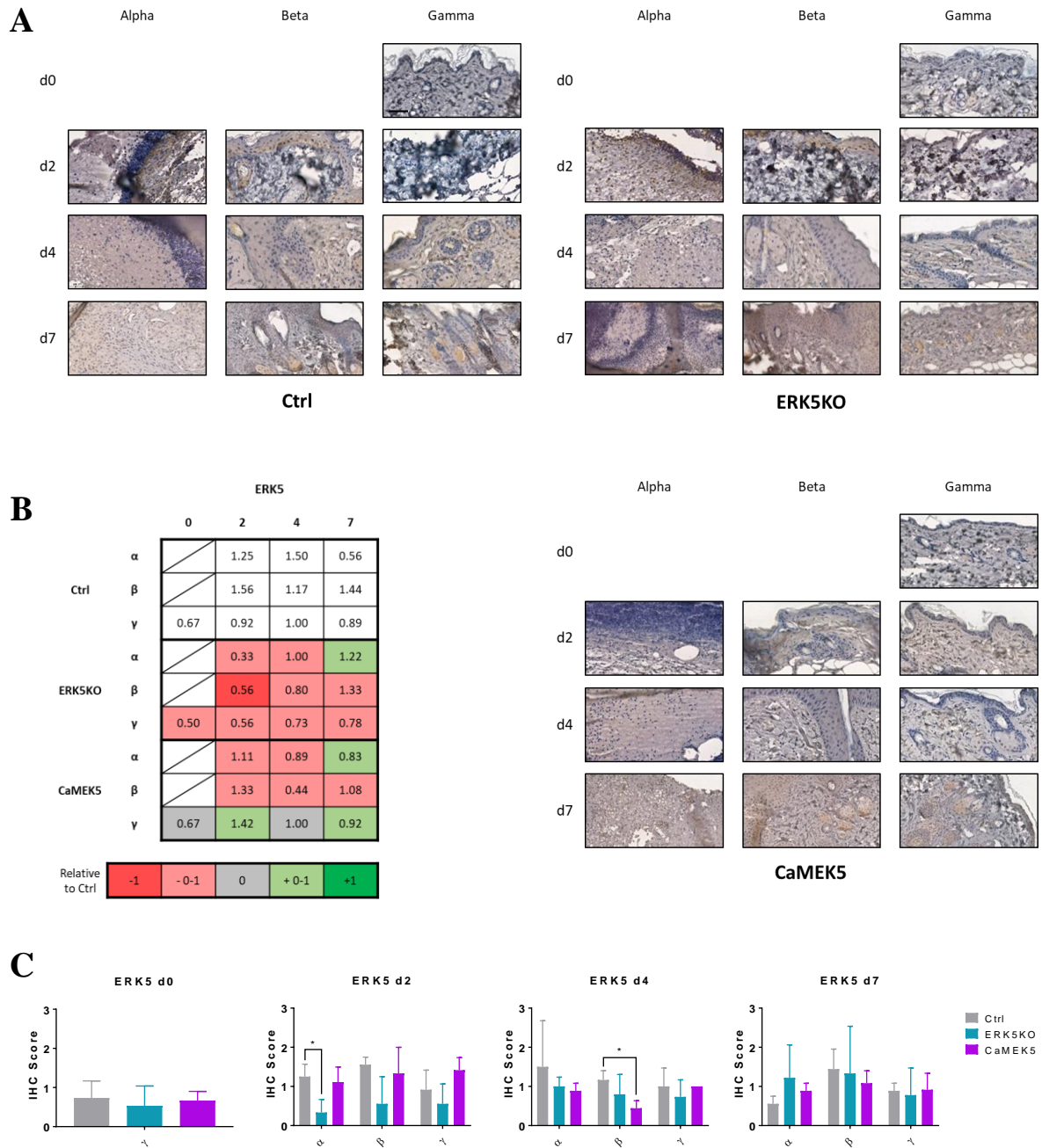


Figure 3.5. ERK5 was lower in ERK5KO wounds but similar in CaMEK5 wounds as determined by immunohistochemistry analysis. (A) Representative images of ERK5 staining in the wounds of control, ERK5KO and CaMEK5 mice. Black bar = 20µm. (B) Table of the quantified scoring analysis of ERK5 staining. Grey = 0. Light red/green = ± 0.1. Dark red/green = ± 1. (C) Graphs of quantified scoring analysis of ERK5 staining in control, ERK5KO and CaMEK5 mice over the wound healing time course at d0 (n=12), d2 (n=4), d4 (n=4) and d7 (n=4). (ns=P>0.05, *=P<0.05).

3.4.2 Neutrophils are more abundant in both ERK5KO and CaMEK5 murine models

NIMP-R14 expression peaked at day 2, particularly in the alpha region (1.67), which decreased by day 4 (α 0.78, β 0.89, γ 0.44) and day 7 (α 1.11, β 0.22, γ 0.00) in control mice (Figure 3.6.A). This is typical of neutrophil migration during the early stages of inflammation in wound healing, followed by their departure as the wound area closes. Interestingly, both loss and overexpression of ERK5 in the keratinocyte led to a consistent and slight increased expression of NIMP-R14 in the alpha (ERK5KO - d2 1.22, d4 2.07, d7 1.89; CaMEK5 - d2 1.89, d4 1.67, d7 1.88) and beta (ERK5KO - d2 1.22, d4 1.20, d7 0.56; CaMEK5 - d2 1.89, d4 1.11, d7 0.56) regions of the wound (Figure 3.6.C). Therefore, modification of ERK5 expression to inactivate or hyperactivate could influence how and when neutrophils enter the wound site.

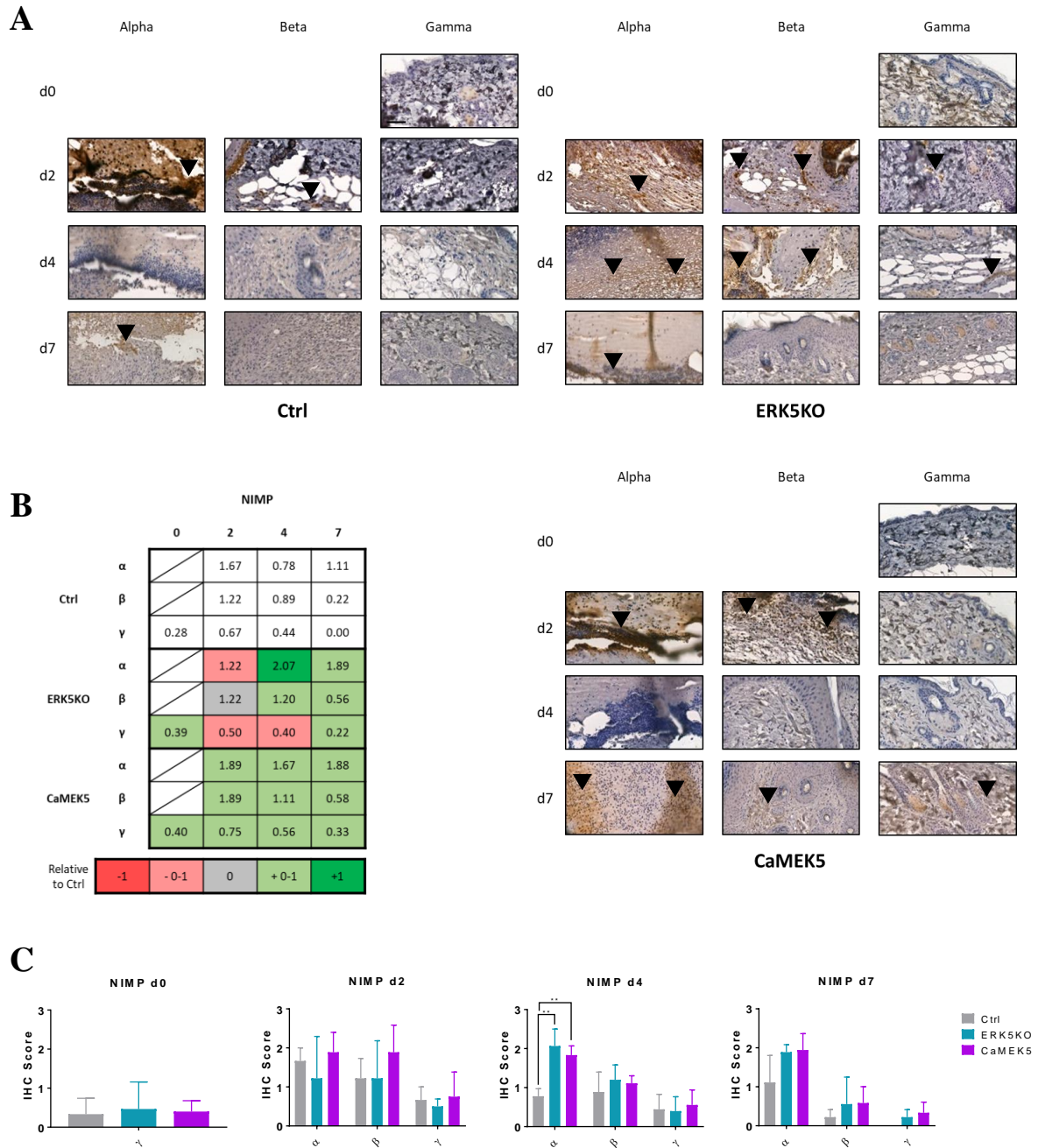


Figure 3.6. Neutrophils were more abundant in both ERK5KO and CaMEK5 wounds as determined by immunohistochemistry analysis. (A) Representative images of NIMP-R14 staining in the wounds of control, ERK5KO and CaMEK5 mice. Black bar = 20µm. Black triangles indicate sites of positive NIMP-R14 staining. (B) Table of the quantified scoring analysis of NIMP-R14 staining. Grey = 0. Light red/green = ± 0.1. Dark red/green = ± 1. (C) Graphs of quantified scoring analysis of NIMP-R14 staining in control, ERK5KO and CaMEK5 mice over the wound healing time course at d0 (n=12), d2 (n=4), d4 (n=4) and d7 (n=4). (ns=P>0.05, *=P<0.05, **=P<0.01).

3.4.3 F4/80 macrophage profiles are similar in both ERK5KO and CaMEK5 murine models when compared to control

F4/80 macrophages remained largely consistent across day 0 (γ 1.44), day 2 (α 1.78, β 1.39, γ 1.44) and day 4 (α 1.67, β 1.44, γ 1.11) in control mice, with most in the alpha region (Figure 3.7.A). Macrophages were found to be most abundant on day 7 (α 2.22, β 2.67, γ 1.89) in control mice. ERK5KO mice had a similar profile to control mice with the exception of day 2 where there were fewer macrophages in the alpha region (1.78 vs 1.25) but more macrophages in the beta (1.39 vs 1.67) and gamma regions (1.44 vs 1.83). Our results also reveal that CaMEK5 mice had a similar pattern of macrophages in day 0, day 2 and day 4. However, there were fewer F4/80 macrophages on day 7 (Ctrl - α 2.22, β 2.67, γ 1.89 vs CaMEK5 - α 1.92, β 1.79, γ 1.33) when compared to control mice (Figure 3.7.C).

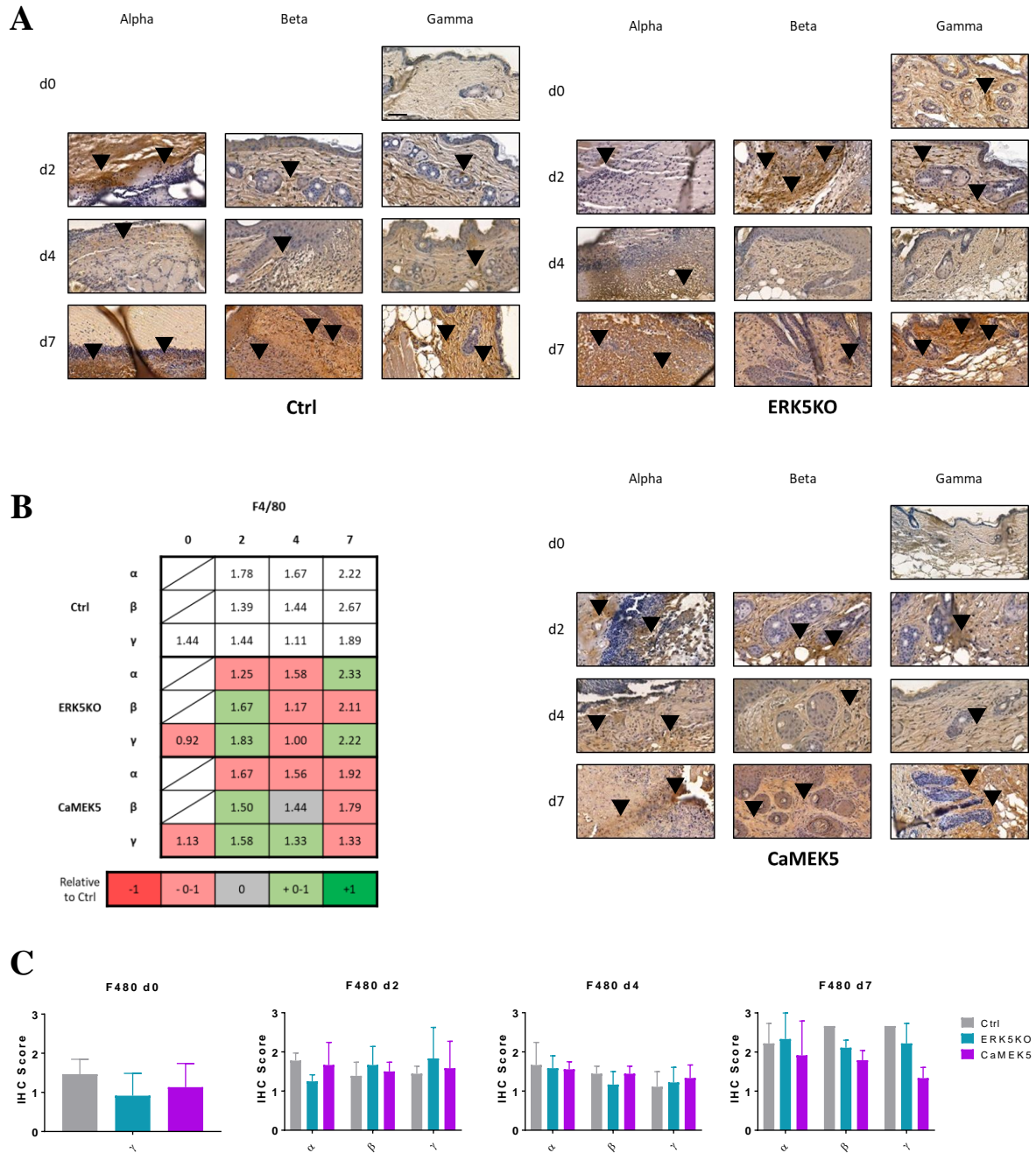


Figure 3.7. Macrophage presence is unchanged in both ERK5KO and CaMEK5 wounds as determined by immunohistochemistry analysis. (A) Representative images of F4/80 staining in the wounds of control, ERK5KO and CaMEK5 mice. Black bar = 20 μ m. Black triangles indicate sites of positive F4/80 staining. (B) Table of the quantified scoring analysis of F4/80 staining. Grey = 0. Light red/green = \pm 0-1. Dark red/green = \pm 1. (C) Graphs of quantified scoring analysis of F4/80 staining in control, ERK5KO and CaMEK5 mice over the wound healing time course at d0 (n=12), d2 (n=4), d4 (n=4) and d7 (n=4). (ns=P>0.05, *=-P<0.05).

3.4.4 iNOS expression levels was lower in ERK5KO and persisted in CaMEK5 murine models

In an attempt to delineate the polarity state of macrophages throughout the wound healing process, our study aimed to distinguish M1- and M2-like macrophages with iNOS and Arg1 as markers of an inflammatory and reparative state, respectively.

Nitric oxide synthase (iNOS) is a catalytic enzyme that mediates the production of nitric oxide, which is expressed by inflammatory macrophages. It should be noted, that iNOS can be expressed on multiple other cell types including keratinocytes, skeletal muscle cells, myocytes, and fibroblasts. Interestingly, a study in aging related inflammation found that increased ERK5 activity in skeletal muscle cells led to peroxisome proliferator-activated receptor (PPAR) stimulation and the subsequent inhibition of iNOS expression (Woo *et al.*, 2006). An additional caveat to note, iNOS has been observed to be induced in keratinocytes, endothelial cells and fibroblasts. This was in relation to homeostatic functions and maintenance of barrier functions (Luo and Chen, 2005). The inflammatory microenvironment of psoriatic plaque lesions with increased IL-1 β and TNF- α can stimulate human keratinocytes to upregulate their gene expression of iNOS (Sirsjö *et al.*, 1996).

However, the majority of studies investigate the murine macrophage expression of iNOS in response to LPS and inflammatory cytokines such as IL-1 β , IL-6 and TNF- α . A wide range of signalling pathways have been studied that influence iNOS expression including PPAR, STAT, Protein Kinase A/C, Suppressor of Cytokine Signalling (SOCS) and MAPKs (Kleinert, Schwarz and Förstermann, 2003). In particular, in the context of murine wound healing, iNOS is regularly utilised as a tool to identify M1-like macrophages in the cutaneous wound environment (Gordon, Plüddemann and Martinez Estrada, 2014; Koo *et al.*, 2019).

However, although iNOS is expressed in human macrophages, they do not over-express it to the same inflammatory stimuli of LPS or IFN γ . Taking all this into account, iNOS can be confidently utilised to assess inflammatory murine macrophages, and wider as a measure of the inflammatory context in the cutaneous wound.

iNOS was relatively low in expression across all regions and all time points in control mice, where it peaked in day 4 (α 0.89, β 0.67, γ 0.56) (Figure 3.8.A). Notably, ERK5KO mice had higher iNOS expression in day 2 (Ctrl - α 0.78, β 0.33, γ 0.44 vs ERK5KO - α 1.22, β 1.67, γ 0.78) which then diminished to comparable levels to control mice in the remaining days post-wounding. Whereas, interestingly iNOS expression persisted in CaMEK5 mice up to day 7 (Ctrl - α 0.22, β 0.22, γ 0.00 vs CaMEK5 - α 0.92, β 0.58, γ 0.25) when compared to control (Figure 3.8.C). In the earliest time point of day 2 in control and ERK5KO mice, it was noted that iNOS expression was present in the epidermal site of the gamma, non-wounded, normal skin region (Figure 3.8.A). This upregulated iNOS expression may be due to proximal inflammatory signalling from the adjacent wound regions at these early time points, i.e. primary inflammatory effects in the central alpha wound region having secondary effects on the proximal gamma, non-wounded region.

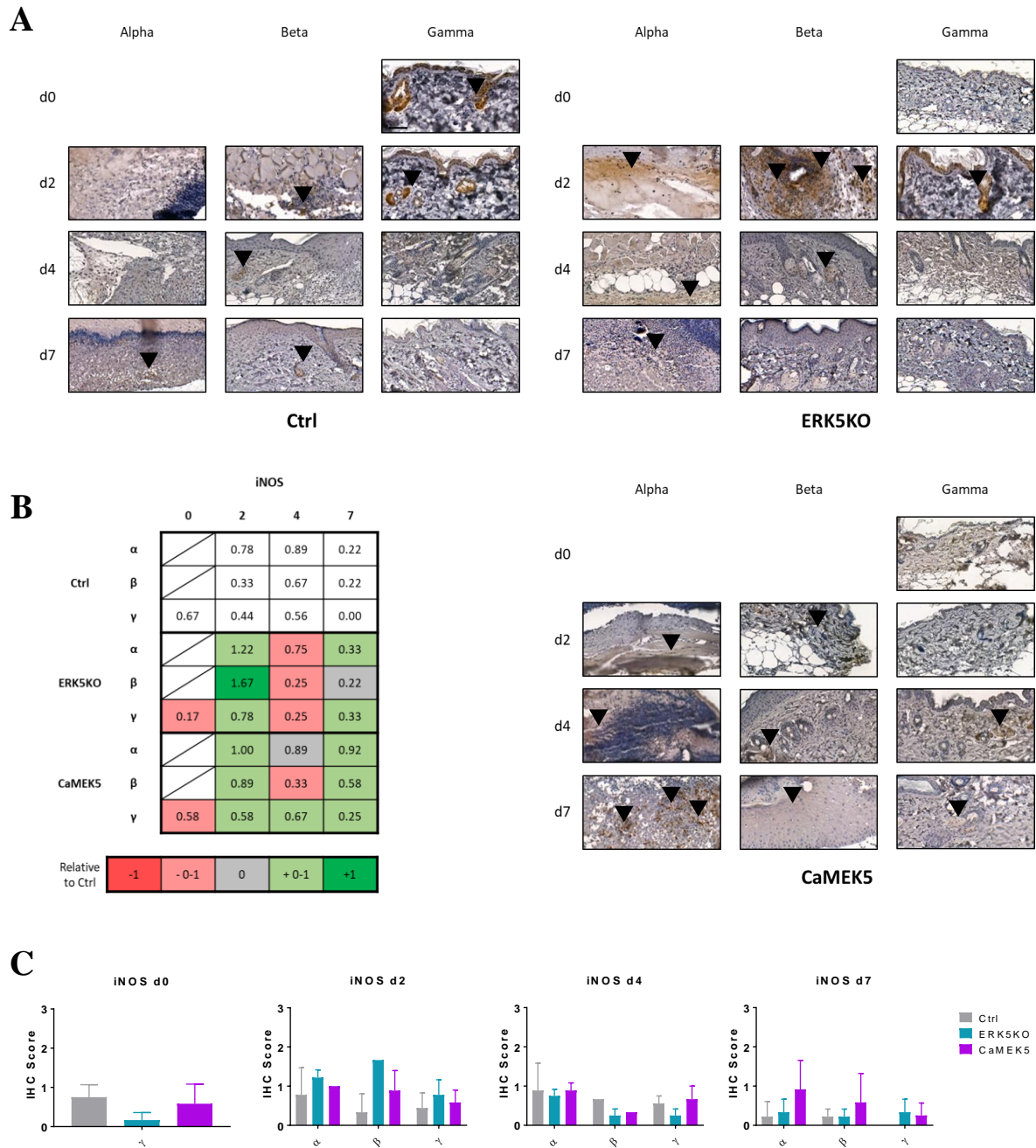


Figure 3.8. iNOS expression decreased in ERK5KO but persisted in CaMEK5 wounds as determined by immunohistochemistry analysis. (A) Representative images of iNOS staining in the wounds of control, ERK5KO and CaMEK5 mice. Black bar = 20µm. Black triangles indicate sites of positive iNOS staining. (B) Table of the quantified scoring analysis of iNOS staining. Grey = 0. Light red/green = ± 0-1. Dark red/green = ± 1. (C) Graphs of quantified scoring analysis of iNOS staining in control, ERK5KO and CaMEK5 mice over the wound healing time course at d0 (n=12), d2 (n=4), d4 (n=4) and d7 (n=4). (ns=P>0.05, *=P<0.05).

3.4.5 Arg1 expression profile was similar in both ERK5KO and CaMEK5 murine models

Type-I arginase (Arg1) is upregulated in M2-like murine macrophages in the context of a repair response (Yang and Ming, 2014; Krzyszczyk *et al.*, 2018). In mice, Arg1 transcription can be induced by TGF- β through IL-4 and STAT6 mediated signalling, as is typical of reparative macrophage polarisation. Arg1 is an enzyme that metabolises L-arginine to produce polyamines and L-proline which are used for cell proliferation, fibrosis and collagen associated tissue repair.

Additionally, Arg1 metabolism of L-arginine can inhibit L-arginine dependent immune functions of CD4⁺ T-cells and inflammatory macrophages. It is widely accepted that Arg1 in M2-like macrophages consume L-arginine, depriving iNOS from M1-like macrophages of its substrate and downregulating nitric oxide production used for microbial killing and inflammation. However, increasing the abundance of L-arginine into the environment is not enough to shift polarity towards M1-like iNOS expressing macrophages. The nitric oxide activity in M1-like macrophages is dependent on their expression of iNOS and the inflammatory context that stimulates this. Equally, Arg1 expression in M2-like macrophages is driven by the reparative and tissue healing context (Roszer, 2015).

Arg1 is known to be expressed in multiple cells types including keratinocytes, fibroblasts, hepatic cells and myeloid derived suppressor cells. And similarly to iNOS, Arg1 is not a biologically relevant marker of human repair mechanisms. However, Arg1 is associated with M2-like macrophages in murine models, where genetic studies found that ablation of Arg1 led to impaired healing, reduction in re-epithelisation, reduced collagen deposition and increased influx of neutrophils and M1-like macrophages (Campbell *et al.*, 2013).

Arg1 expression was consistently highly expressed in control mice across the time course, particularly in the alpha (d2 1.67, d4, 1.33, d7 2.33) and beta (d2 1.67, d4 1.78, d7 3.00) regions

(Figure 3.9.A). Notably, its expression in the keratinocyte and epidermal layer was higher than originally anticipated. The profile in both ERK5KO and CaMEK5 were largely indistinguishable from the control mice, and followed the same pattern and expression levels (Figure 3.9.C). This suggests that modification of ERK5 by inactivation and hyperactivation had little to no impact on proximal effects towards a reparative environment mediated by Arg1 compared to control cutaneous wounds.

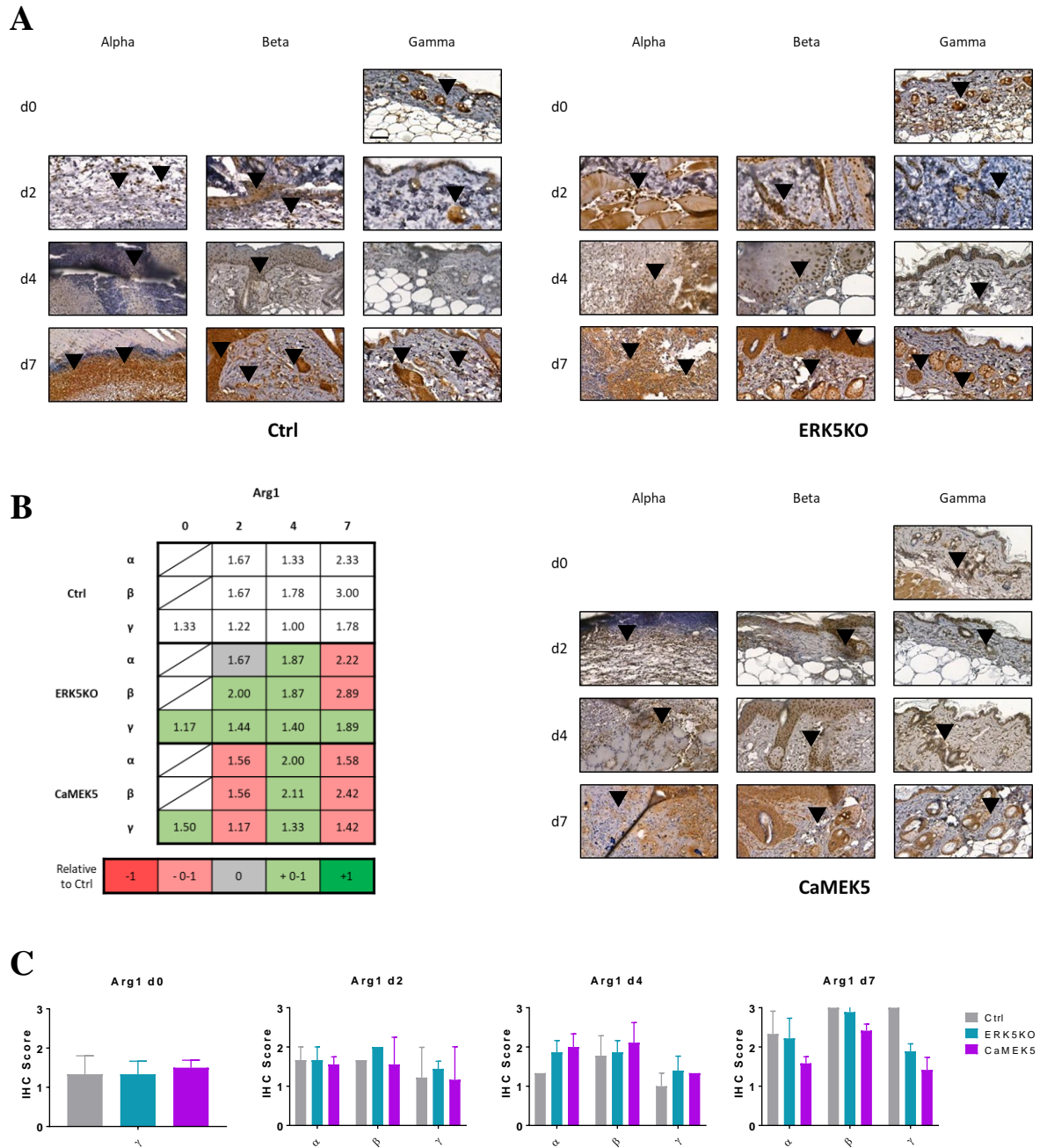


Figure 3.9. Arg1 expression remained unchanged in both ERK5KO and CaMEK5 wounds as determined by immunohistochemistry analysis. (A) Representative images of Arg1 staining in the wounds of control, ERK5KO and CaMEK5 mice. Black bar = 20 μ m. Black triangles indicate sites of positive Arg1 staining. (B) Table of the quantified scoring analysis of Arg1 staining. Grey = 0. Light red/green = \pm 0-1. Dark red/green = \pm 1. (C) Graphs of quantified scoring analysis of Arg1 staining in control, ERK5KO and CaMEK5 mice over the wound healing time course at d0 (n=12), d2 (n=4), d4 (n=4) and d7 (n=4). (ns=P>0.05, *=P<0.05).

3.4.6 Collagen deposition was decreased in ERK5KO and CaMEK5 wounds

The precursor work by the Finegan and Mace Labs showed that ERK5 inactivation led to reduced scarring and ECM build up in these closed, excisional wounds. Excessive ECM is a hallmark of impaired healing in dysfunctional cases such as hypertrophic scarring (Feng *et al.*, 2019). Studies have shown that healthy M2-like macrophages are influential in the balance of MMP-mediated breakdown and generation of ECM components such as collagen and fibronectin (Mirza, DiPietro and Koh, 2009; Delavary *et al.*, 2011).

Additionally, in the context of triple-negative breast cancer biology, ERK5 signalling promotes ECM deposition and matrix integrity. Namely, a study by Hoang *et al.*, depleted ERK5 in cancer cell lines MDA-MB-231 and Hs-578T through a CRISPR/Cas9 system to assess the functional effect on ECM composition. Inactivation of ERK5 led to an altered ECM profile with reduced levels of genes associated to collagens, laminins, and matrix linking proteins (Hoang *et al.*, 2020). However, a previous study in the context of diabetic neuropathy found that ERK5 inactivation of human microvascular endothelial cells of dermal and retinal origins led to increased level of TGF- β which can drive collagen deposition (Wu *et al.*, 2012). Their converse model of hyperactive ERK5 through virally transfected CaMEK5 cells led to decreased levels of fibronectin, an important protein of ECM structures. This reiterates that ERK5 signalling can deliver differing functions dependent on the biological context.

In order to determine if these genetic ERK5 modifications resulted in changes in collagen deposition in murine cutaneous wound environments, the wounds of control, ERK5KO and CaMEK5 mice were stained with picrosirius red. Collagen staining was quantified by the area of red staining at a set threshold as a percentage of the total area and graphed as mean \pm SEM. A representative bright field image used for quantification has been depicted, and represent the data point closest to the mean for that sample set.

Total collagen based on picrosirius red staining had an increasing trend at all three regions over the time points from day 0 (31.4%), day 2 (α 20.1%, β 30.2%, γ 36.3%), day 4 (α 26.4%, β 41.1%, γ 34.8%), and day 7 (α 33.9%, β 48.9%, γ 40.4%) in control mice (Figure 3.10.A). Loss of ERK5 resulted in a decrease in collagen deposition when compared to control in the alpha regions of day 2 (20.1% vs 9.4%) and day 7 (33.9% vs 21.9%), and in the beta region on day 4 (41.1% vs 27.9%). Whereas CaMEK5 mice exhibited a similarly decreased collagen profile compared to control, with a marked decrease in the alpha region on day 7 (33.9% vs 11.7%) when compared to control (Figure 3.10.C).

Collagen synthesis, deposition, remodelling and subsequent formation of ECM architecture in wound healing requires a carefully coordinated process. Decreased collagen deposition in healthy wounds like in the above genetic model context of ERK5KO could be detrimental as they can no longer recruit fibroblasts and encourage deposition of collagen to finalise remodelling. However, loss of excessive collagen production would be beneficial in the dysfunctional context of hypertrophic scarring and pathological impaired wound healing.

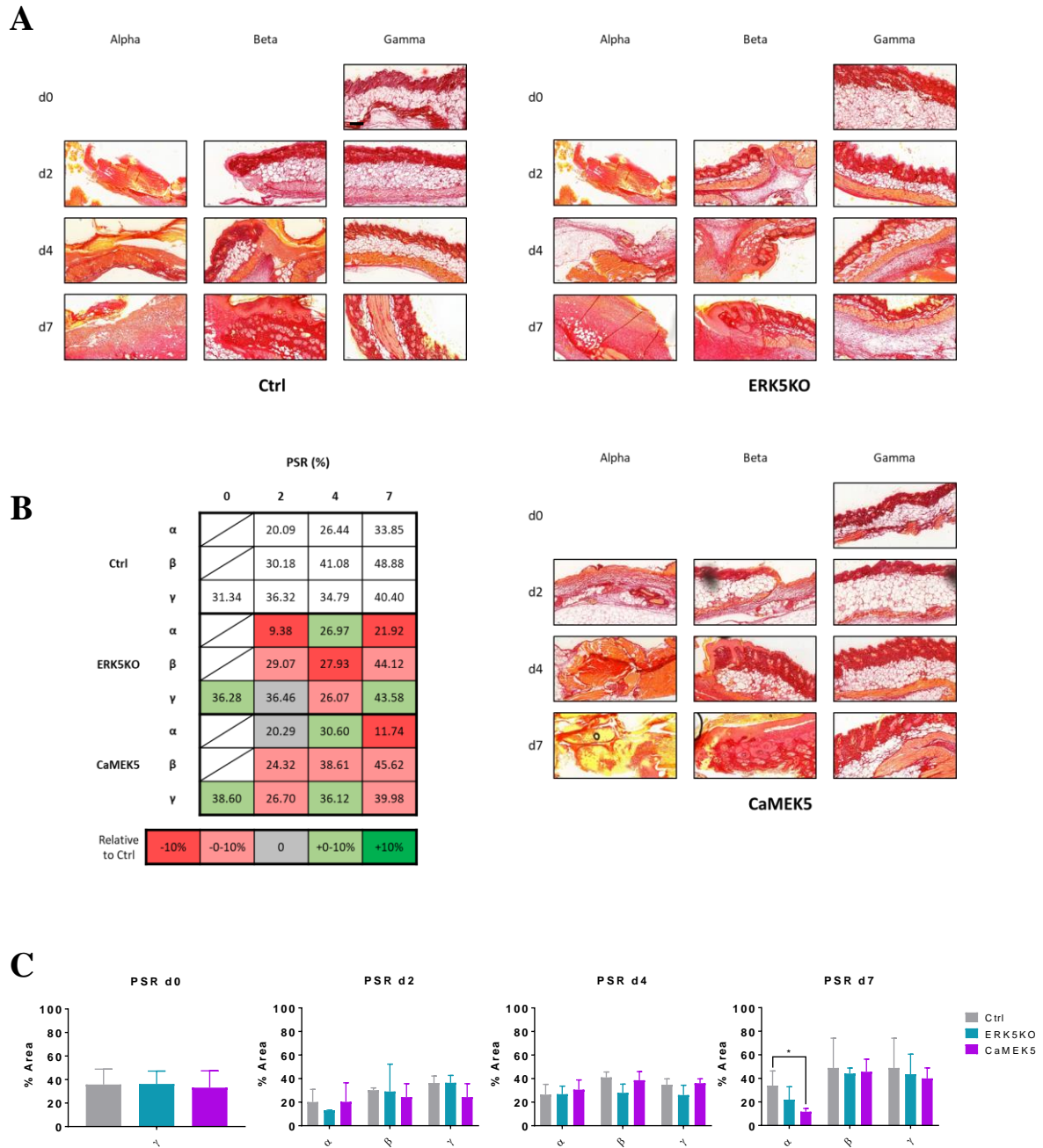


Figure 3.10. Collagen deposition decreased in ERK5KO and CaMEK5 wounds as determined by immunohistochemistry analysis. Collagen staining was quantified by the area of red staining from picrosirius red, at a set threshold as a percentage of the total area and graphed as mean \pm SEM, in control, ERK5KO and CaMEK5 mice wounds over the wound healing time course. (A) Representative images of picrosirius red staining in the wounds of control, ERK5KO and CaMEK5 mice. Black bar = 50 μ m. (B) Table of the quantified scoring analysis of picrosirius red staining. (C) Graphs of quantified scoring analysis of picrosirius red staining in control, ERK5KO and CaMEK5 mice over the wound healing time course at d0 (n=12), d2 (n=4), d4 (n=4) and d7 (n=4). (ns=P>0.05, *=P<0.05).

3.5 Discussion

ERK5 is involved in a myriad of immune and epidermal contexts. In particular various studies have shown its role in driving inflammation-associated tumorigenesis in skin cancer, and proliferative and metastatic function in osteosarcoma, as well as developmental and homeostatic function in cardiac biology (Finegan *et al.*, 2015; Huang *et al.*, 2017). Precursor work by the Finegan and Mace Labs, indicated that genetic inactivation of ERK5 in the keratinocyte population led to earlier wound closure, reduced inflammation and decreased scarring in both healthy and diabetic mice (Figure 1.8). This provided the foundation of our hypotheses: that early changes to the inflammatory environment were responsible for the differences observed in wound closure in keratinocyte specific ERK5KO mice. We therefore looked at time points up to day 7 as we focussed on the inflammatory events in this window that could dictate overall wound closure phenotype. We extended the previous work, which was histology based, to explore a more in-depth immune profile of the wounds (e.g. by FACS) at the early phase of inflammatory wound healing in ERK5 inactivated keratinocyte models (ERK5KO). In addition, we investigated the converse model, to investigate what impact ERK5 hyperactivation in keratinocytes (CaMEK5) would have on cutaneous wound healing and gain novel insight into whether ERK5 signalling can drive aberrant inflammation in *in vivo* wound healing.

In this study, we demonstrate successful keratinocyte specific inactivation or hyperactivation of ERK5 in ERK5KO and CaMEK5 mice, respectively via histological staining with an ERK5 antibody. Absence of ERK5 staining was evident in the keratinocyte layer of ERK5KO mice compared to control mice epidermis and the rest of the non-K14 expressing murine tissue. It should be additionally noted that hair follicles are another important skin structure with functions in thermoregulation, sebum production and cellular regeneration. This highly conserved sensory organ is a known site of cellular regeneration with sources in the dermal

papilla (bottom of the hair follicle) and the follicular bulge (Ji *et al.*, 2021). However, K15, rather than K14, has been used as the prominent marker to identify follicular stem cells. K14-expressing cells have been previously observed in the follicular bulge but to a lesser extent (Sieber-Blum, 2011). Thus, ERK5 inactivation was expected to be less effective in the hair follicle site of the ERK5KO murine model. This was partially observed in our ERK5KO keratinocytes where there was decreased ERK5 expression in the basal keratinocytes but slightly higher expression in the hair follicle bulges. This limits the potential for full ERK5 inactivation in the keratinocyte layer of the skin, as non-K14 expressing hair follicle based epidermal cells could contribute to inflammation and wound healing through their compensatory functioning ERK5 proteins. Thus, the main caveat of the immunological phenotype observed in this ERK5KO study is that we were looking at ERK5 inactivation only in K14 expressing basal keratinocytes and not in other cell types that could dictate wound healing.

An additional limitation that may prevent complete ERK5 modulation is the potential for some K14-expressing cells to avoid tamoxifen induction or not correctly express the K14CreER; ERK5KO. These would be a rare occurrence and have minimal impact compared to the majority of ERK5 inactivated K14 expressing keratinocytes. However, given enough time after the initial ERK5 genetic inactivation, it is possible that keratinocytes that have escaped modification could have a proliferative advantage to their ERK5 modified counterparts, given the clear role for ERK5 in keratinocyte proliferation *in vivo* (Finegan *et al.*, 2015). Therefore, over the course of several months, some mice may have “leaky” ERK5 expressing keratinocytes in the epidermal layer, as is anecdotally seen in long-term skin carcinogenesis studies. This has partially been avoided by ensuring mice have been experimentally wounded within 2-6 weeks after tamoxifen induction. A similar prospect would be possible in CaMEK5 mice, whereby a proportion of cells could arise that do not contain the K14-inducible

constitutive active MEK5. Although, perhaps to a lesser extent, given the presence of CaMEK5 would be hypothesised to provide a proliferative advantage to cells, in contrast to the disadvantages embedded by ERK5 loss.

Assessment of successful ERK5 hyperactivation in CaMEK5 was based on the increased localisation in the nucleus and overall increased expression in the keratinocyte layer. MEK5 mediated phosphorylation of ERK5 can lead to a hyperactivated state with increased nuclear localisation, but equally phosphorylated ERK5 can be found abundantly in the cytoplasm. Additionally, the active state of ERK5 is potentially more stable and could manifest itself in the observed appearance of increased expression of ERK5 staining in the CaMEK5 keratinocyte cytoplasm. However, an alternative method to assess the activated status of ERK5 in keratinocytes of CaMEK5 would be to process these cells for western blot analysis. This has previously been conducted by the Tournier Lab to confirm the validity of the CaMEK5 murine model system.

Using our successfully established genetically engineered models, it was found that genetic inactivation and hyperactivation of ERK5 led to no discernible differences in wound closure compared to control over the 7 day time period studied. As this study focussed on such a short and early phase of wound healing, we anticipated that changes in ERK5 profile of the epidermal layer may have little effect on the wound healing rate. Typically, wound modulators rarely show closure efficacy within the first seven days, but rather alter the immune profile that leads to faster wound closure overall, at later time points (Ashcroft *et al.*, 1999; Su *et al.*, 2016; Thangavel *et al.*, 2017). This altered wound microenvironment can set the pace for later accelerated closure effect, as observed in precursor work that exhibited faster overall closure of wounds lacking ERK5 (Figure 1.8).

We typically see most of our inflammatory immune cells playing a key role in this earlier window of time (Eming, Martin and Tomic-Canic, 2014). Our initial H&E analysis suggested that both ERK5 inactivation and hyperactivation led to no impactful changes in the total quantity of immune infiltrates. However, a more in-depth investigation with a combination of histology (Figure 3.11.A) and flow cytometry analysis (Figure 3.11.B) suggest that, compared to control, ERK5KO mice exhibited an earlier and more pronounced inflammatory phase of wound healing (Figure 3.11.C, red), followed by an earlier shift to the resolution phase of wound healing (Figure 3.11.C, blue). Conversely, CaMEK5 mice had a more persistent inflammatory profile, compared to control (Figure 3.11.C, red).

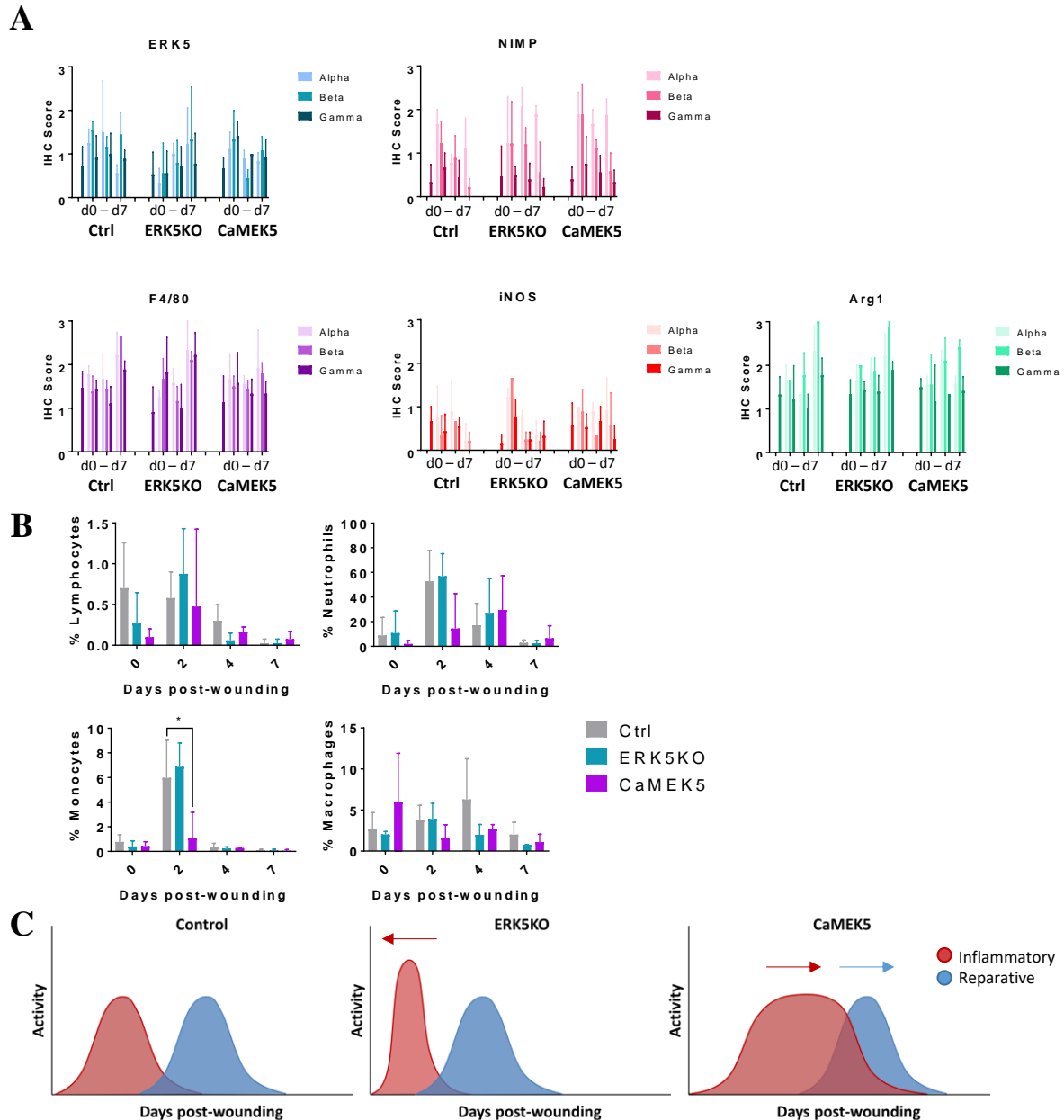


Figure 3.11. Summary wound healing profile of ERK5 modification. (A) Summary IHC data of control, ERK5KO and CaMEK5 in targets for ERK5, neutrophils (NIMP-R14), macrophages (F4/80), M1-like (iNOS) and M2-like phenotype (Arg1). (B) Summary FACS data of % population of lymphocytes, neutrophils, monocytes and macrophages. (C) Based on our data from the ERK5 genetic models, we hypothesise that ERK5 inactivation (ERK5KO) in the epidermis may promote earlier and greater inflammatory activity (red). This was followed by an earlier wave of reparative activity (blue). Conversely we hypothesise that ERK5 hyperactivation (CaMEK5) in the epidermis may promote persistent inflammation and delay wound repair mechanisms, reflecting phenotypes observed in chronic wounds of aged and diabetic models.

Our findings that aberrant ERK5 signalling contributing to inflammation was consistent with literature focussing on cancer progression and metastatic potential (Simões *et al.*, 2015). These ERK5 associated colon cancers have been characterised as aggressive and correlate with poor prognosis. At the time points studied here, we found that ERK5 hyperactivation in the skin through our model CaMEK5 led to a more prolonged and chronic inflammatory phase. Neutrophil NIMP-R14 staining was more abundant in day 2 and 7, compared to control mice suggesting an inability to completely remove these cells, conducive of a pro-inflammatory environment. In parallel, iNOS expression persisted and was higher at the later time points of day 7. As previously highlighted, this could represent both M1-like macrophages and an inflammatory environment.

This persistently inflammatory state could additionally mean that repair mechanisms were slower to arrive, as suggested by the slight decrease in Arg1 expression at day 7 which are representative of M2-like macrophages and healing associated environment. Additionally, our FACS analysis of CaMEK5 mice wounds found a reduction in monocytes at day 2. Efficient recruitment of bone marrow derived monocytes are necessary to polarise these cells to either M1 or M2-like macrophages. The deficiency of monocytes at an early stage of wound healing could lead to a smaller pool of monocytes to polarise towards M2-like macrophages needed around day 4 and day 7.

This observed immunological profile in hyperactive ERK5 wounds was analogous to that seen in chronic and unresolved inflammation typical of many pathological wounds such as those associated with diabetes, leg ulcers and hypertrophic scars. This chronic inflammatory state has often been observed with increased presence of M1-like macrophages, which have been shown to propagate TLR4 and NLRP3 signalling (Wicks, Torbica and Mace, 2014). Additionally these abnormal macrophages can often be defective in their phagocytic capacity.

This could reflect the hyperglycaemic wound environments which inhibit M2 polarisation (Khanna *et al.*, 2010; Mirza and Koh, 2011).

Although a limitation to note is that constitutively active MEK5 and the subsequent hyperactive state of ERK5 may not necessary translate and represent patients with overexpressed ERK5. Various cancer patient studies have found elevated levels of MEK5 and ERK5 in cancers of breast, prostate, colon, and osteosarcoma. Moreover, unpublished data from the Tournier group using this murine model demonstrate that hyperactivation of ERK5 lead to higher tumour burden and an enhanced inflammatory phenotype. What remains uncertain is the direct relationship between ERK5 and wound patient cohorts.

This impaired wound healing profile we observed in CaMEK5 animals suggests that higher expression of ERK5 could indicate wounds that are unlikely to resolve, and provide further rationale for therapeutically targeting ERK5. Further investigations are required to compare the similarity of CaMEK5 wounds to chronic wound models such as those associated with diabetes. Doing so could elucidate the patterns between dysfunctional macrophages in diabetics and how ERK5 could be involved in driving these immune cells and the inflammatory environment.

However, unexpectedly, genetic inactivation of ERK5 through our model of ERK5KO, we induced an increase in magnitude of the inflammatory phase of wound healing, before progressing to an earlier transition towards the resolution phase. In concordance with precursor work by the Finegan and Mace Labs, our studies focussing on the first seven days of wound healing in ERK5KO mice, observed more rapid and increased influx of inflammatory cells, namely neutrophils and M1-like macrophages. Efficient influx of these neutrophils, which occurs in the first few days (Kim *et al.*, 2008), is needed to target and clear pathogens and infections. Their recruitment is signalled by IL-8 from inflammatory and danger signals in the

wound microenvironment, and the associated increased endothelial permeability (Wang, 2018). Once neutrophils have successfully phagocytosed and killed pathogens with ROS, proteases and AMP, they produce a myriad of factors to recruit inflammatory macrophages. These macrophages phagocytosed the spent neutrophils and initiate a transition away from inflammation (Ellis, Lin and Tartar, 2018). This was observed in our studies by the earlier arrival of reparative associated immune cells such as M2-like macrophages. The arrival of these M2-like macrophages are vital in reducing inflammation and stimulating tissue repair, moving wound healing to the resolution phase (Ellis, Lin and Tartar, 2018; Louiselle *et al.*, 2021).

M2-like macrophages are needed in this later stage of wound healing to facilitate the production of fibrotic and regulatory factors such as TGF- β , VEGF, EGF and MMPs (Hesketh *et al.*, 2017). This creates an environment that can carefully coordinate the ECM architecture and vascularisation for final remodelling and scar formation. Our studies indicate a slight decrease in the levels of collagen staining in ERK5KO mice, however this may not indicate much impact as the first seven days are not known to be associated with role of fibrosis. This would typically occur from day 7 onwards in healthy wound healing. Therefore, studies that look at collagen deposition at later time points and in closed, excisional wounds would be needed to determine if ERK5KO models affect collagen deposition and scar formation.

Our studies here have identified M1-like vs M2-like phenotypes of macrophages based on the simplified model of iNOS and Arg1 expression, respectively. This model has limitations in that some other cell types including keratinocytes and fibroblasts can also express these markers dependent on an inflammatory or reparative stimuli. So, although they may not be specific to macrophages, they remain robust indicators of the environmental status. Additionally, as recent research has indicated, macrophage populations are much more complex than a simple dichotomy of M1 vs M2. The reality is likely to be a plastic spectrum of macrophage phenotypes dependent on timing, location and strength of stimuli. A wider panel of markers or

gene signatures to identify these subsets of macrophages would be more accurate in defining these populations. Additional histology markers such as TSPO or MR could be used in conjunction to identify M1-like and M2-like macrophages. This could be conducted as co-stained IF with macrophage markers such as F4/80 to specifically identify macrophages expressing these inflammatory or reparative markers. This was attempted in early studies, however, several technical issues and background staining concerns inhibited our investigation.

Another rational alternative would be expansion of the FACS panel to include macrophage polarity states using the suggested markers above. Preliminary work on this was conducted to identify F4/80 and Ly6C positive populations as macrophages and further separate them into their iNOS and Arg1 expression, but further optimisation was required. This would permit another technique to assess M1, M2 and hybrid macrophage populations from the wound site. However it was additionally noted that the general gating strategy could be re-optimised as CD11b is limited in its ability to identify lymphocytes. Alternative gating strategies could be utilised on the current data set to better separate the immune cell populations. Namely, CD45⁺F4/80⁺ for macrophages and CD45⁺F4/80⁻Ly6G⁺Ly6C⁻ for lymphocytes.

iNOS and Arg1 are well-established markers to identify murine macrophage polarity states, however they are limited in their relevance in the human context. Additional markers, such as TSPO and MR as suggested above could be utilised in the murine context, and would permit comparison between the murine and human wound healing context. Moreover, a limitation of the histology analysis conducted in this study, is that it was a subjective scoring based on the degree of brown staining observed. This was confounded by the blinded nature of the analysis which enabled non-specific staining to potentially be included in positive scoring. Future analysis may require automated scoring software or counting number of cells that are positively stained.

Taken together, this study has found that hyperactive ERK5 in the keratinocytes led to persistent and prolonged inflammatory phase, with a delay in the onset of the reparative phase of wound healing. Conversely, removing ERK5 from the keratinocytes in the wound environment, triggers the inflammatory phase to occur more rapidly and at a higher magnitude. In addition, loss of ERK5 causes the inflammatory phase to end sooner and is accompanied by an earlier onset of the reparative phase of wound healing. Thus, targeting ERK5 therapeutically could enable improvements in wound healing, particularly in chronic wounds that are sustained in the inflammatory phase, by shifting the balance of inflammation toward reparative functions and ultimately wound resolution.

Chapter 4: Therapeutic inactivation of ERK5 with OS1 in *in vitro* models of HaCaTs and THP-1s promotes an overall reparative phenotype

In the previous chapter we showed that genetic inactivation of ERK5 in keratinocytes led to improved wound healing due to earlier and more rapid initiation of inflammation and earlier repair mechanisms. However, there are limitations to the genetic models used: i) this approach is not translatable as a therapeutic for humans (Bulaklak and Gersbach, 2020; Wong *et al.*, 2020). ii) Genetic inactivation was restricted to the K14 expressing keratinocytes and not other compartments of the skin and proximal wound regions.

Targeting ERK5 therapeutically to reduce inflammation could be clinically beneficial for those who suffer from chronic wounds and associated morbidities. There are many ERK5 specific kinase inhibitors available, but recent research in the last five years indicate some clear limitations. Many functions of ERK5, crucially those associated with inflammation, are independent of the kinase activity of the protein. Highly selective ERK5 kinase inhibitors, such as AX15836, failed to exhibit any effect on inflammation or proliferation. Conversely significantly altered inflammatory profiles are seen in response to loss of ERK5 protein through genetic inactivation in both cells and murine models (Woo *et al.*, 2006; Finegan *et al.*, 2015; Green *et al.*, 2020). Moreover, XMD-892, the ERK5 kinase inhibitor that did show reduced inflammation and anti-proliferative effects had off-target inhibitory effects to bromodomain protein 4 (BRD4), which accounted for the immunological phenotype observed (Lin *et al.*, 2016).

To compound issues with the therapeutic use of ERK5 kinase inhibitors further, studies have found a paradoxical activation phenomenon with the use of ERK5 kinase inhibitors, whereby kinase inhibition of ERK5 causes distal C-terminus activation in the protein (Lochhead *et al.*,

2020). Taken together, this data show that in order to target ERK5 for therapeutic gain, we need to remove ERK5 from the cells, rather than simply inhibit its catalytic kinase function.

To address this, we used a compound developed in-house by our collaborators in the Butterworth Lab, via CRUK Drug Discovery funding. This compound, named OS1, after its creator Dr Olly Smith, degrades ERK5 protein via a small molecule approach. Parallel work in the Finegan Lab (unpublished) has successfully shown effective pharmacological-knockdown of ERK5 in triple negative breast cancer inducing an immunological phenotype that was not observed with ERK5 kinase inhibition alone. These compounds are currently being patented and as a result further detail, such as exact mechanism of action and structure, cannot be provided in this thesis.

Our preliminary studies in chapter 3 used *in vivo* murine genetic modulation to inactivate and hyperactivate ERK5 signalling specifically in keratinocytes. Using the HaCaT model permits investigation into translatability of the murine data into a human model system. Moreover, with our unique access to OS1, the novel ERK5 therapeutic, we can assess if the ERK5KO genetic model phenotype can be recapitulated using a small molecule compound.

4.1 *In vitro* therapeutic degradation of ERK5 in HaCaTs

Our initial *in vitro* work aimed to assess our hypothesis that degradation of ERK5 in HaCaTs could promote migration and repair mechanisms while inhibiting inflammation. We investigated whether modifying ERK5 signalling with OS1 would alter the behaviour and function of the keratinocyte layer by using the *in vitro* model of HaCaTs. HaCaT cells are an immortalised human epidermal keratinocyte cell line extensively used to study epidermal homeostasis and its pathophysiology in impaired wound healing and skin carcinogenesis. Appropriately timed proliferation and migration of epidermal cells such as keratinocytes are essential for healthy wound healing. Multiple growth factors, cytokines and signalling

pathways studied in HaCaTs have been described to influence the process of wound healing (Arnoux *et al.*, 2008; Zampetti *et al.*, 2009; Su *et al.*, 2016).

Our *in vitro* workflow utilised AX15836 (named AX throughout) to compare ERK5 specific kinase inhibition to degradation of the whole protein, via OS1. Additionally, we generated HaCaTs with stable genetic lentiviral knockdown of ERK5 (named shERK5) to allow comparison of our *in vitro* cell model to the genetic inactivation of ERK5 observed in the previous chapter with ERK5KO mice. This would provide a phenotypic benchmark for the knockdown we hoped to achieve with OS1 in HaCaTs. However, it should be noted that the ERK5 knockout created in shERK5 cells is at the RNA level whereas OS1 mediated degradation is at the protein level.

After HaCaTs were treated with various ERK5 specific compounds, OS1 and AX, we examined ERK5 expression, cell proliferation, migration and downstream functional outputs. This enabled us to understand how ERK5 signalling influences keratinocytes to replicate and migrate to close wounds, and the signalling factors it generates to facilitate the inflammatory environment of wound healing.

4.1.1 OS1 specifically targets and degrades ERK5 protein in HaCaTs

To compare the effect of ERK5 degradation and kinase inhibition on HaCaT cells, ERK5 expression was assessed over a treatment time course of OS1 and AX, and analysed by western blot. The changes in protein expression were expressed as a ratio density of the protein of interest, ERK5, to the density of the loading control β -actin or GAPDH.

From on-going research within the Finegan Lab in the oncology context, it has previously been found that the optimum concentration to degrade ERK5 with OS1 was at 1 μ M for at least 24h. We therefore initially tested OS1 at concentrations in this range; 0.1 μ M, 1 μ M, and 10 μ M, and over three time points; 8h, 16h, and 24h (Figure 4.1.A), to determine the optimum

concentration and time point needed to degrade ERK5. OS1 led to degradation (-70%) of ERK5 by 16h – 24h in response to 0.1 μ M and 1 μ M of OS1 (Figure 4.1.B). At the highest concentration of 10 μ M we observed little to no degradation of ERK5. This was due to a previously observed phenomenon known as the “hook effect”. OS1 is a tri-partite compound, where one warhead specifically binds to ERK5 and the other to degradation machinery within the cell. If the concentration of OS1 is too high, only bi-partite complexes form, preventing the tri-partite molecule from forming, thereby preventing OS1 from effectively degrading ERK5 (Figure 4.1.C). This phenomenon is common within molecules of this type and is mitigated for by appropriate dosing below the hook effect threshold.

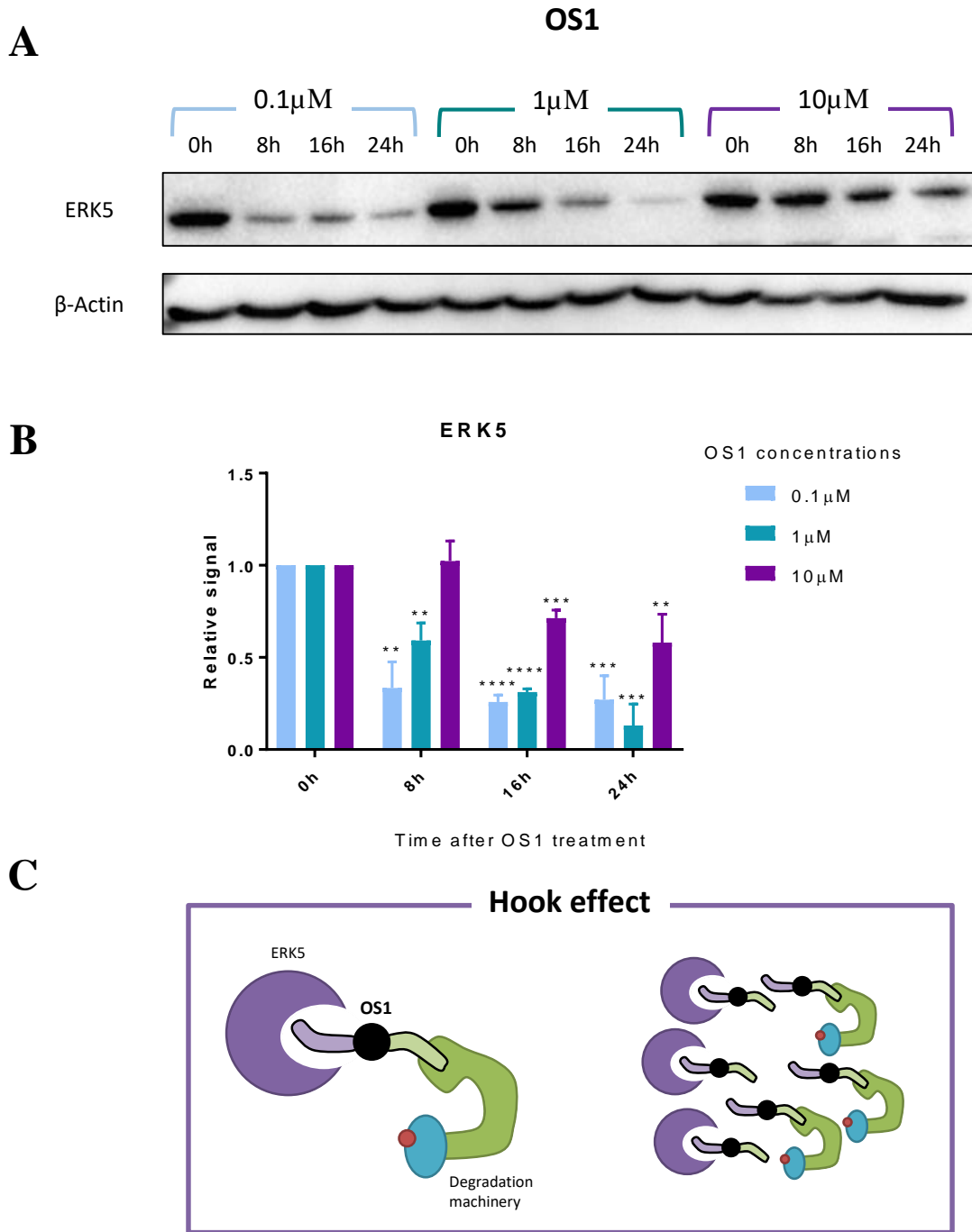


Figure 4.1. OS1 targets and degrades ERK5 in HaCaTs. (A) Representative blots after HaCaT cells were treated with OS1 at 0.1 μ M, 1 μ M and 10 μ M over a 24h time course to assess ERK5 and β -actin (n=3). (B) ERK5 protein levels were normalised and graphed against corresponding β -actin (n=3). (C) Graphical summary of OS1 mechanism. OS1 is a tri-partite compound, where one warhead (purple) specifically binds to ERK5 and the other arm (green) to degradation machinery within the cell. If the concentration of OS1 is too high, only bi-partite complex form, preventing the tri-partite complex (ERK5-OS1-Degradation machinery) from forming, thereby preventing OS1 from degrading ERK5 effectively. (ns = P>0.05, *= <0.05 , **= <0.01 , ***= <0.001 , ****= <0.0001).

We continued the remainder of our investigation with the 1 μ M concentration of OS1 as it was the most effective dose to degrade ERK5 which was consistent with data generated from ongoing research in the Finegan Lab in the oncology context. Next, the efficacy of OS1 was explored at longer time points of 48h and 96h, to assess the duration of ERK5 degradation with a single dose of OS1. Concurrent research in the Finegan Lab, using OS1 has shown that the drug loses efficacy and degrades over time (typically 48h-72h) permitting ERK5 protein to rebound (unpublished).

OS1 significantly degraded ERK5 at 1 μ M within 24h (-58%) and remained degraded in keratinocytes for up to 96h (-68%), following a single dose of OS1 (Figure x A). This was comparable to genetic lentiviral knockdown of ERK5 (shERK5), which had a reduction of ERK5 protein by -64%. The shERK5 HaCaTs, represented an *in vitro* cell model of the genetic *in vivo* inactivation of ERK5 (chapter 3). However, it should be noted that the shERK5 HaCaT cell line was less effective at removing ERK5 compared to OS1, throughout the study.

4.1.2 OS1 does not affect potential off-target proteins: ERK1/2 and BRD4

As previously mentioned, some ERK5 kinase inhibitors have certain limitations including known off-target effects on proteins such as ERK1/2 and BRD4 (Lin, 2016). As OS1 has never been previously used in HaCaTs, these were additionally assessed by western blot analysis. Current work in oncology has shown that OS1 is specific to ERK5, and does not affect these targets.

In this study, no discernible effect was noted on ERK1/2 expression, which is a kinase of similar structure to ERK5, highlighting specificity of OS1 to ERK5 (Figure 4.2.A). However, it should be noted that OS1 treatment has led to a subtle shift in ERK1/2 which is indicative of its phosphorylation. This could be a signalling compensation for the loss of ERK5. There were also no off-target effects on BRD4, a known off-target of other ERK5 kinase inhibitors, such as XMD8-92 (Figure 4.2.A).

4.1.3. OS1 vs AX inhibition of ERK5 phosphorylation

We compared OS1 to AX at 5 μ M, a selective kinase ERK5 inhibitor, which does not have off-target effects on BRD4 (Lin *et al.*, 2016; Lochhead *et al.*, 2020). This is a known and effective dose at inhibiting ERK5 kinase activity and prevents its phosphorylation (Lin *et al.*, 2016; Wright *et al.*, 2020). Addition of d-sorbitol at 500mM for 30 minutes induces ERK5 specific phosphorylation, ~56% of total ERK5 (Figure 4.2.E). AX successfully inhibited the phosphorylation of ERK5 induced by d-sorbitol, whereas OS1 completely degrades the protein (Figure 4.2.D and E). Interestingly, it should be noted that addition of d-sorbitol induces an overall shift of ERK5 which is unaffected by OS1 degradation or AX kinase inhibition (Figure 4.2.C). This is reflective of kinase-independent phosphorylation of ERK5 on the C-terminus, whereas AX only inhibits the N-terminus kinase activity.

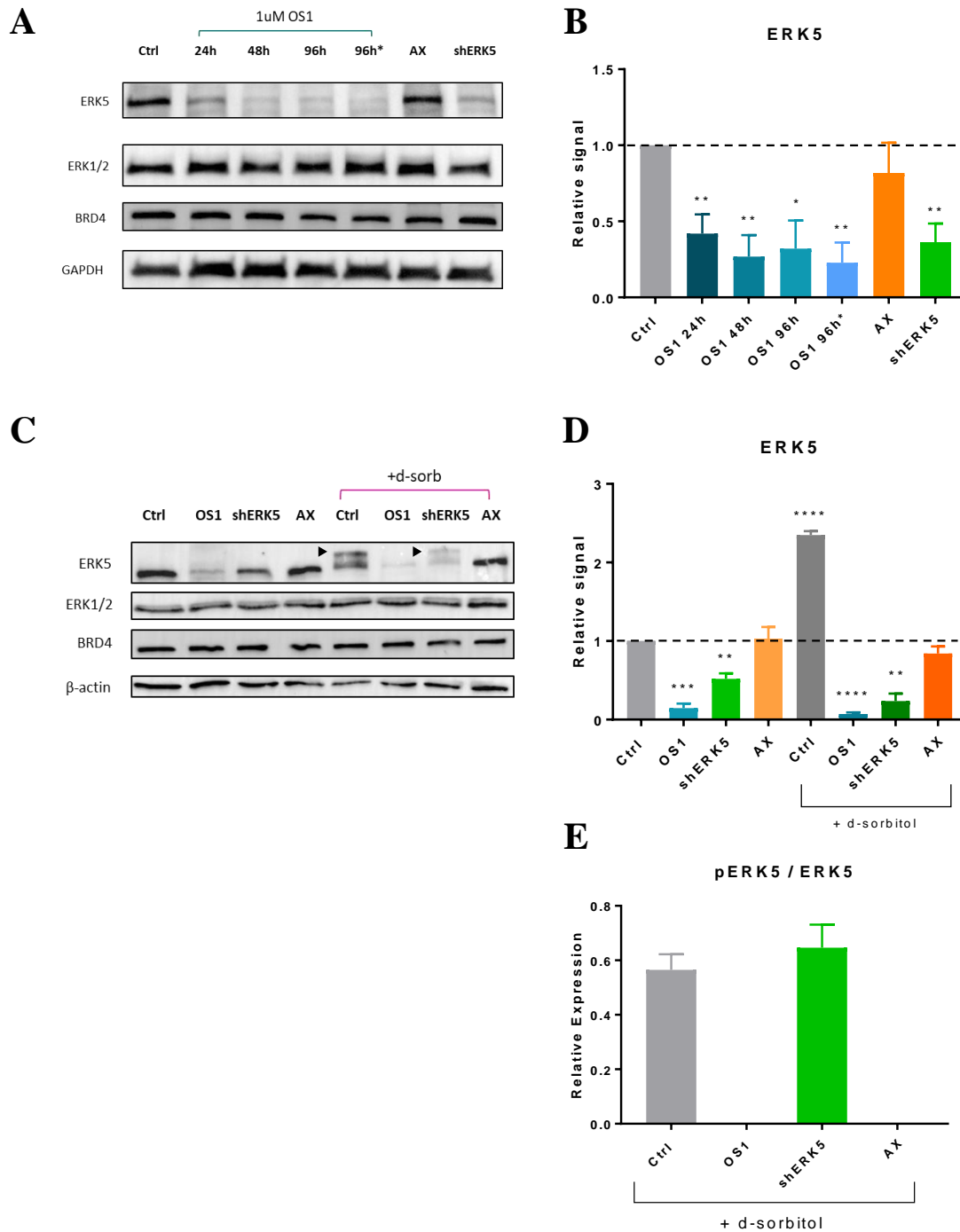


Figure 4.2. OS1 targets and degrades ERK5 in HaCaTs, not affecting potential known off-targets of ERK5 inhibitors: ERK1/2 and BRD4. (A) Representative blots after HaCaT cells were treated with a single dose of OS1 (1 μ M) and monitored over a 96h time course, two doses of OS1 (1 μ M) at 48h intervals (96h*), AX (5 μ M) and shERK5 to assess ERK5, ERK1/2, BRD4 and GAPDH (n=4). (B) ERK5 protein levels were normalised and graphed against corresponding GAPDH (n=4). (C) Representative blots after HaCaT cells were treated with OS1 (1 μ M), shERK5, AX (5 μ M) with and without d-sorbitol (500mM, 30 minutes) to assess ERK5, ERK1/2, BRD4 and GAPDH (n=3). pERK5 band indicated by black triangles. (D) ERK5 protein levels were normalised and graphed against corresponding β -actin (n=4). (E) Phosphorylated ERK5 protein levels as a ratio to the total ERK5 protein in d-sorbitol treated cells (n=4). (ns = P>0.05, *=<0.05, **=<0.01, ***=<0.001, ****=<0.0001).

4.1.4 ERK5 inactivation with OS1 had no effect on cell growth

Both MTT and SRB colorimetric assays were conducted to indirectly assess if ERK5 inhibition alters the proliferation of HaCaTs. These two techniques measure cellular metabolic activity and cellular protein quantity, respectively, to quantify cell density in a 96-well plate to infer a cell's level of proliferation over a time course. The MTT assay determines cell density based on cell metabolic activity by measuring mitochondrial NAD(P)H-dependent cellular oxidoreductase enzymes capacity to reduce tetrazolium dye MTT to insoluble formazan. Whereas the SRB assay measures protein content by stoichiometric binding under mild acidic conditions, which can be inferred as a measure of cell proliferation. Comparison between the two assays would firstly provide robust measurement of the effect of ERK5 on proliferation in these cells. Secondly, comparing the results from the MTT and the SRB assay would delineate any specific effects the ERK5 inhibition may have on mitochondrial activity. This would manifest by differing patterns from the MTT assay, which is reliant on mitochondrial number and function, compared to SRB, which is a direct measure of cellular protein content.

Results of MTT and SRB assays were expressed as fold change of absorbance over a 72 hour time course, in response to a range of OS1 drug concentrations (Figure 4.3.B). This was followed by a comparison between OS1, AX and shERK5. Both MTT and SRB assays revealed no significant difference in proliferation and cell density between all OS1 drug concentrations, AX or shERK5 HaCaTs compared to control (Figure 4.3.A). As both SRB and MTT assays showed similar trends in proliferation rate, it suggests that ERK5 inactivation does not affect mitochondrial-mediated pathways in this context.

4.1.5 ERK5 inactivation with OS1 had no effect on cell migration

Previous studies using lentiviral transfection of a shRNA specific to ERK5, have shown that ERK5 inactivated HaCaTs exhibited altered morphology and disrupted their ability to migrate and close scratch wounds (Arnoux *et al.*, 2008). Therefore, we wanted to determine if OS1 mediated degradation of ERK5 had similar effects. After growing to confluence and being scratched, HaCaT cells were treated with either OS1 (1 μ M), AX (5 μ M), or compared to shERK5 HaCaT cells to inactivate the ERK5 pathway and assess the effect on migration. HaCaTs cells were dosed after the scratch model to allow for comparability to future *in vivo* wounding studies, and to consider translatability as a treatment for existing wound pathology, as opposed to pre-treatment, prior to a wound forming, which is unlikely to be the way any therapeutic would be used to treat wound healing. Notably, ERK5 protein will only be degraded by -50% in the first 8 hours, and to a further -70% by 16h after dosing (Figure 4.1.A). Results of scratch assays were expressed as fold change comparison to the scratch gap area at 0h arbitrarily set to 1.

There was no discernible difference in rate of migration within the first 16h between all groups as they similarly closed the first ~40% of the scratch gap. However, by 24h onwards, control and OS1 treated HaCaT scratches continued to close at an equal rate that was faster than AX treated and shERK5 HaCaT cells (Figure 4.3.C). ERK5 kinase inhibition and shERK5 cells had detrimentally affected migratory function of HaCaTs when compared to control. Previous research (Arnoux *et al.*, 2008) had similarly shown that lentiviral inactivation of ERK5 negatively impacted the migratory function by reducing cell-cell adherence. However, it was unexpected to see that therapeutic degradation of ERK5 using OS1 had no negative affect, and was more similar to control.

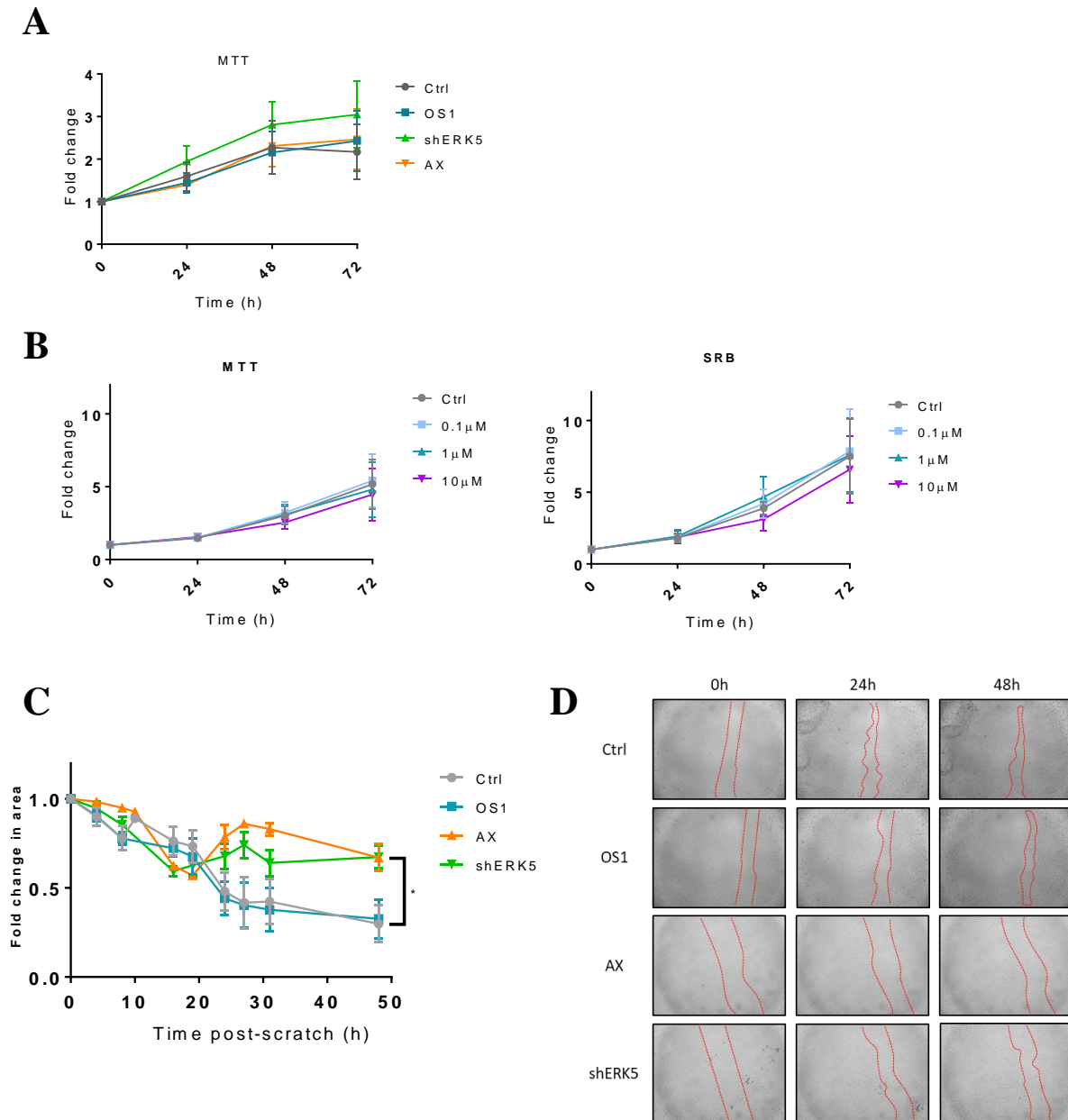


Figure 4.3. OS1 degradation of ERK5 has no effect on HaCaT proliferation and migration. HaCaT cells seeded at 1000 cells per well and underwent MTT or SRB assays as indirect assessments of proliferation. (A) MTT assays were conducted following treatment with DMSO control, OS1 (1 μ M), shERK5, AX (5 μ M) after selected time points of 0, 24, 48, and 72h. Data points plotted represent the mean of three independent experiments \pm SEM. (B) MTT and SRB assays following a time course of varying doses of OS1. Data points plotted represent the mean of three independent experiments \pm SEM. (C) HaCaTs were subjected to scratch assay, then they were treated with DMSO control (n=9), OS1 (1 μ M) (n=8), AX (5 μ M) (n=4) and shERK5 (n=5). Images were taken at 0, 4, 8, 10, 16, 19, 24, 27, 31, 48h. Scratch gap area at 0h for each group was arbitrarily set at 1. Data points plotted represent the mean of at least four independent experiments \pm SEM. (D) Representative images of scratch assay demonstrating the effects of ERK5 inactivation on HaCaT cell migration. Dashed red line indicate wound edge. (ns = P>0.05, *=<0.05).

4.1.6 ERK5 inactivation by OS1 promotes the mRNA expression of a range of both inflammatory and repair associated cytokines

Previous literature and our own studies have shown that inactivation of ERK5 in the keratinocytes, dampens the inflammation that drives tumorigenesis in cancer models. In the context of cancer, it was hypothesised that the lack of proliferative activity in the keratinocytes led to lack of a signal to initiate inflammation (Arnoux *et al.*, 2008; Finegan *et al.*, 2015). What remains unclear is whether a similar mechanisms exists in wound healing, or whether loss of ERK5 can directly influence the production of inflammatory and repair mediators in HaCaTs, that alter the wound microenvironment to promote closure.

RT-qPCR analysis was used to investigate the gene expression of inflammatory (TNF- α , IL-1 β , IL-6, IL-8, IL-12) and regulatory (TGF- β , VEGF, MMP9, SLUG, N-Cad, E-Cad, Vimentin) mediated cytokines in HaCaTs in response to treatment with 1 μ M OS1 at 6h and 24h, and shERK5 HaCaTs. We have previously shown that ERK5 protein can be degraded as early as 8h (Figure 4.1.A), and the comparison of gene expression changes between 6h and 24h permits investigation of the early and later gene expression effects of loss of ERK5 signalling. Analysis was completed with the $\Delta\Delta$ CT method, as relative expression to β -actin, and statistical testing was done on the Δ CT values.

Keratinocytes activated by inflammatory stimulation or in response to danger signals can produce a variety of key inflammatory cytokines to regulate the immune response in wound healing. TNF- α is a multifunctional cytokine that can induce apoptosis and drive complex inflammatory cascades. A study in aged related inflammation found that ERK5 activation inhibits TNF- α expression in a murine myocyte (muscle) cell line (Woo *et al.*, 2006). Similarly, a study by Wilhelmsen *et al.*, found that inhibiting ERK5 and MEK5 in human endothelial cell lines and monocytes led to a reduction in the secretion of TNF- α and IL-1 β (Wilhelmsen *et al.*, 2015). IL-1 β is a very powerful and important mediator of inflammation that induces fever and

is notably associated with NLRP3 inflammasome. A skin carcinoma study that genetically inactivated ERK5 in the keratinocytes of mice found reduced levels of IL-1 β after inflammatory stimulation (Finegan *et al.*, 2015).

IL-6 is a pleiotropic cytokine with key roles in both inflammatory and reparative process, and requires correct spatiotemporal expression to regulate wound healing. Abundant IL-8 expression is crucial as a neutrophil chemoattractant and can further induce more potent pro-inflammatory activity (Zampetti *et al.*, 2009). Both IL-6 and IL-8 were found to be driven by ERK5 and MEK5 activity, and subsequently siERK5 RNA interference led to reduction in their cytokine production (Wilhelmsen *et al.*, 2015; Lin *et al.*, 2016). IL-12 is another pro-inflammatory cytokine where studies have found it has an additional role in reducing angiogenesis in the diabetic context (Zampetti *et al.*, 2009; Koh and DiPietro, 2011; Ali *et al.*, 2017).

TNF- α expression was increased after 6h (4.42 fold) and 24h (4.73 fold) of 1 μ M OS1 treatment, but was unaffected in shERK5 cells (Figure 4.4.A). IL-1 β mRNA expression was largely unchanged by the experimental conditions, but exhibited the greatest increase in expression in shERK5 cells (1.43 fold) (Figure 4.4.B). IL-6 expression increased after 6h (5.64 fold) and 24h (6.26 fold) of OS1 treatment (Figure 4.4.C). IL-8 expression was unchanged compared to control (Figure 4.4.D). IL-12 expression exhibited an increased trend of expression after 6h (3.14 fold) and 24h (3.00 fold) of OS1 treatment (Figure 4.4.E). Taken together, these results suggest that degradation of ERK5 with OS1 leads to an increased induction of pro-inflammatory gene expression in HaCaTs.

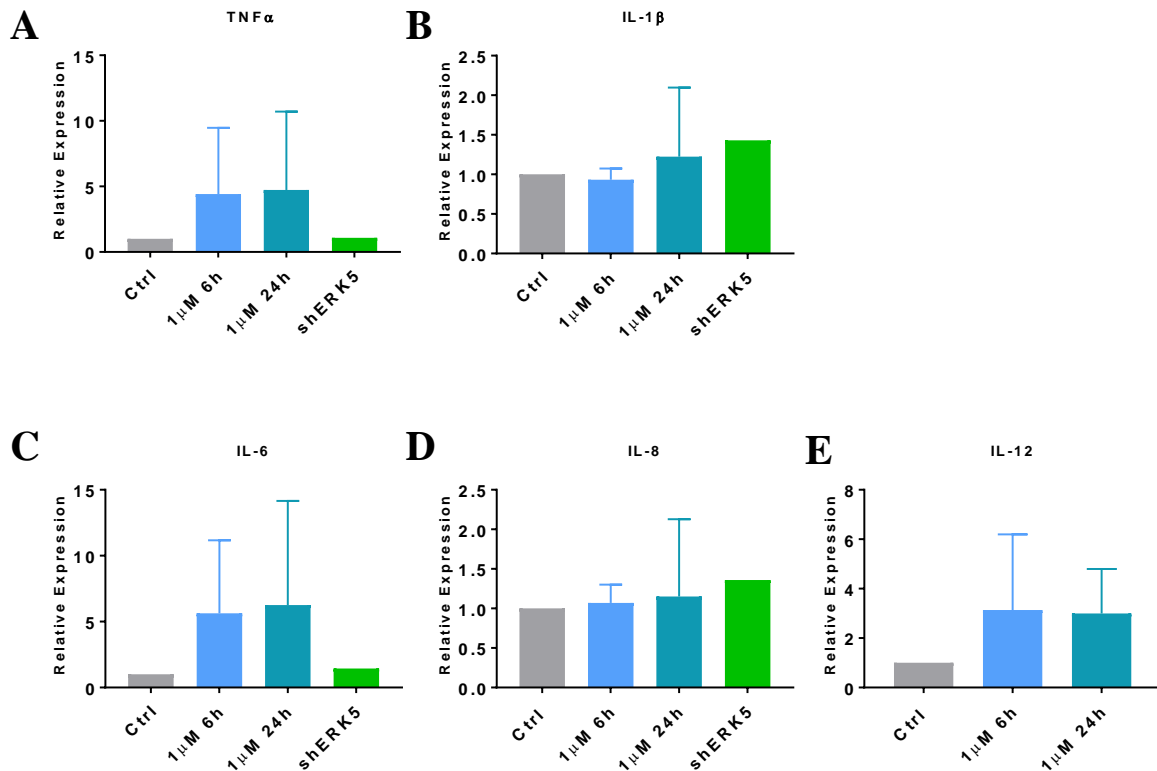


Figure 4.4. ERK5 inactivation by OS1 promotes gene expression of inflammatory targets. Total RNA was extracted and RT-qPCR was performed on a panel of genes after HaCaTs were treated with DMSO control and OS1 (1μM) after 6h and 24h, and compared with shERK5 (n=1). Inflammatory gene targets: (A) TNFα, (B) IL-1β, (C) IL-6, (D) IL-8, and (E) IL-12. (n=3). Values represent the mean expression of cDNA of the various genes relative to β-actin. (ns = P>0.05, *=<0.05).

Alongside timely inflammatory cytokine expression during this initial phase of wound healing, we need regulatory and remodelling signals to be induced next to coordinate healthy wound closure. Keratinocytes alongside other cell types in the wound produce TGF-β, which plays a role in regulating inflammation. And specifically in the context in wound healing and scarring, TGF-β is involved in stimulating fibroblasts, collagen synthesis and remodelling of extracellular matrix (Penn, Grobelaar and Rolfe, 2012; Eming, Martin and Tomic-Canic, 2014). MMP9 is one of many key effectors of ECM remodelling and has been observed to be upregulated in chronic murine wound models. Moreover, MMP9 is a known downstream target of ERK5 that acts as a driving force for bone cancer metastasis (Reiss *et al.*, 2010; Huang *et*

al., 2017; Green *et al.*, 2020). VEGF is required for timely angiogenesis to re-establish the supply of oxygen and nutrients to the wounded tissue (Okonkwo and Dipietro, 2017; Gurevich *et al.*, 2018).

Relative expression of TGF- β increased markedly with a 22.6 fold increase after 6h, and a 547.6 fold increase after 24h of OS1 treatment (Figure 4.5.A). A similarly increased expression pattern was observed in the MMP9 gene, with a peak 3104.4 fold increase in response to 24h 1 μ M OS1 treatment (Figure 4.5.D). VEGF expression was affected to a lesser extent than MMP9 and TGF- β , but nonetheless exhibited the greatest increase after 24h (8.40 fold) with OS1 treatment (Figure 4.5.B).

Additionally, our study focussed on genes related to migration. In the context of cancer biology and ERK5 signalling, Epithelial-to-Mesenchymal (EMT) is a driving force for migratory behaviour and is crucial for promoting metastasis. A known phenomenon during EMT is the upregulation of N-cadherin (N-Cad) and downregulation of E-cadherin (E-Cad) (Loh *et al.*, 2019). Moreover, the coordinated expression of these cell-cell adhesion molecules are required for collective cell migration to close wounds (Li *et al.*, 2013). Vimentin is an intermediate filament protein known to maintain cellular integrity with additional functions in resisting stressed environments. In wound healing, its presence can mediate repair by facilitating the development of myofibroblasts (Walker *et al.*, 2018).

There was increased expression of both N-Cad and E-Cad, with the peak expression after 24h (2479.91 fold and 1973.52 fold, respectively) of 1 μ M OS1 treatment (Figure 4.5.F and G). Vimentin was also upregulated by 2.7 fold after 24h of OS1 treatment (Figure 4.5.C). SLUG is a known downstream transcriptional target of ERK5 signalling and associated with re-epithelisation during keratinocyte wound healing, studied through shERK5 HaCaT models, and invasive osteosarcoma activity in an ERK5 siRNA silencing system (Arnoux *et al.*, 2008;

Yue *et al.*, 2014). However, we found that treatment with OS1 had no effect on the expression of SLUG within 6h and 24h (Figure 4.5.E).

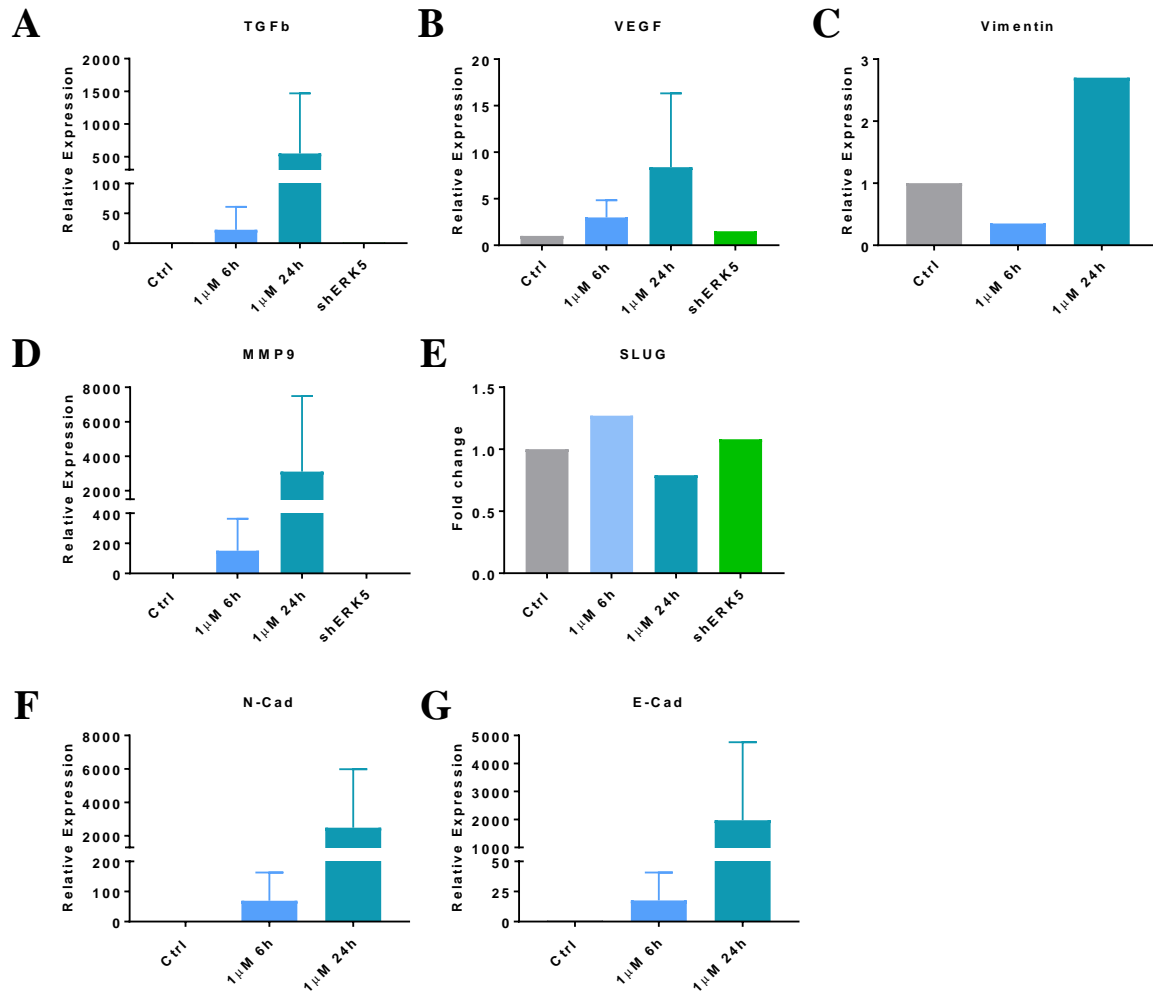


Figure 4.5. ERK5 inactivation by OS1 promotes gene expression of reparative targets. Total RNA was extracted and quantitative RT-qPCR was performed on a panel of genes after HaCaTs were treated with DMSO control and OS1 (1 μM) after 6h and 24h, and compared with shERK5 (n=1). Regulatory and reparative gene targets: (A) TGFβ, (B) VEGF, (C) Vimentin (n=1), (D) MMP9, (E) SLUG (n=1), (F) N-Cadherin, and (G) E-Cadherin. (n=3) Values represent the mean expression of cDNA of the various genes relative to β-actin. (ns = P>0.05, * = <0.05).

4.2 *In vitro* therapeutic degradation of ERK5 with OS1 primes THP-1 macrophages towards a reparative phenotype

Previous studies have demonstrated that manipulating the ERK5 pathway can have a dramatic effect on the polarity and behaviour of macrophages. Using a genetic murine model where *erk5* was inactivated specifically in the myeloid lineage through a LysM-Cre system, a predisposition towards M1-like macrophage polarisation was identified (Giurisato *et al.*, 2018; Luiz *et al.*, 2020). This provided the foundation for our next hypothesis that degradation of ERK5 in human THP-1 cells could influence polarisation of macrophages. We investigated whether a similar phenotype to the genetic model would be observed in the context of wound healing by using our novel ERK5 degrading compound, OS1. THP-1s were used as a model for human monocytes and can be differentiated into macrophages with PMA. These can be further polarised with either LPS and IFN γ or IL-4 and IL-13 to polarise towards M1 or M2 – like macrophages, respectively (Figure 4.6.A), as a robust *in vitro* experimental model (Genin *et al.*, 2015; Baxter *et al.*, 2020). In addition to gaining biological insight into ERK5 signalling in macrophage cell behaviour, using THP-1, this work allowed us to gain an early indication of murine to human model translation.

4.2.1 Morphology and profile of THP-1 macrophages

To determine the success of the differentiation and polarisation protocol we completed an initial screening study based on morphology, as conducted in previous studies (Genin *et al.*, 2015; Rios de la Rosa *et al.*, 2017). Concurring with the literature, after 24h of PMA, the THP-1 M0 macrophages became small, adherent and round body shaped structures (Figure 4.6.B). M2-like macrophages were similarly round in shape, but larger in diameter (unquantified, and only assessed by eye) compared to M0 macrophages. M1-like macrophages exhibited long and spindle like protrusions, which indicates a response to increase its interaction with the surrounding areas and surfaces (Bertani *et al.*, 2017).

In addition, differentiation with PMA to M0 macrophages caused these cells to no longer proliferate, as observed in the SRB and MTT assays (Figure 4.6.C) which was in line with previous studies (Rios de la Rosa *et al.*, 2017; Starr *et al.*, 2018). As previously utilised above, SRB and MTT assays are robust methodologies to measure cell density and proliferation based on cellular protein content or cellular metabolic activity, respectively.

During an initial SRB study, THP-1's were seeded at three densities (5,000, 10,000, and 20,000 cells per well) and collected at 24h, 48h, 72h, and 96h after differentiation with PMA. It was expected that differentiation from monocytes to macrophages would inhibit proliferation (Genin *et al.*, 2015; Baxter *et al.*, 2020), but our observations by SRB yielded inconsistent and unexpected results, where the 5,000 cells per well THP-1 M0 macrophages increased their cell number across the 96h time course (Figure 4.6.C). It was discovered that during the SRB protocol, THP-1 cells were detached during the washing step. The MTT assay was then conducted as the more appropriate approach to assess the cell density of THP-1s to investigate their proliferation, as it allowed cells to remain *in situ* for the study without washes.

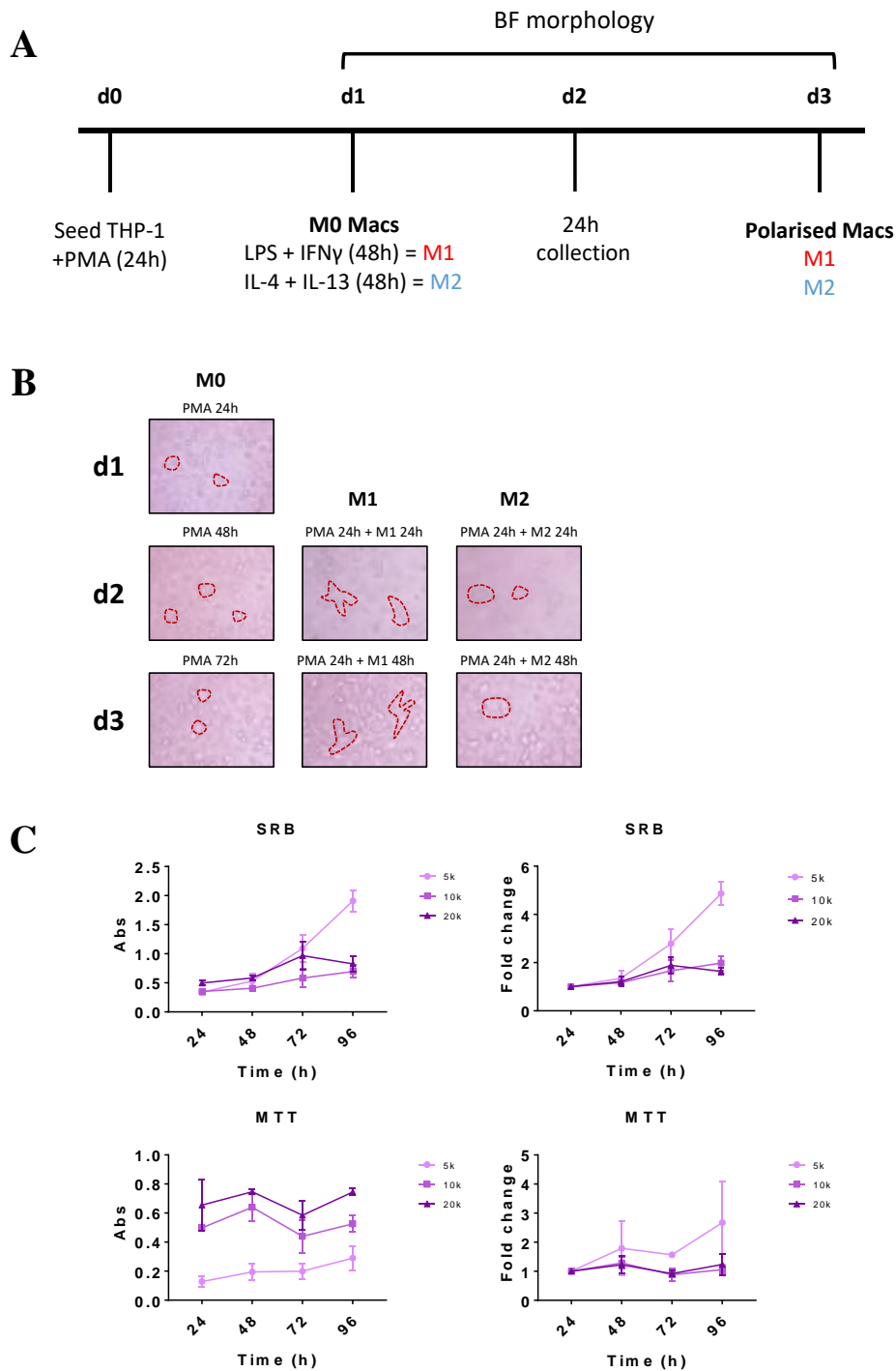


Figure 4.6. THP-1 macrophage model. (A) Experimental *in vitro* workflow with THP-1 model of monocytes. Treatment with PMA for 24h differentiates monocytes to M0 macrophages. These were then further polarised to M1-like (LPS and IFN γ) or M2-like (IL-4 and IL-13) macrophages. (B) Representative bright field images of differentiated and polarised THP-1 cells to demonstrate morphological differences. Dotted red line outline example cells. M0 and M2-like exhibit similar round bodied structures, whereas M1-like macrophages exhibit long and spindle like protrusions. (C) SRB and MTT assays were conducted at varying densities (5,000 vs 10,000 vs 20,000) to assess cell numbers after THP-1 monocyte differentiation with PMA to M0 macrophages (n=4). Left graphs are absorbance, right graphs are fold change from 24h. (ns = P>0.05, * = <0.05).

Given these clear morphological differences observed by bright field analysis, experiments were repeated using the same conditions and cells analysed for cytoskeletal changes using phalloidin: a highly selective peptide for staining actin filaments. These actin filaments are a major component of cytoskeletal structure and are known to change in structure, quantity and location in the cells of M0 macrophages during their transition to M1-like or M2-like macrophages (Pergola *et al.*, 2017; Rios de la Rosa *et al.*, 2017).

Similar observations to the literature and our bright field images were made, where M1 polarised macrophages exhibited long and spindle like protrusions, whereas M2 polarised macrophages remained circular and large in diameter. Phalloidin stain in these cells were quantified by area of total red fluorescence divided by the DAPI count (Figure 4.7.A). This represented the average area of phalloidin per cell. Actin filaments have key functions in motility, endocytosis and polarisation, thus its upregulation can be indicative of the polarised and morphological state of M1-like and M2-like phenotypes (Pergola *et al.*, 2017). Our quantification of the phalloidin indicated that M1 (1.16 fold) and M2 (1.49 fold) macrophages had increased levels of actin filaments, with M2 macrophages being significantly increased compared to M0 macrophage controls (Figure 4.7.A).

We additionally confirmed the successful differentiation of monocytes to macrophages with immunofluorescence staining for CD68. This is a protein highly expressed in the macrophage lineage and if the differentiation protocol of THP-1 has been successful, we should expect to see positive CD68 staining across M0, M1 and M2 macrophages (Genin *et al.*, 2015). Accordingly, our data show its consistent expression across all THP-1 macrophage states in this study: M0, M1-like and M2-like, indicating successful differentiation as concurrent with previous studies (Figure 4.7.B). There was a significant increase in CD68 expression in M2 macrophages (1.79 fold) compared to M0 macrophage control.

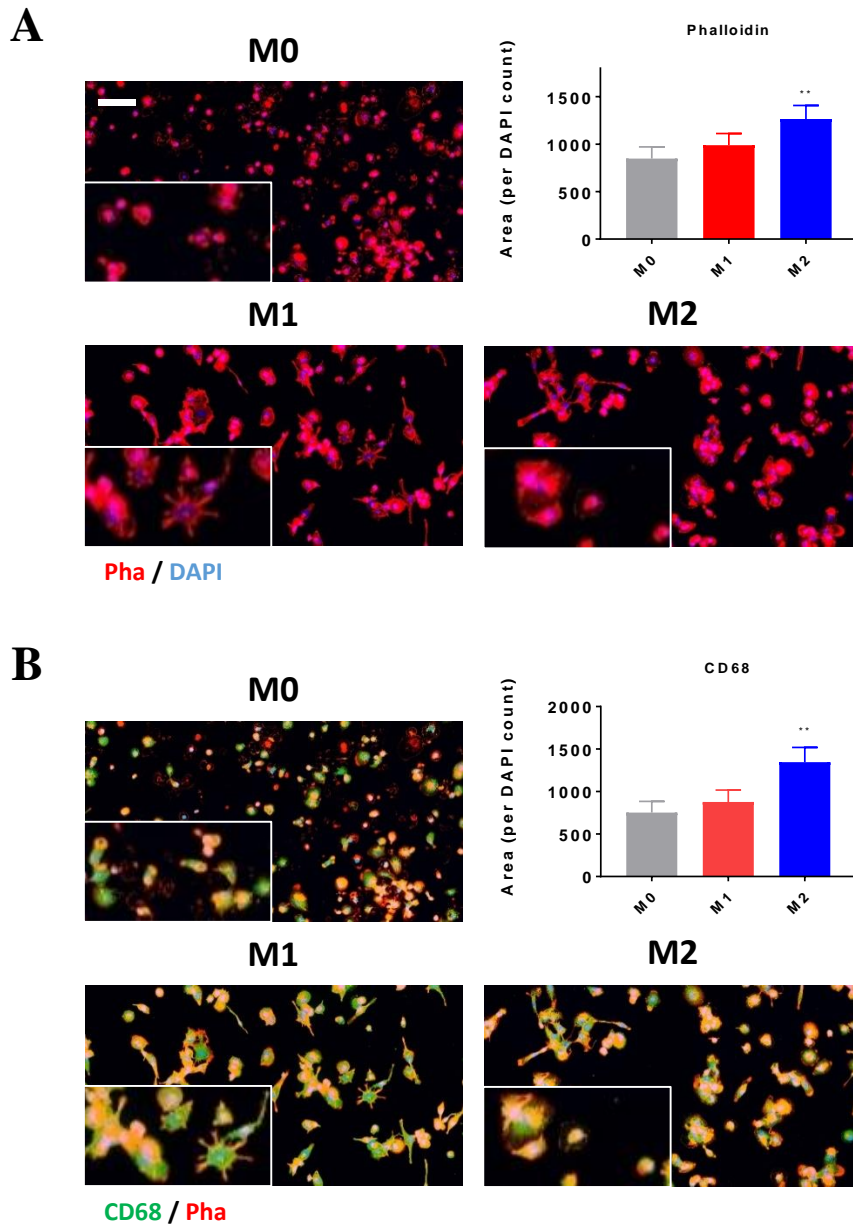


Figure 4.7. Immunofluorescent expression of phalloidin and CD68 in THP-1 macrophages. M0 = THP-1 macrophages treated with PMA for 24h. M1 = M0 + (LPS+IFN γ) for 48h. M2 = M0 + (IL4+IL13) for 48h. (A) Phalloidin stain for M0, M1, and M2 THP-1 macrophages. Red indicates phalloidin, and blue indicates DAPI. Magnification of objective was 20x, with expanded inserts at 40x (white border). White bar = 50 μ m. Graph represents average area of phalloidin stain divided by number of DAPI positive cells as processed by ImageJ. Five fields were counted from three independent samples (n=3). (B) CD68 stain for M0, M1, and M2 THP-1 macrophages. Green indicates CD68. Magnification of objective was 20x, with expanded inserts at 40x (white border). Graph represents average area of CD68 stain divided by number of DAPI positive cells as processed by ImageJ. Five fields were counted from three independent samples (n=3). (ns = P>0.05, *=<0.05, **=<0.01).

4.2.2 Differentiating M1/M2 –like macrophages by their gene expression of inflammatory and repair associated mediators

RT-qPCR analysis was used to investigate the gene expression of key immune and repair mediated cytokines that are known to significantly change in response to successful THP-1 polarisation to M1-like and M2-like macrophages. Control M0 macrophages (Ctrl) were THP-1 cells differentiated into THP-1 M0 macrophages after PMA treatment for 24h. We additionally included samples of THP-1 cells which were treated with PMA for 48h to time match to polarising conditions. M1-like macrophage polarisation was induced with LPS and IFN γ treatment on THP-1 M0 macrophages and were collected after 24h and 48h to assess both early and later polarising effects on mRNA expression. This was similarly conducted with M2-like polarisation with IL-4 and IL-13 treatment on THP-1 M0 macrophages. Analysis was completed with the $\Delta\Delta$ CT method, as relative expression to β -actin, and statistical testing was done on the Δ CT values.

In concordance with previous studies in M1 macrophage polarisation, inflammatory markers; TNF- α , IL-1 β , IL6, and IL-8 were upregulated in M1-like macrophages (Genin *et al.*, 2015). Notably there was significant increase in IL-1 β (16.65 fold) and IL-8 (31.46 fold) in M1 24h macrophages when compared to M0 controls (Figure 4.8.A). Additionally MR, an M2 associated marker, gene expression was significantly lower in M1 24h macrophages (0.18 fold; -82%). There was also significantly increased gene expression of MMP9 in M1 polarity state at 24h (2.21 fold) and 48h (1.81 fold) (Figure 4.8.B). MMP9 has previously been observed to increase in M1-like phenotypes and required in inflammatory response to efficiently migrate in damaged tissue or breakdown atherosclerotic plaques in vessel walls (Lepidi *et al.*, 2001; Hanania *et al.*, 2012).

The profile was less consistent in repair markers for M2-like macrophages. There was increased expression of TGF- β (24.28 fold), MR (10.86 fold), and VEGF (5.58 fold) in M2-

like macrophages within 24h of polarising agent, which matched trends seen in previous studies (Genin *et al.*, 2015; Rios de la Rosa *et al.*, 2017; Baxter *et al.*, 2020) but this was not significant due to large variability (Figure 4.8.B). Unexpectedly, there was similarly high expression of TGF- β (9.94 fold) in M1-like macrophages, and again the large variability was a factor. Typically studies have found M2-like polarisation with IL-4 and IL-13 result in robust and increased expression in MR, TGF- β and VEGF.

This investigation in establishing parameters to understand the polarity states of THP-1 macrophages suggested that M1-like macrophage polarisation was a simpler and more robust model to generate. However, the large variability in M2-like macrophage gene expression profile suggest that the *in vitro* model may be difficult to study wound repair macrophages and require further experimental investigation and development. This is unsurprising when considering the large spectrum that M2-like macrophages can sit under, and that simply trying to polarise and identify repair macrophages without the correct biological context may be difficult.

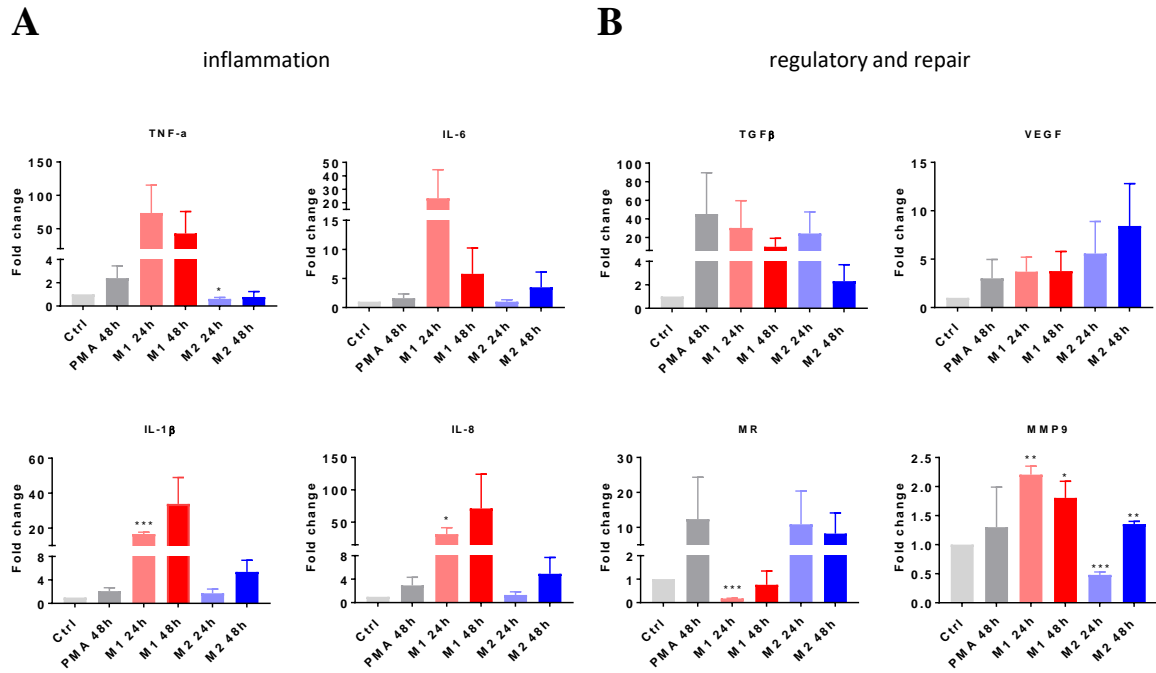


Figure 4.8. Gene expression profile of THP-1 cells. Total RNA was extracted and RT-qPCR was performed on a panel of genes after THP-1 cells were treated with PMA, M1 (LPS and IFN γ) and M2 (IL-4 and IL-13) polarising agents for 24h and 48h. (A) Inflammatory gene targets: TNF- α , IL-1 β , IL-6, and IL-8. (B) Regulatory and reparative gene targets: TGF- β , VEGF, MR, and MMP9. Values represent the mean expression of cDNA of the various genes relative to β -actin (n=3). (ns = P>0.05, *= <0.05 , **= <0.01 , ***= <0.001).

4.2.3 OS1 specifically targets and degrades ERK5 protein in THP-1 cells

Progressing forward we used the above simplified profile and categorisation to investigate the effects that using OS1 treatment to degrade ERK5 on THP-1 M0 macrophages would have in terms of their morphology, function and predisposition to become more inflammatory or reparative macrophage phenotypes. This was based on our previous observations in chapter 3, where *in vivo* systems showed that loss of ERK5 initially invoked an earlier and rapid inflammatory response followed by the earlier arrival of repair mechanisms to assist the wound healing process.

We first focussed our studies into whether OS1 could knockdown ERK5 in THP-1 cells differentiated into macrophages. We wanted to understand what the ERK5 expression in

myeloid cells was and if manipulation of this signalling pathway led to improved wound healing and reduced inflammation as reflected in the genetic model.

To investigate the effect of ERK5 inhibition on THP-1 cells, ERK5 expression was assessed in M0 (PMA for 24h), M1 (M0 polarised with LPS + IFN γ for 48h) and M2 (M0 polarised with IL4 + IL-13 for 48h) polarised states of THP-1 macrophages after treatment of 0.1 μ M and 1 μ M OS1 for 24h, as analysed by western blot. These were effective concentrations that would knockdown ERK5 for the required duration as shown in the HaCaT cell workflow (Figure 4.1.B), and parallel work in the Finegan Lab (unpublished). The changes in protein expression were expressed as a ratio density of the protein of interest, ERK5, to the density of the loading control GAPDH or β -actin.

Polarisation to M1-like or M2-like macrophages slightly reduced levels of ERK5 expression (-15% and -36%, respectively), and it should be noted this was not consistently observed, nor was it significant (Figure 4.9.A). The variance could be due a heterogeneous population of macrophages following polarisation, i.e. not all cells have been polarised to the same degree or in the same time frame. We tested OS1 at two concentrations (0.1 μ M and 1 μ M), and found that 1 μ M treatment for 24h continued to be an effective dose which reduced the levels of ERK5 (-81%) (Figure 4.9.A). It was pragmatic to continue our downstream workflow with the 1 μ M OS1 treatment concentration for 24h, which had previously been effective in HaCaTs and to ensure consistency in workflow comparisons between cell lines. As seen in HaCaT cells, OS1 had no impact on the known off-target proteins of other ERK5 kinase inhibitors (BRD4) and similar kinase proteins such as ERK1/2 in THP-1 cells (Figure 4.9.B).

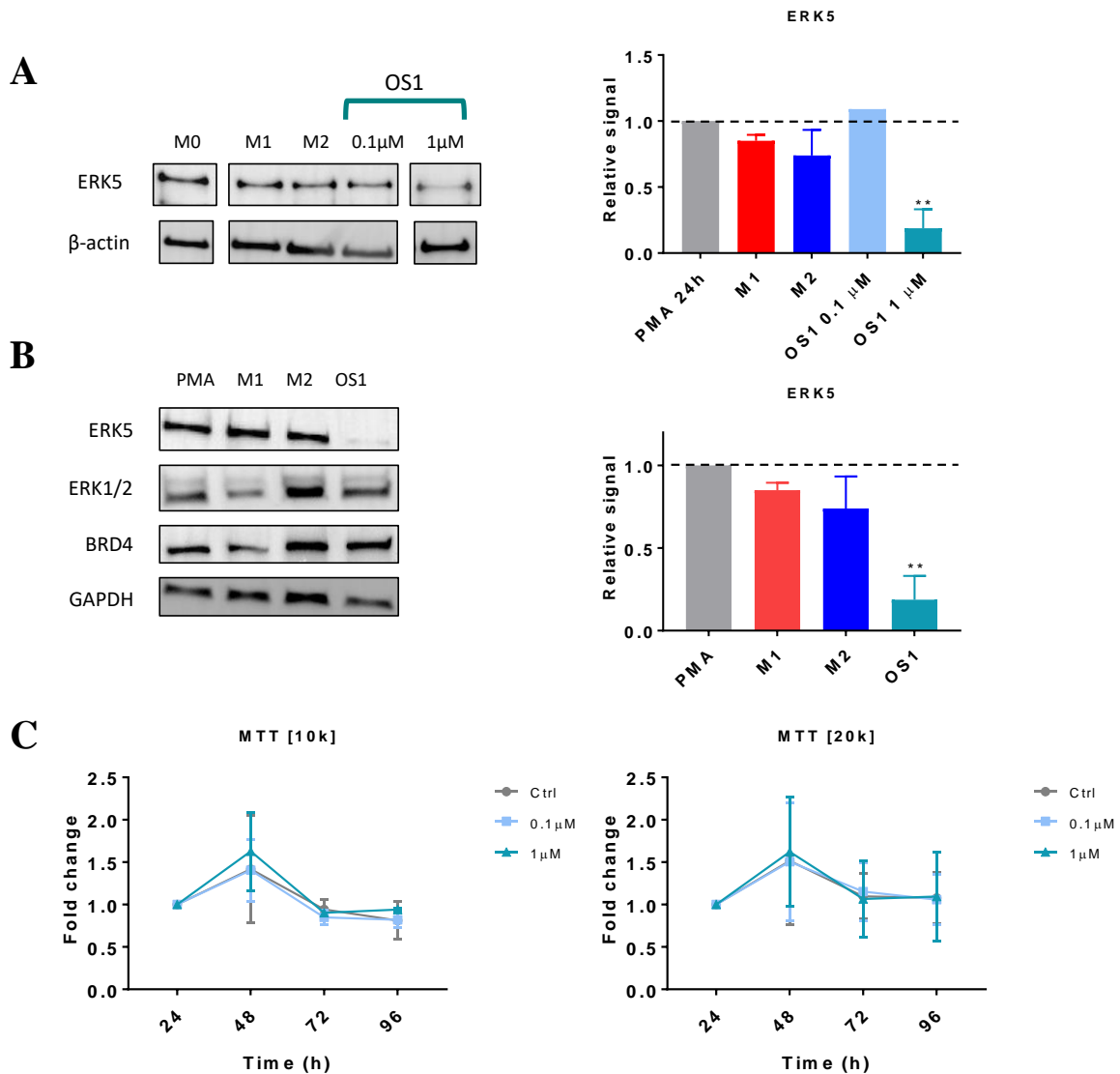


Figure 4.9. OS1 targets and degrades ERK5 in THP-1s and did not affect proliferation. (A) Representative blots after THP-1 cells were M1/M2-like polarised or treated with OS1 at 0.1 μ M and 1 μ M to assess ERK5, and β -actin (n=3). (B) Representative blots after THP-1 cells were M1/M2-like polarised or treated with OS1 at 1 μ M to assess ERK5, ERK1/2, BRD4, and GAPDH (n=3). (C) MTT assays were conducted following treatment with DMSO control, and OS1 (0.1 μ M vs 1 μ M) after selected time points of 24h, 48h, 72h and 96h. Data points plotted represent the mean of three independent experiments \pm SEM. (ns = $P > 0.05$, * = $P < 0.05$, ** = $P < 0.01$, *** = $P < 0.001$, **** = $P < 0.0001$).

The cell density of THP-1 differentiated M0 cells were assessed by MTT, as a measure of cellular mitochondrial activity, to investigate whether treatment of OS1 would have an effect on proliferation or cytotoxicity. THP-1 M0 macrophages were treated with a single dose of OS1 at 0.1 μ M and 1 μ M and collected for MTT analysis over a 96h time course. Assessing the cell density over this time course would indicate if OS1 promoted proliferation (increased cell

density), or had a cytotoxic effect (decreased cell density). With the exception of some large variability at 48h, there was no significant difference in THP-1 cell density. This concluded that OS1 mediated degradation of ERK5 did not promote proliferation or induce a cytotoxic effect on THP-1 macrophages (Figure 4.9.C).

Upon confirmation that ERK5 was successfully degraded in THP-1 M0 macrophages, these cells were assessed for morphology by bright field and immunofluorescence staining for phalloidin and CD68. This would provide insight into how loss of ERK5 may impact cellular structure and marker expression that indicates its status as a healthy M0 macrophage. In our study we found that M0 macrophages treated with a single dose of 1 μ M OS1 for up to 48h showed no obvious morphological changes and remained small and round bodied in shape (Figure 4.10.A), as previously seen in other M0 macrophages (Genin *et al.*, 2015; Rios de la Rosa *et al.*, 2017).

Similarly to our initial profiling workflow, we stained for actin filaments with phalloidin in the M0 macrophages treated with OS1 and observed a slight increased trend (1.39 fold) but of no statistical significance (Figure 4.10.A). As actin filaments are important in motility, endocytosis and polarisation, this subtle increase could indicate a predisposition towards a polarity state. We additionally, confirmed that treatment with OS1 did not affect CD68 staining, a marker for macrophage differentiation, and observed only a small and insignificant decrease in OS1 treated M0 macrophages (Figure 4.10.B).

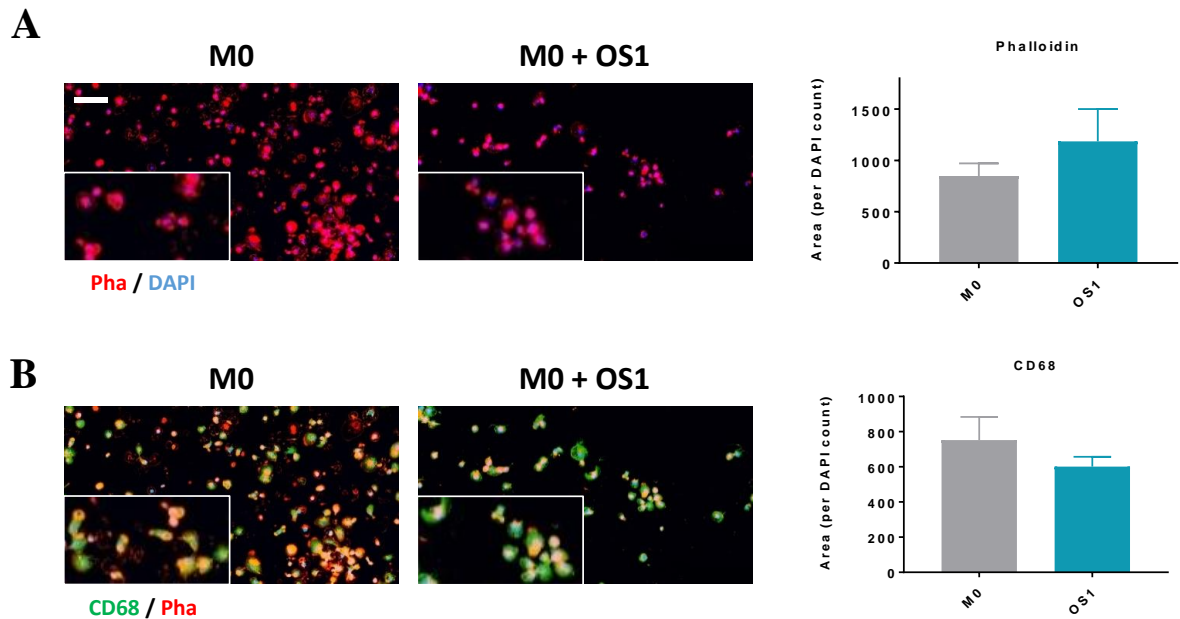


Figure 4.10. OS1 treatment in THP-1s did not affect morphology. M0 = THP-1 macrophages treated with PMA for 24h. M0 + OS1 = M0 + 1 μ M OS1 treatment for 24h. (A) Phalloidin stains for M0 and M0 + OS1 treated THP-1 macrophages. Red indicates phalloidin, and blue indicates DAPI. Magnification of objective was 20x, with expanded inserts at 40x (white border). White bar = 50 μ m. Graph represents average area of phalloidin stain divided by number of DAPI positive cells as processed by ImageJ. Five fields were counted from three independent samples (n=3). (B) CD68 stain for M0 and M0 + OS1 treated THP-1 macrophages. Green indicates CD68. Magnification of objective was 20x, with expanded inserts at 40x (white border). Graph represents average area of CD68 stain divided by number of DAPI positive cells as processed by ImageJ. Five fields were counted from three independent samples (n=3). (ns = P>0.05, *=<0.05).

4.2.4 Identifying changes to cell surface markers by immunofluorescence after ERK5 inactivation with OS1

To determine if ERK5 signalling is involved in human macrophage polarisation towards either an M1 or M2-like phenotype, we then focussed on how OS1 mediated degradation of ERK5 in M0, M1 and M2 polarity states would affect their surface expression markers based on immunofluorescence. Previous studies using bone-marrow derived monocytes isolated from ERK5 deficient myeloid models indicate a pre-disposition towards an M1-like phenotype, with reduced expression of M2-related genes such as *Arg1*, *Fizz1* and *Ym1* (Heo *et al.*, 2014; Giurisato *et al.*, 2018). However, studies in the human model context have been limited. An inflammatory context such as LPS induction or statin treatment have been shown to increase ERK5 phosphorylation and transcriptional activity in THP-1 macrophages (Heo *et al.*, 2014; Richter *et al.*, 2016). However, describing a direct link between ERK5 signalling in the human macrophage polarisation model has yet to be achieved. In addition, using OS1 in this context permits an early indication into whether this small molecule has the potential as a novel therapeutic to alter macrophage polarisation.

We conducted a similar workflow as previously, where THP-1 monocytes were differentiated with PMA to generate M0 macrophages. These M0 macrophages were either polarised to M1 or M2-like macrophages alone, or in conjunction with 1 μ M OS1 treatment. This would permit studies into how ERK5 degradation during the polarisation stage impacts their phenotype based on morphology and expression profiles, as assessed after 24h, 48h, and 72h of combination treatment of polarising agent and OS1 (Figure 4.11.A). Moreover, we were able to confirm that OS1 treatment for 24h in combination with LPS + IFN γ (M1) or IL-4 + IL-13 (M2) leads to degradation of ERK5 (Figure 4.11.B and C).

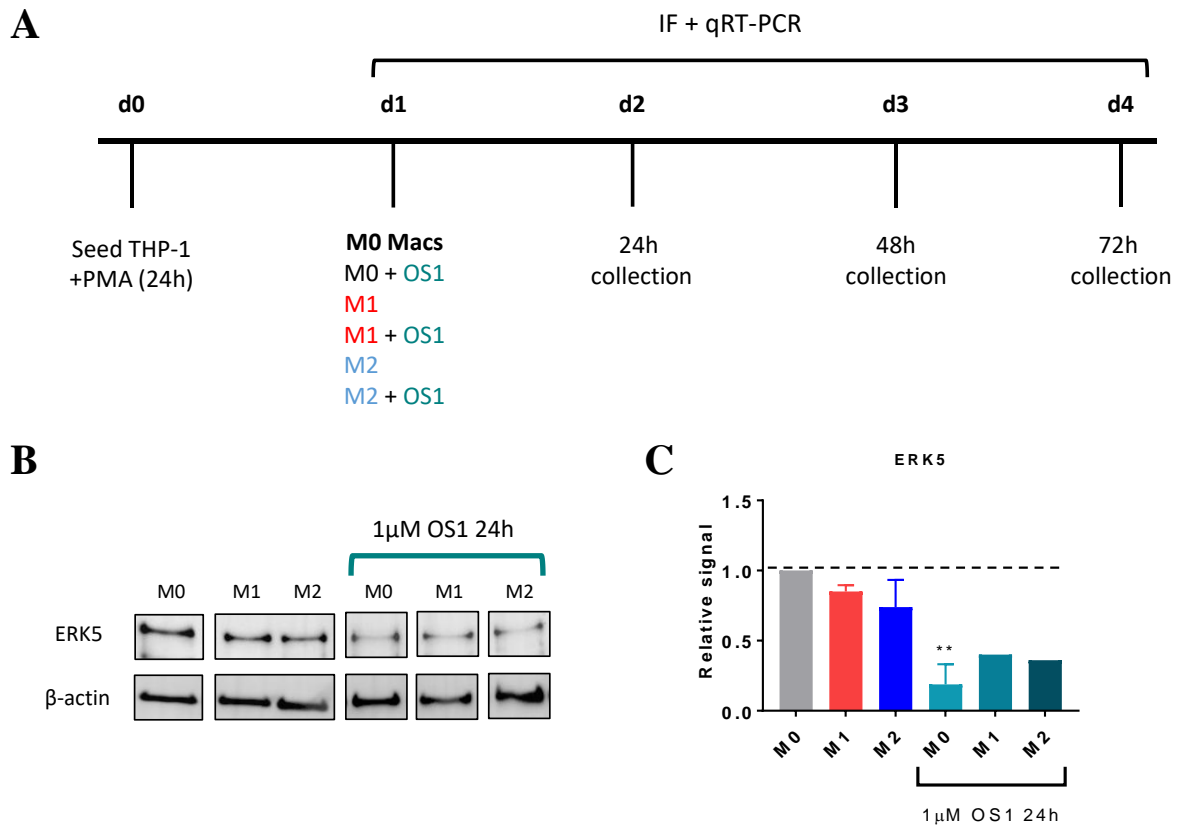


Figure 4.11. OS1 treatment in M0, M1 and M2 THP-1 macrophages degrades ERK5. (A) Experimental *in vitro* workflow with THP-1 model of monocytes. Treatment with PMA for 24h differentiates monocytes to M0 macrophages. These were further polarised to M1-like (LPS and IFN γ) or M2-like (IL-4 and IL-13), or treated in combination with 1 μ M OS1 for 24h, 48h and 72h. (i.e. M1+OS1 cohort were M0 THP-1 macrophages treated with LPS, IFN γ and OS1, in combination). (B) Representative blots after THP-1 cells were M1/M2 polarised or treated with 1 μ M OS1 for 24h to assess ERK5 and β -actin (n=3). (C) ERK5 protein levels were normalised and graphed against corresponding β -actin. (ns = P>0.05, *=<0.05, **=<0.01).

Our range of targets to be investigated by immunofluorescence included, ERK5, phalloidin, and markers of M1-like (TSPO) and M2-like (MR and CD163) polarity states. Assessing ERK5 by immunofluorescence would allow us to reflect the previous western blot protein quantification with the additional advantage of visualising the localisation of ERK5 distribution in the THP-1 cells. Translocator protein (TSPO), is a mitochondrial protein found to be upregulated in expression in inflammatory and M1-like macrophages (Boutin and Pinborg, 2015; Lanfranca *et al.*, 2018). A previous study within the Finegan Lab, in the cancer context, has shown that loss of ERK5 signalling with shERK5 143B (osteosarcoma cells)

suppressed infiltration and the number of TSPO expressing inflammatory macrophages (Green *et al.*, 2020). Mannose receptor is an effective endocytic receptor that binds to a broad range of microbial carbohydrates, and is typically expressed in regulatory and reparative macrophages of an M2-like phenotype (Martinez-Pomares, 2012; Novak and Koh, 2013; Genin *et al.*, 2015; Gantzel *et al.*, 2021). This has additionally been a target of M2-like tumour associated macrophages, and found to be co-localised with ERK5 expression (Green *et al.*, 2020). CD163 is a high affinity scavenger receptor for haemoglobin that often characterises tumour associated macrophages with an immunosuppressive M2-like phenotype (Kubota *et al.*, 2017; Giurisato *et al.*, 2018; Gantzel *et al.*, 2021). The study by Giurasato *et al.*, found ERK5 to be highly expressed in CD163 expressing human tumour associated macrophages, and so the loss of ERK5 could reduce this M2-like phenotype.

4.2.5 ERK5 expression decreased with OS1 treatment and increased with M1/M2 polarisation

We wanted to assess ERK5 expression by IF staining in order to reflect our previous western blot analysis which showed effective ERK5 degradation with 1 μ M OS1 treatment. Additionally, we aimed to investigate and visualise the localisation of ERK5 protein in the myeloid cell lineage in these different polarity states (Figure 4.12.A). As previously mentioned, activated and phosphorylated ERK5 results in exposure of its NLS domain in the C-terminus, promoting its localisation to the nucleus (Nithianandarajah-Jones *et al.*, 2012; Pearson *et al.*, 2020). Most of the ERK5 in these THP-1 cells was observed to remain in the cytoplasm, suggesting a non-phosphorylated and basal activation state throughout M0, M1 and M2 –like polarisation. In this study, we found that OS1 treatment in both M1 (-59%) and M2 (-52%) macrophages led to reduced levels of ERK5 compared to their non OS1 treated counterparts. Additionally, less of the ERK5 was observed to be localised in the nucleus, and what ERK5 remained appeared primarily in the cytoplasm.

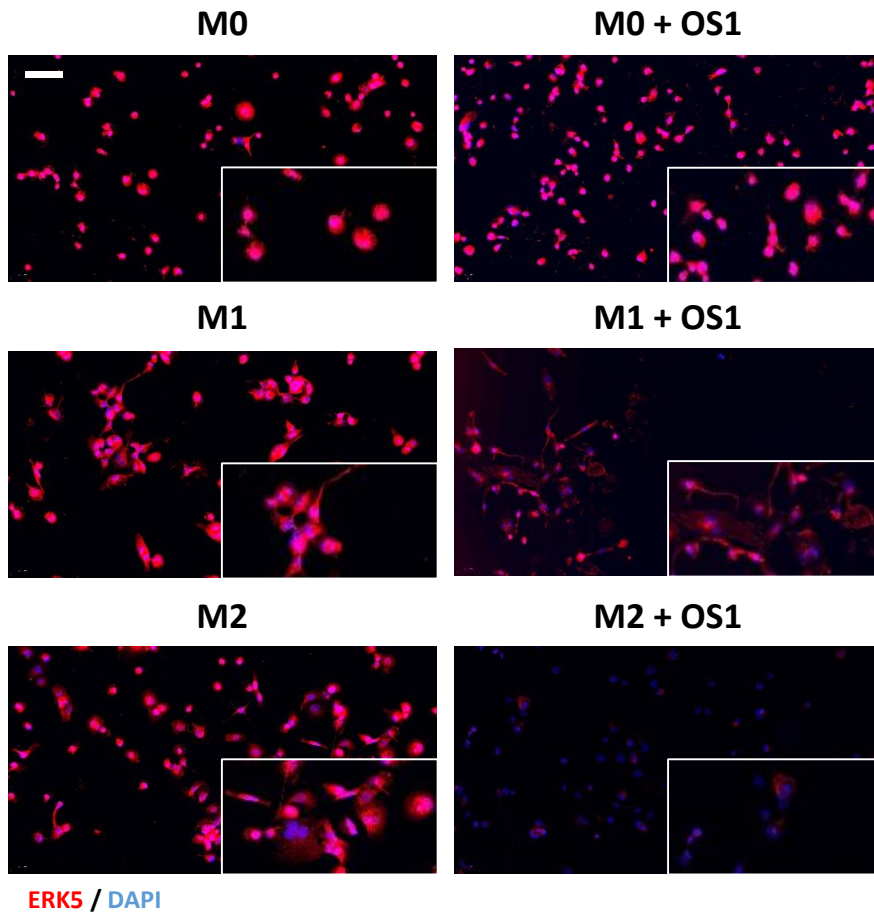
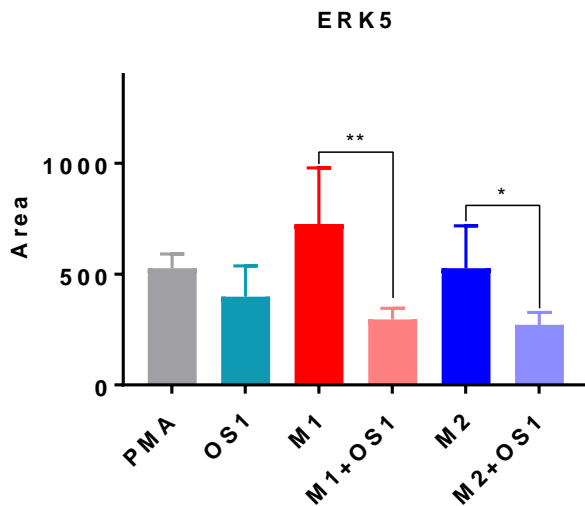
A**B**

Figure 4.12. Increased expression of ERK5 in M1/M2 THP-1 macrophages which decreased after OS1 treatment. M0 = THP-1 macrophages treated with PMA for 24h. M1 = M0 + (LPS+IFN γ) for 24h. M2 = M0 + (IL-4+IL-13) for 24h. 1 μ M OS1 treatment for 24h was simultaneously added with polarisation agents. (A) ERK5 stain for M0, M1, M2 and OS1 treated THP-1. Red indicates ERK5, and blue indicates DAPI. Magnification of objective was 20x, with expanded inserts at 40x (white border). White bar = 50 μ m. (B) Graph represents average area of ERK5 stain divided by number of DAPI positive cells as processed by ImageJ (n=3). (ns = P>0.05, * = <0.05, ** = <0.01).

The investigation into ERK5 expression, polarity states and the effect of OS1 was widened to a time course of up to 72h (Figure 4.13.A). These longer time points were investigated to assess how ERK5 localisation and protein levels may change throughout a 72h window after a single dose of OS1, or M1/M2 polarisation treatment. In particular, as seen in our studies and in previous literature, full polarisation requires at least 48h (Rios de la Rosa *et al.*, 2017), thus with the longer time course we gain a wider insight into how OS1 mediated ERK5 degradation may impact this polarisation.

We unexpectedly found that ERK5 expression significantly decreased in M0 macrophages in PMA alone over 72h (-73%). However, concurrent with our western blot analysis, addition of 1 μ M OS1 in M0 macrophages for 48h and 72h significantly reduced the levels of ERK5 by (-33%) and (-44%) respectively. Polarisation to M1 and M2 macrophages within 24h increased ERK5 expression compared to M0 macrophage controls. Following this initial stage of polarisation, we observed a trend of decreased ERK5 in both M1 and M2 states after 48h and 72h. Additionally, we show that OS1 treatment reduced the levels of ERK5 in both states, but significantly in the M2 macrophages treated with 1 μ M OS1 after 24h (-61%), 48h (-59%), and 72h (-79%). Notably, we observe that OS1 treatment appears to limit ERK5 expression in the nucleus as it primarily sequesters in the cytoplasm of M0 and M1 macrophages after 24h treatment of OS1. This again indicates what ERK5 remains, may be in a basal and non-phosphorylated state.

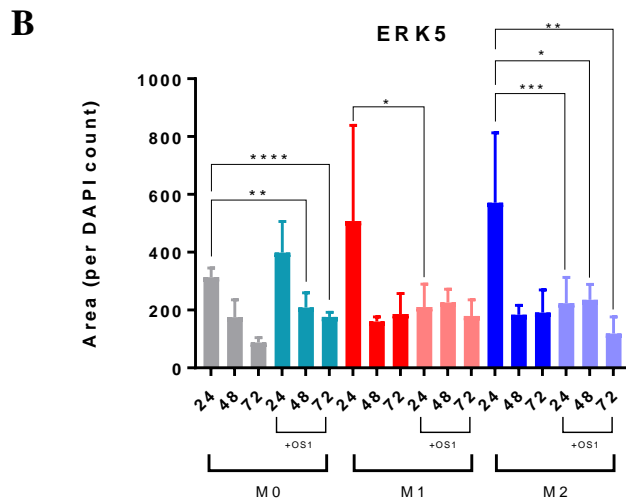
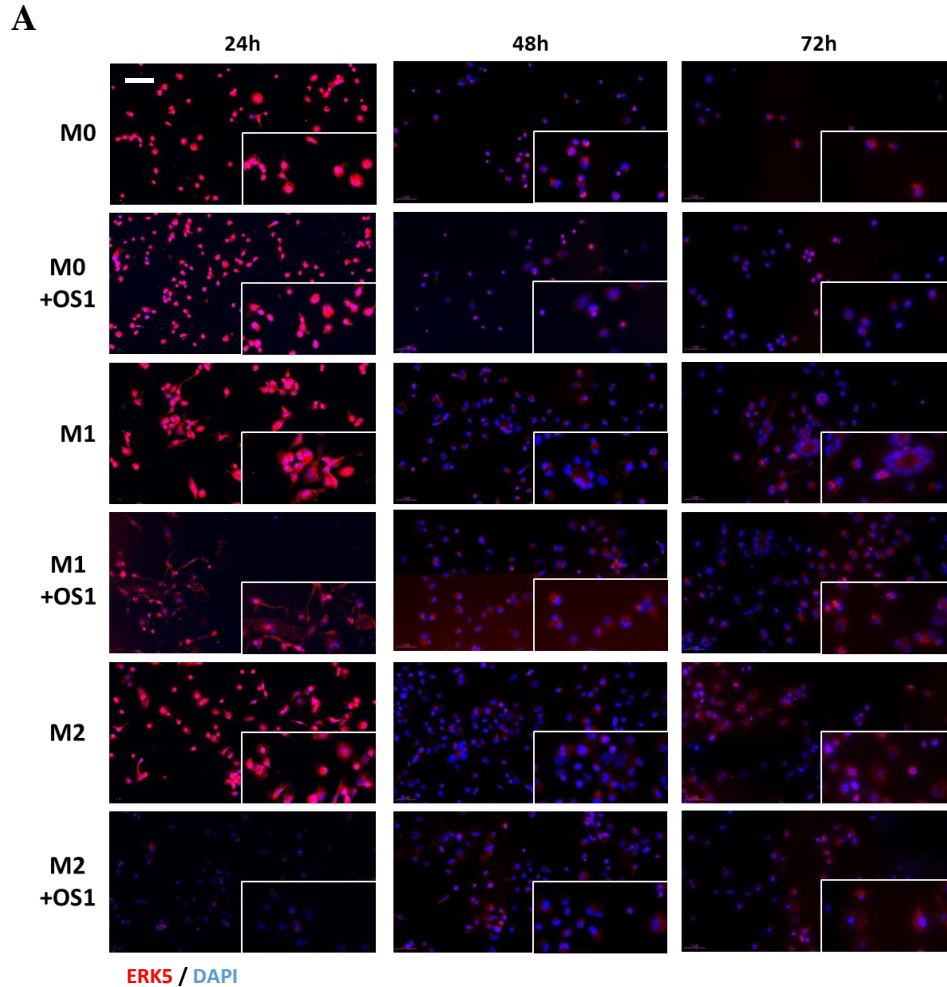


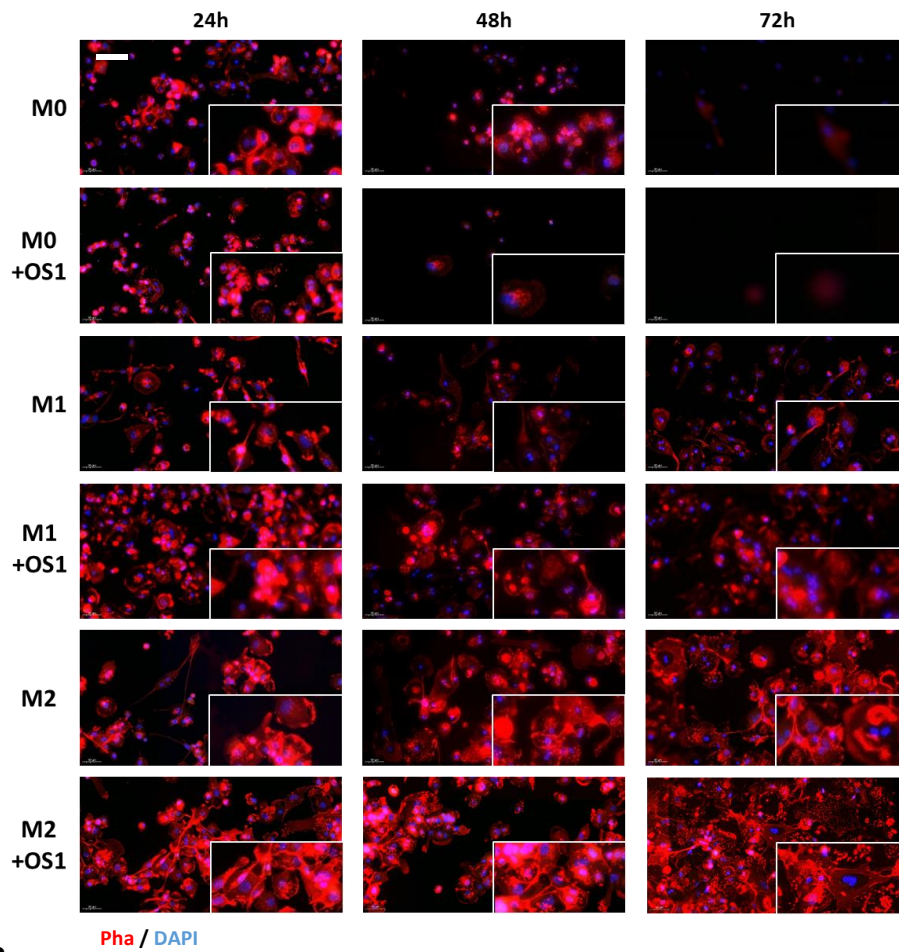
Figure 4.13. OS1 decreased expression of ERK5 which was sequestered into the cytoplasm of THP-1 macrophages. M0 = THP-1 macrophages treated with PMA for 24h. M1 = M0 + (LPS+IFN γ). M2 = M0 + (IL-4+IL-13). 1 μ M OS1 treatment was simultaneously added with polarisation agents. (A) ERK5 stain for M0, M1, M2 and OS1 treated THP-1. Red indicates ERK5, and blue indicates DAPI. Magnification of objective was 20x, with expanded inserts at 40x (white border). White bar = 50 μ m. (B) Graph represents average area of ERK5 stain divided by number of DAPI positive cells as processed by ImageJ (n=3). (ns = P>0.05, * = P<0.05, ** = P<0.01, *** = P<0.001, **** = P<0.0001).

4.2.6 ERK5 inactivation by OS1 had limited effect on phalloidin expression

We re-examined phalloidin expression in the M1 and M2-like macrophage polarity states at these longer time points of 72h (Figure 4.14.A). We previously showed that phalloidin immunofluorescence staining increased in both M1 and M2 macrophages with distinct morphology in each. That is, spindle like protrusions in M1-like, and wide circular structures in M2-like macrophages. Here we studied the actin filament staining in polarised macrophages over the course of 72h, with and without 1 μ M OS1 treatment to assess how ERK5 degradation may impact quantity and morphology pattern of these THP-1 macrophages.

M0 macrophages significantly decreased the levels of actin filaments after 72h (0.20 fold; -80%). M1 macrophages showed a similar profile over the 72h time course. M2 macrophages increased the most, and maintained a high level of actin filaments at 48h (2.13 fold) and 72h (2.30 fold) compared to M2 macrophages at 24h. Treatment with OS1 over the time course had limited impact on actin filament quantity in M0 and M1 macrophages, but exhibited an increased trend in the M2 macrophage (Figure 4.14.B). This could indicate that degradation of ERK5 in M2 polarised macrophages may encourage it to increase in size and quantity of actin filaments required for its motility and polarisation.

A



B

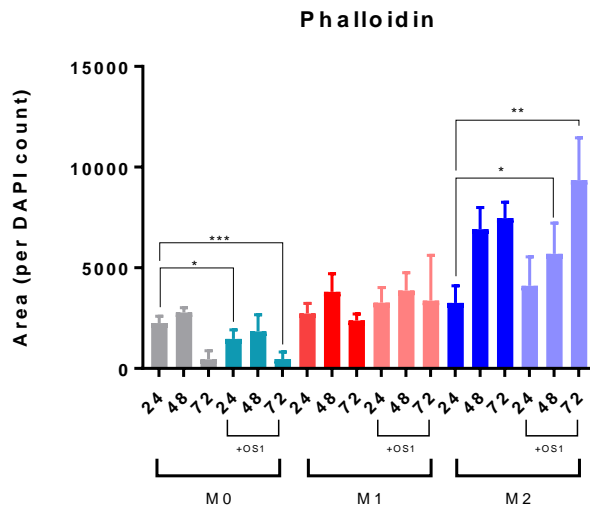


Figure 4.14. OS1 had limited effect on phalloidin expression in THP-1 macrophages. M0 = THP-1 macrophages treated with PMA for 24h. M1 = M0 + (LPS+IFN γ). M2 = M0 + (IL-4+IL-13). 1 μ M OS1 treatment was simultaneously added with polarisation agents. (A) Phalloidin stain for M0, M1, M2 and OS1 treated THP-1. Red indicates phalloidin, and blue indicates DAPI. Magnification of objective was 20x, with expanded inserts at 40x (white border). White bar = 50 μ m. (B) Graph represents average area of phalloidin stain divided by number of DAPI positive cells as processed by ImageJ (n=3). (ns = P>0.05, * = <0.05, ** = <0.01, *** = <0.001).

4.2.7 TSPO expression was largely unchanged by OS1 treatment

TSPO is a mitochondrial based receptor often associated with macrophages in an inflammatory context. We aimed to use this marker to identify M1 polarisation in the THP-1 macrophage model, and to assess how OS1 mediated degradation of ERK5 may influence polarisation (Boutin and Pinborg, 2015; Lanfranca *et al.*, 2018).

Concurring with the literature, we found that M1 polarisation increased the expression levels of TSPO by 1.5 fold. However, unexpectedly we observed this increased expression of TSPO to be greater in M2 polarised THP-1 macrophages by 1.95 fold. OS1 treatment increased TSPO expression in M0 (1.80 fold) and M1 macrophages (1.29 fold), but slightly decreased the TSPO expression in M2 macrophages (0.87 fold; -13%) (Figure 4.15.A and B).

TSPO expression decreased after 72h in M0 (0.40 fold; -60%), M1 (0.38 fold; -62%) and in M2 (0.18 fold; -82%) macrophages compared to their 24h counterparts. This similar pattern was observed after OS1 treatment, suggesting that degradation of ERK5 over 72h had no impact on TSPO expression and polarisation towards an M1-like phenotype (Figure 4.16.B).

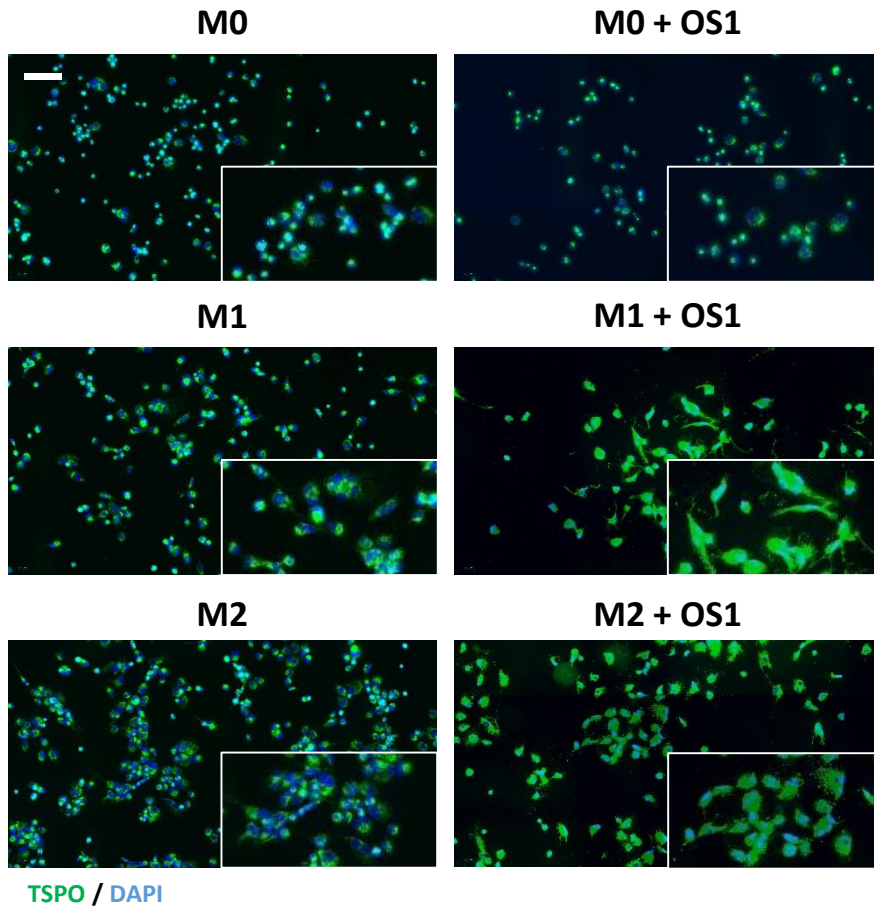
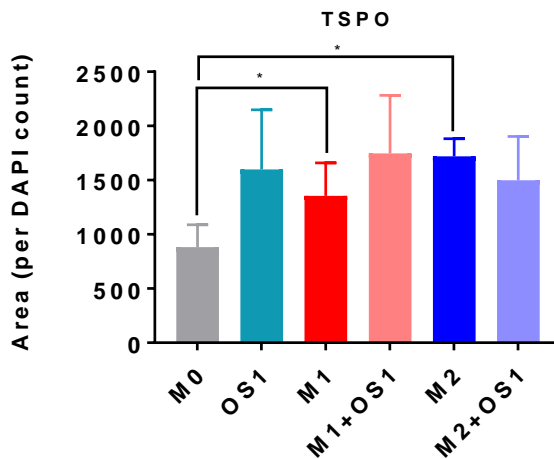
A**B**

Figure 4.15. OS1 had no effect on TSPO expression in THP-1 macrophages within 24h. M0 = THP-1 macrophages treated with PMA for 24h. M1 = M0 + (LPS+IFN γ) for 48h. M2 = M0 + (IL-4+IL-13) for 48h. 1 μ M OS1 treatment for 24h was simultaneously added with polarisation agents. (A) TSPO stain for M0, M1, M2 and OS1 treated THP-1. Green indicates TSPO and blue indicates DAPI. Magnification of objective was 20x, with expanded inserts at 40x (white border). White bar = 50 μ m. (B) Graph represents average area of TSPO stain divided by number of DAPI positive cells as processed by ImageJ (n=4). (ns = P>0.05, *=<0.05).

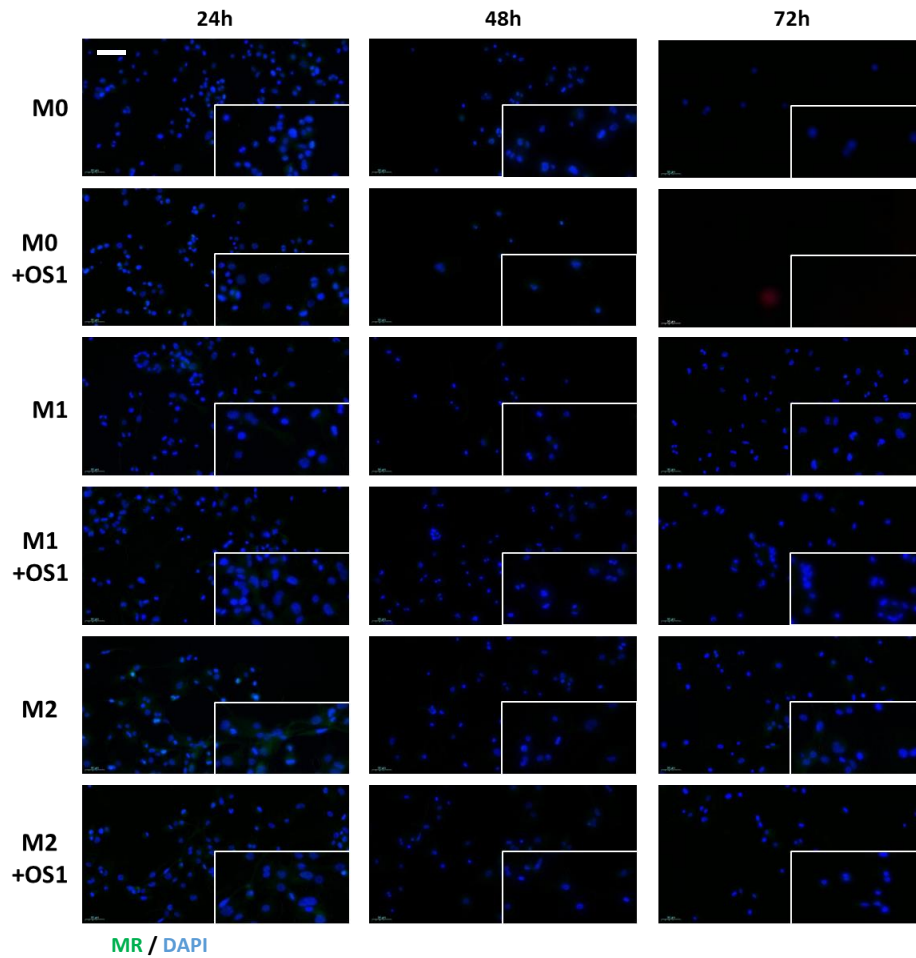
4.2.8 MR expression was largely unchanged by OS1 treatment

Mannose receptor (MR) is a scavenger receptor associated with a reparative and regulatory context. We aimed to measure MR expression in these THP-1 macrophage models to identify M2-like polarisation, and assess how OS1 mediated degradation of ERK5 may influence macrophage reparative behaviour.

There was low expression, which decreased over 72h in M0 macrophages compared to 24h control. MR was found to be expressed in M1 macrophages after the initial 24h of polarisation, but this was significantly reduced after 48h (0.08 fold; -92%) and 72h (0.11 fold; -89%) of M1 polarising agent. M2 macrophages also initially expressed MR to a similar extent to their M0 counterpart. Again, MR expression did decrease over the time course after 48h (0.38 fold; -62%) and 72h (0.60 fold; -40%), although it persisted at a higher level compared to M1 macrophages. OS1 treatment elicited no discernible effects on MR expression in M0, M1 or M2 macrophages compared to controls (Figure 4.17.B).

Taken together, this initially suggests that OS1 mediated degradation of ERK5 had little impact on MR expression and its associated M2-like polarisation. However, we have found very low expression of this standardised marker, MR, in this study. Thus, this may not be a robust immunofluorescence marker to identify M2 THP-1 macrophages with confidence, or an alternative MR antibody requires testing.

A



B

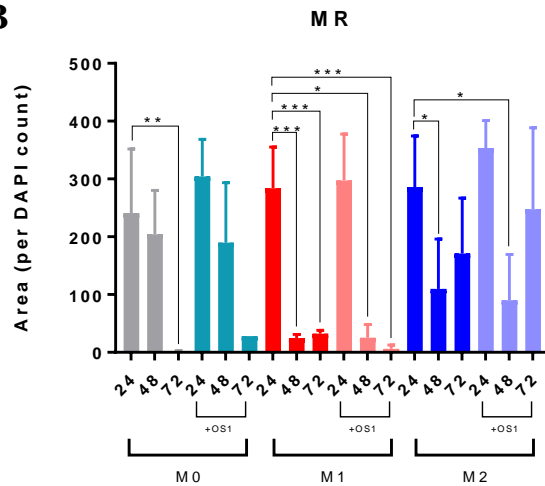


Figure 4.17. OS1 had no effect on MR expression in THP-1 macrophages. M0 = THP-1 macrophages treated with PMA for 24h. M1 = M0 + (LPS+IFN γ). M2 = M0 + (IL-4+IL-13). 1 μ M OS1 treatment was simultaneously added with polarisation agents. (A) MR stain for M0, M1, M2 and OS1 treated THP-1. Green indicates MR and blue indicates DAPI. Magnification of objective was 20x, with expanded inserts at 40x (white border). White bar = 50 μ m. (B) Graph represents average area of MR stain divided by number of DAPI positive cells as processed by ImageJ (n=3). (ns = P>0.05, *=<0.05, **=<0.01, ***=<0.001).

4.2.9 CD163 expression was largely unchanged by OS1 treatment

CD163 expression was assessed as it is a high affinity scavenger receptor associated with an immunosuppressive M2-like phenotype (Kubota *et al.*, 2017; Giurisato *et al.*, 2018). We investigated its expression in both M1 and M2 polarity states in the THP-1 model to replicate its previous use in murine *in vivo* studies and human *ex vivo* studies as an M2 macrophage marker. In addition, we wanted to assess how OS1 mediated ERK5 degradation may impact on CD163 expression, and its influence on polarisation states of human THP-1 macrophages.

CD163 expression was low but consistently expressed across both M1 and M2 polarity states with no difference compared to OS1 treated cells. It was anticipated this would be more highly expressed in the M2-like macrophages, and the lack of this trend further suggests more work is required in the polarisation and immunofluorescence analysis protocol.

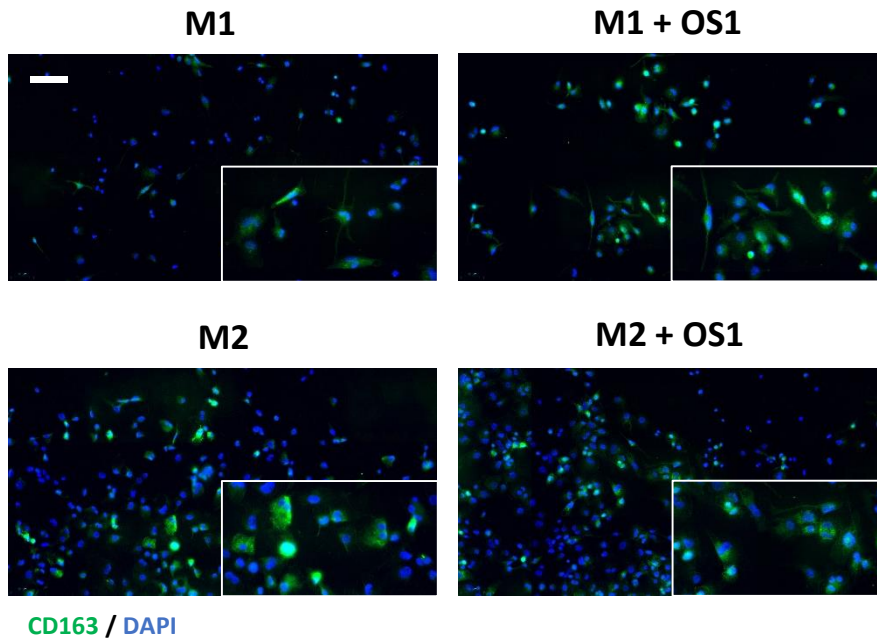
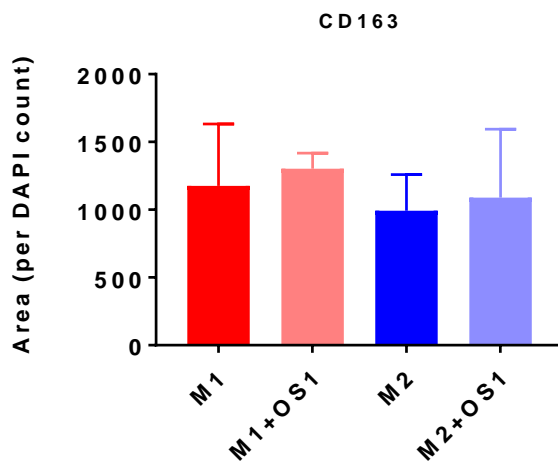
A**B**

Figure 4.18. OS1 had no effect on CD163 expression in THP-1 macrophages. M0 = THP-1 macrophages treated with PMA for 24h. M1 = M0 + (LPS+IFN γ) for 48h. M2 = M0 + (IL-4+IL-13) for 48h. 1 μ M OS1 treatment for 24h was simultaneously added with polarisation agents. (A) CD163 stain for M1, M2 and OS1 treated THP-1. Green indicates CD163 and blue indicates DAPI. Magnification of objective was 20x, with expanded inserts at 40x (white border). White bar = 50 μ m. (B) Graph represents average area of CD163 stain divided by number of DAPI positive cells as processed by ImageJ (n=5). (ns = P>0.05, *=<0.05).

4.2.10 ERK5 inactivation by OS1 caused transient increase on the mRNA expression of a range of repair mediated cytokines

RT-qPCR analysis was used to investigate the gene expression of an established group of inflammatory and repair mediated cytokines in THP-1 M0 macrophages treated with OS1 after 24h and 48h. These time points permit investigation into the early and later effects of OS1 mediated ERK5 degradation on human THP-1 M0 macrophages and an indication on its influence on driving polarisation. Analysis was completed with the $\Delta\Delta\text{CT}$ method, as relative expression to β -actin, and statistical testing was done on the ΔCT values.

The inflammatory markers assessed were TNF- α , IL-1 β , IL-6 and IL-8. Typically these are increased in expression during the inflammatory phase of wound healing, and in M1-like macrophage phenotypes. TNF- α , IL-1 β and IL-6 were largely unaffected, but had slightly decreased after 1 μM OS1 treatment in THP-1 M0 macrophages. Only IL-8 gene expression was significantly decreased at both 24h (0.52 fold; -48%) and 48h (0.42 fold; -58%) after OS1 treatment (Figure 4.19.A). IL-8 is a chemoattractant signal for neutrophils, and so its reduction following ERK5 degradation could result in a reduced inflammatory environment.

Reparative markers investigated in this study were TGF- β , VEGF, MR, MMP9 and SLUG. TGF- β , VEGF and MMP9 are key regulatory signalling factors found in wound healing, and required to reduce inflammation, promote angiogenesis and drive ECM remodelling, respectively (Lepidi *et al.*, 2001; Penn, Grobbelaar and Rolfe, 2012; Ding *et al.*, 2019). MR is an established marker of M2-like macrophages (Martinez-Pomares, 2012). SLUG is a transcription factor with known association with ERK5 signalling, MMP9 activity and keratinocyte activation (Arnoux *et al.*, 2008; Yue *et al.*, 2014).

In this study, we observed increased expression of TGF- β (34.69 fold), MR (3.81 fold), and VEGF (1.58 fold), after 24h of OS1 treatment in THP-1 M0 macrophages. However, these

increased expressions were transient and only seen within 24h, and returned to baseline levels after 48h with OS1 treatment (Figure 4.19.B). In addition, these genes of interest had large variability and inconsistency across the replicates. Overall, our evidence suggests minimal influence on polarisation, but potentially pre-empted the THP-1 M0 macrophages towards a reparative phenotype.

Following from our findings that ERK5 degradation promoted a reparative phenotype in THP-1 M0 macrophages, we next assessed if treatment with 1 μ M OS1 on polarised M1 or M2 macrophages for 24h could both reduce an inflammatory M1 profile and promote a reparative M2 profile. However, this study found that OS1 mediated degradation of ERK5 in polarised THP-1 macrophages results in no effective impact on RNA expression for the selected inflammatory or reparative markers (Figure 4.19.C). This suggests that loss of ERK5 by OS1 does not affect polarised macrophages. There is currently limited research in the mechanism of repolarising macrophages, however studies have shown that M2-like macrophages are more amenable than M1-like macrophages. LPS and IFN- γ stimulation to polarise toward M1-like macrophages inhibits mitochondrial activity, which is necessary for M2-like polarisation (Van den Bossche *et al.*, 2016; Oyarce *et al.*, 2021).

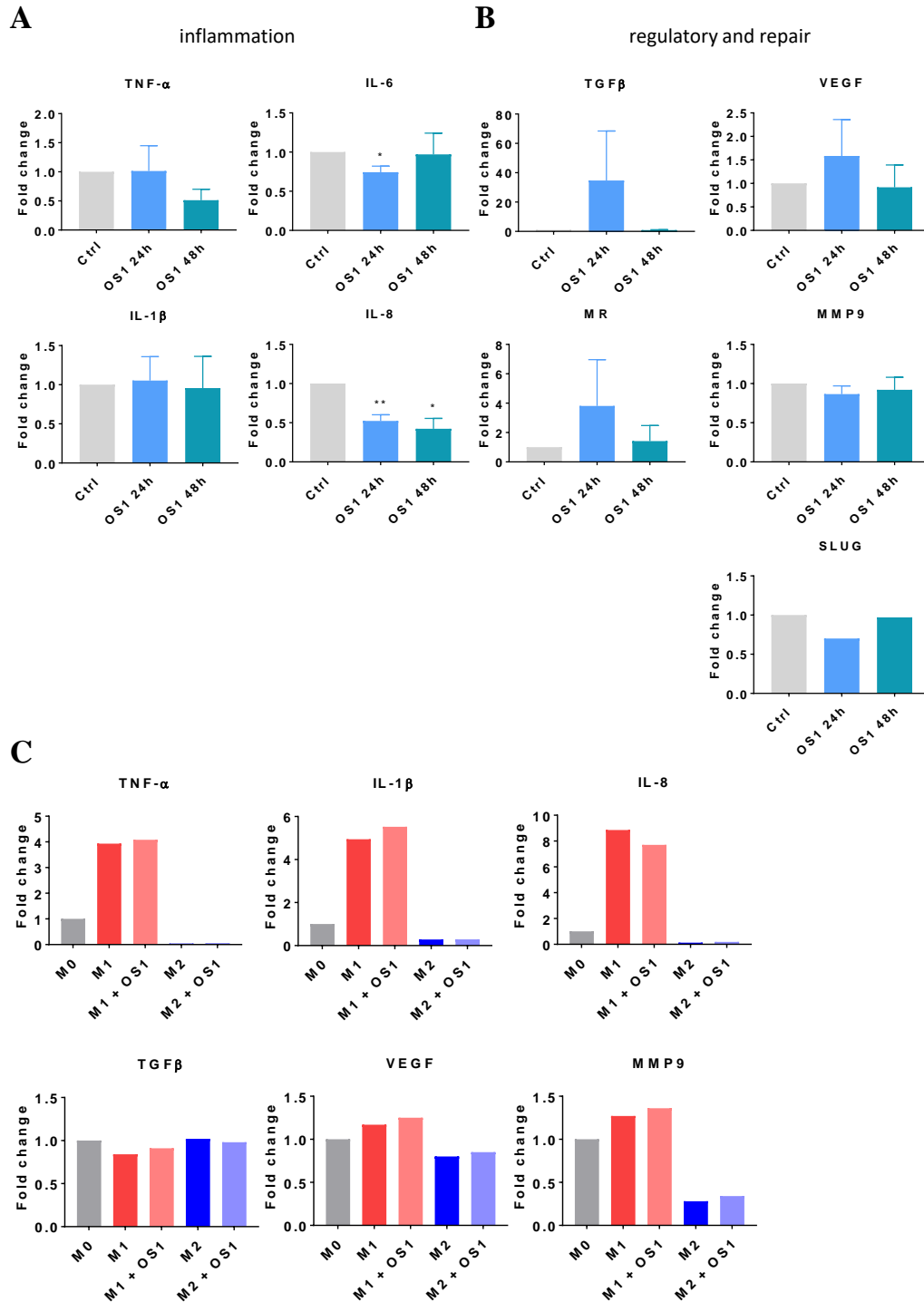


Figure 4.19. ERK5 inactivation with OS1 caused transient increase on the mRNA expression of a range of repair mediated cytokines. Total RNA was extracted and RT-qPCR was performed on a panel of genes after THP-1 cells were treated with PMA, M1/M2 polarising agents and OS1. THP-1 M0 macrophages after treatment with 1 μ M OS1 were investigated in panel A and B (A) Inflammatory gene targets: TNF α , IL-1 β , IL-6, and IL-8 (n=3). (B) Regulatory and reparative gene targets: TGF β , VEGF, MR, MMP9 (n=3), and SLUG (n=1). (C) Inflammatory and regulatory gene expressions of THP-1 macrophages which were polarised towards M1/M2-like macrophages and then treated with 1 μ M OS1 for 24h (n=1). Values represent the mean expression of cDNA of the various genes relative to β -actin. (ns = P>0.05, *= <0.05 , **= <0.01).

4.3 Discussion

The data in chapter 3 showed that *in vivo* genetic inactivation of ERK5 in keratinocytes can benefit wound healing, and so we pursued a workflow of therapeutic driven research by testing the novel compound OS1 in a human *in vitro* model system with HaCaT cells and THP-1 macrophages. This small molecule compound, OS1, has been used in parallel cancer research in the Finegan Lab (unpublished) and shown effective pharmacological degradation of ERK5 in triple negative breast cancer. We aimed to investigate how OS1 mediated degradation of ERK5 can influence the behaviour and function of HaCaTs and THP-1s as robust models of keratinocyte pathophysiology and macrophage behaviour and polarisation, respectively.

In our initial study using HaCaT cells, we successfully degraded the whole ERK5 protein after 24h of 1 μ M OS1 treatment. Moreover, there was no impact on BRD4, which is a known off-target of the ERK5 kinase inhibitor, XMD8-92. OS1 was proved to be specific to ERK5, and had no inhibitory effect on ERK1/2, which is a kinase of similar structure.

However, we did observe a subtle shift in ERK1/2 in OS1 treated HaCaTs over a 96h time course. This suggests that loss of ERK5 in these HaCaT cells may induce a compensatory pathway by driving phosphorylation activity in ERK1/2. These MAPK proteins share many downstream functions including cellular proliferation, migration, and survival (Guo *et al.*, 2020). It's been previously shown that ERK5 activation can occur as a compensatory pathway upon ERK1/2 inhibition (Tubita, Tusa and Rovida, 2021). Conversely, studies using lentiviral knockdown with shRNA or kinase inhibition with XMD8-92 to target ERK5 show no impact on ERK1/2 (Shukla *et al.*, 2013; Bhatt, Patel, *et al.*, 2021). However, our novel therapeutic compound, OS1 differs in its ability to target and degrade the whole ERK5 protein. This upregulation in ERK1/2 activity may influence functional outcomes as a compensatory pathway in OS1 mediated degradation of ERK5, and should be considered in the future.

After confirming OS1 effectively degrades ERK5 in HaCaTs, we showed this compound had no detrimental effect on proliferation, as assessed by MTT and SRB assays. However, a recent study has found that ERK5 inactivation using XMD8-92, siRNA and CRISPR-Cas9 technology led to increased mitochondrial accumulation and reduction in acidic lysosomal activity (Craig *et al.*, 2020). As MTT assays are a surrogate for cell density based on mitochondrial number and function, and ERK5 signalling has been shown to drive mitochondrial degradation, our MTT data may be less reflective of proliferation. However, as we also examined cell density changes with the SRB assay, we could mitigate for these nuances and show that OS1 had no detrimental impact on proliferation.

We additionally showed that OS1 mediated ERK5 degradation had no impact on migration of HaCaT cells, and was comparable with control. This was contradictory to previous studies which found that lentiviral shRNA mediated knockdown of ERK5 in HaCaTs exhibited altered morphology and impaired ability to migrate and close scratch wounds (Arnoux *et al.*, 2008). Notably, in this study we treated cells with OS1 after they were scratched, and so HaCaT cells would express normal levels of ERK5 up until ~16h before degradation of the protein would be observed. However, even at later time points of 24h – 48h, we had comparable rates of closure to control scratches. Perhaps, OS1 may impact wound closure if observed at later time points when ERK5 is degraded for longer. Potential studies to assess this could include; extending the time course to 96h or full wound closure, or pre-treating HaCaT cells with OS1 for 24h before scratching the cells. However, the study was designed to try reflect translatability to future *in vivo* studies, by treating with OS1 after the scratch to mirror the wounding studies used in murine models.

Previous studies by Finegan *et al.*, showed that ERK5 inactivation in keratinocytes led to a reduction in inflammation in skin carcinoma studies (Finegan *et al.*, 2015). However, our data in chapter 3 showed that using this genetic model in the context of wound healing led to an

initial increase in inflammation and an earlier induction of repair mediated signalling. This profile was reflected in our *in vitro* data, where we showed that degradation of ERK5 with OS1 in HaCaTs stimulated a range of both inflammatory and reparative genes to increase in expression. This suggests that loss of ERK5 in these HaCaTs may have primed them to promote both inflammation and repair mechanisms to occur more quickly and sensitively. Most markedly, the largest changes were observed in the reparative associated genes. However, it should be noted that there was large variability in gene expression changes across the replicates. Additionally, only a single successful experiment was conducted with SLUG and Vimentin, and so the results for these targets require replicates before any conclusions can be made in relation to ERK5 degradation by OS1 treatment.

In addition, the HaCaTs cells studied in this context were in a basal state without any additional stimulation. It has been previously shown that HaCaT cells can become activated and inflammatory upon stimulation with external stress factors such as pathogens or physical damage (Zampetti *et al.*, 2009). It is feasible that the increased inflammatory profile seen in our data could be amplified in HaCaTs that have been previously stimulated by LPS or a multi-scratch model. This could emulate an infected or severely wounded keratinocyte context in pathophysiology of chronic wounds.

However, despite the stimulated effect in increased gene expression profile observed, our data also showed some contradictory discrepancy between OS1 mediated degradation of ERK5 and lentiviral knockdown of ERK5 in the shERK5 HaCaT cells. OS1 treatment degrades the ERK5 at a protein level in the HaCaT cells, whereas shERK5 HaCaT cells have been modified to remove it an mRNA level. There may be factors within the non-coding region of the DNA, such as functional micro-RNA, encoded within the mRNA of ERK5 that continue to persist in OS1 treated cells as opposed to the shERK5 model, that limit its comparability. Additionally, it should be noted that shERK5 HaCaT cells were less effective at removing ERK5 compared

to OS1 throughout this study. This may be the result of incomplete GFP cell sorting (encoded in their selection), permitting some non-shERK5 cells to grow or only partial transfection that permitted some ERK5 to remain in the HaCaT cells.

Moreover, OS1 treatment triggers an acute response to loss of ERK5 compared to the chronic loss of ERK5 through shERK5. As ERK5 and MAPK signalling is an evolutionary conserved pathways associated with stress (Drew, Burow and Beckman, 2012; Nithianandarajah-Jones *et al.*, 2012), there may be compensatory systems that deal with acute and chronic response differently. Additionally, it is known that the effects of OS1 can wear off and allow ERK5 to rebound. To investigate this, a long term study will need to be conducted to assess how repeat dosing of OS1 treatment in HaCaTs influences the phenotype and function in these cells over the course of ~2 weeks.

As briefly stated in this chapter, shERK5 cells were not fully ablated of ERK5 and some HaCaT cells with less knockdown maybe be perceived as “fitter”. These cells could proliferate and compete better than their shERK5 counterparts and over time eventually lead to a more mixed population where the culture of shERK5 cells shift towards a lesser ERK5 knockdown. Taken together, these factors in the shERK5 cell line may shape the gene expression and phenotype we observed, and explain the discrepancy we see between OS1 treatment and lentiviral knockdown.

In addition to the crucial role that keratinocytes play in homeostasis and pathology in wound healing, it is well established that immune cells such as macrophages can coordinate healthy repair mechanisms. From the literature we know that loss of ERK5 in myeloid lineages, primes macrophages towards an M1-like and anti-tumour phenotype in cancer models (Giurisato *et al.*, 2018; Luiz *et al.*, 2020). By using OS1 in THP-1 cells, an *in vitro* model of monocytes which can be differentiated and polarised to macrophages, we aimed to test if this could be

replicated. This would enable us to gain an understanding in the therapeutic potential of modifying macrophage behaviour in wound healing.

From our initial studies characterising various macrophage populations by morphology, surface marker immunofluorescence and qPCR gene markers, we found that M0 and M1-like macrophages were the most simple to identify. The profile was less clear in M2-like macrophages, in part due to their heterogeneous and complex behaviour.

THP-1 cells were differentiated into M0 macrophages after induction with PMA for 24h, where they became adherent, small and round bodied structures. This was identified by their morphology using bright field and phalloidin staining for actin filaments, and positive staining for CD68. By stimulating these M0 macrophages with IL-4 and IL-13 for 48h, we polarised them towards M2-like macrophages which were similarly round, but larger in diameter and increased in phalloidin area per cell. M1-like macrophages were polarised with LPS and IFN γ for 48h, and were identified by their distinct morphology of long spindle like protrusions.

These M1-like macrophages were further characterised by their consistent and increased expression of inflammatory genes including TNF- α , IL-1 β , and IL-8. We aimed to identify M2-like macrophages similarly, with their increased expression of TGF- β , MR and VEGF. However, there was a larger degree of variability within these repair associated gene expression markers. The addition of other previously established repair and M2 associated markers could be introduced to capture a wider spectrum, including TGM2, Ym1, Fizz1, fibronectin and Fc γ RIIa (Martinez and Gordon, 2014; Orecchioni *et al.*, 2019).

The variance we observed may also be an artefact of incomplete polarisation. Our data from the bright field and phalloidin stain show that not all M1 and M2 polarised cells exhibit their characteristic morphology of long spindle like protrusions or large circular structures, respectively. Some THP-1 M0 macrophages may not respond or are responding slower to

polarisation over the 48h time course. Therefore, it is possible in this study, that what we categorise as M2-like macrophages (as an example) for analysis by IF or RT-qPCR, may in fact be a heterogeneous population of unpolarised M0 macrophages, polarised M2-like macrophages and a spectrum of those in between. This could be one explanation of the variability often observed in our data. This could be taken into account better in future studies by focussing analysis on true M1 and M2 cells, by generating co-IF or flow cytometry studies to identify and separate these cells from a heterogeneous population.

This investigation in establishing parameters to understand the polarity states of THP-1 macrophages suggested that M1-like macrophage polarisation was a simpler and more robust model to generate. However, this large variability in M2-like macrophage gene expression profile suggest that the *in vitro* model may be difficult to study wound repair macrophages and require further experimental investigation and development. This is additionally unsurprising when considering the large spectrum that M2-like macrophages can sit under, and that simply trying to polarise repair macrophages without the correct biological context may be difficult. The traditional M2 paradigm has been broken down to three types: M2a (IL-4 + IL-13), M2b (TLR/IL-1R ligands), M2c (IL-10), based on its stimulants (Krzyszczuk *et al.*, 2018). These have been documented in playing distinct roles associated with Th2-like response, immune regulation and tissue remodelling, respectively. The simplified model used in this experimental workflow has only focussed on M2a macrophage polarisation and may not truly reflect wound macrophages, which may be more associated with M2c. Other recent studies on cytokine signalling and macrophage biology reveal that this model is much more complex (Martinez and Gordon, 2014). What needs to be taken into account, is that the reality may be more complex than discrete macrophage populations. There is a spectrum or coexistence of M1/M2-like signatures that can lead to a mixed population with overlapping functions in inflammation, regulation and repair.

However, we progressed forward and switched our focus to understand if OS1 and the degradation of ERK5 could prime these THP-1 M0 macrophages towards one polarity state or another. Previous studies have primarily focused on murine derived monocytes and macrophages and shown that ERK5 deficiency pre-disposes these macrophages towards an M1-like and inflammatory phenotype (Giurisato *et al.*, 2018; Luiz *et al.*, 2020). Limited studies have been conducted in the human model context, and so this research permits a novel and early indication into the potential of OS1 to alter human macrophage polarisation.

We successfully degraded the whole ERK5 protein in THP-1 cells to a comparable rate to that observed in HaCaTs, as observed by our western blot and IF analysis. Although we made early attempts to visualise localisation of ERK5 in either the cytoplasm, perinuclear or nuclear sites in the cell, to infer on the functional state of ERK5, these were difficult to quantify based on IF on a 2D axis. One avenue could be the introduction of confocal microscopy to image at three axes to generate a 3D profile of cells and ERK5 expression. Alternatively, cell fractionation to separate nuclear and cytosolic fractions, would permit investigation of ERK5 protein levels in these distinct compartments (Rovida *et al.*, 2008).

We additionally showed that OS1 again had no effect on the proliferation of THP-1s. Unfortunately, our characterisation of cell surface markers by immunofluorescence remains unclear. We were unable to clearly establish TSPO as a marker for M1-like macrophages or CD163 and MR for M2-like macrophages. For example, it should be noted that although it appeared that fluorescence was more intense in some of these images (e.g. TSPO in M1+OS1, Figure 4.15.A), our current processing analysis through ImageJ was unable to take this into account, which may have impaired the accuracy of the data. A major constraint of our analysis was that ImageJ can only assess the area of fluorescent stain, and was unable to measure the intensity of the colour. And so although OS1 treatment made no impact on these markers,

further optimisation, such as more suitable analysis, wider range of IF targets or isolation of fully polarised macrophages may be required.

Interestingly, we found that OS1 treated M0 macrophages upregulated a panel of reparative and regulatory genes of interest; TGF- β , MR and VEGF, suggesting that they may be more M2-like inclined in their polarity. This is contradictory to previous studies in the cancer context using the *in vivo* genetic inactivation of myeloid lineage which lead to priming towards an M1-like phenotype.

We also showed that OS1 treatment for 24h on polarised macrophages had no impact on their gene expression profiles. Thus, we were unable to repolarise M1-like macrophages towards a reparative phenotype, nor were we able to promote this profile in M2-like macrophages. This would require further investigation by assessing OS1 in polarised macrophages at extended time points and with repeated dosing of OS1 to ensure ERK5 remains ablated. However, the limited research available, suggests that repolarising macrophages can be difficult in M1-like macrophages, and only M2-like macrophages are amenable to this approach (Van den Bossche *et al.*, 2016; Oyarce *et al.*, 2021).

It has been previously established that ERK5 drives polarisation and function of macrophages in the context of cancer using myeloid specific ablation studies (Giurisato *et al.*, 2018; Luiz *et al.*, 2020). Our data shows that OS1 can degrade ERK5 and subtly shift its polarity towards an M2-like phenotype. However, a limitation of OS1 is that it can have off-target effect on endothelial cells and drive a major loss of ERK5 in the local microenvironment. A preliminary study was conducted to overcome this potential issue and compared OS1 to three similar novel compounds; ABP-1, ABP-2, ABP-3. These were three variants of OS1 that were redesigned and tagged with CCL2, made by our collaborators from the Butterworth Lab and Aidan Pidd. The aim was to generate ERK5 degrading compounds which specifically targeted monocyte

and macrophage cells that express CCR2. ABP-2 was the only compound to successfully target and degrade ERK5 (-35%) but less efficiently when compared to OS1 (-69%) (Figure 4.20.B). This data has been returned to the Butterworth Lab to inform on further improvements in the drug development process.

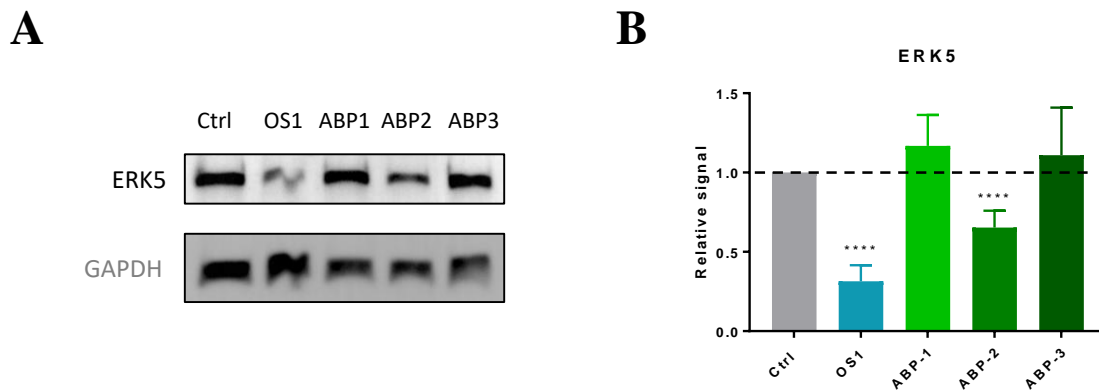


Figure 4.20. OS1 targets and degrades ERK5 in THP-1s more effectively than CCR2 specific variants. (A) Representative blots after M0 THP-1 macrophages were treated with 1 μ M OS1, ABP-1, ABP-2, and ABP-3, to assess ERK5, and GAPDH (n=3). (B) ERK5 protein levels were normalised and graphed against corresponding GAPDH (n=3). Data points plotted represent the mean of three independent experiments \pm SEM. (ns = P>0.05, *=<0.05, **=<0.01, ***=<0.001, ****=<0.0001).

Another limiting factor of this *in vitro* study with HaCaTs and THP-1s is that we are making a simple predicted effect on how loss of ERK5 in keratinocytes or macrophages alone may influence on inflammation and repair mediated signalling in a complex wound microenvironment. Beyond the immediate effect on the epidermal layer of the keratinocytes is an intricate conversation between immune cells, ECM, fibroblasts, endothelial cells and a systemic immune system. Similarly, in addition to the complexity within the macrophage system, the model of M2-like wound macrophages may be difficult to recapitulate without the full environment context. Whereas M1 and inflammatory response is evolutionary conserved with a clear function to target infection and can be simply polarised with LPS alone (Orecchioni *et al.*, 2019; Zhao *et al.*, 2021). Generating an appropriate M2 and reparative response can be nuanced and require more complex *in vitro* systems. Studying the human cell model of keratinocytes or macrophages alone is unable to reflect the continuous cross talk between the

microenvironment and how these inflammatory and reparative signals could be potentiated. This could include multiple stress factors and external triggers such as DAMPs, PAMPs and hypoxia (Eming, Krieg and Davidson, 2007; Koh and DiPietro, 2011; Ellis, Lin and Tartar, 2018).

The alternative would be to investigate the efficacy and functional outcome OS1 treatment in a more complex *in vitro* co-culture systems or utilising an *in vivo* wounding model to explore its impact on inflammation, repair and homeostasis in the skin.

Chapter 5: Therapeutic inactivation of ERK5 with OS1 in *in vivo* models of wound healing promotes a reparative phenotype

In the previous chapters we have shown that inactivation of ERK5 can alter the wound microenvironment and the coordination of inflammation and repair. Notably, we have observed a shift of increased inflammation during the initial stages, followed by an earlier phase of repair mechanisms (Chapter 3). Additionally, we found that by using OS1, a therapeutic compound to target and degrade ERK5, we were able to influence *in vitro* models of keratinocyte and macrophages to reflect this similar pattern of increased inflammation, and pre-emptive repair (Chapter 4). Following from this, we hypothesised that topical *in vivo* dosing of OS1 in the wound could improve the wound healing process by altering this immune profile as our data has previously shown using genetic models. In addition, this study would allow an insight into the impact of ERK5 loss across the full multicellular environment of the wound: keratinocytes, immune cells, endothelial cells, fibroblasts and ECM. This will provide a holistic picture of the influence targeting ERK5 can have on wound healing.

5.1 Topical OS1 treatment led to decreased ERK5 expression and quicker wound closure

Data in chapter 4 showed that the most effective dose *in vitro* to degrade ERK5 and induce a pro-wound healing phenotype in HaCaTs and THP-1 macrophages was at 1 μ M for 24h. We replicated this by generating a 1 μ M topical dose of OS1 in 1% methylcellulose at 50 μ L. Topical dosing at the healthy wound edge (gamma/beta regions) ensures that ERK5 degradation is limited to the local wound environment and associated epidermal, fibrotic and immune cells. We used methylcellulose as a standardised drug carrier due to its characteristics of hydrophilicity, capacity to facilitate permeation across the epidermis and the viscosity for ease of application (Vlaia *et al.*, 2016; Willerth, 2017). Additionally, to ensure ERK5 remained

degraded throughout the wound healing time course, the OS1 cohort were given repeat doses every 48h.

Mice were wounded on the lower-back on day 0, a cohort were dosed with OS1 (1 μ M in 1% methylcellulose) at day 2, and wound samples were collected on a range of time points including day 1, 4, 7, 14, 16 and 29. Samples were processed to evaluate their immune profile via FACS, immunohistochemistry, and RT-qPCR. Furthermore, we visually tracked the wound healing process by continuously photographing, tracing and measuring wounds throughout the course of the experiment (Figure 5.1.B).

There was an initial phase within the first few days where the size of the wound increases (1.5 fold), and was then followed by a decrease in wound size over the time course (Figure 5.1.B). As previously shown in chapter 3, this is typical of normal wound closure. The wound was completely closed by day 14 to day 16. There was no significant difference in the rate of wound closure between control and OS1 treated mice, but there was a slight trend in faster wound closure in the OS1 treated mice. A cohort of animals were maintained up until day 29 to permit investigation into the post-wound closure remodelling phase and the impact ERK5 has on collagen deposition and ECM architecture.

As conducted previously, we assessed the ERK5 profile in the wound environment by ERK5 specific histology of control and OS1 treated mice. Immunostaining skin sections with an ERK5 antibody demonstrate that OS1 successfully removed ERK5 from the gamma regions of wound (Figure 5.1.C), further investigated in Figure 5.4. However, we were able to observe ERK5 in the beta regions of the OS1 treated mice. As OS1 was topically injected at the healthy skin of the wound edge (gamma/beta region), it is feasible the limited ERK5 degradation may be indicative of the methylcellulose vehicle successfully limiting the spread. Additionally, the

loss of ERK5 in the gamma region may induce a compensatory drive in the beta regions to upregulate ERK5 expression.

Following this, an initial assessment of architecture and immune profile by H&E suggested that ERK5 degradation with OS1 led to no obvious physical changes. Additionally, there was no immediate differences in overall immune infiltrate observed between control and OS1 treated wounds across all the time points (Figure 5.1.D). This reflected our genetically modified ERK5 *in vivo* models used in chapter 3, suggesting that ERK5 degradation with OS1 had not detrimental impact on physical phenotype of wounds.

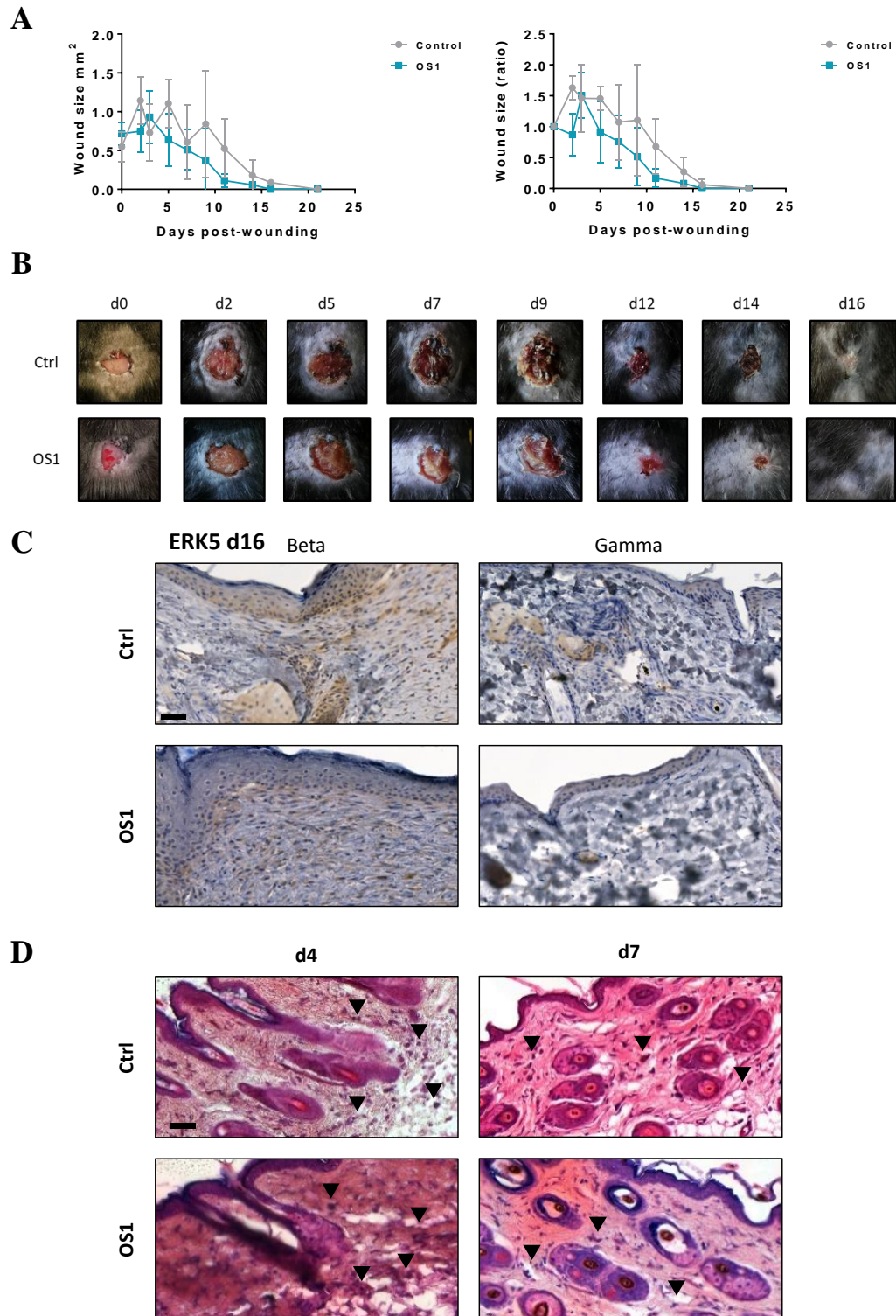


Figure 5.1. Topical OS1 mediated ERK5 inactivation increased wound closure rate. (A) Wounds were imaged and the area calculated on ImageJ to quantify wound closure. Data points plotted represent the mean of multiple difference mice \pm SD (d0 = 8, d2 = 8, d3 = 8, d5 = 5, d7 = 5, d9 = 5, d11 = 5, d14 = 5, d16 = 3, d21 = 3). (B) Representative images of wounds in control and OS1 treated mice. (C) Wound sections in the β and γ regions of mice were assessed for ERK5 expression (brown) by immunohistochemistry and counterstained with Harris Haematoxylin. (D) H&E staining and representative bright field images of γ region sections from control and OS1 treated wounds at d4 and d7. Black triangles represent site of haematopoietic or immune cells. Black bar = 20 μ m. (ns = $P > 0.05$, * = < 0.05).

5.2 Therapeutic inactivation of ERK5 with OS1 increased the proportions of macrophage, monocyte and neutrophil populations

To delineate the dynamic immune response of the wound healing process, the immune cell populations in the wounds over various time points were analysed by flow cytometry at day 0, 1, 4, 7, 14, 16, and 29. Single cell suspensions collected from the wound tissue were subjected to FACS and gated as shown in (Figure 5.2.A). Immune cell populations were expressed as a percentage of the total cell population collected, and the remaining cells were categorised as “others”.

Our data in control animals shows a pattern of early influx of immune cells within day 1 of wound healing, which persisted until day 7. At this point, the percentage of immune cells tended to decrease. This was most clearly observed in the granulocytes, which increased from 32% to 65% of cells between day 0 and day 1 (Figure 5.2.B). Compared to the control, the granulocyte population remained higher in the OS1 treated mice on day 4 (58.5% vs 81.1%), day 7 (61.8% vs 76.1%), day 14 (12.8% vs 38.4%), day 16 (27.5% vs 54.9%), and day 29 (54.8% vs 64.4%).

The lymphocyte population remained largely unchanged compared to control but was slightly lower in the OS1 treated mice on day 4 (2.7% vs 0.03%), day 7 (2.3% vs 0.2%), day 14 (1.0% vs 0.6%) and day 16 (0.8% vs 0.6%). These changes are diluted in the context of the granulocyte numbers (Figure 5.2.B). However, these are potentially stark reductions in lymphocyte populations which account for both T and B-cells in the role of ERK5 mediated wound healing, and could contribute to the OS1 mediated phenotype observed. Although beyond the scope of this study, lymphocytes and their role in wound healing may require further investigation. In particular T-cells are found as both skin residential and recruited cells

with functions in both inflammation and homeostatic repair (Martin and Muir, 1990; Toulon *et al.*, 2009).

In control mice, the percentage population of macrophages (F4/80) increased from 12.8% to 41% between days 0 to day 1, and persisted up to day 7. The macrophage population then decreased on day 14, onwards. Compared to control, treatment with OS1 increased the percentage proportion of macrophages compared to control on day 4 (35.4% vs 54.1%), day 7 (40.5% vs 44.1%), day 14 (9.5% vs 11.9%), day 16 (8.4% vs 19.9%), and day 29 (0.8% vs 5.3%), (Figure 5.2.C).

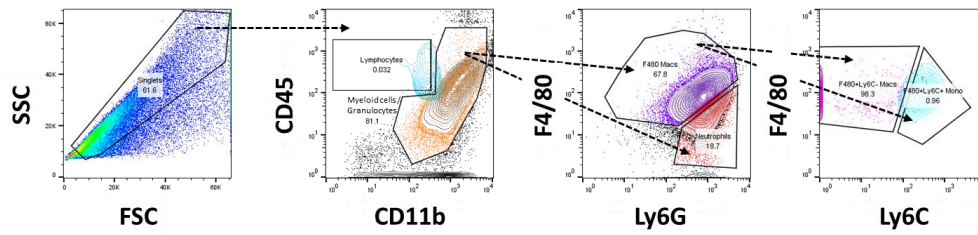
The monocyte (Ly6C) population remained a relatively small proportion of the immune cell constitution in control mice. It increased from 8.9% to 12.1% between day 0 and day 1, then decreased to 6.4% on day 4. OS1 treated mice had lower levels of monocytes compared to control on day 4 (6.4% vs 0.5%) and day 7 (6.7% vs 1.0%). However, compared to control, OS1 treated mice had higher levels of monocytes in the later time points during wound closure of day 14 (1.2% vs 3.1%), day 16 (1.7% vs 12.2%) and day 29 (0.8% vs 5.3%), (Figure 5.2.C). These monocytes recruited to the wound site can differentiate to macrophages and have the potential to polarise to either inflammatory or reparative macrophages dependent on the context. The stark changes in OS1 treated mice suggest that ERK5 can influence the recruitment and potential macrophage landscape in the wound environment.

The neutrophil (Ly6G) population in control animals followed the expected pattern of increased influx in the early stages of wound healing by increasing between day 0 (0.97%), day 1 (2.8%) and peaking at day 4 (6.5%). Our results reveal that OS1 treatment enabled the neutrophil population to persist at a higher level compared to control on day 4 (6.5% vs 15.2%), day 7 (5.2% vs 17.3%), day 14 (0.04% vs 10.8%) and day 16 (0.3% vs 16.1%). It should be noted, that control mice on day 29 exhibited an unusually higher level of neutrophils (38.2%)

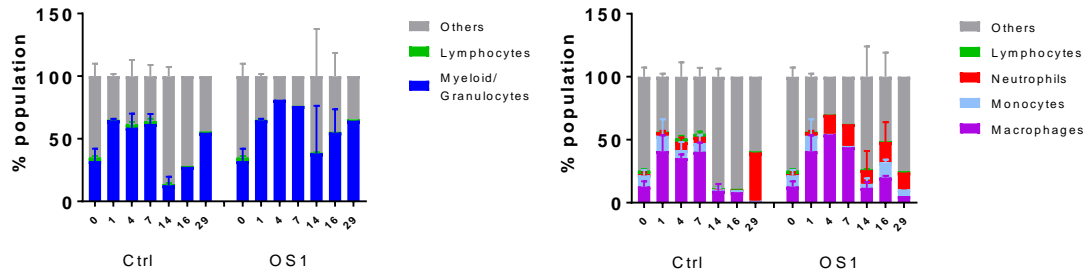
than expected, compared to an already high level found in the OS1 treated mice at day 29 (13.4%).

Taken together, this FACS study suggests that topical OS1 mediated degradation of ERK5 influenced inflammation by increasing neutrophil, macrophage and late monocyte accumulation, but decreasing early monocyte infiltration (Figure 5.2.C).

A



B



C

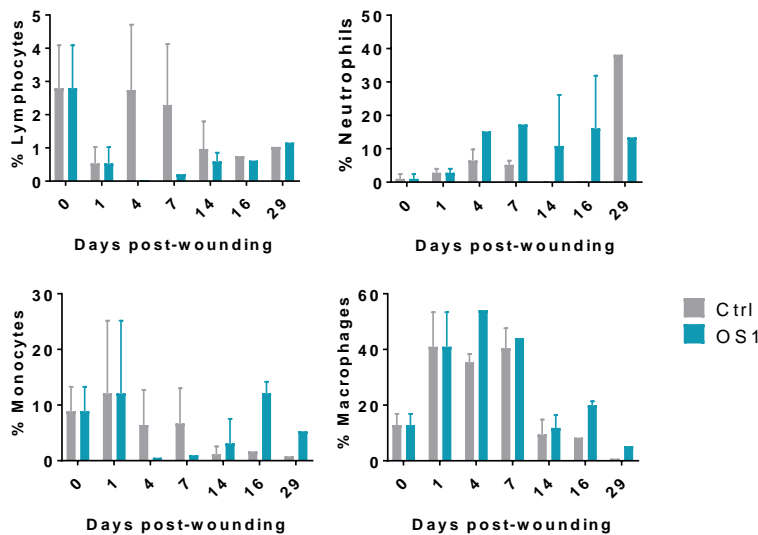


Figure 5.2. FACS analysis showed that OS1 mediated ERK5 inactivation increased monocyte, macrophage and neutrophil proportions. Various populations of immune cells were quantitatively evaluated in wound tissue collected at day 0, 1, 4, 7, 14, 16 and 29 by flow cytometry. (A) Representative flow cytometry plots of the gating strategy. Live cells were gated according to size and granularity. Lymphocytes and granulocytes were distinguished according to CD45 and CD11b expression. Macrophages and neutrophils were identified from the granulocyte population based on their expression of F4/80 and Ly6G. Monocytes were further distinguished from the macrophage population according to their expression of F4/80 and Ly6C. (B) Quantified population distribution of lymphocytes, granulocytes, macrophages, monocytes, neutrophils and other cells in control and OS1 treated wounds on day 0 (n=15), 1 (n=2), 4 (n=3), 7 (n=3), 14 (n=2), 16 (n=2) and 29 (n=1) as a percentage of total cells. (C) Separated graphs indicating the percentage population distribution of lymphocytes, neutrophils, monocytes, and macrophages. (ns = $P > 0.05$, $* = < 0.05$).

5.3 Assessing changes to immune response in OS1 treated wounds by histology

Our initial H&E assessment (Figure 5.1.D) indicated no recognisable difference in immune cell infiltrates despite our prior hypothesis that local inactivation of ERK5 may promote early inflammation and subsequent repair mechanisms in the process of wound healing. We therefore continued our histological analysis with the same panel of targets as previously in chapter 3 for macrophages (F4/80), neutrophils (NIMP-R14), M1-like polarity (iNOS), M2-polarity (Arg1), collagen (Picrosirius red) and ERK5 expression.

IHC on the three regions of the wound; alpha (centre of wound), beta (wound-edge) and gamma (healthy skin) (Figure 5.3.A), was semi-quantitatively assessed and scored out of three (zero = negative, one = low, two = positive, three = high positive), as in (Figure 5.3.B).

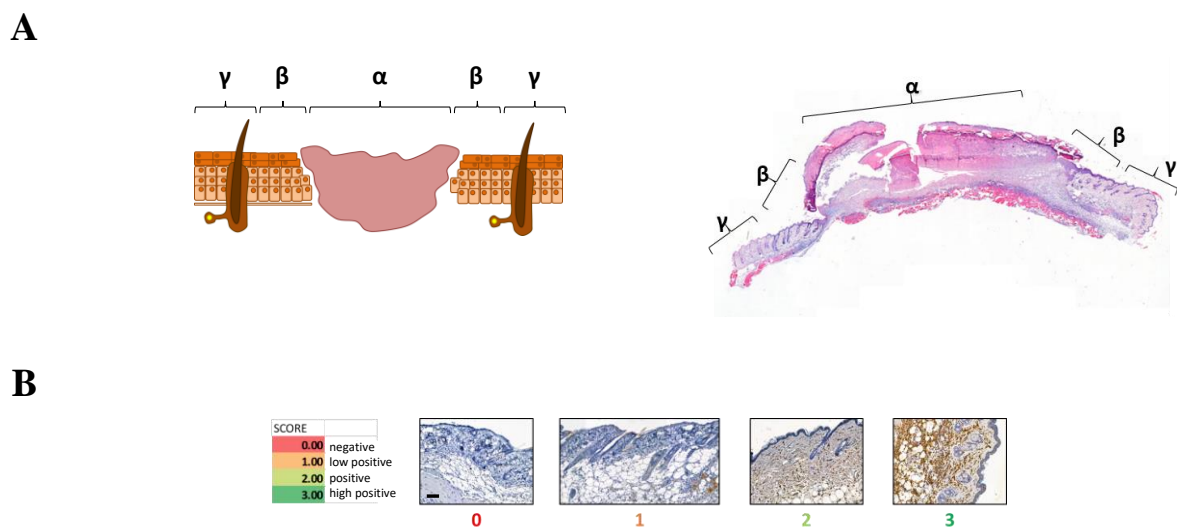
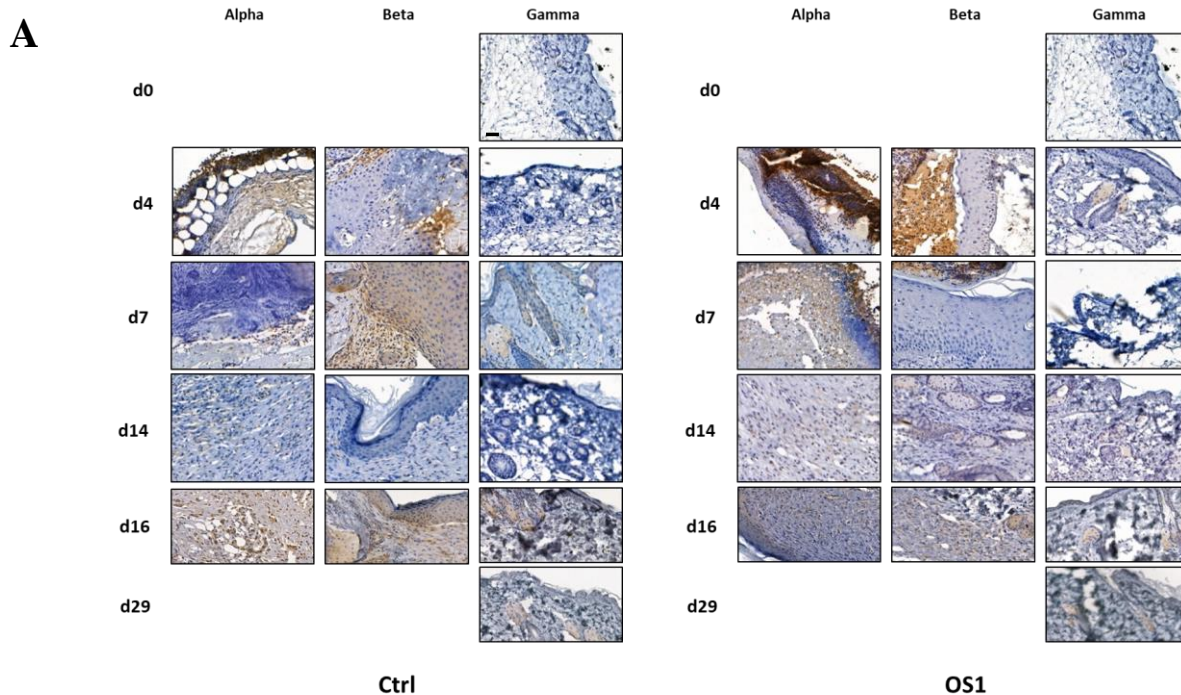


Figure 5.3. Method to assess changes to immune response in OS1 treated wound healing by histology. (A) Wound schematic depicting the three regions of the wound: alpha (α), beta (β), and gamma (γ). (B) Representative images of the scoring system of immunohistochemistry staining intensity: (0) = negative, (1) = low positive, (2) = positive, and (3) = high positive. Black bar = 50 μ m.

5.3.1 ERK5 expression decreases throughout the wound region after OS1 treatment

ERK5 expression increases throughout the wound healing period, with a peak at day 16 in the control wounds. This expression was attenuated after treatment with OS1, where it decreased the expression of ERK5 in all regions of the wound in the majority of the time points indicated (Figure 5.4.C). However, our scoring suggests that relatively early on in wounds, around two days after dosing with OS1, there was an increase in ERK5 expression at day 4 when compared to control (Ctrl - α 0.17, β 0.94, γ 0.86 vs OS1 - α 0.33, β 1.67, γ 1.00). As previously suggested, it may be that this concentration of dosing was unable to successfully degrade the ERK5 at this early time point, and it may have activated some compensatory pathways to overcome this initial loss of ERK5. Additionally, some of the brown staining could be an artefact of non-specific uptake in the acellular scab, which may obscure visualisation (Figure 5.4.A, d4). However, as the ERK5 expression decreased at later time points, we can conclude that dosing every 48h with OS1 reduced the levels of ERK5 over time compared to control wounds.



B

ERK5

	0	3	4	7	14	16	29
Ctrl	α	0.33	0.17	0.17	0.75	2.33	
	β	1.00	0.94	1.25	0.53	1.33	
	γ	0.50	0.00	0.86	0.25	0.22	2.00
OS1	α		0.33	2.00	0.17	0.67	
	β		1.67	0.67	0.00	1.00	
	γ	0.00	1.00	0.00	0.17	1.17	0.67

Relative to Ctrl: -1 (dark red), -0.1 (light red), 0 (grey), +0.1 (light green), +1 (dark green)

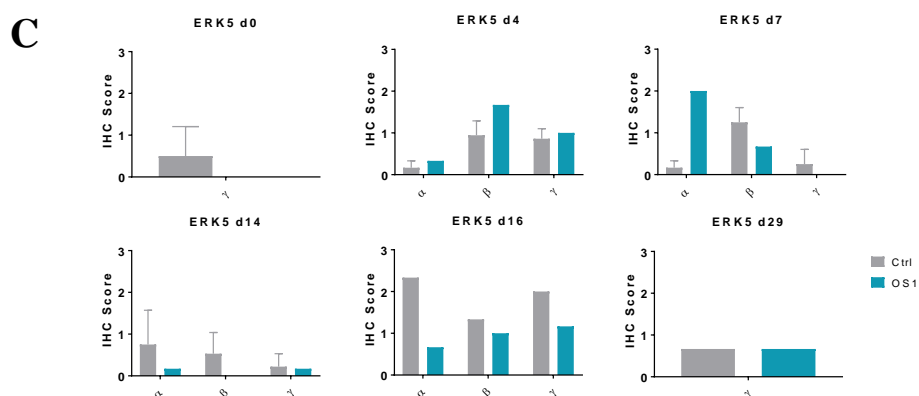
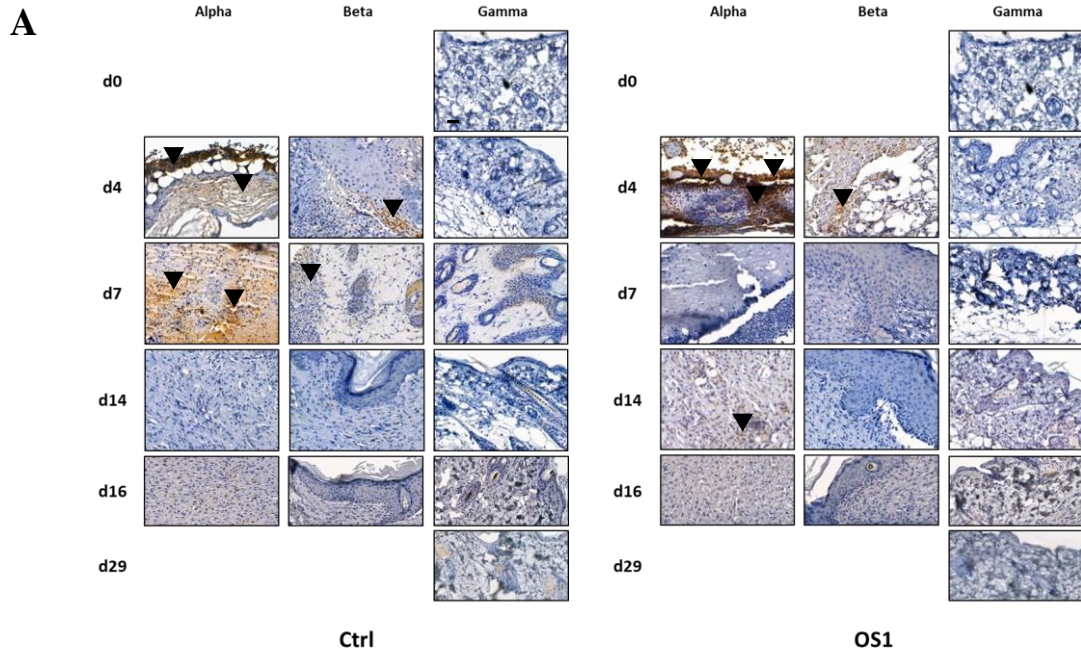


Figure 5.4. ERK5 expression decreased in OS1 treated wounds as determined by immunohistochemistry analysis. (A) Representative images of ERK5 staining in the wounds of control and OS1 treated mice. Black bar = 20 μ m. (C) Table of the quantified scoring analysis of ERK5 staining. Grey = 0. Light red/green = \pm 0.1. Dark red/green = \pm 1. (C) Graphs of quantified scoring analysis of ERK5 staining in control and OS1 treated mice over the wound healing time course on day 0 (n=11), 1 (n=2), 4 (n=2), 7 (n=2), 14 (n=2), 16 (n=2) and 29 (n=1). (ns=P>0.05, *=P<0.05).

5.3.2 ERK5 degradation with OS1 led to reduction in neutrophils

Neutrophils are an early inflammatory cells recruited to the site of the wound to fight infections and typically accumulate and peak around day 1 to day 3 post wounding. Neutrophils stained with NIMP-R14 increased throughout the early time points and was most abundant on day 4 in the alpha (2.39) and beta regions (1.67), (Figure 5.5.C). The expression of NIMP-R14 was relatively low for the remaining days in control mice. However, intervention with OS1 to degrade ERK5 in the wound led to reduction of neutrophils. In particular, they were scarcely observed in all regions on day 7 of OS1 treated mice when compared to control mice (Ctrl - α 1.00, β 0.50, γ 0.17 vs OS1 - α 0.00, β 0.00, γ 0.00), (Figure 5.5.C).

It should be noted, neutrophils role in healthy wound healing typically occurs within the first three to four days. As OS1 was only introduced into wounds at day 2, the influence of ERK5 degradation would be anticipated to only influence egressing neutrophils. In order to investigate the relationship between OS1 mediated degradation of ERK5 and neutrophil recruitment, mice will need to be pre-treated prior to wounding. Additionally, our study using NIMP-R14, collectively stains for murine Ly6G and Ly6C as a standardised marker for neutrophils. However, NIMP-R14 may also account for granulocyte differentiation of eosinophils, basophils, and mast cells as well as identifying other Ly6C cell populations such as monocytes and myeloid-derived suppressor cells (Gabilovich, 2017). This could account for the upregulated expression at late time points (day 7 to day 16) in control animals, when inflammation has resolved and wounds are repairing and remodelling.



B

		NIMP						
		0	3	4	7	14	16	29
Ctrl	α	1.00	2.39	1.00	0.17	0.00		
	β	0.67	1.67	0.50	0.17	0.33		
	γ	0.17	0.00	0.30	0.17	0.28	1.00	0.00
OS1	α		2.33	0.00	0.33	0.67		
	β		1.67	0.00	0.00	0.33		
	γ	0.00		0.00	0.00	0.00	0.00	0.00

Relative to Ctrl: -1 (Dark Red), -0-1 (Light Red), 0 (Grey), +0-1 (Light Green), +1 (Dark Green)

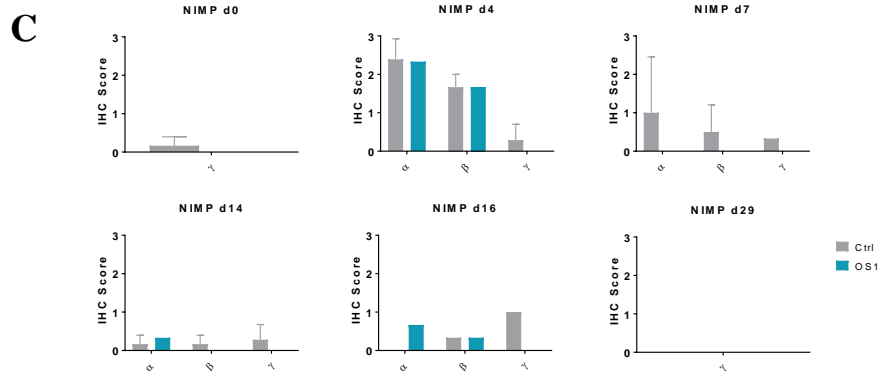


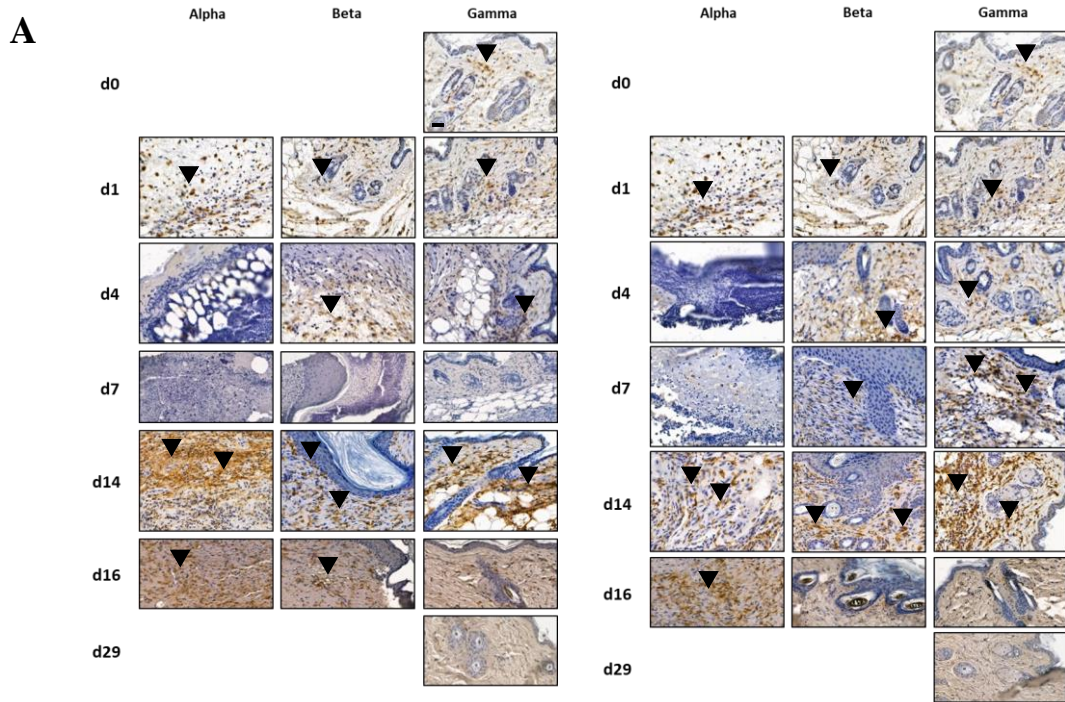
Figure 5.5. Fewer neutrophils were observed in OS1 treated wounds as determined by immunohistochemistry analysis. (A) Representative images of NIMP-R14 staining in the wounds of control and OS1 treated mice. Black triangles represent site of NIMP-R14 staining. Black bar = 20µm. (C) Table of the quantified scoring analysis of NIMP-R14 staining. Grey = 0. Light red/green = ± 0-1. Dark red/green = ± 1. (C) Graphs of quantified scoring analysis of NIMP-R14 staining in control and OS1 treated mice over the wound healing time course on day 0 (n=11), 1 (n=2), 4 (n=2), 7 (n=2), 14 (n=2), 16 (n=2) and 29 (n=1). (ns=P>0.05, *=P<0.05).

5.3.3 ERK5 degradation with OS1 led to modest increase in F4/80 expression at later time points

Macrophages are another crucial immune cell that regulate the inflammatory response and progression through the phases of wound healing. This includes an evolving spectrum from M1-like inflammatory macrophages to support an initial response to fight infection and phagocytose depleted neutrophils, to a transition towards M2-like reparative macrophages to assist in dampening inflammation, repair and remodelling (Snyder *et al.*, 2016; Wynn and Vannella, 2016).

We assessed their presence by the expression of F4/80, a pan-marker for macrophages (Gordon, Plüddemann and Martinez Estrada, 2014; Bio-Rad Laboratories Inc., 2015), through various time points of wound healing when compared to treatment with topical OS1. Macrophage presence in the wound increased and peaked at all three regions on day 16 (α 2.67, β 3.00, γ 1.67) in control mice. A similar pattern was observed in mice treated with OS1, but there was an increased trend with higher numbers on day 4 in the beta region (0.97 vs 2.00), day 7 in the gamma region (0.67 vs 2.00), and day 14 in the gamma region (1.06 vs 2.33), when compared to control mice (Figure 5.6.C).

Although previous studies have similarly found F4/80 macrophages to persist in late stage and healing wounds, they typically peak around day 4-5 and are reduced by wound closure between day 10-14 (Lucas *et al.*, 2010; Wynn and Vannella, 2016; Krzyszczyk *et al.*, 2018). This discrepancy may be due to our analysis widening the region of interest across the whole wound environment; alpha, beta and gamma.



B

		Ctrl							OS1								
		F480															
		0	1	3	4	7	14	16	29	0	1	3	4	7	14	16	29
Ctrl	α	/	0.83	0.00	0.19	0.67	2.36	2.67	/	/	0.83	0.00	0.19	0.67	2.36	2.67	/
	β	1.00	/	0.00	0.97	1.08	1.84	3.00	/	1.00	/	0.00	0.97	1.08	1.84	3.00	/
	γ	0.28	0.83	0.00	0.92	0.67	1.06	1.67	1.33	0.28	0.83	0.00	0.92	0.67	1.06	1.67	1.33
OS1	α	0.83	/	/	0.00	0.33	2.33	2.67	/	0.83	/	/	0.00	0.33	2.33	2.67	/
	β	1.00	/	/	2.00	1.33	2.33	2.33	/	1.00	/	/	2.00	1.33	2.33	2.33	/
	γ	0.56	0.83	/	1.00	2.00	2.33	2.17	1.67	0.56	0.83	/	1.00	2.00	2.33	2.17	1.67

Relative to Ctrl: -1 (dark red), -0.1 (light red), 0 (grey), +0.1 (light green), +1 (dark green)

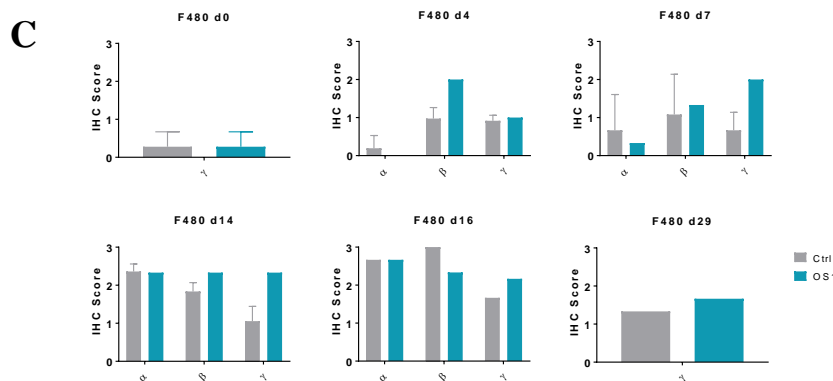
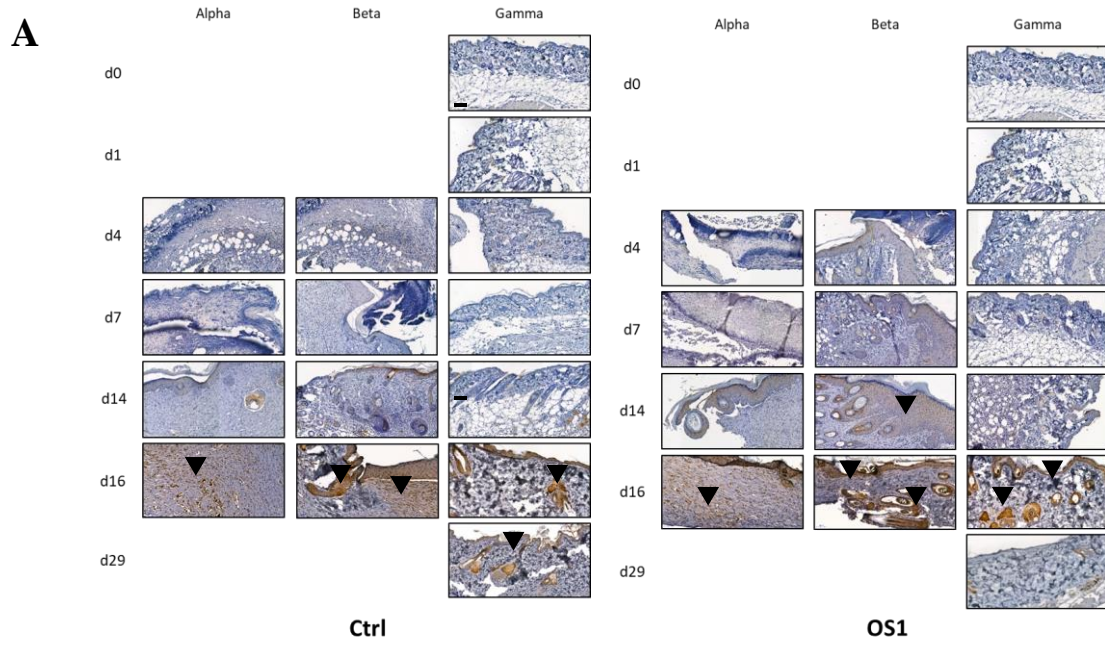


Figure 5.6. Macrophage levels increased in OS1 treated wounds as determined by immunohistochemistry analysis. (A) Representative images of F4/80 staining in the wounds of control and OS1 treated mice. Black triangles represent site of F4/80 staining. Black bar = 20µm. (B) Table of the quantified scoring analysis of F4/80 staining. Grey = 0. Light red/green = ± 0-1. Dark red/green = ± 1. (C) Graphs of quantified scoring analysis of F4/80 staining in control and OS1 treated mice over the wound healing time course on day 0 (n=11), 1 (n=2), 4 (n=2), 7 (n=2), 14 (n=2), 16 (n=2) and 29 (n=1). (ns=P>0.05, *=P<0.05).

5.3.4 ERK5 degradation with OS1 led to no changes in iNOS expression

To better understand the polarity state of macrophages that were contributing to the wound healing process, their inflammatory and reparative profiles were assessed by staining for iNOS and Arg1, respectively.

iNOS is a catalytic enzyme that mediates nitric oxide production which is expressed by M1-like macrophages in response to an inflammatory environment. iNOS expression was relatively low throughout the course of wound healing, peaking at day 16 (α 2.00, β 1.33, γ 1.33) in control mice, and was similar in trend in the OS1 treated mice at day 16 (α 1.67, β 1.67, γ 0.83), (Figure 5.7.C). This was in contrast with the expected profile of inflammatory macrophages and iNOS expression arriving at earlier time points of wound healing (Eming, Krieg and Davidson, 2007; Krzyszczyk *et al.*, 2018). It is additionally worth noting that iNOS expression was concentrated in the keratinocyte region of the skin at later time points of day 7 onwards and is often required for homeostatic functions beyond inflammation (Luo and Chen, 2005). Alternative markers to identify inflammatory macrophages, such as IL-1 β or CD86, in combination with co-staining immunofluorescence studies may be more informative in further clarifying the role of ERK5 in M1-like macrophage behaviour (Louiselle *et al.*, 2021; Wolf, Melvin and Gallagher, 2021).



B

		iNOS							
		0	1	3	4	7	14	16	29
Ctrl	α			0.33	0.33	0.00	0.33	2.00	
	β			0.33	0.34	0.00	0.50	1.33	
	γ	0.00	0.00	0.00	0.34	0.00	0.17	1.33	0.00
OS1	α				0.00	0.00	0.33	1.67	
	β				0.33	0.33	0.67	1.67	
	γ	0.00	0.00		0.00	0.00	0.17	0.83	1.00

Relative to Ctrl: -1 (Dark Red), -0.1 (Light Red), 0 (Grey), +0.1 (Light Green), +1 (Dark Green)

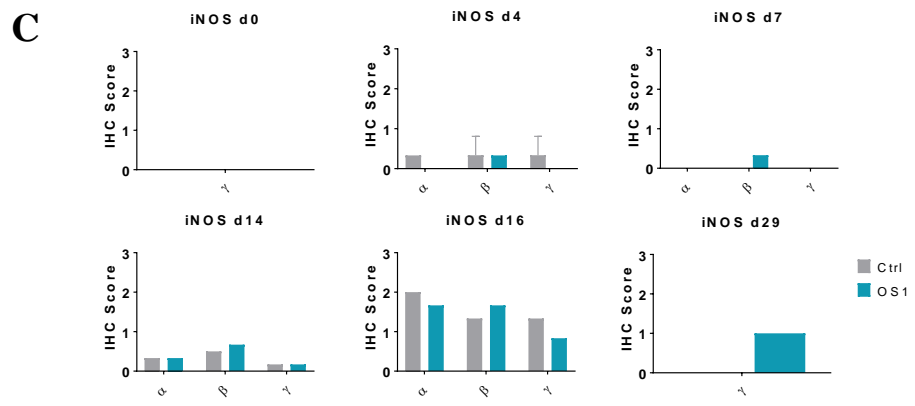
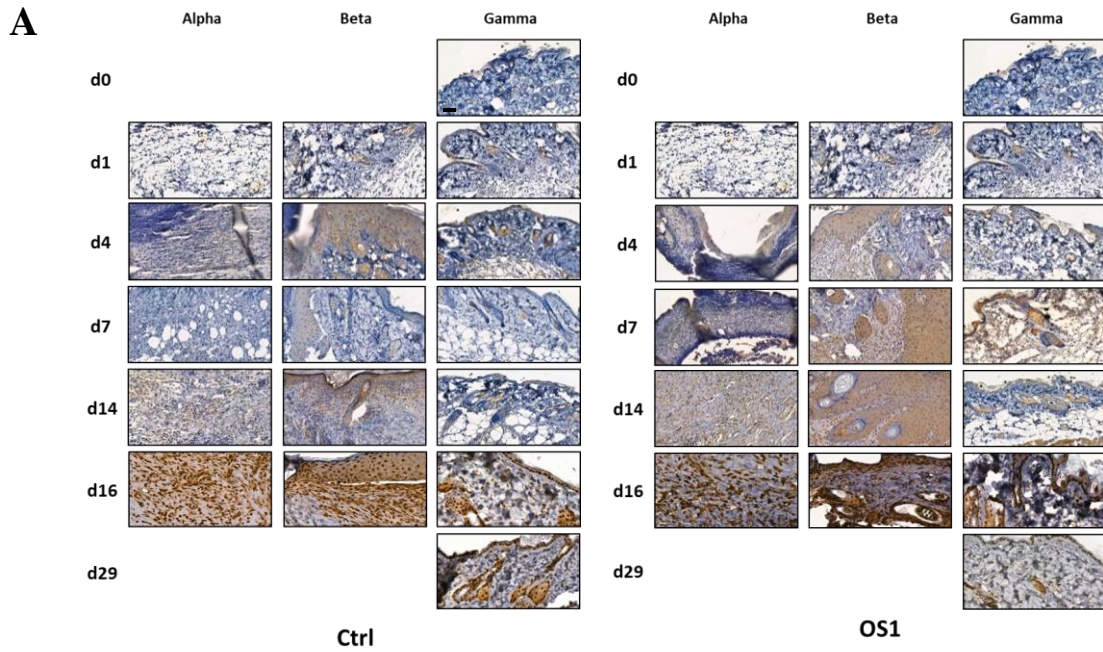


Figure 5.7. iNOS expression remains unchanged in OS1 treated wounds by immunohistochemistry analysis. (A) Representative images of iNOS staining in the wounds of control and OS1 treated mice. Black triangles represent site of iNOS staining. Black bar = 20µm. (B) Table of the quantified scoring analysis of iNOS staining. Grey = 0. Light red/green = ± 0-1. Dark red/green = ± 1. (C) Graphs of quantified scoring analysis of iNOS staining in control and OS1 treated mice over the wound healing time course on day 0 (n=11), 1 (n=2), 4 (n=2), 7 (n=2), 14 (n=2), 16 (n=2) and 29 (n=1). (ns=P>0.05, *=P<0.05).

5.3.5 ERK5 degradation with OS1 led to similar but slight increased Arg1 expression at later time points

Arg1, previously employed as a marker in chapter 3, is an enzyme that is upregulated in M2-like murine macrophages that metabolises L-arginine for functions in cell proliferation, fibrosis and collagen associated repair (Yang and Ming, 2014; Krzyszczyk *et al.*, 2018). Arg1 expression increased over the course of wound healing, and peaked on day 16 in control mice (α 2.67, β 2.67, γ 2.33). A similar trend was observed in OS1, however it was notable that the increase of its expression was most evident at day 7 when compared to control (Ctrl - α 0.17, β 0.67, γ 0.00 vs OS1 - α 0.33, β 2.67, γ 1.67). This trend of increased expression in OS1 treated mice (α 2.00, β 2.00) continued to be observed at day 14 but to a lesser extent when compared to control (α 1.50, β 1.33), (Figure 5.8.C).

This suggests that ERK5 degradation by OS1 shifts macrophages and the environment towards a more M2-like and reparative environment, particularly during the time course when we expect these types of healing activities to occur (from day 7 until wound closure). As previously observed in chapter 3, Arg1 expression was high in the keratinocyte and epidermal layer. Although beyond the scope of this study, investigating the role ERK5 plays in Arg1 expression in epidermal cells to regulate wound healing and local reparative mechanisms should be considered in future work.



B

Arg1

		0	1	3	4	7	14	16	29
Ctrl	α	0.00	0.33	0.83	0.17	1.50	2.67		
	β	1.00	0.33	1.17	0.67	1.33	2.67		
	γ	0.56	1.00	0.00	1.00	0.00	0.67	2.33	1.67
OS1	α	0.00		1.33	0.33	2.00	2.67		
	β	1.00		1.67	2.67	2.00	2.33		
	γ	0.11	1.00	1.33	1.67	0.67	2.33	2.33	

Relative to Ctrl

-1	-0.1	0	+0.1	+1
----	------	---	------	----

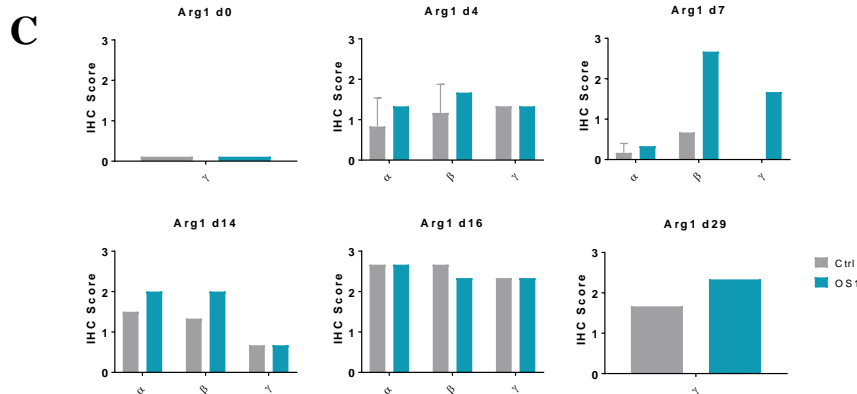


Figure 5.8. Arg1 expression increased in OS1 treated wounds by immunohistochemistry analysis. (A) Representative images of Arg1 staining in the wounds of control and OS1 treated mice. Black triangles represent site of Arg1 staining. Black bar = 20µm. (B) Table of the quantified scoring analysis of Arg1 staining. Grey = 0. Light red/green = ± 0.1. Dark red/green = ± 1. (C) Graphs of quantified scoring analysis of Arg1 staining in control and OS1 treated mice over the wound healing time course on day 0 (n=11), 1 (n=2), 4 (n=2), 7 (n=2), 14 (n=2), 16 (n=2) and 29 (n=1). (ns=P>0.05, *=P<0.05).

5.3.6 ERK5 inactivation with OS1 led to no changes in collagen deposition

Collagen is a key component of ECM architecture, and can be indicative of the progress of remodelling stages of wound healing. A careful balance is necessary, as excess can be a hallmark of dysfunction and hypertrophic scarring, but deficiency can be detrimental for complete wound closure (Eming, Wynn and Martin, 2017). M2-like macrophages are critical drivers and producers of ECM components such as fibronectin and collagen (Mirza, DiPietro and Koh, 2009; Delavary *et al.*, 2011). Our data has shown that ERK5 degradation shifts the local environment and macrophages towards an M2-like profile which could promote collagen deposition. As OS1 treatment affects the wider local environment of the wound, how it impacts other cells needs to be considered. Studies inactivating ERK5 in vascular endothelial cells of dermal and retinal cells in the context of diabetic neuropathy resulted in increased levels of TGF- β which are known to drive collagen deposition (Wu *et al.*, 2012).

As previously described, in order to determine if ERK5 degradation by topical OS1 treatment resulted in changes in collagen deposition in mice, the wounds of control and treated mice were stained with picrosirius red. Collagen staining was quantified by the area of red staining at a set threshold as a percentage of the total area and graphed as mean \pm SEM. A representative bright field image used for quantification has been depicted, and represent the data point closest to the mean for that sample set.

Total collagen based on picrosirius red staining had a gradual and increased trend across the three regions over the time course from d0 (γ 21.55%), d1 (γ 23.74%), d4 (α 1.08%, β 25.52%, γ 34.56%) and d7 (α 20.63%, β 37.00%, γ 40.56%) in control mice. Collagen staining peaked at d16 in all three regions (α 79.21%, β 75.72%, γ 72.27%) at the point of murine wound closure. At d29, almost two weeks after complete closure, only γ region skin remained and this had lower levels of collagen staining (53.04%), (Figure 5.9.C).

Treatment with OS1 led to a similar profile of increased collagen staining throughout the time course, as expected during the wound healing process. Differences observed were slightly decreased collagen staining at d7 (Ctrl - α 20.63%, β 37.00%, γ 40.56% vs OS1 - α 2.62%, β 30.56%, γ 30.20%), d16 (Ctrl - α 79.21%, β 75.72%, γ 72.27% vs OS1 - α 64.86%, β 63.27%, γ 53.36%) and d29 (Ctrl - γ 53.04% vs OS1 - γ 38.81%), but increase staining at d14 (Ctrl - α 41.00%, β 36.15%, γ 22.65% vs OS1 - α 43.68%, β 52.45%, γ 32.66%) when compared to control (Figure 5.9.C).

The difference in collagen content between OS1 treated and control wounds are subtle, and suggest that ERK5 degradation with OS1 has limited impact on altering the ECM architecture over the full wound healing time course.

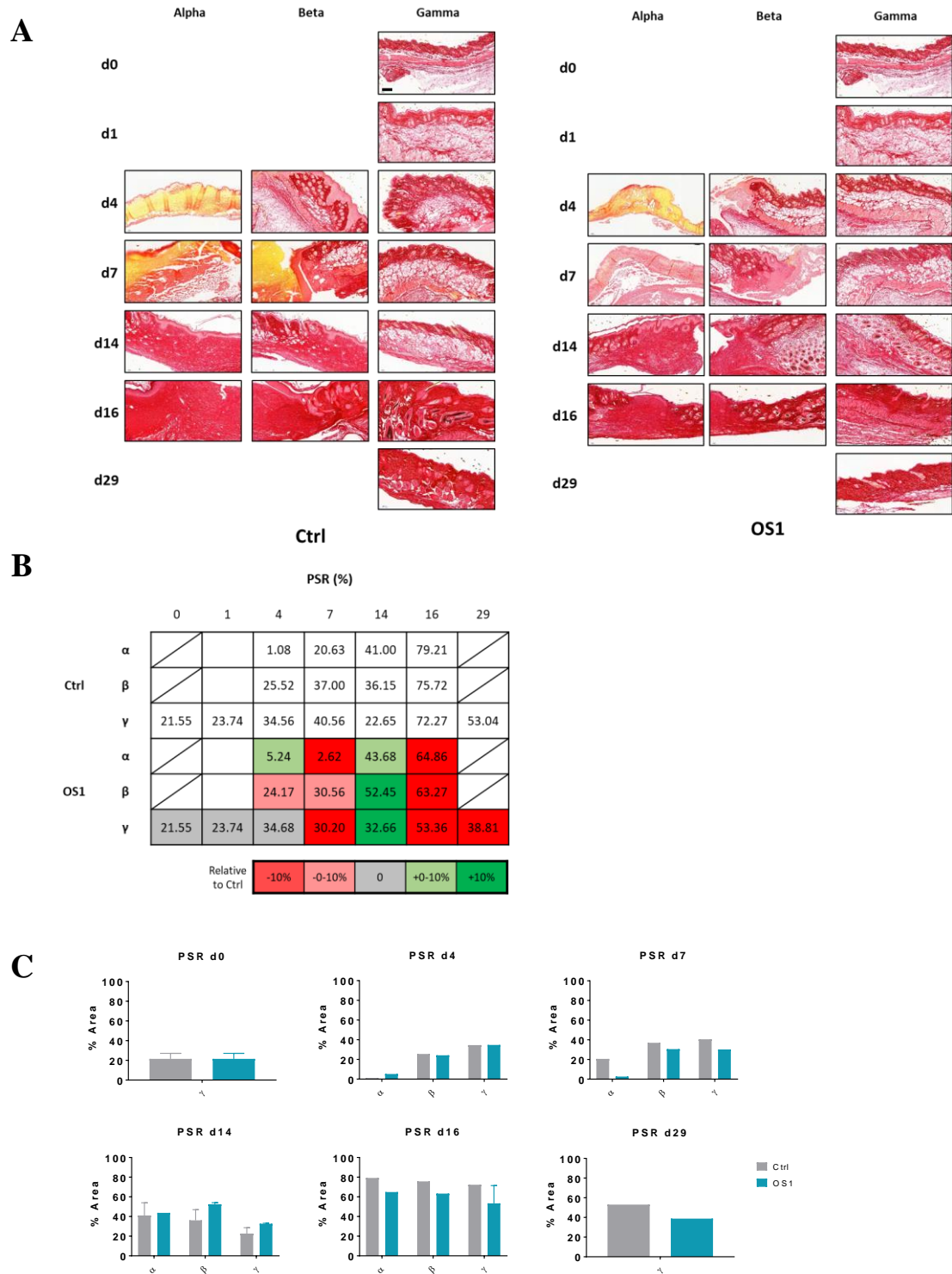


Figure 5.9. Collagen deposition remain unchanged in OS1 treated wounds by immunohistochemistry analysis. Collagen staining was quantified by the area of red staining from picosirius red, at a set threshold as a percentage of the total area and graphed as a mean \pm SEM, in control and OS1 treated wounds over the wound healing time-course. (A) Representative images of picosirius red staining in the wounds of control and OS1 treated mice. (B) Table of the quantified scoring analysis of picosirius red staining. Black bar = 50 μ m. Graphs of quantified scoring analysis of picosirius staining in control and OS1 treated mice over the wound healing time course on day 0 (n=11), 1 (n=2), 4 (n=2), 7 (n=2), 14 (n=2), 16 (n=2) and 29 (n=1). (ns= $P > 0.05$, *= $P < 0.05$).

5.4 OS1 modifies the mRNA expression of various inflammatory associated mediators

The data in our studies and previous literature have shown that inactivation of ERK5 reduces an inflammatory response, and promotes an earlier repair phenotype as indicated by the upregulation of Arg1, F4/80 macrophages and collagen staining. However, how loss of ERK5 drives this phenotype in wounds remains unclear and required further investigation on how OS1 treatment influences inflammatory and repair mediators in the total wound environment.

RT-qPCR analysis was used to investigate the gene expression of inflammatory (IL-1 β , TNF- α , CXCL1, CXCR2, and CCL2) and reparative (TGF- β and VEGF) mediated cytokines in murine wound sections collected over a time course and compared with topical OS1 treatment. Analysis was completed with the $\Delta\Delta$ CT method, as relative expression to β -actin, and statistical testing was done on the Δ CT values.

5.4.1 ERK5 inactivation by OS1 inhibits the mRNA expression of early inflammatory mediators

IL-1 β gene expression was significantly upregulated in the early time points of wounding at d1 (337.70 fold) and d4 (22080.03 fold) when compared to d0 wound tissue. This was followed by a typical resolution stage where IL-1 β gene expression decreased at d7 (8011.57 fold) and d14 (50.13 fold). OS1 treatment had no significant effect on IL-1 β expression at later time-points of d7 and d14, but compared to control, expression was lower at d4 (22080.03 fold vs 8841.00 fold) compared to control (Figure 5.10.A).

A similar pattern was also observed with TNF- α gene expression. There was increased expression at d1 (1.50 fold) followed by significantly upregulated expression at d4 (69.53 fold). Similarly at resolution, this increased expression was lower at d7 (54.37 fold) and reduced by d14 (0.87 fold; -13%). Again, compared to control, OS1 treatment resulted in reduced

expression of an inflammatory gene of interest at the earlier stages of d4 (69.53 fold vs 47.60 fold) and d7 (54.37 fold vs 29.70 fold), (Figure 5.10.A).

5.4.2 ERK5 inactivation by OS1 has limited influence on mRNA expression of chemokine mediators

Following from our previous observations in FACS and IHC of changes in immune cell accumulation in the wound tissue, we investigated whether OS1 treatment had an effect on expression of chemokines associated with macrophages and neutrophils.

CXCL1 is a chemoattractant for neutrophils at the site of injury or infection. It can exist as a monomer or dimer, which are able to bind to CXCR2. It is produced by multiple immune cells including macrophages and neutrophils, as well as epithelial cells and its expression can be induced by IL-1 and TNF- α . When CXCL1 binds to CXCR2 it activates the phosphoinositide 3-kinase (PI3K) and MAPK pathways including ERK1/2 to trigger inflammation, as well as signalling events to coordinate neutrophil adhesion and transmigration across the endothelium (Kim *et al.*, 2008; Wang, 2018).

CXCL1 gene expression initially decreased at d1 (0.59 fold; -41%), and was then followed by increased expression at d4 (4.08 fold) and d7 (6.67 fold) in control mice. As anticipated, the expression of CXCL1 was relatively low at later time points, as this time period is more associated with resolution when the wound was almost completely closed: d14 (0.87 fold; -13%) and d16 (1.67 fold). Compared to control, OS1 treatment resulted in a similar trend, but led to slightly higher expression of CXCL1 at d4 (4.08 fold vs 6.15 fold), and lower expression at d7 (6.67 fold vs 2.86 fold) and d14 (0.87 fold vs 0.07 fold). Unexpectedly, we found that OS1 treatment led to high expression of CXCL1 at d29 (11.02 fold) when the inflammation phase was typically resolved, and wounds would be actively remodelling the collagen architecture (Figure 5.10.A).

We then assessed CXCR2, the receptor counterpart to CXCL1 and observed what changes occurred in CXCR2 relative gene expression over the time course of wound healing. There was a significant increase in d1 (80.85 fold) and d4 (2002.65 fold), when compared to d0 wound tissue. Again a similar profile was observed by the resolution stage where this increased expression was lower on d7 (567.20 fold) and more so by d14 (5.77 fold). Interestingly, compared to control, OS1 treatment shifted the timing of CXCR2 expression and was lower at d4 (2002.65 fold vs 543.10 fold) but higher by d7 (567.20 fold vs 828.90 fold), (Figure 5.10.A).

To try to determine the signalling mechanisms underpinning the changes seen in macrophage accumulation after OS1 treatment, we investigated the changes in CCL2 gene expression. This chemokine primarily attracts myeloid cells such as monocytes and basophils. CCL2 expression can be stimulated by an array of inflammatory stimuli including IL-6, TNF- α , LPS and IFN γ (Ridiandries, Tan and Bursill, 2018). It has been previously shown that pre-treatment of ERK5 kinase inhibition in LPS challenged mice resulted in a reduction in CCL2 plasma concentrations (Wilhelmsen *et al.*, 2015).

In control mice, we observed a significant increase in the expression of CCL2 at d1 (44.95 fold) when compared to d0 wound tissue. Following from this, there was a trend of lower level of relative expression of CCL2 at d4 (15.05 fold), d7 (9.65 fold), d14 (3.35 fold), and d16 (0.86 fold; -14%). OS1 treatment resulted in no discernible difference to control animals, with the exception of d16 where that was a slight but significantly higher level in OS1 murine wounds (0.86 fold vs 2.59 fold), (Figure 5.10.A).

5.4.3 ERK5 inactivation by OS1 has no effect on the mRNA expression of reparative mediators

We turned our attention to reparative gene markers of interest, including TGF- β and VEGF. These reparative mediators play crucial roles in regulating inflammation and stimulating repair

and angiogenesis (Eming, Martin and Tomic-Canic, 2014; Okonkwo and Dipietro, 2017). Our previous *in vitro* workflow in chapter 4 found that OS1 mediated degradation in HaCaTs led to increased TGF- β and VEGF expression. This was similarly observed in OS1 treated M0 THP-1 macrophages, and further indicated that ERK5 inactivation could stimulate a reparative wound healing response. However, compared to the inflammatory markers discussed above in this study, the relative gene expression changes in TGF- β and VEGF were limited.

Initially, there was a slight and significant increased expression of TGF β at d1 (6.65 fold), which was lower by d4 (2.45 fold) in control mice (Figure 5.10.B). The latter time point's revealed similarly low expression of this gene, which was not considerably different from OS1 treated wounds.

Again, this pattern was observed in VEGF gene expression, where it significantly increased at d1 (2.15 fold) and less so by d4 (1.35 fold) in control mice. Interestingly, by the resolution and wound closure stage of d14, there was a significant decrease in expression (0.45 fold; -55%). Similarly to TGF- β , OS1 treatment led to no considerable differences in relative gene expression of VEGF (Figure 5.10.B). However, it should be noted that low replicate numbers prevented statistical analysis being conducted at these later time points and require further investigation.

It is possible that differences in macrophage and neutrophil accumulation in the wound tissue between control and OS1 treated wound was caused by altered chemokine signalling pathways, as observed in the subtle shifts in gene expression patterns in this study. Another theory along a similar theme could be that ERK5 modifies accessibility and permeability of endothelial cells and blood vessels to assist the recruitment of immune cells. However, our assessment of VEGF and CD34 (not shown here) show little to no changes, and so this hypothesis seems less likely.

Further studies investigating chemokine and recruitment signalling in *in vitro* endothelial models such as HUVEC and the cytokine mediators produced could prove insightful.

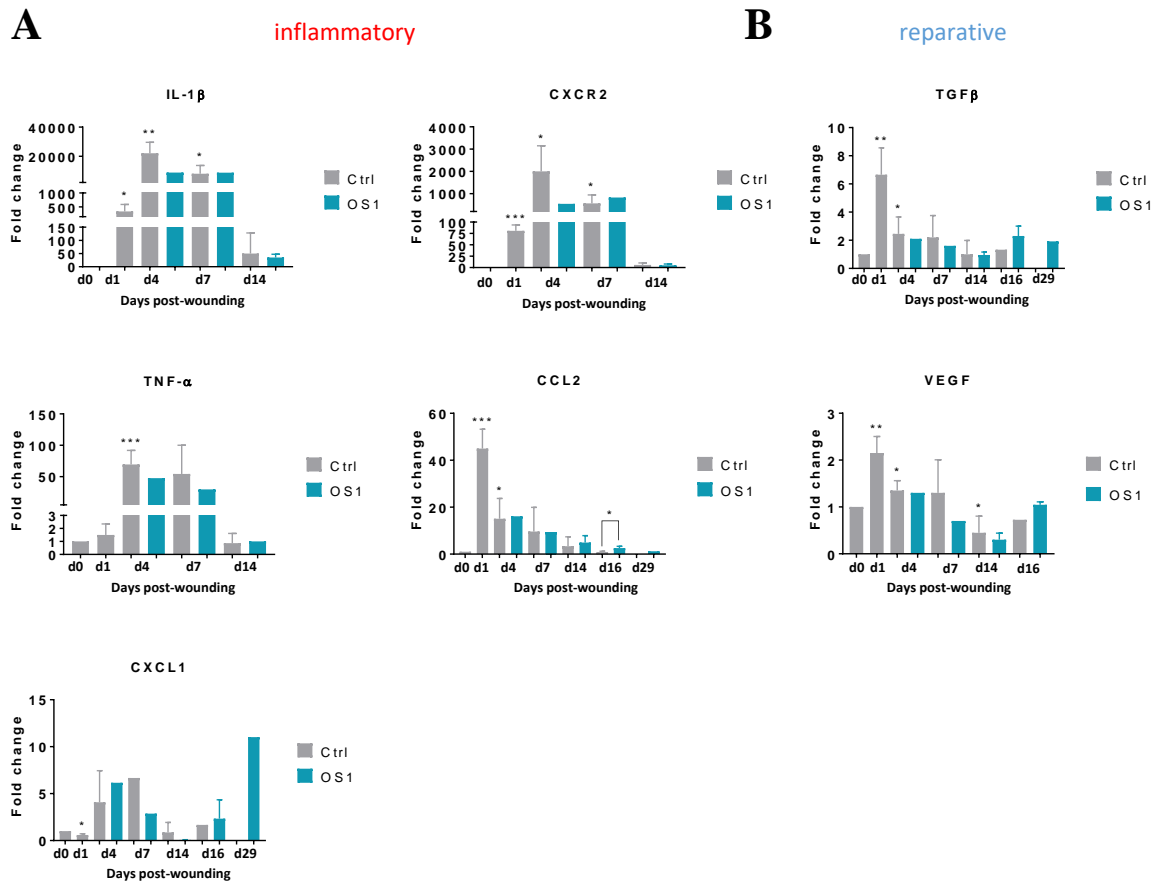


Figure 5.10. ERK5 inactivation by OS1 has limited effects on gene expression of inflammatory and reparative targets. Total RNA was extracted from wound samples and RT-qPCR was performed on a panel of genes from wounded mice that were treated with DMSO control, and OS1 (1 μ M). (A) Inflammatory gene targets: TNF α , IL-1 β , CXCL1, CXCR2 and CCL2. (B) Regulatory and reparative gene targets: TGF β , and VEGF. Values represent the mean expression of cDNA of the various genes relative to β -actin. (n=2) (ns=P>0.05, *=P<0.05, **=P<0.01, ***=P<0.001).

5.5 Discussion

The aim of this chapter was to evaluate whether therapeutic intervention with OS1 to degrade ERK5 in the wound could influence inflammation and promote wound healing. This was on the basis of our previous data which showed that genetic *in vivo* ERK5 inactivation in the keratinocytes exhibiting a phenotype of earlier inflammation and repair mechanisms, which was further reflected in our *in vitro* workflow in HaCaTs and THP-1 cells treated with 1 μ M of OS1.

We aimed to reproduce the effect of 1 μ M treatment with OS1 by topical delivery directly on the wound site. This would induce ERK5 knockdown at a multicellular level but limited to the wound environment, and infiltrating cells. However, as this was a simple proof-of-principle study, multiple factors still need to be considered in the future. We have based our 1 μ M concentration on our *in vitro* data which resulted in successful degradation of ERK5 in both HaCaT and THP-1 cells after 24h. The data in this chapter showed that although ERK5 expression was lower in OS1 treated mice compared to control, the protein was not completely knocked down, and so a wider range of concentrations will need to be evaluated. This future line of work would fully elucidate the *in vivo* efficacy of OS1 to degrade ERK5. In this study, we used methylcellulose as our choice of carrier as an established vehicle for topical drug delivery into the wound environment, due to its characteristics of hydrophilicity, capacity to facilitate permeation across the epidermis and the viscosity for ease of application (Cai, Mesquida and Jones, 2016; Tundisi *et al.*, 2021). This carrier may have successfully limited overt diffusion of OS1, and so the reduction of ERK5 expression observed may have been restrained to locations at the dosing site (gamma/beta; healthy wound edge). This may in turn have triggered proximal regions to compensate and increase the activation and expression of ERK5 in the alpha (centre of wound) and beta (wound edge) areas. Although, beyond the scope of this study, designing an effective drug delivery system for skin penetration will be required.

Present day technology ranges from patches, gels and ointments that permit drugs to be delivered in site specific and controlled dosages (Benson *et al.*, 2019).

In this chapter, we showed that although OS1 treatment did not completely ablate ERK5 protein from the wound environment, it resulted in modest but quicker wound closure with no adverse architectural changes in the wound environment. This occurred alongside an altered profile in immune cell infiltrates. In particular, we observed almost absent neutrophils and increased abundance of macrophages and Arg1 expression from day seven onwards in OS1 treated mice when compared to controls. This was indicative of ERK5 loss resulting in a reparative and M2-like polarised state in healing wounds. Conversely, iNOS expression remained relatively low and consistent across both control and OS1 treated mice. This was consistent with our previous data and suggests that although OS1 may prime and promote M2-like polarisation, it may not necessarily have the capacity to repolarise existing M1-like macrophages.

Additionally, our FACS analysis showed that OS1 treatment led to a reduction in monocytes at day 4 and day 7. This could be an acute response to ERK5 degradation, and limit the pool of myeloid cells able to differentiate and polarise to have functions in the wound environment. Notably, this loss of monocytes was recovered by day 14 onwards, and the percentage of monocytes increased starkly compared to control. This coincided with the increase in Arg1 expression and macrophages. However as highlighted in chapter 3, it was noted that the general gating strategy could be re-optimised. Alternative gating strategies could be utilised on the current data set to better separate the immune cell populations. Namely, CD45⁺F4/80⁺ for macrophages and CD45⁺F4/80⁻Ly6G⁻Ly6C⁻ for lymphocytes.

Furthermore, identifying these polarity states could be improved in this study with a FACS panel that could further characterise macrophages based on their expression of iNOS and Arg1, as we have done by IHC. We could also further expand our panel of IHC markers to include

MR as another established marker for M2-like phenotype. In addition, this could be conducted as co-stained immunofluorescence in conjunction with F4/80 as a pan-macrophage marker to specifically identify macrophages with a polarised state. This was initiated but faced several technical issues.

Moreover, as previously highlighted in Chapter 3, a limitation of the histology analysis conducted in this study, was that it was a subjectively scored from 0-3 based on the degree of brown staining observed. This was further limited by the blinded nature of the analysis which enabled non-specific staining to potentially be included in positive scoring. Future analysis may require automated scoring software or counting number of cells that are positively stained.

We additionally assessed the gene expression profile in these OS1 treated wounds and found that in parallel with earlier initiation of repair mechanisms with the increase in Arg1 expression, we observed earlier decrease of inflammatory mediators including IL-1 β and TNF- α . However, it should still be noted that many of these immune based changes after treatment with OS1 should be taken with caution. Though the results seem to parallel with the pattern of decreased inflammation and earlier reparative mechanisms, many of these changes are modest.

The timing of dosing, is a key factor that may have limited its effect on early inflammatory players such as neutrophils. These are alerted and recruited by early danger signals generated from wounds within hours of damage. As dosing of OS1 only occurred on day 2, many of the inflammatory recruitment actions have already been initiated and are less likely to be affected by OS1 treatment. In order to have an impact on inflammation of healthy wounds, animals would have to be pre-treated with OS1 prior to wounding. This earlier window of time would take into account the role of OS1 treatment on the inflammatory environment of resident cells and infiltrating neutrophils. How therapeutic ERK5 inactivation may play a role in accessibility, permeability and recruitment of neutrophils remains an open question.

Particularly, when our histological analysis of NIMP-R14 suggests such a stark inhibition of their presence at later time points. Notably, we observed abundant and continued expression of NIMP-R14 throughout the wound healing time course up until day 16. It was anticipated this histology marker would only be dominant and present within the first five days to parallel the expected physiology of neutrophils. It is possible that as NIMP-R14 identifies a combination of Ly6G and Ly6C, other cell populations such as monocytes and myeloid-derived suppressor cells could be categorised in these wound samples. In particular, myeloid-derived suppressor cells which have dual functions in regulating inflammation and stimulating cell proliferation, have predominantly been researched in cancers, but have recently been identified in the healing context and their significance is yet to be fully understood (Ou *et al.*, 2015; Gabrilovich, 2017). Thus, in our study where we treat with OS1 after day 2, it may be that OS1 only had a major influence on the departing inflammatory phase and incoming circulating macrophage populations that are likely to be more reparative as examined through Arg1, F4/80 and the genes of interest; TGF- β and VEGF by RT-qPCR.

What would be of potential interest in the future, would be to delineate these inflammatory changes by testing the OS1 compound in a diseased context such as diabetic *in vivo* models. The prolonged chronic inflammation and delayed wound healing from these models associated with diabetes could enable the modest pro-healing effects of using OS1 in healthy skin to be amplified. Namely, would OS1 be able to counteract the chronic inflammation associated with these dysfunctional wounds?

A final technical element to discuss in the scope of this study, is the limitation of snapshot pathology approach to investigate various time points of the wound healing process. An animal has to be culled and collected at each time point from day 1, 4, 7, 14, 16 and 29 to generate six datasets relevant to that timeframe. As we have chosen to focus our studies on the early phases

of wound healing, we gain additional insight from day 4 and day 7. However, there are several interim steps in between those days, and prior that could have relevant information. Additionally, there are large gaps between day 16 and day 29 where activity associated with repair and remodelling would have occurred, and not investigated within the scope of this study. Novel technology is required that would permit dynamic and longitudinal study of wound healing and immune cell behaviour while refining and reducing the number of animals needed for this type of research.

Chapter 6: Development of macrophage PET imaging modality

One of the major limitations in recent decades has been the reliance on static snapshot pathology to understand macrophage behaviour (Yona *et al.*, 2013; Minutti *et al.*, 2017). Recent developments in *in vivo* imaging modalities provides a non-invasive method to investigate the dynamic behaviour of macrophages at a cellular and molecular level. This growing field of technology has become indispensable for clinical research and medical practice, as it enables real-time examination of living subjects with accuracy and sensitive characterisation to better understand biological behaviour and evaluate treatment efficacy (Velikyan, 2012; Rua and McGavern, 2015; Arlauckas *et al.*, 2017).

Positron Emission Tomography (PET) imaging has been a favoured tool due to its high specificity and sensitivity to map biological processes. These tools enable the stratification of patients to specific therapies. In the context of this project, targeting distinct populations of immune cells such as discrete macrophage polarities has been possible with the development of several pre-clinical radiotracers specific to TSPO, expressed on M1-like macrophages and MR, expressed on M2-like macrophages. PET imaging has enabled evaluation of the behaviour of these macrophage phenotypes and has been informative in evaluating the progressive immunopathology of rheumatoid arthritis, Alzheimer's disease and cancer (Boutin and Pinborg, 2015; Henderson *et al.*, 2018). We hypothesised that utilising this established tool in the context of wound healing would enable a novel and refined approach to evaluate the dynamic behaviour of M1-like and M2-like macrophages during the entire wound healing time course.

6.1. Inflammatory macrophage infiltration was not successfully identified with TSPO-PET imaging in the wound healing model

Translocator protein (TSPO) is a mitochondrion associated receptor complex that is increased in expression in inflammatory cells such as infiltrating macrophages. TSPO is involved in multiple biological functions such as apoptosis, cell proliferation, immunomodulation and inflammation (Hatori *et al.*, 2015). TSPO-PET probes have enabled the spatial-temporal visualisation of glial cells and infiltrating macrophages, particularly in the context of stroke, neuroinflammation and cancer (Henderson *et al.*, 2018; Green *et al.*, 2020).

To evaluate the longitudinal real-time behaviour of inflammatory macrophages in wound healing, we used the [¹⁸F]-DPA-714 PET tracer to measure TSPO expression *in vivo*. As standard practice, mice were anaesthetised with isoflurane, and the tracer injected into the tail vein before PET scanning (Figure 6.1.A). Analysis was performed based on the manually drawn regions of interest (ROI) processed as the standardised uptake value (SUV) which represented the mathematically derived ratio of tissue radioactivity based on the weight of the subject. We additionally analysed the SUV as a ratio against control muscle tissue and heart tissue (Henderson *et al.*, 2018; Green *et al.*, 2020).

At all time points, TSPO-PET detected no substantial inflammation in the wound site (Figure 6.1.B). It has been previously shown that [¹⁸F]-DPA-714 can be used as TSPO specific PET tracer in the context of neuroinflammation, stroke and cancer (Boutin and Pinborg, 2015; Henderson *et al.*, 2018). However, in this study in the context of wound healing, only one animal had tracer uptake at the wound area in day 1 and day 4 (Figure 6.1.A).

Conversely, wound sections that were processed for histology and stained for TSPO exhibited positive and strong presence of this target in several regions across the wound environment (Figure 6.1.C). Namely in the keratinocytes and in regions of immune cell influx. Additionally,

our previous analysis with histology, FACS and qPCR indicate a definitive influx of inflammation in the early phases of wound healing in all animals.

One potential explanation for the discrepancy between the overt TSPO expression detected by IHC and the lack of signal from the TSPO-based PET tracer is that the PET tracer could not penetrate the wound site due to lack of vasculature but H&E and CD34 staining (not shown), and presence of VEGF gene expression indicates that this was unlikely. It remains uncertain why this tracer unsuccessfully reached macrophages in the wound site.

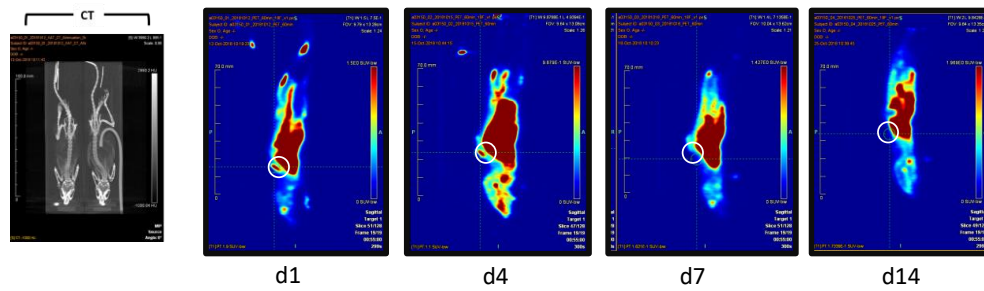
6.2 Reparative macrophage infiltration was not successfully identified with MR-PET imaging in the wound healing model

We conducted a pilot study using a novel [¹⁸F]-MR nanobody based tracer to examine M2-like macrophage activity in the wound site (Figure 6.1.D). Macrophage mannose receptor (MR) is a C-type lectin receptor with key roles in scavenging, immune homeostasis and regulation of insulin sensitivity (Martinez-Pomares, 2012; Roszer, 2015). It is a well characterised marker for M2-like macrophages in both mice and humans. Nanobody technology utilises the unique antibody-binding fragments from camelid heavy chain antibodies, designed specific to MR, which can be labelled with radioisotopes that can be detected by PET scanning (Blykers *et al.*, 2015). Unfortunately, MR-PET detected no substantial presence of tracer uptake in the wound site (Figure 6.1.F). Furthermore, due to technical errors in this single study, we were only able to attempt two imaging sessions, on day 2 and day 8. And of the six animals that underwent imaging, no tracer uptake was observed at the wound site.

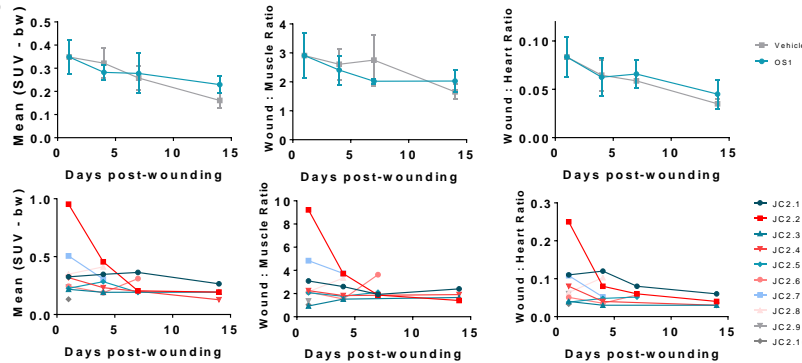
Again, this was contrary to histology of MR staining which demonstrated high MR presence in the skin and wound site, as well as evidence showing presence of M2-like macrophages and repair mechanisms in place in the wound site throughout the wound healing process (Figure 6.1.E). However, one caveat may be that we anticipated presence of M2-like macrophages to

be greatest at later time points during the reparative phase of wound healing (day 7 onwards). This could be one reason why we failed to observe tracer uptake at this earlier phase of wound healing. Unfortunately due to the technical issues mentioned above, we were unable to image on the planned d14/16 time point and therefore were unable to prove or disprove our hypothesis that MR-based PET imaging would be more effective at later phases of wound healing.

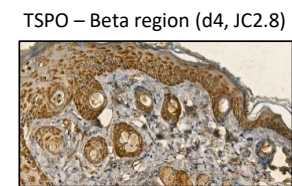
A



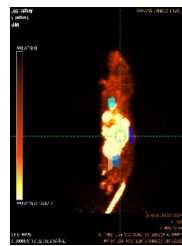
B



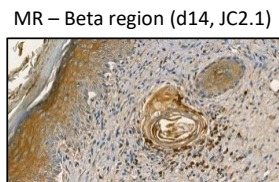
C



D



E



F

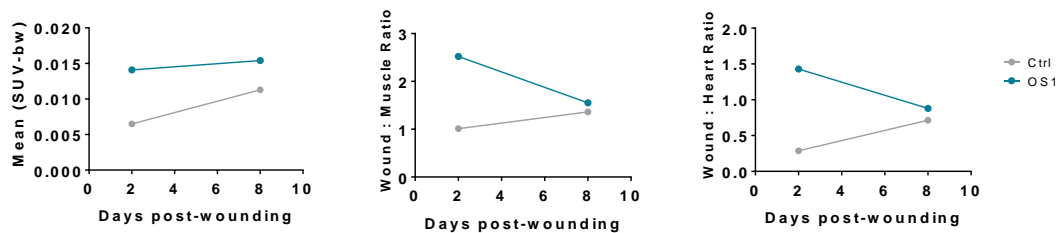


Figure 6.1. Development of TSPO and MR PET imaging technology for wound macrophage investigation. (A) CT-scan and coronal plane $[^{18}\text{F}]$ -TSPO uptake in wound healing murine model at d1, d4, d7 and d14 post-wounding. Yellow circles indicate area of wound. (B) Quantified tracer uptake graphs using Mean SUV, body weight, SUV in muscle tissue or heart tissue. Data has been shown as a group of control and OS1 treated mice, or as individual mice. (C) Representative image of TSPO staining in wound of control mice. (D) Coronal plane of $[^{18}\text{F}]$ -MR uptake in wound healing murine model. (E) Representative image of MR staining in wound of OS1 treated mice. (F) Quantified tracer uptake graphs using Mean SUV, body weight, SUV in muscle or heart tissue. (ns=P>0.05, *=P<0.05).

6.3 Discussion

Much of the approach in this type of *in vivo* study throughout this PhD is focussed on a snapshot pathology, whereby numerous animals are culled to generate data at multiple time points in the pathophysiology. Development of novel PET imaging technology was aimed to permit investigation of the dynamic behaviour of macrophages where a single animal could be tracked during the entire wound healing process. This would additionally provide refinement and reduction in the number of animals needed for this type of research.

Despite TSPO and MR being present in wound tissue based on our histology, we were unable to develop PET imaging as a valid and effective tool in this study. This technology is well-established in cancer and neuroinflammation research, but it remains uncertain why it failed to be recapitulated in the context of wound healing. Potential explanations range from inability for the PET tracer to penetrate to the wound site, or failure to image at the appropriate time range for MR-PET tracers.

Troubleshooting these issues will be necessary and may include workflows such as: assessing vasculature of wounds, *ex vivo* radiography analysis of post-PET imaged animals and conducting PET imaging over the full wound healing time course. Additionally, as intravital imaging continues to develop, there will be greater access to novel technology including nanoparticle imaging agents and fluorescent probes as alternative imaging tracers to non-invasively track immune cell behaviour (MacRitchie *et al.*, 2018, 2020).

Dysfunctional changes in molecular and cellular behaviour can occur well in advance of disease phenotypes being recognisable. Further research into this field will be necessary and beneficial within the wound healing context and beyond. Developing a robust imaging modality that can investigate these initial molecular and cellular changes can permit earlier diagnosis, patient stratification and therapeutic intervention. Moreover, these imaging tools

could be used to assess the efficacy of novel compounds and the impact at a molecular or cellular level.

Chapter 7: General Discussion

Using a combination of ERK5 genetically modified murine *in vivo* models and a novel ERK5 specific therapeutic, OS1, tested in human *in vitro* and murine *in vivo* systems, we show that inactivation of ERK5 can improve wound closure, alter inflammation and enhance reparative mechanisms throughout the wound healing time course. These are novel insights into how ERK5 signalling drives macrophage polarisation and immune infiltration in homeostatic cutaneous wound healing. Moreover, as ERK5 specific therapies continue to develop across multiple pathologies, this study reiterates the need to deviate from kinase inhibitors, as OS1-mediated degradation of ERK5 can better recapitulate the immune phenotypes observed in genetic ablation studies.

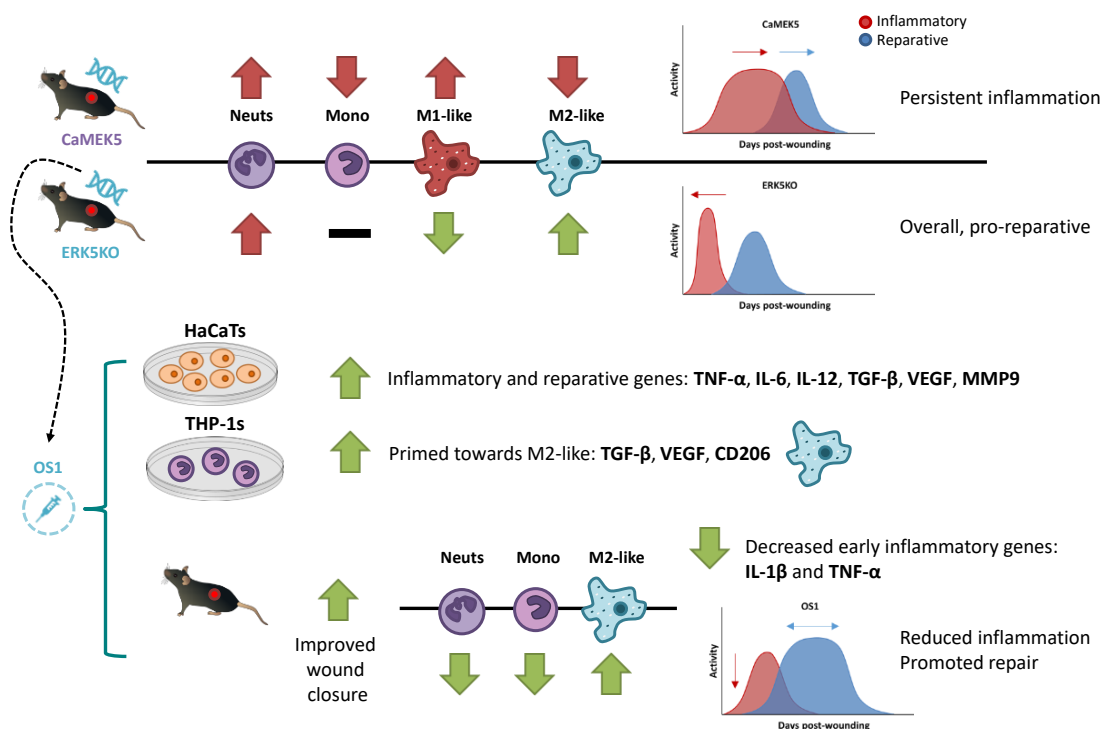


Figure 7.1. ERK5 inactivation drives reparative activity in wound healing. Genetic hyperactivation of ERK5 in keratinocytes (CaMEK5) drives persistent pathological inflammation in wound healing. Conversely, genetic inactivation of ERK5 in keratinocytes (ERK5KO) induces an initial increase and earlier shift of inflammation, followed by earlier repair activity. This ERK5-reparative phenotype was recapitulated using the novel OS1 therapeutic which targeted and degraded ERK5 *in vitro* models of HaCaTs and THP-1s and in *in vivo* wounding models to generate an overall improved reparative phenotype in cutaneous wound healing.

It's expected that over 150 million individuals are affected by impaired wound healing and this number continues to grow worldwide. This has been particularly prevalent in two growing demographics: diabetics and the elderly. Up to 25% of diabetics will suffer from chronic wound pathologies such as diabetic foot ulcers, which often end in lower limb amputations (Sen *et al.*, 2009; Järbrink *et al.*, 2016; Martinengo *et al.*, 2019). Part of the reason this problem persists is because of an incomplete understanding of the process of wound healing. Recently, there has been growing interest which highlights a significant role of the immune system in the homeostasis and pathophysiology of wound healing (Delavary *et al.*, 2011; Snyder *et al.*, 2016).

It is well understood that the wound healing process is based on overlapping and coordinated phases of inflammation, granulation and remodelling. Dysfunction in any of these stages can result in impaired and incomplete healing. One of the crucial cells involved in multiple stages of this wound healing process are macrophages. They are multifunctional with roles in responding to damage, removing apoptotic cells, transitioning to repair and restructuring the collagen and ECM structure (Mirza, DiPietro and Koh, 2009; Snyder *et al.*, 2016; Wynn and Vannella, 2016). The disadvantage of such a pleiotropic cell type, is that dysfunction can be more likely. Conversely, the plasticity of macrophage behaviour has the potential to be exploited as a therapeutic target to treat dysregulated wounds.

In parallel, much research has been conducted to understand the role of macrophages in the context of cancer and metastasis (Nielsen and Schmid, 2017). A similarity has been previously described, and associated cancers as a “wound that never heals”. It was assumed that many of the characteristics of chronic wounds such as abnormal inflammation are similar in their contributions to tumour progression. Thus, there is very likely a crossover of these mechanisms in the context of dysfunctional wound healing. Throughout this line of cancer research, ERK5 has been found to be an important signalling pathway at controlling inflammation and polarity

states of macrophages (Giurisato *et al.*, 2018; Luiz *et al.*, 2020). Moreover, ERK5 has additional crucial roles in regulating angiogenesis, migration and oncogenic function in skin carcinomas (Finegan *et al.*, 2015; Stecca and Rovida, 2019; Bhatt, Wright, *et al.*, 2021).

Although many parallels exist between the chronic inflammation of cancers and diabetic wounds, there are equally many differences in their respective microenvironments and signalling pathways. What remains unanswered is how the potential role ERK5 signalling observed in cancer studies may play a role in influencing the behaviour of immune cells such as macrophages and neutrophils in the context of wound healing.

The hypotheses of this study were:

- i) Hyperactivation of ERK5 may contribute to chronic inflammation that disrupts healthy wound healing.
- ii) With the complex and multi-factorial role ERK5 plays, it had the potential to be therapeutically targeted with the novel compound OS1, to attenuate inflammation and promote repair mechanisms e.g. M2-like macrophage activity.

This PhD study investigated these hypotheses by using a variety of genetic and therapeutic tools to examine how ERK5 signalling regulates key factors of immunity in healthy wound healing.

7.1 Aims of PhD:

- To determine if *in vivo* genetic inactivation of ERK5 and constitutive activation of MEK5 affects wound healing and inflammation.
- To determine if therapeutic inactivation of ERK5 using novel compound OS1 affects *in vitro* models of keratinocytes (HaCaTs) and macrophages (THP-1s) in relation to wound healing and inflammation.

- To determine if therapeutic inactivation of ERK5 using novel compound OS1 affects *in vivo* model of murine wound healing and inflammation.

7.2 Genetic *in vivo* hyperactivation of ERK5 in keratinocytes drive local inflammation in wound healing

Despite no discernible difference in wound closure rate between ERK5KO, CaMEK5 and control mice, we found some interesting changes in immune cell composition. Our analysis suggested that ERK5KO mice exhibited an earlier and more inflammatory response, whereas CaMEK5 mice had a more persistent inflammatory profile.

Our data on hyperactivated ERK5 signalling (via constitutively activated MEK5, CaMEK5) contributing to pathological inflammation was consistent with studies showing ERK5 hyperactivation driving aggressive cancer progression and metastatic potential (Simões *et al.*, 2015). The wounds of CaMEK5 mice were more pathologically inflammatory based on the increased profile of neutrophils and persistent expression levels of iNOS. Moreover, we found a decreased pool of monocytes which may have contributed to the decreased level of Arg1 and F4/80 expression in day 4 and 7 associated with M2-like reparative phenotype required for wound healing.

Unexpectedly, in our opposing model to ERK5 hyperactivation: genetic inactivation of ERK5 also resulted in a brief increase in inflammation. However, overall we observed an earlier shift of both onset of the inflammatory phase and resolution phase of wound healing in the ERK5KO model. Our ERK5KO murine wounds had increased iNOS expression at early time points of day 2, which then decreased to similar or lower levels to control. In parallel we observed slightly higher and earlier influx of Arg1 expression at day 4. Together this could suggest an earlier shift in macrophage activity towards a reparative and M2-like phenotype. Additionally,

we had an increased abundance of neutrophils. Genetic inactivation of ERK5 was observed to promote initial inflammation of wound healing, followed by an earlier repair phenotype with a slight reduction in collagen deposition.

This was in contradiction with previous studies where inactivation of ERK5 in cancer models induced a sharp reduction in inflammation. These studies showed reduced inflammatory mediators (IL-6, IL-8, CXCL1, CXCL2, IL-1, COX2) and fewer infiltrating immune cells, including neutrophils (Finegan *et al.*, 2015; Wilhelmssen *et al.*, 2015). Furthermore, when specifically investigating the role of ERK5 in myeloid cells, studies have found that myeloid-specific inactivation of ERK5 led to an increase in inflammatory M1-like macrophage associated genes including iNOS. These ERK5 myeloid ablation models, also exhibited a reduction in M2 associated genes, e.g. Arg1, TGF- β , and IL-10 (Giurisato *et al.*, 2018; Luiz *et al.*, 2020). One study has additionally found that these ERK5 ablated macrophages are hindered in their ability to phagocytose and have negatively impacted the progression of atherosclerosis (Heo *et al.*, 2014).

To explain the discrepancy between our finding and that of previous studies of ERK5 in inflammation, we must consider context. The role of ERK5 plays will be cell type and context dependent. Notably, much of the research to resolve the role of ERK5 in inflammation has been conducted in cancer cells, which have tumorigenic specific mutations that can contribute to dysfunction and the way ERK5 is “used”, which may be different to that in normal tissue context of wound healing (Stecca and Rovida, 2019). This only reiterates the complex interaction between cells and its microenvironment, as well as the spatiotemporal cues that dictate the coordination of wound healing and its difference to the cancer context.

Interestingly, diabetic murine wounds have an opposite profile to ERK5KO wounds, with diabetic wounds having attenuated initial inflammation but abundance of monocyte and

macrophages at later stages, indicative of a sustained and pathologically inflammatory state (Wolf, Melvin and Gallagher, 2021). Our studies suggested that loss of ERK5 could shift inflammation and repair mechanisms to occur more quickly in wound healing while hyperactivation of ERK5 may in fact deregulate wound repair mechanisms and allow chronic inflammation to persist. This suggests that ERK5 may drive the chronic inflammation associated with diabetic wound healing and inhibiting ERK5 could be leveraged to improve outcomes in diabetic wounds. Indeed, in support of this hypothesis, our precursor data show that loss of ERK5 accelerates wound closure in murine models of diabetes (Figure 1.8.A)

7.3 Therapeutic inactivation of ERK5 with OS1 in *in vitro* models of HaCaTs and THP-1s promotes an overall reparative phenotype

Following from our genetic studies, we were able to replicate whole protein inactivation of ERK5 with the therapeutic use of OS1. A novel compound generated in-house that targets ERK5 for proteolytic degradation within 24h. This study focussed on *in vitro* human models of keratinocytes (HaCaTs) and macrophages (THP-1s) to investigate the role of ERK5 signalling in these crucial wound healing cell types individually, and to validate if our findings in the murine context can be translated to human systems. Our initial studies using HaCaTs found that OS1 specifically degraded ERK5, had no detrimental effects on migration and proliferation, and stimulated various inflammatory and reparative genes of interest. This was in line with many of the changes observed in the genetic *in vivo* inactivation model. However, this was contradictory to previous studies which showed that ERK5 kinase inactivation with AX15836 led to reduced migration and proliferation of keratinocytes (Arnoux *et al.*, 2008).

This was a reminder that many functions of ERK5, in particular those associated with inflammation, has been found to be kinase independent and that a range of selective ERK5 kinase inhibitors such as AX15836, have failed to recapitulate the altered inflammatory profile

observed in genetic knockdown models (Woo *et al.*, 2006; Finegan *et al.*, 2015; Green *et al.*, 2020). Our studies, reiterate these differences in the kinase and non-kinase functions of ERK5 and show that OS1 mediated degradation of ERK5 has therapeutic potential to influence inflammation in the wound healing context.

We also conducted *in vitro* studies to understand how OS1 affects crucial immune cells, such as macrophages, in the human setting. This would enable us to see if our phenotype in murine macrophages can be translated to the human scenario. To achieve this we used the human monocyte cell line, THP-1, and its differentiated and polarised states of M0, M1 and M2 –like macrophages, to test the effects of OS1. We could successfully degrade ERK5 protein in these macrophages, and yielded modest effects on priming M0 macrophages towards the reparative M2-like state. This was contradictory to literature which suggests that inactivation of ERK5 in the murine myeloid lineage can prime them towards the inflammatory M1-like macrophage states (Giurisato *et al.*, 2018; Luiz *et al.*, 2020). However, both studies do highlight that ERK5 may only have a role in IL-4 induced macrophages. Even within this type of M2-like macrophage, it was found to be independent of the STAT3/STAT6 pathway, and related to the c-Myc pathway. Additionally, other research has found that ERK5 deficient macrophages had reduced capacity for efferocytosis and phagocytosis and promoted atherosclerotic lesions. Again, this study provided evidence of ERK5 deficient macrophage being prone to an M1-like phenotype (Heo *et al.*, 2014). However, these discrepancies indicate that whilst genetic myeloid inactivation of ERK5 in these studies primes murine macrophages towards a M1-like phenotype, perhaps therapeutically degrading ERK5 in physiological wild type macrophages can prime them towards an M2-like reparative phenotype as observed in this study. Moreover, this *in vitro* study involves novel insight into how ERK5 signalling regulates human macrophage polarisation, which may have differences with murine macrophage models that

account for the discrepancy. Thus, our data in this chapter may only indicate how ERK5 therapeutics could translate in the human wound healing context.

Another currently open question is if and how we can repolarise macrophages. Whilst data are limited, early indications suggest that M2-like macrophages are more plastic and amenable to repolarisation. Whereas, M1-like macrophages may be more difficult to alter phenotype once committed, due to their impaired mitochondrial activity (Van den Bossche *et al.*, 2016; Oyarce *et al.*, 2021). M1-like macrophages have reduced mitochondrial activity, fatty acid oxidation and tend to use glycolytic pathways. This altered metabolic system is required to polarise towards M1 and inflammatory phenotypes. Notably, studies have found that therapeutic compounds that target and inhibit these metabolic mechanisms can promote M2→M1 polarisation or inhibit M0→M2 polarisation (Van den Bossche *et al.*, 2016; Oyarce *et al.*, 2021). If inactivating ERK5 does promote M2-like polarisation, it is more likely that this occurs by priming M0 towards that phenotype, or by promoting a repair mediated microenvironment. Concurrently our data in THP-1 M0 macrophages studies show that OS1 mediated ERK5 degradation has limited impact on inflammatory M1-like profiles, but increases the gene expression of regulatory and M2-like targets such as TGF- β , CD206 and VEGF.

Taken together, the *in vitro* workflow show that OS1 mediated ERK5 degradation of HaCaTs and THP-1 cells individually, promote an overall reparative phenotype. This suggests that treating human multicellular complex wounds with OS1 can activate keratinocytes to upregulate both inflammatory and reparative genes that are necessary for healthy wound healing. Moreover, OS1 could promote macrophage polarisation towards reparative M2-like phenotype without dampening the necessary M1-like phenotype needed in the early phases of wound healing.

However, as these *in vitro* cell studies were conducted in isolation, we are yet to establish how the integration of these findings on ERK5 in HaCaTs and THP-1s could influence an overall wound healing phenotype in the human context. Further *in vitro* work will be required to examine the direct relationship between keratinocytes and immune cells such as macrophages. For example, it has been previously established that chronically inflamed keratinocytes secrete NF- κ B regulated cytokines such as IL-6 and type 1 IFNs which may further drive the macrophages and wound environment towards inflammation (Wolf, Melvin and Gallagher, 2021). Conversely, how would a pro-reparative keratinocyte profile influence macrophage polarisation and the wider wound healing environment? A more in-depth profile into mediators produced by OS1-treated HaCaTs and how these could affect macrophage behaviour is needed. A workflow could be generated through investigation of cytokine profiles by ELISA and media transfer studies of HaCaT media onto THP-1 cells, and vice versa.

An additional factor to consider is that, although THP-1 cells are a convenient model, there is debate on their biological relevance due to their inability to reproduce a full bone-marrow derived monocyte profile. It may be useful for simple polarisation experiments, but more complex studies in their function and relationship with the microenvironment may be limited. Sourcing human or murine bone-marrow derived monocytes to investigate how ERK5 influences the priming of monocytes and differentiated macrophages at the wound site, could represent more human mimetic future studies into the role of ERK5 in wound healing.

7.4 Therapeutic inactivation of ERK5 with OS1 in *in vivo* models of wound healing promotes a reparative phenotype

Our last aim was a proof-of-principle study to evaluate if OS1 could influence inflammation and promote repair in an *in vivo* wounding model. We anticipated that we would elicit a more reparative immune phenotype in wounds, using OS1, based on the profile we showed in

genetically modified *in vivo* models (Chapter 3) and in *in vitro* human mimetic systems (Chapter 4). Topical treatment with OS1 led to ERK5 loss and increased the wound closure rate. Moreover, we saw a similar pattern to the ERK5KO model (Chapter 3), where degradation of ERK5 enhanced immune cell recruitment and promoted intra-wound conditions that prime a reparative environment at later time points. Notably, at day seven onwards we observed an increase in F4/80 macrophages and expression of Arg1, as well as a lower level of TNF- α gene expression. As previously mentioned, timely transition to M2-like and reparative phenotypes are necessary in healthy wound closure.

What requires further investigation is how ERK5 inactivation drives the recruitment of this reparative macrophage phenotype. For example, studies have found that the exclusive relationship in the CX3CL1-CX3CR1 axis was necessary for reparative macrophage recruitment, leading to improved collagen deposition and expression of repair markers such as TGF β and VEGF (Ishida, Gao and Murphy, 2008; Ishida *et al.*, 2020). Although, our studies show ERK5 degradation increases the gene expression of TGF- β and VEGF in HaCaTs, THP-1 cells and *in vivo* wounds, how this change impacts reparative immune cell infiltration through chemokine signalling remains elusive. It is possible that inactivating ERK5 could have a specific role in driving this chemokine axis and recruit reparative macrophages in wound healing.

Our work provided contradictory information about neutrophil abundance. Our FACS study suggested OS1 mediated ERK5 degradation resulted in persistent neutrophils in the wound environment, whereas histological analysis suggested a brief increase after initial OS1 treatment, followed by almost complete ablation of neutrophil population. Overall, our studies have suggested that ERK5 inactivation would attenuate inflammation. As the histology technique has been more robustly optimised and aligns with the overall pattern of behaviours in terms of improved wound closure in the absence of ERK5, it is likely to be more informative

than the FACS data. Interestingly, some studies suggest that an immunosuppressive low density neutrophil population may exist, with arginase activity which may be actively beneficial to wound repair (Darcy *et al.*, 2014; Scapini *et al.*, 2016). It is therefore possible that the abundant Arg1 histology expression in the wound environment, may coincide with the neutrophil abundance in our Ly6G population by FACS. The inconsistency in neutrophil population will need to be further investigated before elucidating the role of ERK5 in neutrophil function.

What also needs to be conducted in the future, is to assess OS1 mediated ERK5 degradation in chronic diseased contexts of those in diabetic or aged murine models. This could reflect the improved wound healing phenotype we observed in the precursor work in ERK5KO diabetic models, which exhibited improved wound closure and reduced inflammation (Figure 1.8). Additionally, how the timing of ERK5 inactivation effects wound healing remains uncertain. Our study shows that OS1 mediated degradation of ERK5 dosed during the inflammatory phase of wound healing (day 2 post-wounding) results in reduced inflammation and promotes reparative activity in later stages of the wound healing process (day 7 onwards). We are yet to ascertain how OS1 inactivation of ERK5 may influence wound healing: as a pre-treatment, during the earliest stages of inflammation; during granulation and remodelling; or specifically in a chronically inflamed state. These are overlapping but highly diverse microenvironments where ERK5 may play an influential role that can either help or hinder, depending on the context or timing of its signalling. These studies could then confirm whether OS1 and ERK5 inactivation truly has beneficial potential as a treatment option in wound healing.

In our final study, we were unable to develop PET imaging to assess the dynamic behaviour of macrophages in wound healing. By targeting both TSPO and MR markers, we aimed to generate a novel and non-invasive tool to visualise the dynamic behaviour of M1 and M2-like macrophages, and assess this progression in an individual animal throughout the time course

of wound healing. It remains uncertain why this established technique when used in the context of wounds was unable to achieve the efficacy observed in neuroinflammation, stroke and cancer models (Blykers *et al.*, 2015; Henderson *et al.*, 2018; Green *et al.*, 2020). However, one hypothesis to explain this discrepancy is impaired vasculature in the wound site, and the potential hindrance of using a systemic based tracer. Additional studies and improvements could be conducted in the development of PET technology in the context of wound healing. However, there are also a range of emerging imaging modalities such as magnetic resonance imaging (MRI), surface-enhanced Raman spectroscopy and fluorescent dye based *in vivo* imaging which could be utilised to observe the dynamic behaviour of macrophages in wound healing. Some of these technologies are already routinely used as visualisation tools in surgery, and therefore validated and tested in patients. Thus, could be more easily redeveloped for specificity to inflammation and wound healing (Wang and Moore, 2013; Mulder *et al.*, 2014; McArdle, Mikulski and Ley, 2016; MacRitchie *et al.*, 2018).

7.5 Conclusion

Taken together, our studies prove our first hypothesis and show that ERK5 is a signalling pathway that drives inflammation in cutaneous wound healing. This was exemplified from our genetic *in vivo* model, where hyperactivation of ERK5 in the keratinocytes resulted in a pathological inflammatory profile of increased neutrophils and persistent expression of iNOS.

Chronic and dysfunctional wounds often exhibit this persistent and pathological inflammatory profile observed in our CaMEK5 wounds, and therefore it is likely that ERK5 signalling drives dysfunctional wound healing in humans. Work to evaluate ERK5 signalling in patient samples will help prove this hypothesis and support the future use of ERK5 targeted therapies to treat dysfunctional wound healing.

Our second hypothesis, that ERK5 can be therapeutically targeted to attenuate inflammation and promote repair was proved correct. OS1 mediated degradation of ERK5 in our human *in vitro* models of HaCaTs (keratinocytes) and THP-1s (macrophages) resulted in an overall reparative phenotype. These results validate that our findings in the murine context can be translated to human systems. In particular, we found that inactivating ERK5 in THP-1 macrophages promotes the gene expression of key reparative markers: TGF- β , CD206 and VEGF. This primed these macrophages towards a reparative and M2-like phenotype. Moreover, when using OS1 *in vivo* in a complex and multicellular wound environment, we continued to promote this reparative phenotype as indicated by the increase in macrophages, Arg1 expression and reduced expression of IL-1 β and TNF- α .

This thesis provides novel insights into how ERK5 signalling drives macrophage polarisation and immune infiltration in homeostatic wound healing. This will provide the foundation for future studies in macrophage biology and its dysfunction in a diseased context, such as aged and diabetic wounds. Understanding this relationship between ERK5 and wound macrophages, has the potential to improve diagnosis, stratification and treatment for patients of chronic wounds.

ERK5 therapies continues to develop across multiple pathologies, and this study provides further evidence of the need to deviate from kinase inhibitors due to their inability to recapitulate genetic ablation studies. Using OS1 to degrade the whole ERK5 protein more accurately parallels observations in the ERK5KO systems and its ability to influence inflammation. Moreover, we have shown early indications that topical application is the likely path forward for OS1 treatment in cutaneous wound healing.

7.6 Future Studies

As discussed, this thesis has highlighted a novel relationship between ERK5 signalling and wound macrophage functions and explored its role in human *in vitro* systems and murine *in vivo* wounds. In particular, how therapeutic targeting of ERK5 can improve repair mechanism in homeostatic wounds. However, we are yet to elucidate: how these findings translate to human patients; how effective OS1 is in dysfunctional murine models (e.g. diabetes); and how to dynamically interrogate this behaviour via appropriate molecular imaging techniques to track macrophage biology and response to ERK5 targeted therapies. Below are potential future studies, which could facilitate answering these outstanding questions.

7.6.1 Human ex-vivo

There is an on-going collaboration with the NHS Biobank to collect patient wound samples and process them by RT-qPCR, Mass Cytometry and histology to assess their ERK5 wound healing signature. This would help validate whether i) ERK5 pathway markers are upregulated in chronic wounds from non-diabetic and diabetic patients and therefore highlight the potential to utilise ERK5 as a biomarker to identify chronic wound patients and ii) if there is high ERK5 in wounds, this would provide the rationale for employing ERK5 specific therapy in this context.

We have already commenced work in this area in collaboration with wound healing experts at Manchester University NHS Foundation Trust. Our initial collection criteria includes five diabetic and five non-diabetic chronic wound samples, collected from a wide range of patients to make an initial assessment of the ERK5 wound healing signature in the human patient context.

Using our existing panel from *in vitro* and *in vivo* workflow, we will assess various ERK5, immune and repair mediated markers in these human chronic wound samples to generate a

human ERK5 wound healing signature. Focussing on aspects of macrophage, ERK5 and healing markers.

7.6.2 Diabetic model

The introduction and development of the *in vivo* model of diabetic wound healing with *Lep^r^{db/db}* mice, and assessing the changes with OS1 treatment would parallel the precursor work using ERK5KO in diabetic models. Moreover, this could be compared with the CaMEK5 model to test the efficacy of OS1, as a potential patient model of persistent inflammation.

As previously mentioned, chronic inflammation is an established driving force of dysregulation in diabetes and impaired macrophages. Introducing the mice strain that is homozygous for *Lep^r^{db/db}* replicates type 2 diabetes, where these mice are recognisably obese after 3 to 4 weeks. This genetic mutation of the leptin receptor affects hunger and energy use, and the subsequent phenotype of markedly elevated levels of plasma insulin and blood sugar. These mice have delayed wound healing and are regularly utilised as a model for chronic wound healing, that is comparable to dysfunction in human diabetic wounds.

It would be insightful to assess how effective OS1 mediated degradation of ERK5 is in influencing the immune and repair profile of the wounds of these diabetic mice, and compare it to control and wild-type wounds. The precursor work found that the improved wound healing phenotype observed in ERK5KO models was most significant in the diabetic model. It is therefore likely that OS1 may have more impact in the diabetic context compared to the phenotype observed in the healthy wounds. Furthermore, there is the potential to generate diabetic-CaMEK5 murine models to profile a hyperactivated ERK5 diabetic wound, which could theoretically be more persistent and highly inflammatory, i.e. more representative of the patient population most likely to need therapy for dysfunctional wound healing. Therefore is an ideal model to assess the efficacy of OS1 therapy.

7.6.3 Imaging

It has been well established that inflammation and immune cells are key factors contributing to various disorders such as cardiovascular disease, rheumatoid arthritis, diabetes and cancer. Moreover, we have an arsenal of novel therapeutics that can target and dampen the excessive and chronic inflammation associated with these disorders. However, we are yet to establish nuanced differences in stratifying patients where some of these therapeutics may not be viable. In order to achieve this, one potential avenue is our improving molecular imaging tools to direct earlier clinical diagnosis.

As technology develops, we have greater access to a range of cutting-edge science which enables us to dynamically and non-invasively assess the behaviour and location of immune cells at a cellular and molecular level. This will both widen our understanding of biology, and can reduce our usage of animals in research.

PET imaging is an established and clinically translated technology with high sensitivity and is non-invasive. However, its major limitations are the use of radioactive tracers and inability to multiplex. In recent decades, there has been advances in the range of pre-clinical targets developed for PET imaging, but its translation has been slow. The standard of ^{18}F -FDG still accounts for almost 95% of clinical PET scans (Goel *et al.*, 2017).

The field of intravital imaging is an expansive field that enables us to visualise, detect and quantify cellular and molecular immune processes. Currently established techniques in molecular imaging are CT, MRI, ultrasound, fluorescent dyes and the previously described PET (MacRitchie *et al.*, 2020). CT is one of the most widely used imaging techniques that enables 3D anatomical imaging in fast scan times. However, it is often limited to skeletal structures due to its low sensitivity and inability to distinguish with soft tissue. MRI is another widely used tool for anatomical and functional imaging. It can be further utilised for molecular

imaging with the addition of contrast agents. This enables the molecular imaging of soft tissue with a range of sensitivity of 10 μ m to 10mm. Contrast enhanced ultrasound is another developing field which is primarily used for non-invasive imaging of abdominal, breast and musculoskeletal examination. Fluorescent dyes are regularly implemented to guide surgeries and provide real-time visualisation of the operation. These tools all have the potential to be modified to be specific for immune cells such as macrophages and give preliminary insight into a patient's inflammatory and dysfunctional wounding profile and stratify who might respond best to ERK5 targeted therapy.

One of the major challenges for intravital molecular imaging is doing so with minimal tissue damage and enabling deeper tissue analysis. An ideal imaging modality would be one with high sensitivity, spatial resolution, rapid scanning, at depth, quantifiable, reproducible, low economic burden and the ability to multiplex. It may be difficult to attain all in one technique, so utilising hybrid imaging or in conjunction with other techniques such as flow cytometry and transcriptomics may be necessary to fully elucidate dynamic behaviour of immune cells and inflammation.

Chapter 8: References

- Adams, R. L. C. and Bird, R. J. (2009) 'Review article: Coagulation cascade and therapeutics update: Relevance to nephrology. Part 1: Overview of coagulation, thrombophilias and history of anticoagulants', *Nephrology*. doi: 10.1111/j.1440-1797.2009.01128.x.
- Ali, M. *et al.* (2017) 'Essential Role of IL-12 in Angiogenesis in Type 2 Diabetes', *American Journal of Pathology*. doi: 10.1016/j.ajpath.2017.07.021.
- Arlauckas, S. P. *et al.* (2017) 'In vivo imaging reveals a tumor-associated macrophage-mediated resistance pathway in anti-PD-1 therapy', *Science Translational Medicine*. doi: 10.1126/scitranslmed.aal3604.
- Arnoux, V. *et al.* (2008) 'Erk5 controls slug expression and keratinocyte activation during wound healing', *Molecular Biology of the Cell*. doi: 10.1091/mbc.E07-10-1078.
- Ashcroft, G. S. *et al.* (1999) 'Mice lacking Smad3 show accelerated wound healing and an impaired local inflammatory response', *Nature Cell Biology*. doi: 10.1038/12971.
- Ayala, T. S. *et al.* (2019) 'High Glucose Environments Interfere with Bone Marrow-Derived Macrophage Inflammatory Mediator Release, the TLR4 Pathway and Glucose Metabolism', *Scientific Reports*. doi: 10.1038/s41598-019-47836-8.
- Bannon, P. *et al.* (2013) 'Diabetes induces stable intrinsic changes to myeloid cells that contribute to chronic inflammation during wound healing in mice', *DMM Disease Models and Mechanisms*. doi: 10.1242/dmm.012237.
- Bauer, S. M., Bauer, R. J. and Velazquez, O. C. (2005) 'Angiogenesis, vasculogenesis, and induction of healing in chronic wounds', *Vascular and Endovascular Surgery*. doi: 10.1177/153857440503900401.
- Baxter, E. W. *et al.* (2020) 'Standardized protocols for differentiation of THP-1 cells to macrophages with distinct M(IFN γ +LPS), M(IL-4) and M(IL-10) phenotypes', *Journal of Immunological Methods*. doi: 10.1016/j.jim.2019.112721.
- Benson, H. A. E. *et al.* (2019) 'Topical and Transdermal Drug Delivery: From Simple Potions to Smart Technologies', *Current Drug Delivery*. doi: 10.2174/1567201816666190201143457.
- Bertani, F. R. *et al.* (2017) 'Classification of M1/M2-polarized human macrophages by label-free hyperspectral reflectance confocal microscopy and multivariate analysis', *Scientific Reports*. doi: 10.1038/s41598-017-08121-8.
- Bhatt, A. B., Wright, T. D., *et al.* (2021) 'Diverse and converging roles of ERK1/2 and ERK5 pathways on mesenchymal to epithelial transition in breast cancer', *Translational Oncology*. doi: 10.1016/j.tranon.2021.101046.
- Bhatt, A. B., Patel, S., *et al.* (2021) 'Molecular mechanisms of epithelial to mesenchymal transition regulated by ERK5 signaling', *Biomolecules*. doi: 10.3390/biom11020183.
- Bio-Rad Laboratories Inc. (2015) 'F4-80-Antibody-Mini-Review', *Bio-Rad Laboratories, Inc.*
- Blykers, A. *et al.* (2015) 'PET imaging of macrophage mannose receptor-expressing macrophages in tumor stroma using 18F-radiolabeled camelid single-domain antibody fragments', *Journal of Nuclear Medicine*. doi: 10.2967/jnumed.115.156828.
- Van den Bossche, J. *et al.* (2016) 'Mitochondrial Dysfunction Prevents Repolarization of Inflammatory Macrophages', *Cell Reports*. doi: 10.1016/j.celrep.2016.09.008.
- Boutin, H. and Pinborg, L. H. (2015) 'TSPO imaging in stroke: from animal models to human subjects', *Clinical and Translational Imaging*. doi: 10.1007/s40336-015-0146-7.

- Brancato, S. K. and Albina, J. E. (2011) 'Wound macrophages as key regulators of repair: Origin, phenotype, and function', *American Journal of Pathology*. doi: 10.1016/j.ajpath.2010.08.003.
- Bulaklak, K. and Gersbach, C. A. (2020) 'The once and future gene therapy', *Nature Communications*. doi: 10.1038/s41467-020-19505-2.
- Cai, X. J., Mesquida, P. and Jones, S. A. (2016) 'Investigating the ability of nanoparticle-loaded hydroxypropyl methylcellulose and xanthan gum gels to enhance drug penetration into the skin', *International Journal of Pharmaceutics*. doi: 10.1016/j.ijpharm.2016.08.055.
- Caley, M. P., Martins, V. L. C. and O'Toole, E. A. (2015) 'Metalloproteinases and Wound Healing', *Advances in Wound Care*. doi: 10.1089/wound.2014.0581.
- Campbell, L. *et al.* (2013) 'Local arginase 1 activity is required for cutaneous wound healing', *Journal of Investigative Dermatology*. doi: 10.1038/jid.2013.164.
- Chan, R. K. *et al.* (2006) 'Effect of recombinant platelet-derived growth factor (Regranex®) on wound closure in genetically diabetic mice', *Journal of Burn Care and Research*. doi: 10.1097/01.BCR.0000202898.11277.58.
- Colotta, F. *et al.* (2009) 'Cancer-related inflammation, the seventh hallmark of cancer: Links to genetic instability', *Carcinogenesis*. doi: 10.1093/carcin/bgp127.
- Craig, J. E. *et al.* (2020) 'MEKK3-MEK5-ERK5 signaling promotes mitochondrial degradation', *Cell Death Discovery*. doi: 10.1038/s41420-020-00342-7.
- Cullen, B. *et al.* (2002) 'Mechanism of action of PROMOGRAN, a protease modulating matrix, for the treatment of diabetic foot ulcers', *Wound Repair and Regeneration*. doi: 10.1046/j.1524-475X.2002.10703.x.
- Daley, J. M. *et al.* (2010) 'The phenotype of murine wound macrophages', *Journal of Leukocyte Biology*. doi: 10.1189/jlb.0409236.
- Darby, I. A. *et al.* (2014) 'Fibroblasts and myofibroblasts in wound healing', *Clinical, Cosmetic and Investigational Dermatology*. doi: 10.2147/CCID.S50046.
- Darcy, C. J. *et al.* (2014) 'Neutrophils with myeloid derived suppressor function deplete arginine and constrain T cell function in septic shock patients', *Critical Care*. doi: 10.1186/cc14003.
- Delavary, B. M. *et al.* (2011) 'Macrophages in skin injury and repair', *Immunobiology*. doi: 10.1016/j.imbio.2011.01.001.
- Ding, J. *et al.* (2019) 'Macrophages are necessary for skin regeneration during tissue expansion', *Journal of Translational Medicine*. doi: 10.1186/s12967-019-1780-z.
- Drew, B. A., Burow, M. E. and Beckman, B. S. (2012) 'MEK5/ERK5 pathway: The first fifteen years', *Biochimica et Biophysica Acta - Reviews on Cancer*. doi: 10.1016/j.bbcan.2011.10.002.
- Ellis, S., Lin, E. J. and Tartar, D. (2018) 'Immunology of Wound Healing', *Current Dermatology Reports*. doi: 10.1007/s13671-018-0234-9.
- Eming, S. A., Krieg, T. and Davidson, J. M. (2007) 'Inflammation in wound repair: Molecular and cellular mechanisms', *Journal of Investigative Dermatology*. doi: 10.1038/sj.jid.5700701.
- Eming, S. A., Martin, P. and Tomic-Canic, M. (2014) 'Wound repair and regeneration: Mechanisms, signaling, and translation', *Science Translational Medicine*. doi: 10.1126/scitranslmed.3009337.
- Eming, S. A., Wynn, T. A. and Martin, P. (2017) 'Inflammation and metabolism in tissue repair and regeneration', *Science*. doi: 10.1126/science.aam7928.
- Fang, R. C. and Galiano, R. D. (2008) 'A review of becaplermin gel in the treatment of diabetic neuropathic foot ulcers', *Biologics: Targets and Therapy*. doi: 10.2147/btt.s1338.

- Fang, Y. *et al.* (2007) 'Impaired cutaneous wound healing in granulocyte/macrophage colony-stimulating factor knockout mice', *British Journal of Dermatology*. doi: 10.1111/j.1365-2133.2007.07979.x.
- Feng, Y. *et al.* (2019) 'Direct and indirect roles of macrophages in hypertrophic scar formation', *Frontiers in Physiology*. doi: 10.3389/fphys.2019.01101.
- Finegan, K. G. *et al.* (2015) 'ERK5 is a critical mediator of inflammation-driven cancer', *Cancer Research*, 75(4). doi: 10.1158/0008-5472.CAN-13-3043.
- Gabrilovich, D. I. (2017) 'Myeloid-derived suppressor cells', *Cancer Immunology Research*. doi: 10.1158/2326-6066.CIR-16-0297.
- Gantzel, R. H. *et al.* (2021) 'Macrophage Activation Markers, Soluble CD163 and Mannose Receptor, in Liver Fibrosis', *Frontiers in Medicine*. doi: 10.3389/fmed.2020.615599.
- Genin, M. *et al.* (2015) 'M1 and M2 macrophages derived from THP-1 cells differentially modulate the response of cancer cells to etoposide', *BMC Cancer*. doi: 10.1186/s12885-015-1546-9.
- Gilbert, A. S. *et al.* (2017) 'Vomocytosis of live pathogens from macrophages is regulated by the atypical MAP kinase ERK5', *Science Advances*. doi: 10.1126/sciadv.1700898.
- Ginhoux, F. *et al.* (2016) 'New insights into the multidimensional concept of macrophage ontogeny, activation and function', *Nature Immunology*. doi: 10.1038/ni.3324.
- Giurisato, E. *et al.* (2018) 'Myeloid ERK5 deficiency suppresses tumor growth by blocking protumor macrophage polarization via STAT3 inhibition', *Proceedings of the National Academy of Sciences of the United States of America*. doi: 10.1073/pnas.1707929115.
- Giurisato, E., Vermi, W. and Tournier, C. (2016) 'ERK5 is required for pro-tumour macrophage activation', *European Journal of Cancer*. doi: 10.1016/s0959-8049(16)61371-0.
- Goel, S. *et al.* (2017) 'Positron emission tomography and nanotechnology: A dynamic duo for cancer theranostics', *Advanced Drug Delivery Reviews*. doi: 10.1016/j.addr.2016.08.001.
- Gordon, S. (2003) 'Alternative activation of macrophages', *Nature Reviews Immunology*. doi: 10.1038/nri978.
- Gordon, S., Plüddemann, A. and Martinez Estrada, F. (2014) 'Macrophage heterogeneity in tissues: Phenotypic diversity and functions', *Immunological Reviews*. doi: 10.1111/imr.12223.
- Goren, I. *et al.* (2009) 'A transgenic mouse model of inducible macrophage depletion: Effects of diphtheria toxin-driven lysozyme m-specific cell lineage ablation on wound inflammatory, angiogenic, and contractive processes', *American Journal of Pathology*. doi: 10.2353/ajpath.2009.081002.
- Green, D. *et al.* (2020) 'Targeting the MAPK7/MMP9 axis for metastasis in primary bone cancer', *Oncogene*. doi: 10.1038/s41388-020-1379-0.
- Guo, Y. *et al.* (2020) 'ERK/MAPK signalling pathway and tumorigenesis (Review)', *Experimental and Therapeutic Medicine*. doi: 10.3892/etm.2020.8454.
- Gurevich, D. B. *et al.* (2018) 'Live imaging of wound angiogenesis reveals macrophage orchestrated vessel sprouting and regression', *The EMBO Journal*. doi: 10.15252/embj.201797786.
- Gurtner, G. C. *et al.* (2008) 'Wound repair and regeneration', *Nature*. doi: 10.1038/nature07039.
- Han, G. and Ceilley, R. (2017) 'Chronic Wound Healing: A Review of Current Management and Treatments', *Advances in Therapy*. doi: 10.1007/s12325-017-0478-y.
- Hanahan, D. and Weinberg, R. A. (2011) 'Hallmarks of cancer: The next generation', *Cell*. doi: 10.1016/j.cell.2011.02.013.

- Hanania, R. *et al.* (2012) 'Classically activated macrophages use stable microtubules for matrix metalloproteinase-9 (MMP-9) secretion', *Journal of Biological Chemistry*. doi: 10.1074/jbc.M111.290676.
- Hatori, A. *et al.* (2015) 'Utility of translocator protein (18 kDa) as a molecular imaging biomarker to monitor the progression of liver fibrosis', *Scientific Reports*. doi: 10.1038/srep17327.
- Hayashi, M. *et al.* (2004) 'Targeted deletion of BMK1/ERK5 in adult mice perturbs vascular integrity and leads to endothelial failure', *Journal of Clinical Investigation*. doi: 10.1172/JCI200419890.
- Hayashi, M. and Lee, J. D. (2004) 'Role of the BMK1/ERK5 signaling pathway: Lessons from knockout mice', *Journal of Molecular Medicine*. doi: 10.1007/s00109-004-0602-8.
- Henderson, F. *et al.* (2018) 'Multi-modal imaging of long-term recovery post-stroke by positron emission tomography and matrix-assisted laser desorption/ionisation mass spectrometry', *Rapid Communications in Mass Spectrometry*. doi: 10.1002/rcm.8090.
- Heo, K. S. *et al.* (2014) 'ERK5 activation in macrophages promotes efferocytosis and inhibits atherosclerosis', *Circulation*. doi: 10.1161/CIRCULATIONAHA.113.005991.
- Hesketh, M. *et al.* (2017) 'Macrophage phenotypes regulate scar formation and chronic wound healing', *International Journal of Molecular Sciences*. doi: 10.3390/ijms18071545.
- Hoang, V. T. *et al.* (2020) 'ERK5 Is Required for Tumor Growth and Maintenance Through Regulation of the Extracellular Matrix in Triple Negative Breast Cancer', *Frontiers in Oncology*. doi: 10.3389/fonc.2020.01164.
- Huang, Y. *et al.* (2017) 'Mitogen-activated protein kinase 7 promotes cell proliferation, migration and invasion in SOSP-M human osteosarcoma cell line', *Tumori*. doi: 10.5301/tj.5000399.
- Ishida, Y. *et al.* (2020) 'Pivotal Involvement of the CX3CL1-CX3CR1 Axis for the Recruitment of M2 Tumor-Associated Macrophages in Skin Carcinogenesis', *Journal of Investigative Dermatology*. doi: 10.1016/j.jid.2020.02.023.
- Ishida, Y., Gao, J.-L. and Murphy, P. M. (2008) 'Chemokine Receptor CX3CR1 Mediates Skin Wound Healing by Promoting Macrophage and Fibroblast Accumulation and Function', *The Journal of Immunology*. doi: 10.4049/jimmunol.180.1.569.
- Ivashkiv, L. B. (2013) 'Epigenetic regulation of macrophage polarization and function', *Trends in Immunology*. doi: 10.1016/j.it.2012.11.001.
- Jablonski, K. A. *et al.* (2015) 'Novel markers to delineate murine M1 and M2 macrophages', *PLoS ONE*. doi: 10.1371/journal.pone.0145342.
- Järbrink, K. *et al.* (2016) 'Prevalence and incidence of chronic wounds and related complications: A protocol for a systematic review', *Systematic Reviews*. doi: 10.1186/s13643-016-0329-y.
- Ji, S. *et al.* (2021) 'Functional hair follicle regeneration: an updated review', *Signal Transduction and Targeted Therapy*. doi: 10.1038/s41392-020-00441-y.
- Kato, Y. *et al.* (1998) 'Bmk1/Erk5 is required for cell proliferation induced by epidermal growth factor', *Nature*. doi: 10.1038/27234.
- Khanna, S. *et al.* (2010) 'Macrophage dysfunction impairs resolution of inflammation in the wounds of diabetic mice', *PLoS ONE*. doi: 10.1371/journal.pone.0009539.
- Kim, M. H. *et al.* (2008) 'Dynamics of neutrophil infiltration during cutaneous wound healing and infection using fluorescence imaging', *Journal of Investigative Dermatology*. doi: 10.1038/sj.jid.5701223.
- Kleinert, H., Schwarz, P. M. and Förstermann, U. (2003) 'Regulation of the expression of inducible

- nitric oxide synthase', *Biological Chemistry*. doi: 10.1515/BC.2003.152.
- Koh, T. J. and DiPietro, L. A. (2011) 'Inflammation and wound healing: the role of the macrophage.', *Expert reviews in molecular medicine*. doi: 10.1017/S1462399411001943.
- Komaravolu, R. K. *et al.* (2015) 'Erk5 inhibits endothelial migration via KLF2-dependent down-regulation of PAK1', *Cardiovascular Research*. doi: 10.1093/cvr/cvu236.
- Koo, J. H. *et al.* (2019) 'Myeloid cell-specific sirtuin 6 deficiency delays wound healing in mice by modulating inflammation and macrophage phenotypes', *Experimental and Molecular Medicine*. doi: 10.1038/s12276-019-0248-9.
- Kovtun, A. *et al.* (2018) 'Neutrophils in tissue trauma of the skin, bone, and lung: Two sides of the same coin', *Journal of Immunology Research*. doi: 10.1155/2018/8173983.
- Krzyszczczyk, P. *et al.* (2018) 'The role of macrophages in acute and chronic wound healing and interventions to promote pro-wound healing phenotypes', *Frontiers in Physiology*. doi: 10.3389/fphys.2018.00419.
- Kubota, K. *et al.* (2017) 'CD163+CD204+ tumor-associated macrophages contribute to T cell regulation via interleukin-10 and PD-L1 production in oral squamous cell carcinoma', *Scientific Reports*. doi: 10.1038/s41598-017-01661-z.
- Lanfranca, M. P. *et al.* (2018) 'Tracking macrophage infiltration in a mouse model of pancreatic cancer with the positron emission tomography tracer [11C]PBR28', *Journal of Surgical Research*. doi: 10.1016/j.jss.2018.07.015.
- Lavin, Y. *et al.* (2014) 'Tissue-resident macrophage enhancer landscapes are shaped by the local microenvironment', *Cell*. doi: 10.1016/j.cell.2014.11.018.
- Lepidi, S. *et al.* (2001) 'MMP9 production by human monocyte-derived macrophages is decreased on polymerized type I collagen', *Journal of Vascular Surgery*. doi: 10.1067/mva.2001.119401.
- Li, L. *et al.* (2013) 'Collective cell migration: Implications for wound healing and cancer invasion', *Burns and Trauma*. doi: 10.4103/2321-3868.113331.
- Lin, E. C. K. *et al.* (2016) 'ERK5 kinase activity is dispensable for cellular immune response and proliferation', *Proceedings of the National Academy of Sciences of the United States of America*. doi: 10.1073/pnas.1609019113.
- Lindley, L. E. *et al.* (2016) 'Biology and biomarkers for wound healing', *Plastic and Reconstructive Surgery*. doi: 10.1097/PRS.0000000000002682.
- Lochhead, P. A. *et al.* (2020) 'Paradoxical activation of the protein kinase-transcription factor ERK5 by ERK5 kinase inhibitors', *Nature Communications*. doi: 10.1038/s41467-020-15031-3.
- Loh, C. Y. *et al.* (2019) 'The E-Cadherin and N-Cadherin Switch in Epithelial-to-Mesenchymal Transition: Signaling, Therapeutic Implications, and Challenges', *Cells*. doi: 10.3390/cells8101118.
- Louiselle, A. E. *et al.* (2021) 'Macrophage polarization and diabetic wound healing', *Translational Research*. doi: 10.1016/j.trsl.2021.05.006.
- Lucas, T. *et al.* (2010) 'Differential Roles of Macrophages in Diverse Phases of Skin Repair', *The Journal of Immunology*. doi: 10.4049/jimmunol.0903356.
- Luiz, J. P. M. *et al.* (2020) 'MEK5/ERK5 signaling mediates IL-4-induced M2 macrophage differentiation through regulation of c-Myc expression', *Journal of Leukocyte Biology*. doi: 10.1002/JLB.1MA0520-016R.
- Luo, J. D. and Chen, A. F. (2005) 'Nitric oxide: A newly discovered function on wound healing', *Acta Pharmacologica Sinica*. doi: 10.1111/j.1745-7254.2005.00058.x.

- Mace, K. A. *et al.* (2009) 'HOXA3 modulates injury-induced mobilization and recruitment of bone marrow-derived cells', *Stem Cells*. doi: 10.1002/stem.90.
- MacRitchie, N. *et al.* (2018) 'Molecular imaging of atherosclerosis: Spotlight on Raman spectroscopy and surface-enhanced Raman scattering', *Heart*. doi: 10.1136/heartjnl-2017-311447.
- MacRitchie, N. *et al.* (2020) 'Molecular imaging of inflammation - Current and emerging technologies for diagnosis and treatment', *Pharmacology and Therapeutics*. doi: 10.1016/j.pharmthera.2020.107550.
- Marques da Costa, R. *et al.* (1999) 'Randomized, double-blind, placebo-controlled, dose-ranging study of granulocyte-macrophage colony stimulating factor in patients with chronic venous leg ulcers', *Wound Repair and Regeneration*. doi: 10.1046/j.1524-475X.1999.00017.x.
- Martin, C. W. and Muir, I. F. K. (1990) 'The role of lymphocytes in wound healing', *British Journal of Plastic Surgery*. doi: 10.1016/0007-1226(90)90185-3.
- Martinengo, L. *et al.* (2019) 'Prevalence of chronic wounds in the general population: systematic review and meta-analysis of observational studies', *Annals of Epidemiology*. doi: 10.1016/j.annepidem.2018.10.005.
- Martinez-Pomares, L. (2012) 'The mannose receptor', *Journal of Leukocyte Biology*. doi: 10.1189/jlb.0512231.
- Martinez, F. O. *et al.* (2006) 'Transcriptional Profiling of the Human Monocyte-to-Macrophage Differentiation and Polarization: New Molecules and Patterns of Gene Expression', *The Journal of Immunology*. doi: 10.4049/jimmunol.177.10.7303.
- Martinez, F. O. and Gordon, S. (2014) 'The M1 and M2 paradigm of macrophage activation: Time for reassessment', *F1000Prime Reports*. doi: 10.12703/P6-13.
- McArdle, S., Mikulski, Z. and Ley, K. (2016) 'Live cell imaging to understand monocyte, macrophage, and dendritic cell function in atherosclerosis', *Journal of Experimental Medicine*. doi: 10.1084/jem.20151885.
- Mescher, A. L. (2017) 'Macrophages and fibroblasts during inflammation and tissue repair in models of organ regeneration', *Regeneration*. doi: 10.1002/reg2.77.
- Meszaros, A. J., Reichner, J. S. and Albina, J. E. (2000) 'Macrophage-Induced Neutrophil Apoptosis', *The Journal of Immunology*. doi: 10.4049/jimmunol.165.1.435.
- Minutti, C. M. *et al.* (2017) 'Tissue-specific contribution of macrophages to wound healing', *Seminars in Cell and Developmental Biology*. doi: 10.1016/j.semcdb.2016.08.006.
- Mirza, R., DiPietro, L. A. and Koh, T. J. (2009) 'Selective and specific macrophage ablation is detrimental to wound healing in mice', *American Journal of Pathology*. doi: 10.2353/ajpath.2009.090248.
- Mirza, R. E. *et al.* (2014) 'Sustained inflammasome activity in macrophages impairs wound healing in type 2 diabetic humans and mice', *Diabetes*. doi: 10.2337/db13-0927.
- Mirza, R. and Koh, T. J. (2011) 'Dysregulation of monocyte/macrophage phenotype in wounds of diabetic mice', *Cytokine*. doi: 10.1016/j.cyto.2011.06.016.
- Mosser, D. M. and Edwards, J. P. (2008) 'Exploring the full spectrum of macrophage activation', *Nature Reviews Immunology*. doi: 10.1038/nri2448.
- Mowbray, M. *et al.* (2008) 'Topically applied nitric oxide induces T-lymphocyte infiltration in human skin, but minimal inflammation', *Journal of Investigative Dermatology*. doi: 10.1038/sj.jid.5701096.
- Mulder, W. J. M. *et al.* (2014) 'Imaging and nanomedicine in inflammatory atherosclerosis', *Science*

Translational Medicine. doi: 10.1126/scitranslmed.3005101.

Murray, P. J. *et al.* (2014) 'Macrophage Activation and Polarization: Nomenclature and Experimental Guidelines', *Immunity*. doi: 10.1016/j.immuni.2014.06.008.

Narayan, N. *et al.* (2017) 'The macrophage marker translocator protein (TSPO) is down-regulated on pro-inflammatory "M1" human macrophages', *PLoS ONE*. doi: 10.1371/journal.pone.0185767.

Nielsen, S. R. and Schmid, M. C. (2017) 'Macrophages as Key Drivers of Cancer Progression and Metastasis', *Mediators of Inflammation*. doi: 10.1155/2017/9624760.

Nithianandarajah-Jones, G. N. *et al.* (2012) 'ERK5: Structure, regulation and function', *Cellular Signalling*. doi: 10.1016/j.cellsig.2012.07.007.

Novak, M. L. and Koh, T. J. (2013) 'Phenotypic transitions of macrophages orchestrate tissue repair', *American Journal of Pathology*. doi: 10.1016/j.ajpath.2013.06.034.

Okonkwo, U. A. and Dipietro, L. A. (2017) 'Diabetes and wound angiogenesis', *International Journal of Molecular Sciences*. doi: 10.3390/ijms18071419.

Orecchioni, M. *et al.* (2019) 'Macrophage polarization: Different gene signatures in M1(Lps+) vs. Classically and M2(LPS-) vs. Alternatively activated macrophages', *Frontiers in Immunology*. doi: 10.3389/fimmu.2019.01084.

Ou, L. *et al.* (2015) 'Kruppel-like factor KLF4 facilitates cutaneous wound healing by promoting fibrocyte generation from myeloid-derived suppressor cells', *Journal of Investigative Dermatology*. doi: 10.1038/jid.2015.3.

Oyarce, C. *et al.* (2021) 'Re-polarization of immunosuppressive macrophages to tumor-cytotoxic macrophages by repurposed metabolic drugs', *OncoImmunology*. doi: 10.1080/2162402X.2021.1898753.

Pearson, A. J. *et al.* (2020) 'Discovery of a gatekeeper residue in the C-terminal tail of the extracellular signal-regulated protein kinase 5 (ERK5)', *International Journal of Molecular Sciences*. doi: 10.3390/ijms21030929.

Penn, J. W., Grobbelaar, A. O. and Rolfe, K. J. (2012) 'The role of the TGF- β family in wound healing, burns and scarring: a review.', *International journal of burns and trauma*.

Perez-Madrigal, D. *et al.* (2012) 'The extracellular-regulated protein kinase 5 (ERK5) promotes cell proliferation through the down-regulation of inhibitors of cyclin dependent protein kinases (CDKs)', *Cellular Signalling*. doi: 10.1016/j.cellsig.2012.08.001.

Pergola, C. *et al.* (2017) 'Modulation of actin dynamics as potential macrophage subtype-targeting anti-tumour strategy', *Scientific Reports*. doi: 10.1038/srep41434.

Potente, M., Gerhardt, H. and Carmeliet, P. (2011) 'Basic and therapeutic aspects of angiogenesis', *Cell*. doi: 10.1016/j.cell.2011.08.039.

Reinke, J. M. and Sorg, H. (2012) 'Fax +41 61 306 12 34 E-Mail karger@karger.ch Review Articles, Systematic Reviews and Meta-Analyses Wound Repair and Regeneration', *Eur Surg Res*, 49, pp. 35–43. doi: 10.1159/000339613.

Reiss, M. J. *et al.* (2010) 'Matrix metalloproteinase-9 delays wound healing in a murine wound model', *Surgery*. doi: 10.1016/j.surg.2009.10.016.

Richter, E. *et al.* (2016) 'Induction of macrophage function in human THP-1 cells is associated with rewiring of MAPK signaling and activation of MAP3K7 (TAK1) protein kinase', *Frontiers in Cell and Developmental Biology*. doi: 10.3389/fcell.2016.00021.

Ridiandries, A., Tan, J. T. M. and Bursill, C. A. (2018) 'The role of chemokines in wound healing',

International Journal of Molecular Sciences. doi: 10.3390/ijms19103217.

Rios de la Rosa, J. M. *et al.* (2017) 'The CD44-Mediated Uptake of Hyaluronic Acid-Based Carriers in Macrophages', *Advanced Healthcare Materials*. doi: 10.1002/adhm.201601012.

Roszer, T. (2015) 'Understanding the mysterious M2 macrophage through activation markers and effector mechanisms', *Mediators of Inflammation*. doi: 10.1155/2015/816460.

Rovida, E. *et al.* (2008) 'ERK5/BMK1 Is Indispensable for Optimal Colony-Stimulating Factor 1 (CSF-1)-Induced Proliferation in Macrophages in a Src-Dependent Fashion', *The Journal of Immunology*. doi: 10.4049/jimmunol.180.6.4166.

Rovida, E. *et al.* (2015) 'The mitogen-activated protein kinase ERK5 regulates the development and growth of hepatocellular carcinoma', *Gut*. doi: 10.1136/gutjnl-2014-306761.

Rua, R. and McGavern, D. B. (2015) 'Elucidation of monocyte/macrophage dynamics and function by intravital imaging', *Journal of Leukocyte Biology*. doi: 10.1189/jlb.4ri0115-006rr.

Saini, V. (2010) 'Molecular mechanisms of insulin resistance in type 2 diabetes mellitus', *World Journal of Diabetes*. doi: 10.4239/wjd.v1.i3.68.

Scapini, P. *et al.* (2016) 'Human neutrophils in the saga of cellular heterogeneity: insights and open questions', *Immunological Reviews*. doi: 10.1111/imr.12448.

Sen, C. K. *et al.* (2009) 'Human skin wounds: A major and snowballing threat to public health and the economy: PERSPECTIVE ARTICLE', *Wound Repair and Regeneration*. doi: 10.1111/j.1524-475X.2009.00543.x.

Shi, C. and Pamer, E. G. (2011) 'Monocyte recruitment during infection and inflammation', *Nature Reviews Immunology*. doi: 10.1038/nri3070.

Shukla, A. *et al.* (2013) 'Extracellular signal-regulated kinase 5: A potential therapeutic target for malignant mesotheliomas', *Clinical Cancer Research*. doi: 10.1158/1078-0432.CCR-12-3202.

Sieber-Blum, M. (2011) 'Epidermal stem cell dynamics', *Stem Cell Research and Therapy*. doi: 10.1186/scrt70.

Simões, A. *et al.* (2015) 'Aberrant MEK5/ERK5 signalling coSimões, A. *et al.* (2015) "Aberrant MEK5/ERK5 signalling contributes to human colon cancer progression via NF-κB activation", *Cell Death and Disease*. doi: 10.1038/cddis.2015.83.tributes to human colon cancer progression via', *Cell Death and Disease*. doi: 10.1038/cddis.2015.83.

Sirsjö, A. *et al.* (1996) 'Increased expression of inducible nitric oxide synthase in psoriatic skin and cytokine-stimulated cultured keratinocytes', *British Journal of Dermatology*. doi: 10.1111/j.1365-2133.1996.tb06963.x.

Smith, T. D. *et al.* (2017) 'Harnessing macrophage plasticity for tissue regeneration', *Advanced Drug Delivery Reviews*. doi: 10.1016/j.addr.2017.04.012.

Snyder, R. J. *et al.* (2016) 'Macrophages: A review of their role in wound healing and their therapeutic use', *Wound Repair and Regeneration*. doi: 10.1111/wrr.12444.

Spiering, D. *et al.* (2009) 'MEK5/ERK5 signaling modulates endothelial cell migration and focal contact turnover', *Journal of Biological Chemistry*. doi: 10.1074/jbc.M109.042911.

Stackowicz, J., Jönsson, F. and Reber, L. L. (2020) 'Mouse Models and Tools for the in vivo Study of Neutrophils', *Frontiers in Immunology*. doi: 10.3389/fimmu.2019.03130.

Starr, T. *et al.* (2018) 'The phorbol 12-myristate-13-acetate differentiation protocol is critical to the interaction of THP-1 macrophages with Salmonella Typhimurium', *PLoS ONE*. doi: 10.1371/journal.pone.0193601.

- Stecca, B. and Rovida, E. (2019) 'Impact of ERK5 on the hallmarks of cancer', *International Journal of Molecular Sciences*. doi: 10.3390/ijms20061426.
- Su, L. *et al.* (2016) 'Loss of CAR promotes migration and proliferation of HaCaT cells, and accelerates wound healing in rats via Src-p38 MAPK pathway', *Scientific Reports*. doi: 10.1038/srep19735.
- Thangavel, P. *et al.* (2017) 'Accelerated Healing of Diabetic Wounds Treated with L-Glutamic acid Loaded Hydrogels Through Enhanced Collagen Deposition and Angiogenesis: An in Vivo Study', *Scientific Reports*. doi: 10.1038/s41598-017-10882-1.
- Toulon, A. *et al.* (2009) 'A role for human skin-resident T cells in wound healing', *Journal of Experimental Medicine*. doi: 10.1084/jem.20081787.
- Tracy, L. E., Minasian, R. A. and Caterson, E. J. (2016) 'Extracellular Matrix and Dermal Fibroblast Function in the Healing Wound', *Advances in Wound Care*. doi: 10.1089/wound.2014.0561.
- Tubita, A., Tusa, I. and Rovida, E. (2021) 'Playing the Whack-A-Mole Game: ERK5 Activation Emerges Among the Resistance Mechanisms to RAF-MEK1/2-ERK1/2- Targeted Therapy', *Frontiers in Cell and Developmental Biology*. doi: 10.3389/fcell.2021.647311.
- Tundisi, L. L. *et al.* (2021) 'Hydroxypropyl methylcellulose: Physicochemical properties and ocular drug delivery formulations', *European Journal of Pharmaceutical Sciences*. doi: 10.1016/j.ejps.2021.105736.
- Velikyan, I. (2012) 'Molecular imaging and radiotherapy: Theranostics for personalized patient management', *Theranostics*. doi: 10.7150/thno.4428.
- Vlaia, L. *et al.* (2016) 'Cellulose-Derivatives-Based Hydrogels as Vehicles for Dermal and Transdermal Drug Delivery', in *Emerging Concepts in Analysis and Applications of Hydrogels*. doi: 10.5772/63953.
- Walker, J. L. *et al.* (2018) 'In wound repair vimentin mediates the transition of mesenchymal leader cells to a myofibroblast phenotype', *Molecular Biology of the Cell*. doi: 10.1091/mbc.E17-06-0364.
- Wang, J. (2018) 'Neutrophils in tissue injury and repair', *Cell and Tissue Research*. doi: 10.1007/s00441-017-2785-7.
- Wang, P. and Moore, A. (2013) 'Translational Molecular Imaging of Diabetes', *Current Radiology Reports*. doi: 10.1007/s40134-013-0019-7.
- Wetzler, C. *et al.* (2000) 'Large and sustained induction of chemokines during impaired wound healing in the genetically diabetic mouse: Prolonged persistence of neutrophils and macrophages during the late phase of repair', *Journal of Investigative Dermatology*. doi: 10.1046/j.1523-1747.2000.00029.x.
- Wicks, K. *et al.* (2015) 'Diabetes inhibits Gr-1+ myeloid cell maturation via cebpa deregulation', *Diabetes*, 64(12), pp. 4184–4197. doi: 10.2337/DB14-1895.
- Wicks, K., Torbica, T. and Mace, K. A. (2014) 'Myeloid cell dysfunction and the pathogenesis of the diabetic chronic wound', *Seminars in Immunology*, 26(4), pp. 341–353. doi: 10.1016/J.SMIM.2014.04.006.
- Wieman, T. J. (1998) 'Clinical efficacy of becaplermin (rhPDGF-BB) gel. Becaplermin Gel Studies Group.', *American journal of surgery*.
- Wilhelmsen, K. *et al.* (2015) 'Extracellular signalregulated kinase 5 promotes acute cellular and systemic inflammation', *Science Signaling*. doi: 10.1126/scisignal.aaa3206.
- Wilkinson, H. N. *et al.* (2019) 'Tissue Iron Promotes Wound Repair via M2 Macrophage Polarization and the Chemokine (C-C Motif) Ligands 17 and 22', *American Journal of Pathology*. doi:

10.1016/j.ajpath.2019.07.015.

Willerth, S. (2017) 'Natural biomaterials for engineering neural tissue from stem cells', in *Engineering Neural Tissue from Stem Cells*. doi: 10.1016/b978-0-12-811385-1.00005-4.

Wolf, S. J., Melvin, W. J. and Gallagher, K. (2021) 'Macrophage-mediated inflammation in diabetic wound repair', *Seminars in Cell & Developmental Biology*. doi: 10.1016/J.SEMCDB.2021.06.013.

Wong, C. H. *et al.* (2020) 'Estimating the financial impact of gene therapy', *medRxiv*. doi: 10.1101/2020.10.27.20220871.

Woo, C. H. *et al.* (2006) 'ERK5 activation inhibits inflammatory responses via peroxisome proliferator-activated receptor δ (PPAR δ) stimulation', *Journal of Biological Chemistry*. doi: 10.1074/jbc.M602369200.

World Health Organization (2016) 'Global Report on Diabetes', *Isbn*. doi: ISBN 978 92 4 156525 7.

Wright, T. D. *et al.* (2020) 'Pharmacological inhibition of the MEK5/ERK5 and PI3K/Akt signaling pathways synergistically reduces viability in triple-negative breast cancer', *Journal of Cellular Biochemistry*. doi: 10.1002/jcb.29350.

Wu, Y. *et al.* (2012) 'ERK5 regulates glucose-induced increased fibronectin production in the endothelial cells and in the retina in diabetes', *Investigative Ophthalmology and Visual Science*. doi: 10.1167/iovs.12-10553.

Wynn, T. A. and Vannella, K. M. (2016) 'Macrophages in Tissue Repair, Regeneration, and Fibrosis', *Immunity*. doi: 10.1016/j.immuni.2016.02.015.

Xue, J. *et al.* (2014) 'Transcriptome-Based Network Analysis Reveals a Spectrum Model of Human Macrophage Activation', *Immunity*. doi: 10.1016/j.immuni.2014.01.006.

Yang, Z. and Ming, X. F. (2014) 'Functions of arginase isoforms in macrophage inflammatory responses: Impact on cardiovascular diseases and metabolic disorders', *Frontiers in Immunology*. doi: 10.3389/fimmu.2014.00533.

Yona, S. *et al.* (2013) 'Fate Mapping Reveals Origins and Dynamics of Monocytes and Tissue Macrophages under Homeostasis', *Immunity*. doi: 10.1016/j.immuni.2012.12.001.

Yue, B. *et al.* (2014) 'ERK5 silencing inhibits invasion of human osteosarcoma cell via modulating the Slug/MMP-9 pathway', *European Review for Medical and Pharmacological Sciences*. doi: 10.4172/2161-0681.1000182.

Zampetti, A. *et al.* (2009) 'Proinflammatory cytokine production in HaCaT cells treated by eosin: Implications for the topical treatment of psoriasis', *International Journal of Immunopathology and Pharmacology*. doi: 10.1177/039463200902200423.

Zhao, B. *et al.* (2021) 'Sophoridine Inhibits the Tumour Growth of Non-Small Lung Cancer by Inducing Macrophages M1 Polarisation via MAPK-Mediated Inflammatory Pathway', *Frontiers in Oncology*. doi: 10.3389/fonc.2021.634851.

Zhao, R. *et al.* (2016) 'Inflammation in chronic wounds', *International Journal of Molecular Sciences*. doi: 10.3390/ijms17122085.

Zhu, Z. *et al.* (2016) 'Systemic depletion of macrophages in the subacute phase of wound healing reduces hypertrophic scar formation', *Wound Repair and Regeneration*. doi: 10.1111/wrr.12442.